10th INTERNATIONAL CONFERENCE ON MATERIALS SCIENCE AND CONDENSED MATTER PHYSICS

dedicated to
the 60th anniversary of the foundation of the Institute of Applied Physics

ABSTRACTS

CHIȘINAU 2024

Chișinău, Moldova, October 1-4, 2024

10th INTERNATIONAL CONFERENCE ON MATERIALS SCIENCE AND CONDENSED MATTER PHYSICS

dedicated to the 60th anniversary from the foundation of the Institute of Applied Physics

1-4 October, Chisinau 2024

Descrierea CIP a Camerei Naţionale A Cărţii Din Republica Moldova

"Materials Science and Condensed-Matter Physics", intern.ational conference (10; 2024; Chişinău). 10th International Conference on Materials Science and Condensed-Matter Physics : MSCMP : Chisinau 2024 : dedicated to the 60th anniversary from the foundation of the Institute of Applied Physics, October 1-4, 2024 : Book of abstracts / conference organizers: Leonid Culiuc (chair) [et al.]. – Chişinău : [S. n.], 2024 (CEP USM). – 220 p. : fig.

Antetit.: Institute of Applied Physics, Faculty of Physics and Engineering of the Moldova State University, Scientific Association "Materials Science and Engineering" [et al.]. – Referinţe bibliogr. la sfârşitul abstractelor. – [230] ex.

ISBN 978-9975-62-763-4.
538.9/539(082)
M 47

ISBN 978-9975-62-763-4. © CEP USM, 2024

To the reader,

This book includes abstracts of the communications presented at the ***10th International Conference on Materials Science and Condensed-Matter Physics (MSCMP) held in Chisinau, the Republic of Moldova.***

Until 2018, the MSCMP conference was a traditional biennial meeting organized by the Institute of Applied Physics (IAP) of the Academy of Sciences of Moldova. Unfortunately, due to the COVID pandemic and then the unexpected complication of the political situation in our region, which shook the whole scientific community, the organization of the 10th edition of the MSCMP conference was postponed for 4 long years. At the same time, it is in this year, 2024, that the IAP, which, along with other research institutes of Moldova, currently affiliated with Moldova State University, celebrates its 60th anniversary, to which the 10th edition of the MSCMP conference is dedicated.

The aim of this event is two–fold. First, it provides a nice opportunity for discussions and the dissemination of the latest results on selected topics in materials science, condensed-matter physics, and electro-physical and electro-chemical methods of materials treatment. On the other hand, this is an occasion for sketching a broad perspective of scientific research and technological developments for the participants through oral and poster presentations.

The abstracts presented in the book cover a vast range of subjects, such as: advanced materials and fabrication processes; methods of crystal growth, post-growth technological processes, fabrication of solid state structures; defect engineering, engineering of molecular assembly; 2D-materials, nanowires and nanodots; fullerenes and nanotubes, methods of material and structure characterization; structure and mechanical characterization; optical, electrical, magnetic and superconductor properties, transport processes, non-linear phenomena, size and interface effects; advances in condensed matter theory; theory of low dimensional systems; modelling of materials and structure properties; phase transition; advanced quantum physics for nanosystems; device modelling and simulation, device structures and elements; optoelectronics and photonics; micro-sensors; theory and advanced technologies of using electric fields, currents and discharges so as to intensify heat – mass-transfer, to raise the efficiency of treatment of materials, of biological preparations and foodstuff; materials and structures for electromagnetic radiation and detection.

The Program of the Conference consists of plenary lectures, of contributed oral and poster presentations, which are distributed into 6 sections:

- ***Condensed Matter Theory (CMT)***
- ***Growth and Properties of Advanced Materials (GPAM)***
- ***Design and Structural Characterization of Materials (DSCM)***
- ***Solid State Nanophysics and Nanotechnology (SSNN)***
- ***Electromagnetic Radiation Detection and Conversion (EMDC)***
- ***Materials Engineering for Innovative and Sustainable Technologies (MEST)***

Within the current edition of the MSCMP conference, two workshops took place:

- ***NATO Workshop "3D architectures of high entropy materials"***
- ***COST Action CA21144 SuperQuMap Workshop "Emerging Quantum Materials based on Superconducting Nanostructures"***

The Abstracts are published in their original versions. All responsibilities are on the authors.

L. Kulyuk — Conference Chair

S. Vatavu — Co-chair of the Conference

CONFERENCE ORGANIZERS

Leonid Culiuc (Kulyuk)	Conference Chair	Institute of Applied Physics, Moldova State University, Moldova
Sergiu Vatavu	Conference Co-chair	Faculty of Physics and Engineering, Moldova State University, Moldova
Ernest Arushanov	Programme Committee Chair	Institute of Applied Physics, Moldova State University, Moldova
Nikita Siminel	Secretary of the Conference	Institute of Applied Physics, Moldova State University, Moldova

PROGRAMME COMMITTEE

Ernest Arushanov	Programme Committee Chair	Institute of Applied Physics, Moldova State University, Moldova

Section*: **Condensed matter theory (CMT)***

Mihai Macovei - Section Chair	Institute of Applied Physics, Moldova State University, Moldova
Denis Nika	E. Pokatilov Laboratory of Physics and Engineering of Nanostructures, Moldova State University, Moldova

Section: ***Growth and Properties of Advanced Materials (GPAM)***

Vladimir Tsurkan - Section Chair	Institute of Applied Physics, Moldova State University, Moldova; Center for Electronic Correlations and Magnetism, University of Augsburg, Germany
Alexandr Nateprov	Institute of Applied Physics, Moldova State University, Moldova

Section: ***Design and Structural Characterization of Materials (DSCM)***

Victor Kravtsov - Section Chair	Institute of Applied Physics, Moldova State University, Moldova
Svetlana Baca	Institute of Applied Physics, Moldova State University, Moldova

Section: ***Solid State Nanophysics and Nanotehnology (SSNN)***

Veacheslav Ursachi - Section Chair	Academy of Sciences of Moldova, Moldova
Alexandr Cocemasov	E. Pokatilov Laboratory of Physics and Engineering of Nanostructures, Moldova State University, Moldova

Section: ***Electromagnetic Radiation Detection and Conversion (EMDC)***

Marin Rusu - Section Chair	Helmholtz-Zentrum Berlin für Materialien und Energie; Department of Applied Physics and Computer Science, Moldova State University, Moldova
Elena Achimova	Institute of Applied Physics, Moldova State University, Moldova

Section: ***Materials engineering for Innovative and Sustainable Technologies (MEST)***

Tsyntsaru Natalia - Section Chair	Institute of Applied Physics, Moldova State University, Moldova
Oleg Șapoval	Physics of Semiconductors and Devices Laboratory, Moldova State University, Moldova

Section: ***Emerging Quantum Materials Based on Superconducting Nanostructures (SuperQuMap) including Workshop***

Vladimir Fomin - Section Chair	Leibniz Institute for Solid State and Materials Research, Germany

INTERNATIONAL ADVISORY COMMITTEE

Vladimir Fomin - Chair of the International Advisory Committee	Leibniz Institute for Solid State and Materials Research, Germany
Henrikas Cesiulis	Vilnius University, Lithuania
Veaceslav Coropceanu	Department of Chemistry and Biochemistry, University of Arisona, USA
Silvio Decurtins	Department of Chemistry and Biochemistry, University of Bern, Switzerland
Chris S. Ferekides	University of South Florida, USA
Christoph H. Keitel	Max Plank Institute for Nuclear Physics, Germany
Erkki Lähderanta	Lappeenranta University of Technology, Finland
Janusz Lipkowski	Cardinal Stefan Wyszyński University in Warsaw, Poland
Mihael Zaworotko	University of Limerick, Ireland
Dimitris Pavlidis	Florida International University, USA
Susan Schorr	Department Structure and Dynamics of Energy Materials, Helmholtz-Zentrum Berlin für Materialien und Energie, Germany
Jordi Sort	Autonomous University of Barcelona, Spain
Ion Tiginyanu	Academy of Sciences of Moldova, Moldova
Wojciech Knap	CENTERA Laboratories, Institute of High Pressure Physics, Polish Academy of Sciences, Poland
Victor Șontea	Technical University of Moldova , Moldova

CONFERENCE ORGANIZING COMMITTEE

Sergiu Vatavu – Chair of the Organizing Committee — Faculty of Physics and Engineering, MSU, Moldova

Institute of Applied Physics, Moldova State University, Moldova

Olga Shikimaka
Alexei Meshalkin
Dorina Croitori
Marianna Roman
Nicolai Curmei
Oleg Reu
Serghei Ostrovsky
Natalia Kazak
Anatolii Siminel
Alexandru Micu
Valentin Batîr
Anatolii Cuharuc

Scientific association "Materials Science and Engineering"

Irina Filippova
Nina Iuzva

Faculty of Physics and Engineering, Moldova State University, Moldova

Liliana Dmitroglo
Natalia Nedeoglo
Vadim Sirkeli
Arcadi Chirița
Dorin Spoială
Igor Narolschi
Elmira Vatavu
Gheorghe Ghilețchii
Varzari Alexandru
Vlad Moisei
Irina Maistruc
Elena Bercu
Tatiana Iurieva
Eugeniu Spinei
Alisa Moșneaga
Alexandr Belenciuc

ORGANIZED BY

Institute of Applied Physics

Faculty of Physcis and Engineering of Moldova State University

Scientific Association “Materials Science and Engineering”

NATO SPS Project G6153

“Stealth Coatings Based on 3D Architectures of High Entropy Materials"

SUPPORTED BY

Moldova State University

NATO SPS Project G6153

“Stealth Coatings Based on 3D Architectures of High Entropy Materials"

National Institute for Laser, Plasma and Radiation Physics, Romania

COSTAction CA21144 SuperQuMap

“Superconducting Nanodevices and Quantum Materials for Coherent Manipulation”

Labromed Laborator SRL

CONTENTS

NITRIDES VERSUS GRAPHENE FOR TERAHERTZ PLASMONIC OPTOELECTRONICS

P. Sai[1,2], M. Dub[1,2], V. Korotyeyev[1,2,3], G. Cywiński[1,2], W. Knap[1,2,*]
[1]*CENTERA -CEZAMAT Warsaw University of Technology, Warsaw, Poland;*
[2]*Institute of High Pressure Physics, Polish Academy of Sciences, Warsaw, Poland;*
[3]*V. Ye. Lashkaryov Institute of Semiconductor Physics, NASU, Kyiv, Ukraine*
[*]E-mail: wojciech.knap@unipress.waw.pl

The first demonstration of THz amplification by graphene nanostructures achieved by RIEC- Sendai-Tohoku University team [1,2] raised many fundamental questions like : i) is the graphene really necessary ii) can one scale results obtained on sub-wavelength (μm scale) graphene flakes up to practical size (mm scale) THz amplifier devices. In this work we present recent results on GaN/AlGaN based plasmonic structures obtained in CENTERA -Warsaw, showing that in moderate cryogenic conditions (temperatures ~80K) in many aspects (i.e. carrier density , mobility and optical phonon energy) these structures mimic graphene nanostructures used in the first amplification experiments. The results allow us to identify main challenges/difficulties on the way towards realistic (practical size) plasmonic amplifiers of THz radiation [3, 4, 5].

ACKNOWLEDGMENTS: Funded by the European Union (ERC ADAVANCED PROJECT -TERAPLASM #101053716). The work was also supported by the "International Research Agendas" Projects CENTERA &CENTERA2 of the Foundation for Polish Science co-financed by the European Union under the European Regional Development Fund (Grant No. MAB/2018/9 for CENTERA & FENG.02.01-IP.05-T004/23) for CENTERA2).

[1] S. Boubanga-Tombet, W. Knap, D. Yadav, A. Satou, D. B. But, V. V. Popov, I. V. Gorbenko, V. Kachorovskii, and T. Otsuji. *Phys. Rev. X* **10** (2020), 031004
[2] T. Otsuji, S. A. Boubanga-Tombet, A. Satou, D. Yadav, H. Fukidome, T. Watanabe, T. Suemitsu, A. A. Dubinov, V. V. Popov, W. Knap, V. Kachorovskii, K. Narahara, M. Ryzhii, V. Mitin, M. S. Shur and V. Ryzhii. *Nanophotonics*, **11-9** (2022).
[3] P. Sai, V. V. Korotyeyev, M. Dub, M. Słowikowski, M. Filipiak, D. B. But, Yu. Ivonyak, M. Sakowicz, Yu. M. Lyaschuk, S. M. Kukhtaruk, G. Cywiński and W. Knap *Phys. Rev. X* **13** (2023), 041003.
[4] P. Sai, M. Dub, V. Korotyeyev, S. Kukhtaruk, G. Cywinski, and W. Knap. *Lithuanian Journal of Physics* **63-4** (2023), 251–263
[5] Plasmons in AlGaN/GaN grating-gate structure probing with 300 K background illumination. M. Dub, D. B. But, P. Sai, Yu. Ivonyak, M. Słowikowski, M. Filipiak, G. Cywinski, W. Knap and S. Rumyantsev *AIP Advances* **13** (2023), 09501

EARTH-ABUNDANT COMPOUND SEMICONDUCTORS FOR SOLAR ENERGY CONVERSION

Susan Schorr[1,2,*]
[1]*Helmholtz-Zentrum Berlin fuer Materialien und Energie, Germany;*
[2]*Freie Universitaet Berlin, Institute of Geological Siences, Germany*
[*]E-mail: susan.schorr@helmholtz-berlin.de

The need of handling eco-friendly and cheap compound semiconductors in thin film photovoltaics (PV) has constantly pushed the research towards more environmental friendly materials, such as Kesterite-type compound semiconductors Cu_2ZnSnS_4 (CZTS), $Cu_2ZnSnSe_4$ (CZTSe) and $Cu_2ZnSn(S,Se)_4$ (CZTSSe). They present the only critical raw material (CRM) free thin film PV technology with tunable band gap energy and excellent long-term stability. The current record efficiency for CZTSSe solar cells of 14.9 % [1] highlights the great potential of this abundant chalcogenides to support a sustainable energy transition. Additionally, finding alternative semiconductor materials with suitable properties remains a task of utmost importance for the widespread use of renewable energies.

In record devices these chalcogenide absorber materials generally show a non-stoichiometric composition which is possible due to a remarkable flexibility of their crystal structure. This ability to accept deviations from stoichiometry is correlated to the formation of intrinsic point defects [2]. The formation of such defects, like vacancies, ant-sites and interstitials, is driven thermo-dynamically by minimizing the Gibbs free energy of the crystal. The key issue for kesterite solar cells is the large open-circuit voltage deficit which is caused by three main factors: (i) a non-homogeneous absorber composition resulting in bandgap fluctuations [3] and formation of secondary phases, (ii) structural disorder like Cu-Zn disorder [4] or intrinsic point defects [2] causing strong band tailing [3] and (iii) the multi-element composition and the variable valence of Sn resulting in complicated defect properties [5].

Ternary nitrides $ZnGeN_2$ and $ZnSnN_2$ are being considered as promising candidates for photovoltaic absorber materials, containing uniquely elements of low toxicity and low resource criticality. Further to bandgap tuning by alloying we have shown that these compounds possess a second mechanism for bandgap tuning through cation disorder [6].

The presentation will discuss the potential of point defect engineering to optimize the key factors limiting the open circuit voltage of the potential solar cell. Based on the off-stoichiometry type model for quaternary chalcogenides [2] correlating chemical composition and occuring intrinsic point defects in these compound semiconductors, a compositional region for high efficient devices can be revealed. Changing the degree of Cu-Zn disorder varies the band gap energy as well as the value of PL_{max} [7]. The Cu-Zn disorder can be influenced by a thermal annealing process [8] nowadays technologically applied as post-deposition treatment. Cation disorder is also important for the bandgap engineering in $ZnGeN_2$, showing an interplay with the unavoidable oxygen content in the material [6].

The presentation is based on our systematic experimental studies of quaternary compound semiconductors applying advanced analytical methods like neutron and synchrotron X-ray diffraction, photoluminescense and UV-Vis spectroscopy.

[1] Best Research-Cell Efficiency Chart, NREL, www.nrel.gov/pv/cell-efficiency.html
[2] S. Schorr et al., J. Phys.: Energy 2 (2020) 012002
[3] T. Gokman et al., Appl. Phys. Lett. 103 (2013) 103506
[4] S. Schorr et al., Europ. J. Mineral. 19 (2007) 65
[5] R. Fonoll-Rubio et al., Energy Environ. Sci. 14 (2021) 507
[6] Z. Wang et al., J. Mat. Chem. C 12 (2024) 1124
[7] G. Gurieva et al., Sol. En. Mat. Sol. Cells 248 (2022) 112009
[8] D. Többens et al., Phys. Stat. Solidi B 253 (2016) 1890

PULSED LASER DEPOSITION OF THIN FILMS FOR ADVANCED APPLICATIONS

V. Craciun[1,2,*], D. Craciun[1], S. A. Irimiciuc[1], G. Dorcioman[1], P. Garoi[1], A. Trefilov[1], R. Udrea[1,3], V. Grumezescu[1], D. Ursescu[2], G. Bleotu[2], A. Magureanu[2], C. Ticos[2], V. Geanta[4], I. Voiculescu[4], J.C. Marza-Rosca[5]

[1]*National Institute for Laser, Plasma and Radiatio Physics, Magurele, Romania;*
[2]*Extreme Light Infrastructure for Nuclear Physics, Magurele, Romania;*
[3]*Physics Faculty, University of Bucharest, Magurele, Romania;*
[4]*National University of Science and Technology Politehnica of Bucharest, Romania;*
[5]*Mechanical Engineering Department, University of Las Palmas de Gran Canaria, Spain*
[*]E-mail: valentin.craciun@inflpr.ro

Pulsed Laser Deposition remains one of the best laboratory-based technique to synthesize thin films of novel materials to investigate their structure-composition-properties. By changing the laser parameters (fluence and repetition rate), substrate temperature, deposition atmosphere nature (inert to reactive) and pressure (from high vacuum to 100 mbar) one can control the structure, composition and surface morphology of the deposited films and nanostructures. Several examples will illustrate the PLD advantages.

High entropy alloys (HEA), although discovered a couple of centuries ago, have become an active research topic in the last two decades. Incorporating 5 or more elements in approximately equimolar concentrations, HEA materials exhibit superior properties than usual alloys. We used PLD technique to obtain thin films starting from small AlCoCrFeNix buttons of around 15-20 mm diameter to investigate the role of Ni composition on the properties of grown films [1]. Moreover, by performing the depositions under N2 or CH4 gases we successfully incorporated metallic nitrides and carbides in the thin films composition, which increased their hardness and electrochemical properties [2].

Another research topic where PLD grown films were successfully used was the measurement of the fs-Laser Induced Damage Threshold (fs-LIDT) values. Since such experiments using real fs-laser mirrors are destructive and therefore rather expensive, we fabricated small mirrors by PLD technique depositing thin films of HfO2 and ZrO2 of high quality SiO2 substrates. By changing the oxygen pressure during deposition, we obtained films showing different fs-LIDT values, which were measured both using Langmuir probes and the charge compensation current technique [3].

The coupling of extreme high power fs-laser pulses in materials depends on their electronic density. For ELI lasers (800 nm wavelength) this electron density turns out to be achieved for a low Z material such as carbon at a mass density of around 5-10 mg/cm3, which is almost 3 orders of magnitude lower than the normal mass density. We fabricated carbon foam materials using PLD in a very high pressure of CH4. By using Rutherford backscattering spectrometry coupled with cross-sectional scanning electron microscopy we estimated the density of the foams at around 10-15 mg/cm3. Experiments at various laser intensities from 10^{15} W/cm^2 up to 10^{20} W/cm2 clearly showed a better coupling on films covered with 10 μm carbon foam than that measured for simple films.

[1] Characteristics of Thin High Entropy Alloy Films Grown by Pulsed Laser Deposition, Laszlo, EA; Craciun, D; Dorcioman, G; Craciun, G; Geanta, V; Voiculescu, I; Cristea, D; Craciun, V, COATINGS, Volume 12, Issue8, Article Number1211, DOI10.3390/coatings12081211, PublishedAUG 2022.
[2] D. Craciun, E.A. Laszlo, J.C. Mirza-Rosca, G. Dorcioman, V. Geanta, I. Voiculescu, G. Craciun, L. Badea, V. Craciun, Structural Parameters and Behavior in Simulated Body Fluid of High Entropy Alloy Thin Films, Materials 17 (2024) 1162. https://doi.org/10.3390/ma17051162
[3] Exploring fs-laser irradiation damage subthreshold behavior of dielectric mirrors via electrical measurements Petrisor Gabriel Bleotu, Radu Udrea, Alice Dumitru, Olivier Uteza, Maria-Diana Mihai, Dan Gh Matei, Daniel Ursescu, Stefan Irimiciuc, Valentin Craciun, High Power Laser Science and Engineering, Vol 12, e15.

ELECTRONIC STRUCTURE OF SURFACES AND INTERFACES BY KELVIN PROBE AND PHOTOELECTRON YIELD SPECTROSCOPY AT AMBIENT PRESSURE

M. Rusu[1,*], T. Unold[1], S. Schorr[1,2]
[1]*Department Structure and Dynamics of Energy Materials, Helmholtz-Zentrum Berlin für Materialien und Energie GmbH, Hahn-Meitner-Platz 1, 14109 Berlin, Germany*
[2]*Institute of Geological Sciences, Freie Universität Berlin, Malteserstr. 74-100, 12249 Berlin, Germany*
[*]E-mail: rusu@helmholtz-berlin.de

Kelvin probe (KP) and photoemission spectroscopies are widely used for characterization of materials surface and interface electronics for modelling and development of new effective optoelectronic devices. Those investigations are usually carried out under ultra-high vacuum conditions. It was however found in recent studies that under the latter conditions the surface species, incl. molecules used for surface functionalization, tend to detach, making it challenging to draw unambiguous conclusions. For this reason, we employ techniques working at ambient pressure, e.g., KP in combination with the photoelectron yield spectroscopy (PYS) [1]. The application of those techniques at atmospheric pressure is still emerging and yet an amount of skepticism might be felt in community. The aim of this work is therefore to show the successful application of combined KP-PYS under inert ambient, e.g., N_2 or Ar, at atmospheric pressure.

KP and PYS use the same Kelvin tip for recording the work function (WF) and ionization energy (IE), i.e., Fermi level and valence band maximum positions, respectively. From PYS spectra we determine in addition the density of states (DOS) for energies > WF. The KP and PYS measurements are conducted successively at the same sample position with energy resolutions of 1-2 meV and ~30 meV, respectively. We calculate PYS information depths of 1-10 nm by considering electron energies <10 eV. Note that for electron energies <50 eV, and especially for the energy range <10 eV (our case), there is still a big lack of experimental data and reliable calculation models.

We demonstrate a good agreement of the measured WFs and IEs of CdS, $Cu(In,Ga)Se_2$, CuI and NiO_x with the available data obtained by other methods [1-3]. We show in addition the applicability of the combined KP-PYS for detection of surface dipoles induced by self-assembled monolayers [4], of the DOS in comparison with theoretical calculations [5], and of negative electron affinity of diamond [6]. We also demonstrate the applicability of the gained KP-PYS data on energy band positions for determination of material charge carrier concentration [1-3]. Finally, we demonstrate mappings on combinatorial thin films for high-throughput material characterisation.

[1] M. Rusu, T. Kodalle, L. Choubrac, N. Barreau, C. A. Kaufmann, R. Schlatmann, T. Unold, *ACS Appl. Mater. Interfaces* **13** (2021) 7745-7755.
[2] A. Crovetto, H. Hempel, M. Rusu, L. Choubrac, D. Kojda, K. Habicht, T. Unold, *ACS Appl. Mater. Interfaces* **12(43)** (2020) 48741-48747.
[3] S. H. B. Vinoth Kumar, R. Muydinov, N. Maticiuc, N. Alktash, M. Rusu, B. B. O. Seibertz, H. Köbler, A. Abate, T. Unold, I. Lauermann, B. Szyszka, *Adv. Energy Sustainability Res.* **5** (2024) 2300201/1-11.
[4] L. Canil, T. Cramer, B. Fraboni, D. Ricciarelli, D. Meggiolaro, A. Singh, M. Liu, M. Rusu, C. M. Wolff, N. Phung, Q. Wang, D. Neher, T. Unold, P. Vivo, A. Gagliardi, F. De Angelis, A. Abate, *Energy Environ. Sci.* **14(3)** (2021) 1429-1438.
[5] Y. T. Huang, S. R. Kavanagh, M. Righetto, M. Rusu, I. Levine, T. Unold, S. J. Zelewski, A. J. Sneyd, K. Zhang, L. Dai, A. J. Britton, J. Ye, J. Julin, M. Napari, Z. Zhang, J. Xiao, M. Laitinen, L. Torrente-Murciano, S. D. Stranks, A. Rao, L. M. Herz, D. O. Scanlon, A. Walsh, R. L. Z. Hoye, *Nature Communications* **13** (2022) 4960(13).
[6] A. Chemin, I. Levine, M. Rusu, R. Vaujour, P. Knittel, P. Reinke, K. Hinrichs, T. Unold, T. Dittrich, and T. Petit, *Small Methods* **7(11)** (2023) 2300423(1-11).

ULTRASONIC STUDIES OF QUANTUM MAGNETS WITH COMPETING INTERACTIONS

J. Sourd[1,*], Y. Skourski[1], L. Prodan[2,3], V. Tsurkan[2,3], T. Kotte[1], P. Wild[4], S. Mühlbauer[4], A. Miyata[5], J. Wosnitza[1,6] and S. Zherlitsyn[1]

[1]*Hochfeld-Magnetlabor Dresden (HLD-EMFL) and Würzburg-Dresden Cluster of Excellence ct.qmat, Helmholtz-Zentrum Dresden-Rossendorf, Dresden, Germany;*

[2]*Experimental Physics V, University of Augsburg, Augsburg, Germany;*

[3]*Institute of Applied Physics, Moldova State University, Chișinău, Republic of Moldova;*

[4]*Heinz Maier-Leibnitz Zentrum (MLZ), Technische Universität München, Garching, Germany;*

[5]*Institute for Solid State Physics, The University of Tokyo, Kashiwa, Japan;*

[6]*Institut für Festkörper und Materialphysik, TU Dresden, Dresden, Germany*

[*]E-mail: j.sourd@hzdr.de

Quantum magnets shows fascinating properties and emergent phenomena at low temperatures. In particular, when competing magnetic interactions are present, very rich phase diagrams can be observed by varying the temperature and an external parameter such as the magnetic field. In this talk, we will be interested in two different magnetic compounds, $Ba_2CuGe_2O_7$ which shows the competition between magnetic exchange and Dzyaloshinskii-Moriya interactions, and $MnSc_2Se_4$ which shows competing ferromagnetic and antiferromagnetic interactions on the frustrated diamond lattice. We use ultrasound measurement to characterize this systems, which permits a symmetry detailed analysis of the ordered phases and of the low energy fluctuations, thanks to the use of compression and shear waves of different symmetry. This permits to identify an exotic coupling of the elastic modes to the cycloidal order of $Ba_2CuGe_2O_7$, and to characterize the enhancement of quantum fluctuations by the magnetic field in $MnSc_2Se_4$.

CURVILINEAR MAGNETISM: FUNDAMENTALS AND APPLICATIONS

D. Makarov*
Helmholtz-Zentrum Dresden-Rossendorf e.V., Bautzner Landstrasse 400, Dresden, Germany
*E-mail: d.makarov@hzdr.de

Curvilinear magnetism is a framework, which helps understanding the impact of geometric curvature on complex magnetic responses of curved 1D wires and 2D shells [1-3]. This approach provides means to modify conventional or to launch novel functionalities by tailoring curvature and 3D shape of magnetic thin films and nanowires [3,4]. In this talk, we will address fundamentals of curvature-induced effects in magnetism and review the envisioned application scenarios. In particular, we will demonstrate that curvature allows tailoring fundamental anisotropic and chiral magnetic interactions [5] and enables fundamentally new non-local chiral symmetry breaking effect [6,7]. 3D shaped magnetic objects enable realization of non-linear systems accommodating multiple solitons with complex interactions [8]. Those are relevant for numerous research and technology fields ranging from non-conventional computing and spin-wave splitters for low-energy magnonics. Application potential of geometrically curved magnetic architectures is currently being explored as mechanically reshapeable magnetic field sensors for automotive applications, spin-wave filters, high-speed racetrack memory devices, magnetic soft robotics [9] as well as on-skin interactive electronics relying on thin films [10-12] as well as printed magnetic composites [13,14] with appealing self-healing performance [15]. This opens perspectives for magnetoelectronics in smart wearables, interactive printed electronics and motivates further explorations towards the realization of eco-sustainable magnetic field sensing relying on biocompatible and biodegradable materials.

[1] P. Gentile et al., Electronic materials with nanoscale curved geometries. *Nature Electronics* (Review) **5** (2022) 551.
[2] P. Makushko et al., A tunable room-temperature nonlinear Hall effect in elemental bismuth thin films. *Nature Electronics* **7** (2024) 207.
[3] D. Makarov et al., New Dimension in Magnetism and Superconductivity: 3D and Curvilinear Nanoarchitectures. *Advanced Materials* (Review) **34** (2022) 2101758.
[4] D. Makarov et al., *Curvilinear micromagnetism: from fundamentals to applications* (Springer, Zurich, 2022).
[5] O. Volkov et al., Experimental observation of exchange-driven chiral effects in curvilinear magnetism. *Physical Review Letters* **123** (2019) 077201.
[6] D. D. Sheka et al., Nonlocal chiral symmetry breaking in curvilinear magnetic shells. *Communications Physics* **3** (2020) 128.
[7] O. M. Volkov et al., Chirality coupling in topological magnetic textures with multiple magnetochiral parameters. *Nature Communications* **14** (2023) 1491.
[8] O. Volkov et al., Three-dimensional magnetic nanotextures with high-order vorticity in soft magnetic wireframes. Nature Communications **15** (2024) 2193.
[9] M. Ha et al., Reconfigurable Magnetic Origami Actuators with On-Board Sensing for Guided Assembly. *Advanced Materials* **33** (2021) 2008751.
[10] G. S. Canon Bermudez et al., Magnetosensitive e-skins for interactive devices. *Advanced Functional Materials* (Review) **31** (2021) 2007788.
[11] J. Ge et al., A bimodal soft electronic skin for tactile and touchless interaction in real time. *Nature Communications* **10** (2019) 4405.
[12] G. S. Canon Bermudez et al., Electronic-skin compasses for geomagnetic field driven artificial magnetoception and interactive electronics. *Nature Electronics* **1** (2018) 589.
[13] M. Ha et al., Printable and Stretchable Giant Magnetoresistive Sensors for Highly Compliant and Skin-Conformal Electronics. *Advanced Materials* **33** (2021) 2005521.
[14] E. S. Oliveros Mata et al., Dispenser printed bismuth-based magnetic field sensors with non-saturating large magnetoresistance for touchless interactive surfaces. *Advanced Materials Technologies* **7** (2022) 2200227.
[15] R. Xu et al., Self-healable printed magnetic field sensors using alternating magnetic fields. *Nature Communications* **13** (2022) 6587.

COMPETITION OF KONDO SCATTERING AND FANO-FESHBACH RESONANT PAIRING IN ARTIFICIAL HIGH-T_C SUPERLATTICES MADE BY QUANTUM DESIGN

A. Bianconi*
Rome International Center Materials Science Superstripes, (RICMASS), Rome, Italy
*Email: antonio.bianconi@ricmass.eu

Recently, the quest for high-T_c superconductivity has evolved from the trial-and-error methodology to the growth of nanostructured artificial high-T_c superlattices (AHTS) with tailor-made superconducting functional properties by quantum design [1-4]. Superlattices are composed of nanoscale superconducting units of modulation doped Mott insulator La_2CuO_4 with thickness *L* intercalated by metallic overdoped $La_{1.55}Sr_{0.45}CuO_4$ and period d. Quantum design based on the multi-gap Bogoliubov theory including spin-orbit coupling (SOC). has been employed for prediction of the amplification of the critical temperature as a function of the conformational parameter L/d which gives origin to the superconducting dome by modulation of the pair transfer exchange interaction.

At the top of the superconducting dome, at the *magic* ratio L/d=2/3, the heterostructures are tuned at the Fano-Feshbach resonance and the normal phase exhibits the Planckian T-linear resistivity. Here, we report experimental evidence that the Kondo proximity effect competes with the Fano-Feshbach resonance suppressing T_c on both sides of the superconducting dome [5]. The Kondo proximity effect is expected in electrical resistance of AHTS nanoscale heterostructures following a Kondo universal scaling obtained by numerical renormalization group theory. We show the vanishing Kondo temperature T_K and Kondo scattering amplitude R_{0K} at L/d=2/3, while T_K and R_{0K} increase on the underdoped (L/d>2/3) and overdoped (L/d<2/3) side of the superconducting dome.

[1] Logvenov, G., Bonmassar, N., Christiani, G., Campi, G., Valletta, A., Bianconi, A. *Condensed Matter,* **8(3)** (2023), 78
[2] Mazziotti, M. V., Valletta, A., Raimondi, R., Bianconi, A. *Physical Review B,* **103(2)** (2021), 024523.
[3] Mazziotti, M. V., Bianconi, A., Raimondi, R., Campi, G., Valletta, A. *Journal of Applied Physics*, **132(19)** (2022).
[4] Valletta, A., Bianconi, A., Perali, A., Logvenov, G., & Campi, G. *arXiv:2407.19069* (2024).
[5] Campi, G., Logvenov, G., Caprara, S., Valletta, A., & Bianconi, A. *arXiv:2407.19068* (2024).

DIRECT OBSERVATION OF A SUPERCONDUCTING VORTEX DIODE

Y. Anahory[1,*], A. Gutfreund[1], H. Matsuki[2], V. Plastovets[3], A. Noah[1],
L. Gorzawski[2], N. Fridman[1], G. Yang[2], A. Buzdin[3], O. Millo[1], J.W.A. Robinson[3]
[1]*The Hebrew University of Jerusalem, Jerusalem, Israel;*
[2]*University of Cambridge, Cambridge, United Kingdom;*
[3]*Université de Bordeaux, Talence, France*
[*]E-mail: yonathan.anahory@mail.huji.ac.il

The interplay between magnetism and superconductivity can lead to unconventional proximity and Josephson effects. A related phenomenon that has recently attracted considerable attention is the superconducting diode effect, in which a non-reciprocal critical current emerges [1–3]. Although superconducting diodes based on superconducting/ferromagnetic (S/F) bilayers were demonstrated more than a decade ago [4], the precise underlying mechanism remains unclear. While not formally linked to this effect, the Fulde-Ferrell-Larkin-Ovchinikov (FFLO) state is a plausible mechanism, due to the 2-fold rotational symmetry breaking caused by the finite center-of-mass-momentum of the Cooper pairs. Here, we directly observe, a tunable superconducting vortex diode in Nb/EuS (S/F) bilayers. Based on our nanoscale SQUID-on-tip (SOT) microscope [5,6] and supported by in-situ transport measurements, we propose a theoretical model that captures our key results. Thus, we determine the origin for the vortex diode effect, which builds a foundation for new device concepts.

[1] F. Ando, Y. Miyasaka, T. Li, J. Ishizuka, T. Arakawa, Y. Shiota, T. Moriyama, Y. Yanase, T. Ono, *Nature* ***584***, 373 (2020).
[2] K.R. Jeon, J.K. Kim, J.Yoon, J.C. Jeon, H. Han, A. Cottet, T. Kontos, S.S.P. Parkin. *Nat. Mater.* ***21***, 1008 (2022).
[3] S. Ilić, F. S. Bergeret. *Phys. Rev. Lett.* **128**, 177001 (2022).
[4] G. Carapella, V. Granata, F. Russo, G. Costabile. *Appl. Phys. Lett.* ***94***, 242504 (2009).
[5] D. Vasyukov, Y. Anahory, et.al. *Nat. Nanotechnol.* ***8***, 639 (2013).
[6] Y. Anahory, et al. *Nanoscale* ***12***, 3174 (2020).

RECENT ADVANCES IN HIGH PERFORMANCE MgB_2 WIRES FOR PRACTICAL APPLICATIONS

A.Gencer[1,3,*], C. Guo[2], S. Safran[1,3], D. Wang[2], H. Koralay[4], E. Coskun[1], Y. Oznal[1], A. Seçkin[5], K. Sönmez[1], Y. Ma[2]

[1]*Ankara University, Superconductor Technologies Application and Research Center, Ankara, Türkiye;*

[2]*Chinese Academy of Sciences, Institute of Electrical Engineering, Key Laboratory of Applied Superconductivity, Beijing, China;*

[3]*Ankara University, Science Faculty, Physics Department, Ankara, Türkiye;*

[4]*Gazi University, Science Faculty, Physics Department, Ankara, Türkiye;*

[5]*Gazi University, Basic and Engineering Sciences Central Laboratory Application and Research Center (GUTMAM), Ankara, Türkiye*

[*]E-mail: Ali.Gencer@science.ankara.edu.tr

MgB_2 is widely recognized as a promising superconductor for practical applications at temperatures around 20 K, offering advantages in cryogenic cooling and cost-effectiveness. In the context of wire production, two primary methods are employed: Powder-In-Tube (PIT) and Internal Mg Diffusion (IMD). These methods yield high-density MgB_2 phases with improved grain connectivity, resulting in high transport critical current density (Jc).

IMD-processed wires have gained prominence in MgB_2 research, particularly due to efforts aimed at enhancing structural uniformity and maximizing the filling factor of IMD-MgB_2 wires. Türkiye, with its abundant and high-purity boron resources, has successfully produced amorphous boron powders crucial for MgB_2 wire fabrication. While PIT has been the dominant method over the past two decades, recent trends favor the production of IMD-MgB_2 wires.

In this presentation, we share our latest findings on developing high-performance MgB_2 long wires using an advanced IMD approach for high-magnetic-field applications. Our objective is to enhance the critical current carrying capacity of IMD-processed wires by incorporating C-coated amorphous boron powders and low-temperature activators such as Cu or Sn. This strategy aims to create MgB_2 wires with higher Technology Readiness Levels (TRL), making them more suitable for potential large-scale applications.

ACKNOWLEDGMENTS: This work has received support from TÜBİTAK and the Chinese Academy of Sciences (CAS) through Bilateral Cooperation under contract No: 123N624.

ON THE MATERIAL CONSIDERATIONS FOR ENERGY HARVESTING IN IOTS

A Vaseashta[1,2,*]
[1]*International Clean Water Institute, Manassas, VA USA, and Institute of Electronic Engineering*
[2]*Technical University of Moldova, D.Ghitu Institute of Electronic Engineering and Nanotechnologies, Chișinău, Republic of Moldova*
[*]E-mail: prof.vaseashta@ieee.org

The current landscape in the 21st century has become exceedingly complex and interconnected by resources, systems, and networks – both physical and virtual. Using cyber-physical systems (CPS), the Internet of Things (IoT) based devices form highly connected and adaptive environments through smart and intelligent systems and protocols to provide enhanced situational awareness. Artificial intelligence plays a pivotal role in augmenting the potential of IoTs, now commonly termed AIoT. Potential applications of AIoT are driving the growth and evolution of IoT, with significant impacts on consumers, the research community, the public sector, as well as the commercial and industrial sectors. One of the constraints that limit such operations is the sources of energy to power such devices. Recent advances in next-generation triboelectric nanogenerators (TENG), the integration of finite-state machines (FSM), and built-in edge computing in onboard IoT devices have reduced the energy requirement, thus shifting the energy storage requirements to built-in power generation and ambient sources. One of the aspects to enhance energy generation efficiency is piezoelectric materials and is studied in terms of the figure of merit [1,3]. Furthermore, it is essential to have the synergetic integration of technologies to minimize energy storage and reduce energy consumption in commercial off-the-shelf (COTS) configurations [4,6]. As the complexity and functionality of systems around us increase exponentially, combinatorial technologies in conjunction with artificial intelligence (AI), machine learning (ML), and data analytics (DA) are used as decision support tools to provide a comprehensive analysis and strategy to optimize usage. The economic and societal potential of such systems is vastly greater than what has been realized, and major investments are being made worldwide to develop the technology, hence CPS, in conjunction with AI with IoT (AIoT) and the Internet of Behavior (IoB) will further expand the boundaries of smart and connected systems to provide numerous societal opportunities. Applications of AIoTs, IoB, and onboard energy harvesting devices also include tactile sensing, smart agriculture, and transportation logistics and will be presented.

[1] A. Vaseashta, Building Cyber Resilience against Hybrid Threats, *IOS Press* (2022)
[2] A. Vaseashta, NATO Science for Peace and Security Series - *E: Human and Societal Dynamics*, **154** (2021), 1-18
[3] H. Thorisson, F. Baiardi, D.G. Angeler, K. Taveter, A. Vasheasta, P.D. Rowe, W. Piotrowicz, T.L. Polmateer, J.H. Lambert, I. Linkov, *NATO Science for Peace and Security Series - D: Information and Communication Security,* **55** (2019), 13-16
[4] N. Bölgen, D. Demir, M. Aşık, B. Sakım, A. Vaseashta. *Introduction and Fundamentals of Electrospinning. Electrospun Nanofibers, Springer, Cham* (2022)
[5] N. Ashammakhi, N. *Electrospinning and Three-Dimensional (3D) Printing for Biofabrication. Electrospun Nanofibers. Springer, Cham* (2022), 555-604
[6] YZ. Long, J. Zhang, Z. Liu, BC. Wang, M. Yu, S. Ramakrishna, *Application of Hand-Held Electrospinning Devices in Medicine, Electrospun Nanofibers. Springer, Cham* (2022), 605-630

SPATIALLY RESOLVED CONDUCTIVITY IN TYPE-II SUPERCONDUCTORS

D.M. Evans*
Department of Physics, University of Warwick, Coventry, UK
*E-mail: donald.evans@warwick.ac.uk

Quantum materials, such as superconductors, are exciting from both fundamental and technological perspectives. Superconductors are defined by their zero-electrical resistivity, typically established using four-probe characterization methods like the van der Pauw method. However, such four-probe measurements assume and require electronic homogeneity to derive their physical meaning. Thus, homogeneous electrical conductivity is an implicit assumption in superconductor research.

In this presentation, we demonstrate the limitations of this assumption using two iron-based superconductors, $RbFe_{2+y}Se_{2+x}$ and Fe(Se,Te), as template materials. We show that even when bulk characterization suggests high-quality homogeneous conductivity, direct spatially resolved measurements reveal that the crystals are electrically heterogeneous. This is illustrated by the macroscopic resistance data and corresponding low-temperature conducting atomic force microscopy (cAFM) data in Figure 1. In both template systems, cAFM provides exciting new insights into the materials. For instance, in $RbFe_{2+y}Se_{2+x}$, the local superconducting transition occurs at a much higher temperature than expected, as illustrated in Figure 1. Meanwhile, in Fe(Se,Te), areas with enhanced conductivity below the superconducting transition exhibit a composition close to $FeSeTe_2$, while the majority insulating phase corresponds to the previously accepted target composition, $FeSe_{0.4}Te_{0.6}$. In Fe(Se,Te), we also observe metastable conductivity above the macroscopic transition, consistent with preformed Cooper pairs, as expected at the crossover from Bardeen-Cooper-Schrieffer (BCS) superconductivity to Bose-Einstein condensation (BEC). Our work underscores the importance of direct measurements of quantum properties and highlights the urgent need for more direct tests of the homogeneity of conductivity in type-II superconductors.

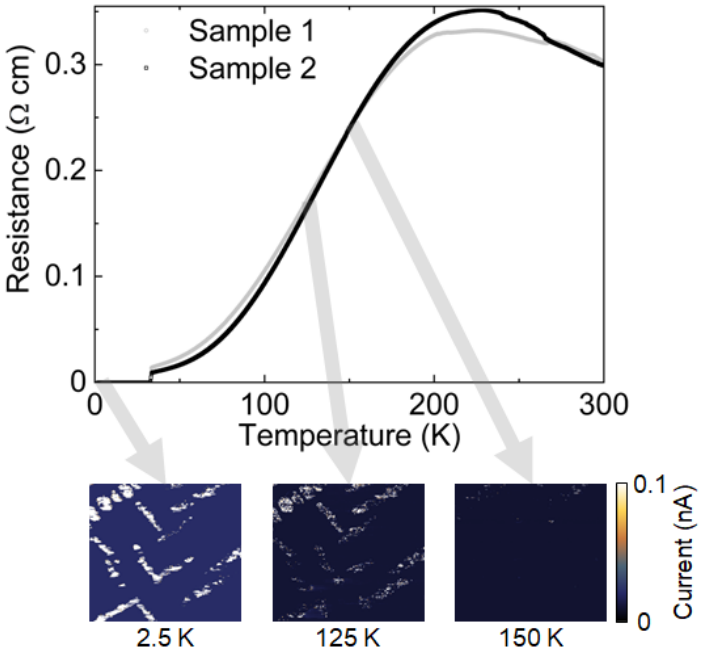

Figure 1. Four-probe resistivity measurements of $RbFe_2Se_2$ and cAFM measurements at different temperatures. In the cAFM images, the white areas are areas of enhanced conductivity while dark areas have no registered currents, indicating highly heterogeneous conductivity within the 10 x 10 µm scan area. This enhanced local conductivity persists well above T_c.

MAGNETIC DOMAIN TOMOGRAPHY

R. Schäfer*
Leibniz Institute for Solid State and Materials Research (IFW), Dresden, Germany
*E-mail: r.schaefer@ifw-dresden.de

Magnetic domains are the elements of the microstructure of magnetic materials that link the fundamental physical properties of a material with its macroscopic properties and applications at a mesoscopic level [1]. Any analysis of magnetization curves, which are primarily measured to characterize magnetic materials, requires an understanding of the underlying domains. While domain analysis in magnetic films, for which all relevant domains can be visualised using numerous experimental methods, is relatively simple, this is not true anymore for massive, non-transparent specimens, which possess the most complex domain patterns. Most imaging techniques have limited information depth, only showing the surface domains that are often significantly different from the bulk domains. Simply cleaving the sample to capture the entire domain pattern would be useless, as the domains would immediately adapt to the new surface. Therefore, in the past, domain analysis on bulk materials was performed by observing surface domains and using arguments from domain theory to infer the internal domains.

In recent years, however, there was impressive progress in the development of magnetic tomography, which has the potential to reveal the entire domain structure. In this presentation those methods, which include soft x-ray spectromicroscopy, hard x-ray tomography, electron holography, and neutron dark-field microscopy, will be reviewed. The focus is on Libovicky tomography [2], which can be used to reveal the true 3D structure of characteristic patterns in ironlike material.

[1] A. Hubert, R. Schäfer: Magnetic Domains. Springer (1998).
[2] R. Schäfer, S. Schinnerling: Phys. Rev. B 101, 214430 (2020)

CHARACTERIZATION OF METALLIC FOAMS AND THE VARIETY OF THEIR APPLICATIONS AS A SUBSTRATE IN ELECTROCHEMICAL TECHNOLOGIES

Henrikas Cesiulis*
Vilnius University, Faculty of Chemistry and Geosciences, Vilnius, Lithuania
*E-mail: henrikas.cesiulis@chf.vu.lt

Due to its porous structure, research on metallic foam is a popular topic due to its diverse industrial applications and unique properties. There are two types of metallic foams: closed cells and open cells foams. Closed-cell foams provide good mechanical properties but do not allow access to their internal surface, whereas open porosity is generally required for functions associated with the material's interior and is mostly used in applications where load-bearing capability is not the primary goal. The important characteristic of foams is an electrochemically active area (EAA). It can be determined by electrochemical impedance spectroscopy. It was shown that EAA depends on the limiting stage of the process occurring on the electrode. It was determined to be 7–14 times higher than that for the flat electrode, whereas charge transfer resistance on the Cu foam electrode is 1.5–1.7 times lower than that on the flat electrode: mass transfer and deposition rate is up to 3 times higher on the foam surface in comparison with a flat surface. The applicability of Cu-foam electrodes for electrowinning of based metals from the leachate of electronic waste in citric solutions and supports for electrodes used in electrocatalytic processes such as methanol oxidation will be discussed. In addition, the applicability of metallic foams including bimetallic as electrodes for supercapacitors, hydrogen, and oxygen electrochemical evolution reactions will be widely discussed.

ACKNOWLEDGMENTS: This work was partially financed from the MSCA grant №778357- SMARTELECTRODES, Research Council of Lithuania grant No. P-MIP-24-676, MSCA4Ukraine program grant No. 1233494.

SUPERCONDUCTOR 3D NANOARCHITECTURES

V.M. Fomin[1,2,*]
[1]*Institute for Emerging Electronic Technologies, Leibniz Institute for Solid State and Materials Research (IFW) Dresden, Dresden, Germany;*
[2]*Faculty of Physics and Engineering, Moldova State University, Chişinău, Republic of Moldova*
[*]E-mail: v.fomin@ifw-dresden.de

Superconductor 3D nanoarchitectures are a subject of a vigorous theoretical and experimental studies [1] as a playground for novel fascinating fundamental superconducting properties and their highly prospective applications in nanoelectronics and optoelectronics, quantum optics and quantum information processing [2]. In 3D superconductor nanoarchitectures, a topological transition between the vortex and phase-slip regimes determines the magnetic-field–voltage and current–voltage characteristics revealing a nontrivial topology of superconducting screening currents. An abrupt switch-on of the transport current triggers the transition from the vortex- to phase-slip-regime in superconductor open nanotubes [3]. Various dynamic topological transitions in superconductor open nanotubes take place under a combined dc+ac transport current [4].

Relying upon the time-dependent Ginzburg-Landau equation, it is found that vortex chains, vortex jets, and phase-slip regimes occur in superconductor open nanotubes due to the inhomogeneity of the normal magnetic field component. Distinct from planar thin films, the vortex jets are constrained within the half-tubes and correlate strongly between them. At lower magnetic fields, vortices follow the same path within the half-tubes, forming single vortex chains. At higher magnetic fields, the vortex trajectories undergo multifurcations, giving rise to patterns composed of vortex jets consisting of two or more vortex chains. Due to a stronger confinement of single vortex chains in tubes of small radii, jumps in the average voltage and frequency of microwave generation are unveiled, which occur when the number of fluxons moving in the half-tubes increases by one [5]. The peaks in the induced voltage and jumps in the microwave generation frequency as a function of the applied magnetic field are predicted for nanotubes of rather small radii pointing to the decisive role of the interaction of vortices in the both half-tubes for the correlated vortex dynamics. Effective steering of vortex chains and jets is realized by tilting the magnetic field in the plane perpendicular to the nanotube axis, with a jet-to-chain transition unseen for planar constrictions [6]. In addition to prospects for the tuning of GHz-frequency spectra and the steering of vortices as information bits, the discussed findings lay the foundation for on-demand tuning of vortex arrangements in superconductor 3D nanoarchitectures in tilted magnetic fields. By introducing a lattice of asymmetric pinning sites along the preferred vortex paths, a non-reciprocal flux transport exhibits a vortex ratchet effect is realized, which is revealed to be twice stronger than in the respective planar membranes. It is attributed to the inhomogeneous-field-induced vortex channeling through the areas containing the asymmetric pinning sites [7].

ACKNOWLEDGEMENTS: I am grateful to I. A. Bogush, R. Córdoba, R. H. de Bragança, O. V. Dobrovolskiy, and R. O. Rezaev for fruitful collaborations. The study was supported by the E-COST via Action #CA21144 “SuperQuMap”.

[1] R. Córdoba, V. M. Fomin. *Appl. Phys. Lett.* **124** (2024) 170501.
[2] V. M. Fomin, O. V. Dobrovolskiy. *Appl. Phys. Lett*. **120** (2022), 090501.
[3] I. Bogush, V. M. Fomin. *Phys. Rev. B* **105** (2022) 094511.
[4] V. M. Fomin, R. O. Rezaev, O. V. Dobrovolskiy. *Scientific Reports* **12** (2022) 10069.
[5] I. Bogush, O. V. Dobrovolskiy, V. M. Fomin. *Phys. Rev. B* **109** (2024) 104516.
[6] I. Bogush, V. M. Fomin, O. V. Dobrovolskiy. *Nanomaterials* **14** (2024) 420.
[7] R. H. de Bragança, I. Bogush, O. V. Dobrovolskiy, V. M. Fomin. https://arxiv.org/abs/2407.20780 (2024).

ATTRACTIVE VORTEX-VORTEX INTERACTION IN LOW-κ SUPERCONDUCTORS

P. Miranović[1,*]
[1]*Faculty of Natural Sciences and Mathematics, University of Montenegro, Podgorica, Montenegro*
[*]E-mail: pedjam@ucg.ac.me

Type II superconductors whose Ginzburg-Landau parameter is close to the limiting value of $1/\sqrt{2}$ experience unusual thermodynamic properties when transitioning from the Meissner state to the mixed state [1]. It is believed that the reason for such behavior is the attractive interaction between the vortices. In order to investigate more deeply the nature of the interaction between vortices in low-κ superconductors, a generalized London model was developed that is valid in low magnetic fields. However, the attractive inter-vortex force is shown to be elusive within the simple picture of pairwise inter-vortex interactions. That's why we started a numerical investigation of the stability of the hexagonal vortex lattice, a structure that is most stable when the inter-vortex interaction is repulsive. It is shown that equilibrium vortex lattice structure undergoes structural phase transition from hexagonal one in high magnetic field to vortex chains in low fields. Structural transformation of vortex lattice is macroscopic manifestation of attractive vortex-vortex interaction in low-k superconductors.

[1] P. Miranović and K. Machida, Phys. Rev. B **67**, 092506 (2003).

KEY PROGRESSES OF SOLUTION BASED KESTERITE SOLAR CELLS

E. Saucedo*
Universitat Politècnica de Catalunya, Barcelona, Spain.
*E-mail: edgardo.saucedo@upc.edu

The synthesis of multinary semiconductors for solar energy conversion applications such as kesterite ($Cu_2ZnSn(S,Se)_4$, CZTSSe) is extremely challenging due to the complexity of this type of compounds. In particular, quaternary kesterite-type compounds are not the exception, and all these detrimental issues explain why during almost 10 years the world record efficiency was unchanged. But the very recent development of molecular inks route with special precursors, allows the accurate control of single kesterite phase with high crystalline quality, contributing to increase the conversion efficiency record of kesterite based solar cells up to 15% in a short time.

This presentation will be focused first in demonstrating how the molecular inks synthesis route was of key relevance for the control of high-quality single phase kesterite, through the modification of the synthesis mechanisms. The relevance of the composition of the ink, the precursor salts, and the interaction between the solvent and the cations in the solution is key for a reliable and reproducible high efficiency kesterite production baseline. Then, diluted alloying/doping strategies will be presented including Cu, Zn and Sn partial substitution with elements such as Ag, Li, Cd or Ge. The positive impact of these cation substitutions will be discussed in regards of their impact on the kesterite quality, as well as on the annihilation of detrimental punctual defects, allowing for new efficiency records at 15% level.

Finally, very recent, and innovative interface passivation strategies will be discussed, showing the pathway to increase the record efficiency beyond 20%.

DEFINITION OF AN UPSCALED KESTERITE (CZTSe) TECHNOLOGY PLATFORM

A. Pérez-Rodríguez[1,2,*], Pedro Vidal-Fuentes[1], J. Andrade-Arvizu[1], D. Payno[1], R. Fonoll[1], M. Guc[1], V. Izquierdo-Roca[1]
[1]*IREC: Catalonia Institute for Energy Research, Barcelona, Spain;*
[2]*Department of Electronic and Biomedical Engineering, University of Barcelona, Barcelona, Spain*
[*]E-mail: aperezr@irec.cat

The development of a novel PV technology is pointless without aiming for its scale-up and the feasibility of its industrialization and commercialization, especially in the frame of EU's transition towards electrification. The current efficiency level of the kesterite technology (15%) is already compatible with innovative integrated PV applications (IoT, BIPV, PIPV, VIPV...) in which high efficiencies are not required, and the target is placed in features that Si cannot offer such as a high degree of customizability, flexibility, high power to weight ratio, low energy payback time and lifetimes adapted to the lifetime of products. In this context, efforts must be made in this direction, going beyond improving "pixel efficiency" and tackling the rest of the critical factors for the industrialization of the kesterite technology such as large area homogeneity and reproducibility using scalable and industrially compatible fabrication processes.

This work reviews the 10 x 10 cm^2 kesterite technology platform that has been defined at IREC for the systematic upscaling of a $Cu_2ZnSnSe_4$ (CZTSe) PV technology. The goal is the demonstration of a 10% pixel device efficiency on up-scaled 10x10 cm^2 flexible substrates with very high process and device uniformity (i.e. relative dispersion of optoelectronic pixel parameters below 10%). The platform is based on a sequential sputtering /reactive annealing process that has allowed demonstration of a 11.9% record device efficiency at cell level [1]. To achieve the proposed goal a systematic methodology has been defined that implies a rigorous standardization and optimization of the different fabrication processes, identifying the main sources of device and process inhomogeneities through the application of high statistic studies and the application of advanced data analysis using Artificial Intelligence (AI) approaches. This goes hand in hand with the development of rigorous PV device fabrication protocols and with the implementation of automated process monitoring inspection platform. This development has enabled assessing the bottlenecks that limit the lab-to-industry adaptation of the CZTSe PV device fabrication process, which are related mainly to the spatial inhomogeneity of the buffer and window deposition processes as well as to equipment stability and operation protocols. The identification of the physico-chemical origin of the main performance loss mechanisms enables the definition of quality control indicators that allow the development of strategies for their mitigation towards the progress of the scale-up of the Kesterite technology, laying the foundations for its future industrialization.

[1] S. Giraldo et al., Energy & Environmental Science **11** (2018), 582-593

MAGNETIC LIGHTNING IN SUPERCONDUCTING FILMS

A. V. Silhanek*
Experimental Physics of Nanostructured Materials, Physics Department, Université de Liège, Liège, Belgium
*E-mail: asilhanek@uliege.be

Magnetic flux lines in superconductors are topologically protected quantum objects which can be deformed when moving at very high velocities. These extreme conditions can be transitorily realised when superconductors undergo a thermomagnetic instability, for which the sample geometry and topology also come into play [1]. In this work, we explore the complex pattern of magnetic field penetration and identify its impact on the resonance frequency of NbTiN and Nb superconducting resonators by combining magneto-optical imaging (Figure 1) and high-frequency measurements [2]. We will also discuss the possibility of improving the performance of superconducting films by introducing periodic surface structures employing a femtosecond UV laser irradiation [3].

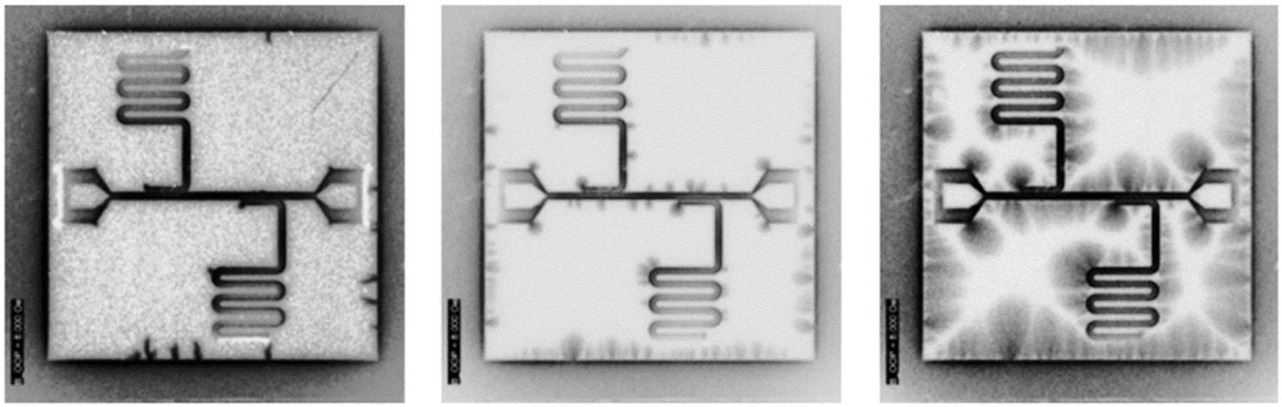

Figure 1. Magneto-optical image of a planar NbTiN superconducting resonator at three different temperatures (lowest to the left, highest to the right) after applying an out-of-plane magnetic field in zero-field-cooling conditions.

[1] S. Blanco Alvarez, J. Brisbois, S. Melinte, R. B. G. Kramer and A.V. Silhanek. *Sci. Rep.* **9** (2019) 3659.
[2] L. Nulens, N. Lejeune, J. Caeyers, S. Marinković, I. Cools, H. Dausy, S. Basov, B. Raes, M. J. Van Bael, A. Geresdi, A. V. Silhanek, J. Van de Vondel. *Communications Physics* **6** (2023) 267.
[3] A. Badía-Majós, E. Martínez, L. A. Angurel, G. F. de la Fuente, E. Fourneau, S. Marinković, A. V. Silhanek. *Applied Surface Science* **649** (2023) 159164; E. Martínez, N. Lejeune, *et al.* (unpublished)

VORTEX COUNTING AND VELOCIMETRY BASED ON SLITTED SUPERCONDUCTING MICROBRIDGES

O. Dobrovolskiy*
Cryogenic Quantum Electronics, EMG and LENA, Technische Universität Braunschweig, Germany
*E-mail: oleksandr.dobrovolskiy@tu-braunschweig.de

The maximal speed $v*$ for magnetic flux quanta is determined by the energy relaxation of unpaired electrons and is thus essential for superconducting microstrip single-photon detectors (SMSPDs). However, the deduction of $v*$ from the current-voltage (*I*-*V*) curves at zero magnetic field is hindered by the unknown number of vortices, *n*, as a small number of fast-moving vortices can induce the same voltage as a large number of slow-moving ones.

In my talk I will introduce an approach for the quantitative determination of *n* and $v*$. The idea is based on the Aslamazov and Larkin prediction of kinks in the *I*-*V* curves of wide and short superconducting constrictions when the number of fluxons crossing the constriction is increased by one. We realized such conditions in wide MoSi thin strips with slits milled by a focused ion beam and revealed quantum effects in a macroscopic system [1]. By observing kinks in the *I*-*V* curves with increase of the transport current, we evidenced a crossover from a single- to multifluxon dynamics and deduced $v*$ of about 12 km/s. Our experimental observations are augmented with numerical modeling results, which reveal a transition from a vortex chain over a vortex jet to a vortex river with increase of *n* and *v*. Overall, our findings are essential for the development of one-dimensional and two-dimensional few-fluxon devices and provide a demanded approach for the deduction of maximal vortex velocities at the SMSPD operation conditions.

[1] V. M. Bevz *et al*, *Phys. Rev. Appl.* **19** (2023) 034098.

NON-INVASIVE PROBING OF SUPERCONDUCTING NANOSTRUCTURES

J.Van de Vondel*
Quantum Solid-State Physics, Department of Physics and Astronomy, KU Leuven, Leuven, Belgium
*E-mail: joris.vandevondel@kuleuven.be

Understanding the dynamics of phase slips, topological fluctuations of the superconducting order parameter, in superconducting loops is very important for the development of future nanodevices. These loops show tremendous potential as building blocks for superconducting qubits [1], could be used for memory devices with topological protection [2], and determine the observed critical current profile in Superconducting Quantum Interference Devices (SQUIDs). Understanding these phase slips necessitates the capability to probe the number of flux quanta and determine the kinetic inductance associated with the Cooper pair density in such structures. Here we utilize a niobium resonator as a non-invasive probe capable of exploring the superconducting properties of an aluminum loop positioned close to the resonator. By locally applying a magnetic field, adjusting the temperature, and modifying the loop dimensions using focused ion beam milling, we induce changes in the kinetic inductance of the loop, which are directly manifested in the resonance frequency [3]. This approach highlights the promise of our proof-of-principle spectroscopy device as a tool for exploring the local Cooper pair density within inductively coupled superconducting nanostructures. Moreover, it provides an effective platform for manipulating and detecting phase slips, offering insights into the dynamics of these quantum phenomena.

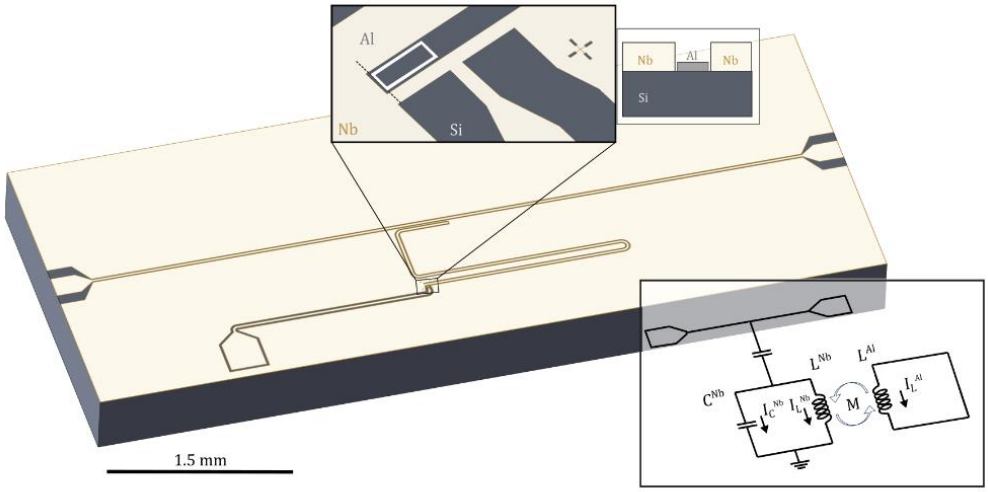

Figure 1. Schematic representation of the device, comprised of a λ/4 resonator capacitively coupled to the central feedline. The circuit diagram representation of the resonator-loop system is provided in the bottom inset.

[1] JE Mooij and CJPM Harmans. New Journal of Physics 7, 219 (2005).
[2] N. Ligato et al., Nat. Commun. 12, 5200 (2021).
[3] L. Nulens et al., (unpublished).

UNLOCKING THE POWER OF ELECTROSPARK ALLOYING AND ELECTROCHEMICAL METHODS FOR SHAPING INNOVATIVE MATERIALS

N. Tsyntsaru[1,2,*]
[1]*Laboratory of Electrophysical and Electrochemical Treatment of Materials Boris Lazarenko, Institute of Applied Physics, Moldova State University, Chișinău, Republic of Moldova;*
[2]*Faculty of Chemistry, Vilnius University, Vilnius, Lithuania*
[*]E-mail: ashra_nt@yahoo.com

Among various surface modification technologies, such as physical vapor deposition, magnetron plasma sputtering, plasma-electrolytic saturation of the surface, etc., electrospark alloying (ESA) or electrospark deposition (ESD) conquers a distinct place due to the following advantages: (1) a wide range of materials which can be used as alloying elements and the possibility to obtain multicomponent coatings and control their properties; (2) strong metallurgical bonds between the modified surface and the substrate; (3) high corrosion and wear resistance of obtained materials. This method is based on transferring anode material to the treated surface by spark discharges in various environments: air, inert gas, dielectric liquid, etc., and vacuum.

The electrospark alloying method was developed by Lazarenko and has been known since 1964 [1], but it has been recognized worldwide as a 21st-century technology. Many researchers have pointed out that this low-heat-input process has great potential for coating applications and the restoration of damaged high-value parts (e.g. [2]).

On the other hand, electrochemical methods are used to synthesise a large number of compounds and materials with versatile applications. The shape, size, and dimensions of the material can be easily controlled by using either template-assisted or template-free electrochemical methods. Some advantages of electrochemical synthesis are (1) a large redox potential range accessible by selecting an appropriate combination of electrode materials, solvents, and supporting electrolytes. (2) precise control over materials composition and current efficiency due to precise choice of potential and current, (3) deposition in deep recesses.

Moreover, nowadays, growing consideration is set on sustainability, characterised by viable changes that enable foreseeing future needs and adjusting them to the present necessities [3]. Sustainability aspects are rising in different branches of materials science too. Thus, there is an increased amount of research focused on the fabrication of advanced materials based on earth-abundant metals (iron, nickel and cobalt), especially for catalytic applications. Moreover, the role of iron and its compounds is significant because iron is the second earth-abundant metal on our planet. They can be found in various applications, but certainly, magnetic, and catalytic properties of iron-based advanced materials are acknowledged foremost.

This presentation is dedicated to celebrating 60 years of establishing the Institute of Applied Physics and will overview the experience gained in obtaining new and advanced materials.

ACKNOWLEDGMENTS. The author gratefully acknowledges the colleagues' contribution and support from MSCA grant №778357- SMARTELECTRODES, the Moldavian National project ANCD project 011204, and the Research Council of Lithuania grant No. P-MIP-24-676.

[1] B.R. Lazarenko, N.I. Lazarenko. Electrospark Machining of Metals; US Cons Bureau: New York, NY, USA, 1964
[2] G. Renna, P. Leo, G. Casalino, E. Cerri. Repairing 2024 Aluminum Alloy via Electrospark Deposition Process: A Feasibility Study. *Adv. Mater. Sci. Eng.* 2018, 8563054.
[3] Our Common Future, Chapter 2: Towards Sustainable Development. UN Documents Gathering a body of global agreements. Available from: http://www.un-documents.net/ocf-02.htm

PULSED LASER DEPOSITION OF HIGH ENTROPY ALLOY THIN FILMS: TAILORING PROPERTIES BY GAS PAHSE PLASMA CHMEISTRY

S. A. Irimiciuc[1,2,*], S. Cichoň[2], P. Hruška[2], S. Vatavu[3], V. Craciun[1,4], J. Lancok[2]
[1]*National Institute for Laser, Plasma and Radiation Physics – NILPRP, Bucharest, Romania;*
[2]*Institute of Physics of the Czech Academy of Sciences, Prague, Czech Republic;*
[3]*Moldova State University, Chișinău, Republic of Moldova;*
[4]*Extreme Light Infrastructure – Nuclear Physics, Horia Hulubei National Institute of Physics and Nuclear Engineering, Magurele, Romania*
[*]E-mail: irimiciuc@fzu.cz

High Entropy Alloys (HEAs) define a new and exciting class of materials that have gradually been introduced as solution for wide range of applications over the past few decades. HEAs are characterized by the presence of multiple principal elements in roughly equal proportions and are defined by sluggish diffusion, lattice distortions and cocktail effects. They represent a key point in the involvement of machine learning algorithms and AI in the development of new materials. The unique composition gives HEAs their name, as they exhibit a high degree of configurational entropy due to the large number of elements in the alloy.

The proposed approach aims to produce complex films based on HfNbTaTiZr, as microwave (MW) and IR absorbers. This technological pursuit is particularly crucial in the context of a rapidly evolving environment characterized by the exponential growth in computational power and the emergence of AI-controlled systems, defining the era of the 4th Industrial Revolution or Industry 4.0.

HEAs coating were produced by pulsed laser ablation using a Nd: YAG laser operated at 266 nm on FuSi and MgO (100) substrates. The films were prepared under diverse experimental conditions: substrate temperature variations (up to 700°C), working atmospheres (Ar, N and O2 atmospheres up to 20 Pa), at a constant fluence of 3.7 J/cm2. The production of the HEA films was monitored in situ by optical emission spectroscopy to analyze the composition of the plasma and the fluctuations that can appear during deposition. The use of OES for deposition revealed a complex plasma with back body radiation from heated nanoparticle and clusters and specific emission from all the elements composing the target.

The deposited films were investigated using several surface analysis techniques such as Atomic Force Microscopy (AFM), Scanning Electron Microscopy (SEM), X-ray Diffraction (XRD), X-ray Photoelectron Spectroscopy (XPS) and electrical measurements. Finally, an optimization procedure was developed to corelate the deposition conditions with the physical properties of the films

ACKNOWLEDGEMENTS: This research is supported by the NATO Science for Peace and Security program through SPS G6153 Project.

CHARACTERIZATION OF LATTICE DEFECTS IN HIGH-ENTROPY ALLOY THIN FILMS BY POSITRON ANNIHILATION SPECTROSCOPY

P. Hruška[1,*], S. Cichoň[1], S. A. Irimiciuc[1], F. Lukáč[2], J. Lančok[1]
[1]*Institute of Physics of the Czech Academy of Sciences, Prague, Czech Republic;*
[2]*Institute of Plasma Physics of the Czech Academy of Sciences, Prague, Czech Republic;*
[*]E-mail: hruskap@fzu.cz

High-entropy alloys (HEAs) represent an exciting novel category of materials that have garnered significant attention due to their unique structure and promising, yet relatively unexplored, potential. Characterized by multiple principal elements, HEAs exhibit local lattice distortions arising from the varying atomic sizes of elements randomly occupying lattice sites. These distortions lead to a broad distribution of interstitial open volumes. HEAs are intensively studied for their design flexibility and superior properties, including excellent mechanical strength, corrosion and oxidation resistance, electrical and superconductive properties, hydrogen absorption capacity, and irradiation resistance. HEA films, typically deposited via magnetron sputtering or pulsed laser deposition, offer tunable microstructures, ranging from amorphous films to multi-phase nanocrystalline and single-phase polycrystalline films.

Positron annihilation spectroscopy (PAS) is a versatile method for characterizing open-volume lattice defects [1]. Two complementary PAS techniques can be used: (1) Positron lifetime spectroscopy, a well-established non-destructive technique, identifies defects and evaluates their concentrations, and (2) coincidence Doppler broadening spectroscopy, which provides insights into the local chemical environment of defects. Utilizing slow positron beams with variable energy allows for depth-resolved defect analysis in thin films. In our previous studies [2], we successfully demonstrated the critical role of defect characterization in HfNbTaTiZr films, establishing a link between defect structures and their oxidation behavior. We will present our recent results, offering the latest insights into defect characterization in HEA films using advanced positron annihilation spectroscopy techniques.

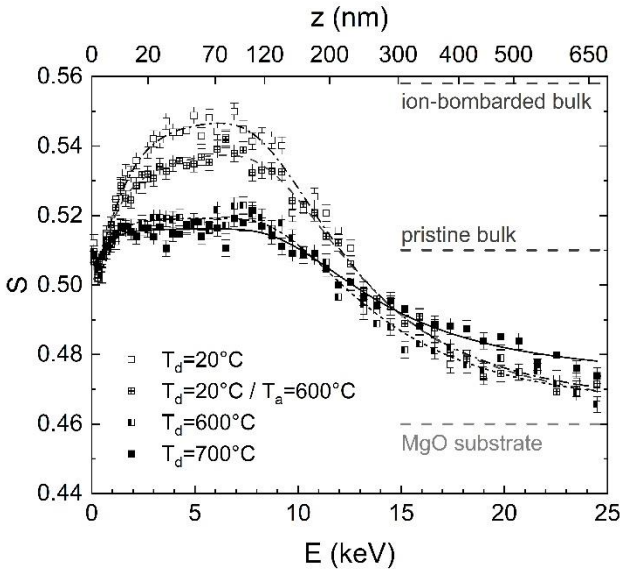

Figure 1. Doppler broadening S parameters as a function of incident positron energy for HfNbTaTiZr films: (a) films deposited at room temperature (RT), 600°C, and 700°C, as well as films deposited at RT and subsequently annealed at 600°C. The corresponding mean positron implantation depth in the HfNbTaTiZr alloy is indicated on the top axis.

[1] J. Čížek, *J. Mater. Sci. Technol.* **34** (2018) 577-598.
[2] P. Hruška, F. Lukáč, S. Cichoň, et al., *J. Alloys Compds.* **862** (2021) 157978.

KEYNOTE LECTURES

COLLECTIVE AND NONLINEAR EXCITATIONS OF SUPERFLUID FERMI GASES

S.N. Klimin*, J. Tempere
TQC, Universiteit Antwerpen, Universiteitsplein 1, Antwerp, Belgium
*E-mail: sergei.klimin@uantwerpen.be

This talk provides a review of our recent research on the collective and nonlinear excitations in neutral and charged fermionic superfluids. We analyze theoretical predictions obtained through different methods, focusing mainly on the finite-temperature effective field theory [1, 2] and the Gaussian pair-and-density fluctuation approximation [3-5].

We explore nonlinear excitations in superfluid Fermi gases, such as soliton and vortex solutions, derived from effective field theory. We also discuss recent advancements in both the Gaussian fluctuation method and the effective field theory and examine the similarity and difference of these approximations, as well as their relation to other approaches and verification by advanced numeric methods.

Additionally, we investigate the spectra of collective excitations in superconducting and superfluid systems across different dimensionalities within the BCS-BEC crossover regime. Special attention is given to the interactions between different branches of collective excitations and their observable manifestations. The study is based on the Gaussian fluctuation method for the effective bosonic action within the path-integral formalism, unified for both neutral and charged superfluid Fermi gases.

[1] S. N. Klimin, J. Tempere, G. Lombardi and J. T. Devreese. *Eur. Phys. Journal B* **88** (2015) 122.
[2] S. N. Klimin, J. Tempere, and J. T. Devreese. *Phys. Rev. A* **90** (2014) 053613.
[3] H. Kurkjian, S. N. Klimin, J. Tempere, and Y. Castin. *Phys. Rev. Lett.* **122** (2019) 093403.
[4] T. Repplinger, S. Klimin, M. Gélédan, J. Tempere, H. Kurkjian. *Phys. Rev. B* **107** (2023) 014504.
[5] S. N. Klimin, J. Tempere, T. Repplinger, and H. Kurkjian. *New J. Phys.* **25** (2023) 063011.

ENTROPY PRODUCTION AND QUANTUM CORRELATIONS OF TWO COUPLED BOSONIC MODES IN A THERMAL ENVIRONMENT

T. Mihaescu, A. Isar*
National Institute of Physics and Nuclear Engineering, Bucharest-Magurele, Romania
*E-mail: isar@theory.nipne.ro

The Markovian time evolution of the entropy production rate as an indicator of the irreversibility, in comparison with the correlations like Rényi-2 mutual information, Rényi-2 quantum discord and entanglement is studied, in a bipartite quantum system consisting of two coupled bosonic modes embedded in a common thermal environment. The dynamics of the system is described in the framework of the theory of open systems based on completely positive quantum dynamical semigroups, for initial two-mode squeezed thermal states, squeezed vacuum states and coherent states. We show that the rate of the entropy production and the considered correlations in the non-equilibrium stationary state, as well as the time evolution of the rate of entropy production and of the correlations, strongly depend on the parameters of the initial Gaussian state (squeezing parameter and average thermal photon numbers), frequencies of the modes, the parameters characterising the thermal reservoir (temperature and dissipation rate) and the coupling between the two bosonic modes [1,2].

[1] T. Mihaescu, A. Isar, Entropy **24** (2022) 696.
[2] T. Mihaescu, A. Isar, European Physical Journal Plus **139** (2024) 82.

MODELING OF PROTON TRANSFER COUPLED SPIN TRANSITION IN THE HL-Cl([Fe(HL-Cl)$_2$])(AsF$_6$)$_2$ COMPOUND

S.I. Klokishner*, O.S. Reu
Institute of Applied Physics, Moldova State University, Chișinău, Republic of Moldova
*E-mail: klokishner@yahoo.com

Traditionally the phenomenon of spin crossover i.e. the transition between the low- and high-spin states of transition metal ions with the electronic configuration d^4-d^7 is observed under action of external stimuli such as temperature, pressure and light. Recently a new trend in the field of spin transitions has been reported that is represented by iron(II) molecular compounds exhibiting proton transfer coupled spin-transition (PCST) behavior [1]. The present communication focuses on the elucidation of the origin of the spin transformation caused by the proton transfer in the titled compound and explanation on this basis of its magnetic behavior. Since the proton lies on the nitrogen of hydrazone and pyridine moieties in the ligand in the high-spin and low-spin states of the iron(II) ion, respectively, the developed model takes into account the proton transfer between these two its positions. The electronic basis for a single molecule accounts for the *low-spin* $^1A_1$ and high spin $^5T_2$ states of the iron (II) ion and two different positions of the proton and, thus, includes 32 different states of the molecule. The cooperativity in the suggested model is assured by electron-deformational interaction and intermolecular dipole-dipole coupling because the PCST transition is accompanied by an appreciable elongation of the bonds between the iron ion and nearest nitrogen atoms as well as by the redistribution of the electron density inside the complex. The model takes into account the proton transfer between its two positions as well. The parameters of the cooperative interactions are estimated with the aid of temperature dependent structural data. The numerical value of the parameter characterizing the proton transfer between the hydrazine and pyridine moieties is obtained through DFT calculations (functional B3LYP, monoelectronic TZVP wavefuctions, ORCA package [2]). The problem of interacting molecules is solved within the mean field approximation. The suggested model captures the main features of the phenomenon and provides quite a good description of the temperature dependence of the χT product (Fig.1).

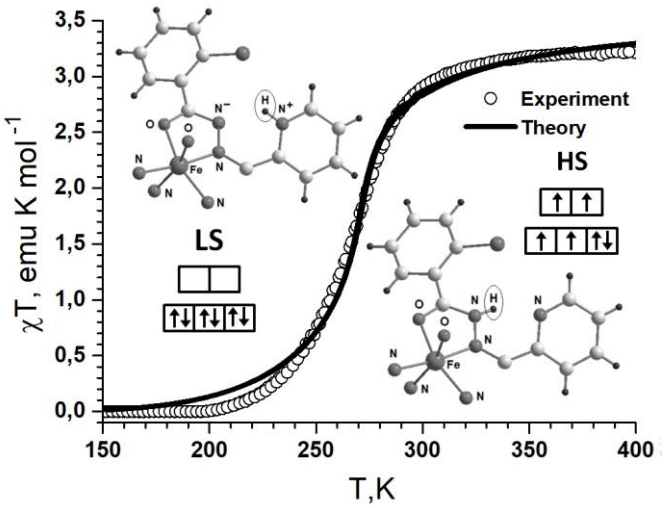

Figure 1. Temperature dependence of the χT product for the HL-Cl([Fe(HL-Cl)$_2$])(AsF$_6$)$_2$ compound (HL-Cl=N`-(di(pyridin-2-yl)-methylene)-2-chlorbenzohydrazide): circles– experimental data [1], solid line – calculated curve.

The theoretical χT curve reflects quite well the observed slow decrease in the temperature range 150-220K , the pronounced change of this product for 230-290 K and its slowdown in the growth at temperatures higher than 300K.

ACKNOWLEDGEMENTS: The authors are grateful to the Ministry of Education and Research of Moldova for financial support (project no. 011201).

[1] T. Nakanishi et al *J.Am.Chem.Soc.***141** (2019) 14384-14393.
[2] F. Neese, Software update: the ORCA program system, version 4.0. WIREs Comput. Mol. Sci. **8**, (2018), e1327.

A PARAMETRIC ANOMALY ASSOCIATED WITH NEGATIVE REFRACTION OF ACOUSTIC WAVES IN THIN PLATES

S. Cojocaru*
Horia Hulubei National Institute for Physics and Nuclear Engineering, Magurele, Romania
*E-mail: scojocaru@theory.nipne.ro

Negative refraction is a key characteristic of acoustic metamaterials commonly designed as sub-wavelength-engineered periodic structures [1]. However, recently it has been found that the same phenomenon can be realized in thin homogeneous elastic plates by exploiting the known dispersion anomaly of the Rayleigh-Lamb modes [2]. The negative refraction of the propagating modes takes place on the side interface between plates when the material parameters of the two plates match certain conditions. To explore these conditions we analyze the variation of the Rayleigh-Lamb (RL) vibration spectrum of an isotropic layer based on the principle of parametric scaling, which allows us to overview the evolution of the RL spectrum in the full parametric space [3]. We find a previously unnoticed anomaly in the dependence of the RL spectrum on parameters (bulk velocities, thicknesses, elastic moduli etc.) of constituent materials. In particular, some of the RL modes would acquire a slower velocity when propagating through a faster material, i.e., having higher bulk velocities. It turns out that these modes are the same as those involved in the observed negative refraction phenomenon, the S1 and A2, due to their strongly anomalous dispersion with a negative group velocity at longer wavelengths. The location of the anomalous parametric dependence on these specific branches of the RL spectrum is at shorter wavelengths, beyond the zero-group velocity point. Our approach covering both dispersion and parametric space in a unified way allows us to demonstrate the correlated character of the two anomalies. We discuss possible applications of this theoretical finding.

[1] G. Aydın, S.E. San. Materials Science and Engineering B **305** (2024) 117384.
[2] F. Legrand, et al., Scientific Reports. 11 (2021) 23901.
[3] S. Cojocaru. Physics Letters A **483** (2023) 129066.

ON THE EQUILIBRIUM STATES OF MULTIPARAMETRIC THERMODYNAMIC SYSTEMS IN A SMALL VICINITY OF THE EQUILIBRIUM VALUES OF PARAMETERS

A.A. Barsuk, F. Paladi*
Department of Theoretical Physics and ePhysMCS Research Laboratory, Moldova State University, Chișinău, Republic of Moldova
*E-mail: fpaladi@yahoo.com

The dynamic behavior of thermodynamic systems described by several order and control parameters is studied in a small neighborhood of ordinary and bifurcation equilibrium values of the system parameters. Using the general methods of investigating the branching (bifurcations) of solutions for nonlinear equations, we performed an exhaustive analysis of the order parameters dependences on the control parameters in a small vicinity of the equilibrium values of parameters, including the stability analysis of the equilibrium states, and the asymptotic behavior of the order parameters dependences on the control parameters (bifurcation diagrams). One shall adopt the most convenient general form of the applied methods, because both the order and control parameters are significantly different for distinct physical systems, and the analyses of equilibrium states relevant, in particular, to the crystal-nucleation phenomena in supercooled liquids as well as protein crystallization by using these general results have been reported [1].

In contrast to thermodynamic systems described by one order parameter, the analysis of multidimensional dynamical systems becomes noticeably more complicated and requires a separate detailed consideration. Note, for example, that dynamical systems with several order parameters naturally arise in the analysis of the dynamic behavior of biological populations. Transition dynamics under the effect of thermal fluctuations is another application of the realistic case of Landau-type kinetic potential with two order parameters. We present a detailed analysis of the equilibrium states in a small neighborhood of ordinary and bifurcation equilibrium values of the system parameters. Asymptotic representations are derived for sensitivity formulae of the equilibrium values of parameters. Stability analyses of the equilibrium states for multidimensional dynamical systems depending on several parameters, e.g., the cases of Landau-type kinetic potential with two order and four control parameters and the Lotka-Volterra model, are examined [2]. Finally, we formulate several general conclusions without specifying functional dependencies describing thermodynamic systems.

Also, we have formulated the stability criteria for linear dynamical systems described by an autonomous system of linear differential equations with constant real coefficients in critical cases of the Lyapunov's theory of stability for both simple and multiple eigenvalues of the matrix of coefficients [3]. The proposed framework is not related to the construction of the Jordan canonical form of the matrix of coefficients, and uses only information about the order of matrix, rank of the corresponding λ-matrix, and the multiplicity of the corresponding eigenvalues to the critical cases. In order to avoid misinterpretation when obtaining the proposed stability criteria, we shall mention that the diagonal canonical form of the matrix of coefficients, i.e. the Smith normal form, and its Jordan canonical form are essentially used, and, thus, the proposed algebraic stability criteria and the classical criteria lead always to the same conclusions.

ACKNOWLEDGEMENTS: Authors gratefully acknowledge support provided by the National Agency for Research and Development and the Moldova State University through the grant number 20.80009.7007.05, and the Ministry of Education and Research of the Republic of Moldova through the grant number 011210.

[1] A. A. Barsuk, F. Paladi, Physica A **527** (2019) 121303-20.
[2] A. A. Barsuk, F. Paladi, Eur. Phys. J. B **95** (2022) 54-14.
[3] A. A. Barsuk, F. Paladi, Physica A **569** (2021) 125787-9.

EFFECTS OF LIGAND DEPROTONATION ON THE SPIN CROSSOVER IN Fe(II) COMPLEXES

S.M. Ostrovsky*, O.S. Reu, S.I. Klokishner*
Institute of Applied Physics, Moldova State University, Chișinău, Republic of Moldova
*E-mail: sm_ostrovsky@yahoo.com; klokishner@yahoo.com

A model based on the crystal field calculations has been developed to examine the effect of ligand deprotonation on the spin crossover behavior of Fe(II) compounds. Due to the observed pronounced changes in the magnetic characteristics of the iron(II) ion, the proton removal from the ligand in the second coordination sphere is modeled by the appearance of a negative charge on one of the neutral nitrogens in the nearest octahedral surrounding of the iron(II) ion thus changing significantly the crystal field acting on this ion and, respectively, the conditions for observation of the low spin ↔ high spin transition. Different symmetries of the nearest nitrogen surrounding of the iron(II) ion and different locations of the negative charge in this surrounding are examined in the frames of the suggested model. It is demonstrated that depending on the symmetry of the complex under examination and the distribution of the negative extra charge on the nitrogen ions, belonging to the first coordination sphere of the Fe(II) ion, removal of protons in the second coordination sphere can either prevent or facilitate the spin transition. The extra charge located on the ligand lying on the middle or long axis of the distorted octahedron with the iron ion in its center aggravates the spin transition. This result explains the experimental data on the $[Fe_4(H_nL_4)]^{(n)+}$(n=8,6,4) compounds [1], where the deprotonation of the terpyridine-like ligand suppresses the thermal spin crossover due to the appearance of a negative charge on more distant nitrogen atoms from the first coordination sphere. Contrary, it has been demonstrated that the reduction of the energy gap between the high spin and low spin configurations takes place for the perfect octahedral surrounding of the iron ion or low symmetry complexes with the extra charge placed on the ligand closest to this ion. In the case when only electrostatic interactions between the extra charge and electrons of the iron ion are accounted for, the configuration with this charge on the closest to iron(II) nitrogen is shown to be energetically unfavorable. The configuration with the perfect octahedral surrounding does not realize due to the Jahn-Teller effect. So, at first glance in this case the situation with the decrease of the energy gap between the high spin and low spin configurations, that facilitates the spin transition, does not occur. Noting that the position of the extra charge is determined not only by the electrostatic interaction with the metal ion but also by some interactions within the ligand as well, it is predicted that due to these interactions it becomes probable the case when the total energy of the complex with the extra charge on the closest to the iron nitrogen acquires the minimum value. In such type systems the effect of facilitation of the spin transition due to deprotonation may take place.

ACKNOWLEDGEMENTS: The authors are grateful to the Ministry of Education and Research of Moldova for financial support (project no. 011201).

[1] S. Dhers, A. Mondal, D. Aguilà, J. Ramírez, S. Vela, P. Dechambenoit, M. Rouzières, J.R. Nitschke, R. Clérac, J.-M. Lehn *J. Am. Chem. Soc.* **140** (2018) 8218-8227.

THERMAL TRANSPORT SUPPRESSION IN INDIUM OXIDE BY RATTLING ATOMS

A.I. Cocemasov*, V.I. Brinzari, D.L. Nika
Moldova State University, Chișinău, Republic of Moldova
*E-mail: kocemasov@live.ru

We report on a first-principles study of electron, phonon and thermal properties in cubic In_2O_3 with a diatomic defect composed of a Sn atom substituting the In atom at a b-site (Sn_b) and a Ga atom embedded in an internode corresponding to a nearest to the b-site structural vacancy (Ga_i). The introduction of Sn_b and Ga_i atoms leads to large local displacements of guest and host atoms in the vicinity of the Sn-Ga defect, resulting in a radical rearrangement of the electronic and phononic properties of the crystal. This is primarily reflected in the displacements of the Sn atom and its nearest neighbors from their initial positions. The latter forms a cage-like structure with 12 O and 12 In atoms surrounding the Sn-Ga pair. Density functional theory calculations within Quantum Espresso software [1-2] have revealed that both Ga and Sn atoms are located in interstitial positions when rather unexpectedly, the Sn atom appears in the role of a rattler. The redistribution of electron density inside this cage changes the neighboring interatomic "spring constants" accompanied by a bond weakening. As a result, significant modifications of phonon spectrum are occurred revealing the flattening of phonon branches with their spatial localization. Overall, the phonon spectrum of In_2O_3 with Sn-Ga defect is characterized by the reduced average group velocities of phonons, including those of acoustic type, and the presence of avoided-crossing features in the low energy range.

To get insight into the thermal properties of In_2O_3 with Sn_b-Ga_i we have calculated the phonon thermal conductivity κ_{ph} within the Peierls-Boltzmann transport equation and accounted for all possible three-phonon scattering channels [3]. The room temperature mean free paths (MFP) of phonons and phonon thermal conductivity ratio in the considered structures are shown in Figure 1.

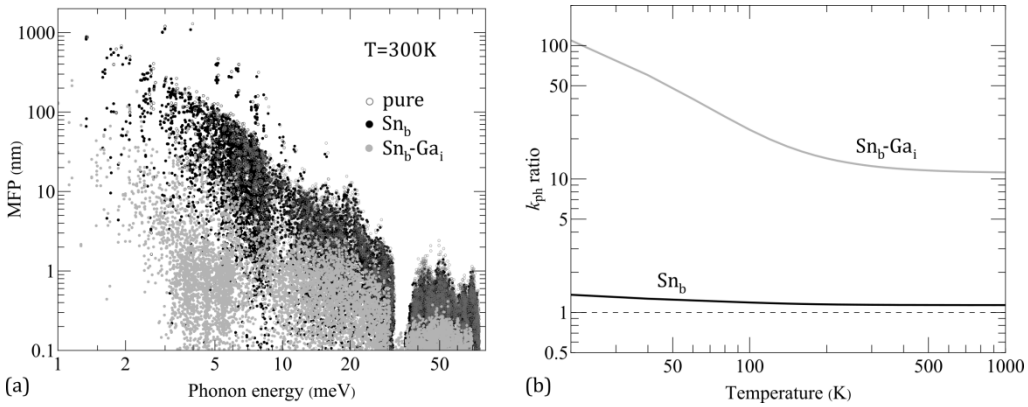

Figure 1. (a) Phonon mean free paths and (b) phonon thermal conductivity ratio in In_2O_3 with Sn_b defect and Sn_b-Ga_i defect relative to pure material.

Rattling vibrations strongly affect heat carrying capability of In_2O_3 with Sn_b-Ga_i point defect with ~12 times suppression of phonon thermal conductivity at room temperature in comparison with pure In_2O_3 [4]. The obtained theoretical results demonstrate the possibility of engineering the thermal conductivity in indium oxide-based compounds by Ga doping and may lead to their practical applications in thermoelectricity.

ACKNOWLEDGMENTS: The authors acknowledge financial support under the Moldovan Government research subprogram no. 011208.

[1] P. Gianozzi et al. *J. Phys.: Condens. Matter* **21** (2009) 395502.
[2] P. Gianozzi et al. *J. Phys.: Condens. Matter* **29** (2017) 465901.
[3] T. Tadano et al. *J. Phys.: Condens. Matter* **26** (2014) 225402.
[4] A. Cocemasov, V. Brinzari, D. Nika, *J. Phys.: Condens. Matter* **35** (2023) 195701.

MOTT TRANSITION OF EXCITONS TO ELECTRON-HOLE PLASMA STATE IN CdTe

A. Varzari*, A. A. Cliucanov, S. Vatavu
Faculty of Physics and Engineering, Moldova State University, Chisinau, Republic of Moldova
*E-mail: alexandru.varzari@usm.md

A theoretical analysis of radiative recombination in the exciton and impurity regions in CdTe was carried out, along with a comparative analysis of experimental photoluminescence (PL) data in CdTe thin films. As a result of theoretical analysis of CdTe PL, a Mott transition of excitons into electron-hole plasma (EHP) state along with increase of the intensity of 1.45 eV PL band was found.
The excitonic PL peaks (1.587 eV and 1.592 eV) in the CdTe PL spectrum at 4.7 K are due to the radiative annihilation of bound excitons in the ground ($n = 1$) state. At 25 K, excitons bound to acceptor (1.587 eV) disappear from the spectrum, while excitons bound to donor (1.592 eV) exhibit a Mott transition to the EHP state at 30 K. There is a thermal quenching of the impurity band (1.45 eV) in the temperature range of 4.7– 30 K, but temperature increase in the range of 30– 45 K, results in an increase in the impurity intensity and a flatteing of its phonon structure. The increase in the intensity of the impurity band is associated with the Mott transition and the increasing concentration and temperature of electrons in the EHP state. The Mott transition of the electron and hole from the bound exciton state to the free EHP state can be directly observed by the disappearance of exciton peaks and the intensity increase of 1.45 eV band. The exciton spectrum and the Mott transition is determined by the Wannier-Mott equation of quantum statistical physics:

$$(\varepsilon_i(k_i) - \varepsilon_m(k_m) - \hbar\omega)\psi_{lm}(q) + \sum_{q_1} V_{q_1} e_{ll'}^{-iq_1 r}\left(n_{l'}(\omega_{ll'}) - n_{m'}(\omega_{mm'})\right)\psi_{l'm'}(q)e_{ll'}^{-iq_1 r} = 0 \quad (1)$$

To determine the criterion for the Mott transition, the variational method and perturbation theory was used. Both of these calculations give similar results for the Mott transition criterion:

$$E_1(a_B/\lambda_D \to 0.86) = 0, \text{in CdTe:} \frac{n}{T_e} = 0.72\frac{k_0}{8\pi G a_B^3} = 7 \cdot 10^{14} cm^{-3}K^{-1} \quad (2)$$

The form-function of the impurity PL spectrum at 1.45 eV depends on the CdTe parameters, but more significantly, the PL spectra depend on the concentration of EHP and the electron temperature:

$$F_A(\omega) = \frac{\omega_g}{\omega}\exp\left(-N_A \coth\frac{\beta}{2}\right)\sum_n e^{-n\frac{\beta}{2}} I_n(z\omega_n)\omega_n^{1/2}\exp(-\beta\omega_n)\,(1 + b_A\omega_n)^{-4} \quad (3)$$

Thus, by comparing the PL spectrum at a lattice temperature of 45 K with the theoretically calculated spectrum from equation (3), the value of n/T_e was determined, considering that the calculated spectrum matches the experimental results. As a result of this calculations, satisfactory agreement was found for the theoretical value of n/T_e (2) and same parameter determined form PL spectrum. The Mott transition of excitons to the interband mechanism of EHP is controlled by both temperature and the power of the exciting laser. It was shown that the photon energy of radiation during exciton annihilation depends weakly on the plasma concentration, since the linear contributions in a_B/λ_D to E_g and to the exciton binding energy E_1 at small momenta are quenched. However, a red shift of the excitonic peak on the order of tenths of a meV is observed with the plasma concentration increase. The red shift is negligibly small and is not observed experimentally. However, a blue shift (on the order of several meV) is observed at the highest excitation levels. The increase in transition frequency with increasing excitation level is due to the Mott transition of the exciton gas into an EHP, which involves a shift from the exciton annihilation mechanism to the interband mechanism, accompanied by a blue shift of the photon energy from the exciton value $\hbar\omega = E_G - E_1(x), E_1(x) \to 0$ to the interband value $\hbar\omega = E_G + k_B T_e/2$, in accordance with the experiment at $W = 3.0\,mW$. At higher excitation levels, the plasma radiative recombination band exhibits a red shift due to the decrease in E_G with increasing EHP temperature.

ACKNOWLEDGEMENTS: MEC subprogram 011207

LONG-LIVED PHONONS IN HYBRID OPTOMECHANICAL DEVICES

V. Ceban*, M. A. Macovei
Institute of Applied Physics, Moldova State University, Chișinău, Republic of Moldova
*E-mail: victor.ceban@ifa.md

We have investigated the quantum dynamics of a laser driven two-level emitter coupled to an optical and to a mechanical resonator. This model represents the case of a polycyclic aromatic molecule placed within an organic crystal or a quantum-dot deposed on a mechanical resonator made of a nanobeam or a vibrating membrane. This kind of hybrid optomechanical devices can be used as quantum memory, by transferring back and forth the bits of information carried by photons to long-lived phonons. The limitations of such type of quantum memory is related to the lifetime of the single-mode phonons of the mechanical resonator.

Here, we show that phonon lifetimes can be enhanced by slowing-down the decay dynamics of the emitter's excited state [1]. This is achieved by oppressing the spontaneous emission effect when placing the emitter within an optical cavity and by modulating its transition frequency. The emitter is off-resonantly driven by an intense laser, creating a dynamic Stark effect which modulates the emitter transition frequency. Within the bad cavity limit, the slow-down effect of the emitter decay dynamics is transferred to the phonon dynamics. Long-lived phonons are estimated to appear within the mechanical resonator. This effect is more prominent for mechanical resonators with lower damping rates, i.e., of the same order of magnitude as the emitter spontaneous emission rate.

[1] V. Ceban, M. A. Macovei. *J. Opt. Soc. Am B* **41** (2024) 216-221.

DYNAMICS OF STRONGLY COUPLED HARMONIC OSCILLATORS IN GAUSSIAN NOISY CHANNELS

T. Mihaescu*, A. Isar
Horia Hulubei National Institute for R&D in Physics and Nuclear Engineering, Măgurele, Romania
*E-mail: mihaescu.tatiana@theory.nipne.ro

We investigate the Markovian evolution of Gaussian entanglement and steering in a system consisting of two strongly coupled harmonic oscillators immersed in a structured environment. Specifically, we analyze the contribution of the interaction between modes when the magnitude of the intermode coupling strength is comparable to the local frequencies of the modes, and the rotating wave approximation does not apply. Previously, the intermode strong coupling was considered in the case of a common thermal bath [1], and presently we extend this investigation to a generalized Gaussian channel, when the environment is modeled by a collection of squeezed bosonic modes. We provide also an extended comparison of the evolution of entanglement and steering in weak and strong coupling regimes [2].

[1] C. Joshi, P. Ohberg, J.D.Cresser, E. Andersson, Markovian evolution of strongly coupled harmonic oscillators, Phys. Rev. A 90, 063815 (2014)
[2] T. Mihaescu, A. Isar, Dynamics of strongly coupled harmonic oscillators in Gaussian noisy channels, (to be published)

CONTROL DYNAMICS OF THE EMMITED PHOTONS IN THE BIOLOGICAL MEDIA

N. Ciobanu[1,*], N.Gubceac[1,2], V.Tronciu[2]
[1]*Department of Human Physiology and Biophysics, State University of Medicine and Pharmacy "Nicolae Testemițanu", Chișinău, Republic of Moldova*
[2]*Department of Physics, Technical University of Moldova, Chișinău, Republic of Moldova*
[*]E-mail: nellu.ciobanu@usmf.md

Recently, the influence of electromagnetic fields on the living matter has become an attractive goal for modern biomedicine [1],[2]. The human body is exposed daily to the radiation of various types of electromagnetic waves through modern technologies, which are extremely widespread in everyday life. The effects produced by these radiations can destroy the body's defense and functional systems. However, some classes of electromagnetic waves, e.g., millimeter waves (MM) and terahertz (THZ) can produce constructive therapeutical effects [3].

The theoretical model describing the evolution of photons and phonons generated by the biological media was discussed in our previous papers [4]. Figure 1 shows the scheme of irradiation of the biological environment by MM wave source, whose profile is described by a function with sinusoidal modulated pump power: $P = P_0(1 + m(cos2\pi\omega t))$, where m is the modulated parameter. The photons emitted by the biological medium are delayed from an external mirror, similar to the model of semiconductor lasers with external feedback. The photons and phonons emitted by the biological medium are described by the system of differential equations

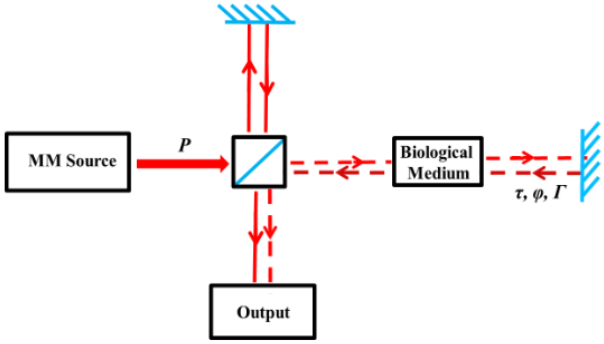

$$\frac{dE_1}{dT} = -\sigma E_1 - (\tilde{\delta} - \tilde{\omega}_0)E_2 + 2\alpha\tilde{\gamma}A_1 + \alpha\{2\tilde{\gamma}[\delta - (A_1^2 + A_2^2)] - 1\}A_2 + P + \Gamma[cos(\varphi)\,E_1(t-\tau) + sin(\varphi)\,E_2(t-\tau)],$$

$$\frac{dE_2}{dT} = (\delta - \tilde{\omega}_0)E_1 - \sigma E_2 + 2\alpha\tilde{\gamma}A_2 + -\alpha\{2\tilde{\gamma}[\delta - (A_1^2 + A_2^2)] - 1\}A_1 + \Gamma[cos(\varphi)\,E_2(t-\tau) - sin(\varphi)\,E_1(t-\tau)],$$

$$\frac{dA_1}{dT} = -\alpha E_2 - A_1 - [\delta - \nu(A_1^2 + A_2^2)]A_2,$$

$$\frac{dA_2}{dT} = -\alpha E_1 + [\delta - \nu(A_1^2 + A_2^2)]A_1 - A_2$$

Figure 1. Schematic representation of the setup

We describe the system dynamics in terms of bifurcation diagrams. Figure 2 shows a typical bifurcation diagram, where feedback strength Γ is considered as bifurcation parameter. The diagram shows the dependence of photon number on the feedback strength for maximum and minimum values and for various pump parameters. Each dot represents a peak of the output power. For small values of the optical feedback the system displaces continuous wave and oscillatory regimes. An increase of feedback leads to a period doubling and chaotic behavior.

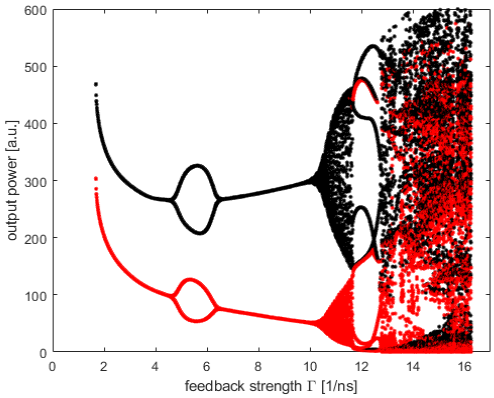

Figure 2. Numerical bifurcation diagram.

[1] D. Arco, M. Di Fabrizio, V. Dolci, M. Petrarca, S. Lupi. Condensed Matter 5 (2), (2020), p. 25.
[2] I. Akinori, L. Stefano, M. Augusto. Condensed Matter, **6**(3), (2021), p. 23.
[3] S. Sarika, K. Neeru. Advances in Biology 1 (2014), p. 24.
[4] N. Gubceac, N. Ciobanu and V. Tronciu. Proc. of E-Health and Bioengineering Conference (EHB), Iasi, Romania, (2022), p. 01-04.

CHARGE TRANSFER INDUCED SPIN TRANSITION IN THE TETRANUCLEAR CYANIDE-BRIDGED [Co_2Fe_2] COMPLEX

S.I. Klokishner*, O.S. Reu*, S.M. Ostrovsky
Institute of Applied Physics, Moldova State University, Chișinău, Republic of Moldova
*E-mail: klokishner@yahoo.com, olegreu@yahoo.com

Recently it has been reported the first tetranuclear compound $[Co_2Fe_2(bpy^*)_4(CN)_6(tp^*)_2]$-$(PF_6)_2\cdot 2CP\cdot 8BN$ ($[Co_2Fe_2]$) [1] which manifests a three step charge transfer induced spin transition with 4 phases involved: the high-temperature phase, containing only clusters with two *low-spin (ls)* Fe^{III} and two *high*-spin (*hs*) Co^{II} ions; two intermediate phases characterized by the ratio 1:1 and 3:1 of clusters in the *low-spin* state ($2ls$-Co^{III}–$2ls$-Fe^{II}) and those in the *hs* state ($2hs$-Co^{II}–$2ls$-Fe^{III}), respectively, and, finally, the low-temperature phase, in which all 4 ions in the cluster are diamagnetic. The structural data also show that (a) at 100 K the Co_2Fe_2 species form two sublattices A and B containing *ls*-Fe^{II} and *ls*-Co^{III} ions; (b) with temperature rise sublattice A splits into two sublattices A and A` containing *hs*-$Co^{II}$ and *ls*-$Co^{III}$ ions, respectively, while sublattice B only includes *ls*-$Co^{III}$ ions; (c) at $T \geq 260K$ the difference between sublattices A and A` disappears, and all squares in these sublattices contain *hs*-Co^{II} and *ls*-Fe^{III} ions, while B clusters still remain diamagnetic up to 260K. Finally, at 320K all clusters contain only paramagnetic ions. Paper [1] provides only a qualitative explanation of the experimental data. In the present communication a quantitative description of the observed spin transformation is given on the basis of DFT calculations of the single point energies as functions of temperatures for spin values S=0,1,2,3,4 of the total complex. The performed DFT analysis (ORCA package [2], B3LYP functional, TZVP-functions) allowed to restore the picture of spin conversion in the Co_2Fe_2 complex and to compare it with the experimental data. It has been demonstrated that at 100K for the two subunits A and B, present in the structure, the lowest is the diamagnetic state containing the *ls*-Fe^{II} and *ls*-Co^{III} ions. From three subunits A, A' and B detected crystallographically in the compound at 200K only for the A ones the ground state possesses the spin value S=4 corresponding to paramagnetic *ls*-Fe^{III} and *hs*-Co^{II} ions, while at 260 K a half of all clusters in the crystal are in this state. From the DFT calculations it also follows that at 320 K in the crystal only two paramagnetic subunits A and B containing *hs*-Co^{II} and *ls*-Fe^{III} ions and possessing the highest ground state spin value S=4 are present. The results obtained [3] are in accordance with the experimental data [1] on the magnetic susceptibility of the examined compound and show the way how to predict new magnetic materials manifesting spin transitions and the most important to give the answer, whether the material under examination can manifest spin transitions and in what range of temperatures these transitions are expected to be observed.

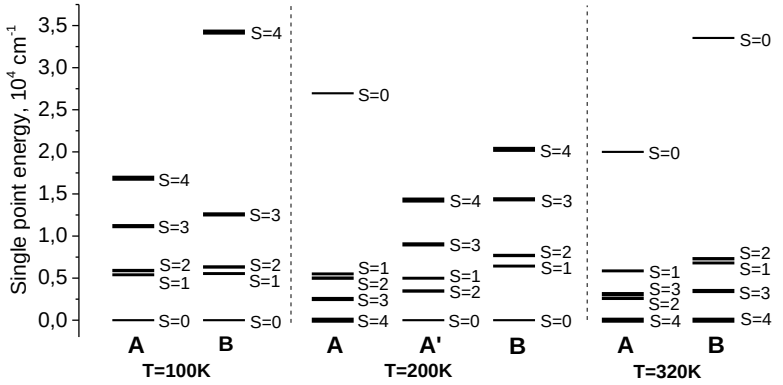

Figure 1. Single point energies corresponding to different values of the total spin S for the tetranuclear clusters of the types A , A` and B in the $[Co_2Fe_2(bpy^*)_4(CN)_6(tp^*)_2]$-$(PF_6)_2\cdot 2CP\cdot 8BN$ compound [2] at T=100K, 200K and 320K.

ACKNOWLEDGEMENTS: The authors are grateful for financial support to the Ministry of Education and Research of Moldova (project no. 011201)

[1] M. Nihei, Y. Yanai, I.-J. Hsu, Y. Sekine, H. Oshio, *Angew. Chem. Int. Ed.* **56** (2017) 591-594.
[2] F. Neese, Software update: the ORCA program system, version 4.0. WIREs Comput. Mol. Sci.5, (2018), e1327.
[3] O. Reu, S. Ostrovsky, S. Klokishner, *J. Phys. Chem. A* **127** (2023) 7496-7500.

ENVIRONMENT-ASSISTED GENERATION OF QUANTUM CORRELATIONS OPEN QUANTUM SYSTEMS

Alina-Alexandra Stoica[1,2,*], Aurelian Isar[*]
[1] *"Horia Hulubei" National Institute of Physics and Nuclear Engineering, Bucharest-Magurele, Romania;*
[2] *Faculty of Physics, University of Bucharest, Bucharest-Magurele, Romania*
[*] E-mail: dobre.alina@theory.nipne.ro, isar@theory.nipne.ro

We analyze the environment-assisted generation of quantum correlations of the type of the geometric Hellinger quantum discord in a system of two bosonic modes embedded in a common environment, by using the characteristic function method to describe the dynamics of the system [1-3]. We consider the two modes initially in factorized squeezed states and consider three types of environments: thermal, squeezed vacuum and squeezed thermal. We show that not only the environment can enhance, but also can generate the two-mode quantum discord. We also describe the influence of the squeezing parameter of the modes and of the environment on the generation of quantum discord [4].

[1] S.-H. Xiang, B. Shao, K.-H. Song, Chin. Phys. Lett. **26** (2009) 030304
[2] X. Yang, G. H. Huang, M. F. Fang, Opt. Comm. **341** (2015) 91
[3] S.-H. Xiang, B. Shao, K.-H. Song, Phys. Rev. A **78** (2008) 052313
[4] A. Stoica, A. Isar (to be published)

PICOSECOND PULSE GENERATION IN InGaN BLUE LASERS WITH SATURABLE ABSORBER

V. Dobrovolschi*, S.Rusu, V.Tronciu
Department of Physics, Technical University of Moldova, Chișinău, Republic of Moldova.
*E-mail: veronica.dobrovolschi@fiz.utm.md

In this paper we report the results of theoretical investigations of generation of ps-pulses by blue InGaN with saturable absorber. We study numerically, using the single mode rate equations, the influence of wavelength of laser, and the length of saturable absorber on the features of output pulses. We investigate also, the impact of different material and laser parameters on properties of pulses. The mechanism belong to pulse generation is also presented. Finally, we discuss the applications of ps-pulses in distant measurements, free-space communications, material processing and spectroscopy.
Figure 1 shows an analytical model of investigated setup. It consists of an InGaN active layer and a saturable absorber (SA). The active layer is composed by six QWs, and the emitting wavelength is 405 nm. Lasers with different cavity length and wavelengths have been investigated theoretically.

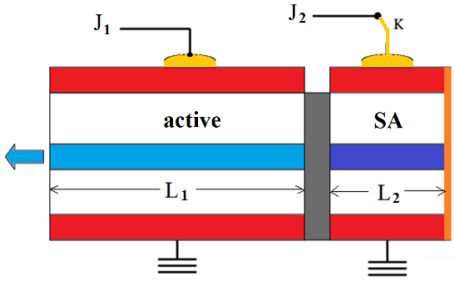

Figure 1. Setup of InGaN laser

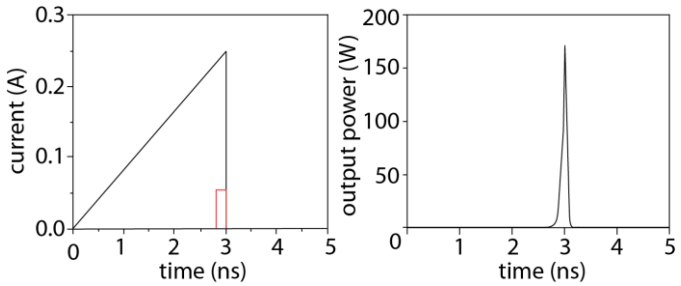

Figure 2. Principle of pulse generation. a) injected current into active (black line) and SA (red line) sections. b) Generated output pulse.

To simulate the generation of pulses in an InGaN lasers we use the single mode model [1], which is given by the following rate equations for photon number S and injected carrier number n_1 in active region and n_2 in the saturable absorber.

$$\frac{dn_1}{d\tau} = -(n_1 - n_{g1})S - \frac{n_1}{\tau_{s1}} + J_1, \quad \frac{dn_2}{d\tau} = -(n_2 - n_{g2})S - \frac{n_2}{\tau_{s2}} + J_2,$$

$$\frac{dS}{d\tau} = (n_1 - n_{g1} + n_2 - n_{g2})S - B_C(n_1 - n_{g1})S - GS + M(n_1 + n_2).$$

We integrate numerically this set of equations by studying the features of pulses in dependence of laser wavelength and length of SA. Figure 3 shows the dependence of pulse energy and maximum of output pulse on the laser wavelength. One can see that a large wavelength implies a low maximum of pulses, as well as a decrease of their energy. Figures 3 c) and d) shows the dependence of the same pulse features on length of SA. Large SA length lead to low energy and peak of pulse due to the increase of losses in SA. We believe that our work provides a good basis for future experimental study of pico-seconds pulses generated by blue InGaN laser with saturable absorber.

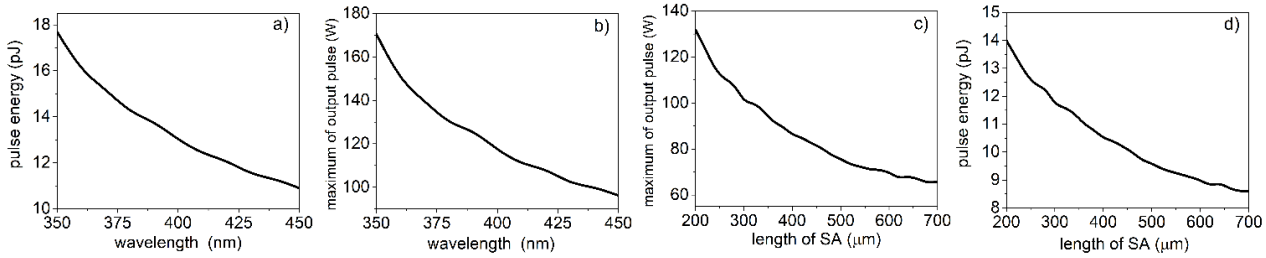

Figure 3. Dependences of pulse features (energy and peak) on the laser parameters.

[1] V.Z. Tronciu et al Optics Communications 235 (2004) 409–414

DIPOLE-DIPOLE INTERACTING FEW-LEVEL EMITTERS IN A THERMOSTAT

Mihai A. Macovei*
Institute of Applied Physics, Moldova State University, Chișinău, Republic of Moldova
*E-mail: mihai.macovei@ifa.usm.md

The interaction of a small atomic ensemble with the incoherent environmental thermal heat bath may surprisingly lead to quantum phenomena. It was demonstrated that the entanglement between two initially independent qubits can be generated if the two qubits interact with a common heat bath in thermal equilibrium [1,2]. Larger two-level ensembles, under the Dicke approximation and in a common thermostat, obey the Bose-Einstein statistics and quantum light features are characteristic only for few atoms in these setups. Actually, the electromagnetic fields emitted on the two transitions of a three-level Dicke-like ensemble, surrounded by the thermostat, are strongly correlated or anticorrelated and exhibit quantum light properties also for larger numbers of atoms which was demonstrated via violation of the Cauchy-Schwarz inequality [3].

Here we shall report our recent results obtained in a dense and dipole-dipole coupled ensemble of two-level emitters interacting via their environmental thermostat. The established thermal equilibrium of ensemble's quantum dynamics is described with respect to the dipole-dipole coupling strengths. We have demonstrated the quantum nature of the spontaneously scattered light field in this process for weaker thermal baths as well as non-negligible dipole-dipole couplings compared to the emitter's transition frequency. Furthermore, the collectively emitted photon intensity suppresses or enhances depending on the environmental thermal baths intensities [4].

[1] A. M. Basharov, Entanglement of Atomic States upon Collective Radiative Decay, JETP Letters **75**, (2002) 123.
[2] D. Braun, Creation of Entanglement by Interaction with a Common Heat Bath, Phys. Rev. Lett. **89**, (2002) 277901.
[3] M. Macovei, J. Evers, and C. H. Keitel, Quantum correlations of an atomic ensemble via an incoherent bath, Phys. Rev. A **72**, (2005) 063809.
[4] M. A. Macovei, Dense dipole-dipole-coupled two-level systems in a thermal bath, Phys.Rev. A. **110**, (2024), 023712

THEORETICAL MODEL OF LIPID PEROXIDATION KINETICS INVOLVING THREE DIFFERENT ANTIOXIDANTS: FLAVONOID, α-TOCOPHEROL AND ASCORBATE

E. Yu. Kanarovskii*, O. V. Yaltychenko, S. A. Baranov
Institute of Applied Physics, Moldova State University, Chișinău, Republic of Moldova
*E-mail: evghenii.canarovschii@ifa.usm.md

Modern experimental and theoretical studies of biological condensed media (CM), which are part of complex multicomponent biosystems, lie at the intersection of biology, physics, and chemistry, requiring also the use of various mathematical methods for processing results and modeling. Among biological CM, as objects of study, a special place belongs to the lipid CM, existing in cells in the form of lipid layers due to the hydrophobic interactions. An interdisciplinary approach led to the emergence (in the early 2000s) of a new, rapidly developing scientific discipline – lipidomics [1], which combines diverse studies at the micro- and macrolevels of various lipid metabolites and lipid CM. Lipid layers are the basis of cell membranes of living organisms and they are also widely used as shells for a number of drugs. And since the structural and functional properties of cell membranes depend significantly on the biochemical processes occurring in their lipid layers, then the ways and means of controlling the LPO process are of primary importance for the stability and normal functioning of cells.

In recent years, there has been increased interest in flavonoids due to their unique biochemical properties [2]. Flavonoids (also known as vitamin P) are the largest class of plant polyphenols. Among them, the most famous are rutin, quercetin and dihydroquercetin, which are widely used in medicines. Also, flavonoids are actively used in the food and nutrition sciences and the food preservation technologies, where they are studied and used as dietary supplements and as components of mixtures for canning. Such attention to them is owing to the fact that most flavonoids and their glycosides have pronounced antioxidant activity, as they are able to both effectively inhibit free radicals and modulate enzyme activity. In addition, their antioxidant activity is associated with the ability to form chelate complexes with transition and heavy metals, thereby protecting lipids, proteins and DNA molecules from oxidative stress induced by ions of variable valence, as well as removing heavy metals from the organism.

This work proposes modeling of the joint antiradical action of flavonoid (vitamin P), α-tocopherol (vitamin E) and ascorbic acid (vitamin C) in the process of lipid peroxidation (LPO) taking into account the synergy effect. This effect is that ascorbate is able to restore lipophilic antioxidants, which include both α-tocopherol and most flavonoids, from their radical forms. The model under consideration is an extension of the previously proposed model with two conjugated antioxidants (vitamins E and C) [3], given that the flavonoid is able to effectively control the initiation stage of LPO, since it significantly reduces the initiation rate. According to the proposed modified LPO scheme, including three antioxidants, a minimal kinetic model was formulated in the form of a system of differential equations. Taking into account the performed approximations and using quasi-stationary conditions for lipid radicals R• and ROO•, this model makes it possible to obtain analytical solutions for the concentrations of lipid antioxidants in their reduced and radical forms, and for the concentration of the main LPO product (lipid hydroperoxide ROOH). An analysis of the characteristics of the LPO process with the participation of the three indicated antioxidants is carried out, the features of the synergy effect of vitamins E, P and C and its significance for the effective control of this process as a whole are discussed.

ACKNOWLEDGEMENTS: The research was founded by the Ministry of Education and Research of RM (subprograms 011201, 011204).

[1] M. R. Wenk. *Nat. Rev. Drug Discov.* **4** (2005) 594–610.
[2] V. A. Kostyuk, A. I. Potapovich. Bioradicals and bioantioxidants: Monograph. Minsk: BSU. 2004. (in Russian)
[3] E. Yu. Kanarovskii, O. V. Yaltychenko. *Surf. Engin. Appl. Electrochem.* **59** (2023) 473-478.

VALENCE TAUTOMERIC TRANSFORMATION IN MOLECULAR [FeCo] COMPOUND: EXPLORATION OF COOPERATIVE INTERACTIONS

S.I. Klokishner*, O.S.Reu*
Institute of Applied Physics, Moldova State University, Chișinău, Republic of Moldova
*E-mail: klokishner@yahoo.com, olegreu@yahoo.com

In the present communication a model is reported to describe the valence tautomeric transformation in a crystal containing as a structural element trinuclear linear Fe–ligand–Co complexes. The following electronic configurations of the complex, revealed on the basis of experimental data, are taken into account: I. $ls\text{-}Fe^{3+}–dhbq^{3-}– ls\text{-}Co^{3+}$, II. $hs\text{-}Fe^{3+}–dhbq^{3-}–ls\text{-}Co^{3+}$ and III. $hs\text{-}Fe^{2+}–dhbq^{2-}–ls\text{-}Co^{3+}$ [1] (*ls*–low-spin, *hs*–high-spin), wherein in configurations I and II the extra electron resides on the ligand, while in configuration III it is transferred from the ligand to the iron ion. In the consideration all states of the complex arising from these configurations are included. As for an individual molecule the model takes into account the electron transfer from the ligand to the iron ion and the Heisenberg exchange interaction in the pairs $ls\text{-}Fe^{3+}–dhbq^{3-}$, $hs\text{-}Fe^{3+}–dhbq^{3-}$. The parameters j_1 and j_2 of Heisenberg exchange in these pairs were evaluated with the aid of the DFT calculations (ORCA package [2], B3LYP functional, TZVP-functions). Through DFT calculations the dipole moments of the cluster in its states arising from configurations I-III were also estimated. The transition between configurations I and II is caused by spin crossover in the iron (III) ions accompanied by the deformation of the intra- and intermolecular spaces. Therefore, the introduced in the model cooperative electron-deformational interaction between the Fe-ligand-Co units accounts for different rigidity of these spaces, the interaction parameter was calculated with the aid of the observed values for the elongations of iron-ligand bonds. Since the electron transfer from the $dhbq^{3-}$-ligand to the $hs\text{-}Fe^{3+}$ ion leads to electronic density redistribution in each trinuclear cluster and transformation of the $hs\text{-}Fe^{3+}$ ion into the $hs\text{-}Fe^{2+}$-one, the model also accounts for ligand-metal electron transfer and cooperative dipole-dipole interaction, The characteristic energy of the latter one was evaluated with the aid of the numerical values of DFT calculated dipole moments. The role of cooperative interactions and, namely, of the electron-deformational and dipole-dipole ones is elucidated. Within the framework of the developed model quite a good agreement is obtained between the calculated and experimental values [1] of the magnetic susceptibility for the [(Fe(RR-cth))(Co(SS-cth))(μ-dhbq)]$(PF_6)_3$ compound represented in the figure given below. The suggested model reproduces quite well the width of the observed hysteresis loop and the temperature of the transition governed by internal parameters of the cluster itself as well as by the strength of intercluster interactions.

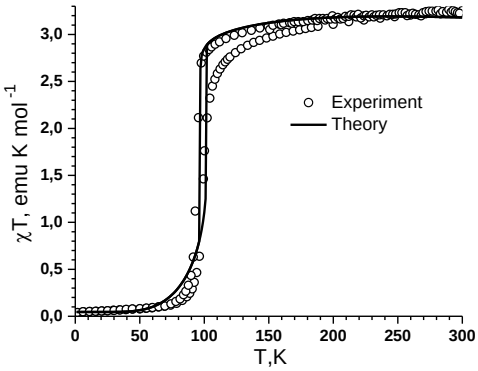

Figure 1. Temperature dependence of the χT product for the the [(Fe(RR-cth))(Co(SS-cth))(μ-dhbq)]$(PF_6)_3$ compound:
circles – experimental data reported in [1],
solid line – calculated theoretical curve

ACKNOWLEDGEMENTS: The authors are grateful for financial support to the Ministry of Education and Research of Moldova (project no. 011201)

[1] P. Sadhukhan, et al, Manipulating electron redistribution to achieve electronic pyroelectricity in molecular [FeCo] crystals, *Nature Communications*, **12** (2021) 4836.
[2] F. Neese, Software update: the ORCA program system, version 4.0. WIREs Comput. Mol. Sci.5, (2018), e1327.

OPTICAL ABSORPTION IN QUANTUM DOT SUPERLATTICES WITH PARABOLIC POTENTIAL

R.Z. Ibayeva*, G.B. Ibragimov
Ministry of Science and Education, İnstitute of Physics, Baku, Azerbaijan
*E-mail: raidaibayeva1@gmail.com

Recently, various nanomaterials and nanostructures are intensively studied. Modern semiconductor technology allows the creation of nanostructures with interesting physical properties. Quantum dots are one of those structures that are of special interest. The uniqueness of quantum dots is that the movement of charge carriers in such systems is quantized in all three directions. All quantum nanostructures are obtained in various dielectric matrices. When obtaining a semiconductor quantum dot, a confinement potential is created at the boundary between the matrix and the quantum dot, the shape of which in most cases depends on the method of quantum dot acquisition. Due to the confinement potential, quantum size effects are created in quantum structures, which allows to control the properties of the quantum dot, which is of interest from the point of view of both fundamental science and its application in nanoelectronics.

The application of charge transport in quantum dot superlattices attracts a lot of attention. The study of intersubband absorption in quantum wells is of great interest because it is used in quantum well infrared detectors [1] and quantum cascade lasers [2, 3, 4, 5, 6].

Light absorption by free charge carriers in the presence of phonons in an anisotropic quantum wire[7], intraband absorption of electromagnetic radiation by electrons with optical phonon participation in quantum dot superlattices [8], light absorption by free charge carriers with scattering mechanisms in a semiconductor superlattice [9] were presented.

In this work, the intraband optical absorption in a quantum dot superlattice with a parabolic potential is studied. Note that the study of intraband optical transitions provides important information about the parameters of the Fermi surface and energy spectrum of electrons. Since parabolic potential confinement is considered in this work, the electron-electron interaction is not taken into account. In quantum dot superlattices, the electron gas is confined by an anisotropic parabolic potential as in the following expression:

$$V(x,y) = \frac{m^*}{2}(\omega_x^2 x^2 + \omega_y^2 y^2) \tag{1}$$

here m^* is the effective mass, ω_x and ω_y are the frequencies of confinement in the x and y directions, respectively.

In the case of an undegenerated electron gas in quantum dot superlattices with anisotropic parabolic potential, it was found that intraband absorption takes place between adjacent sublevels in the first-order excitation theory of electron-photon interaction in the direction of the limiting potential axis of the polarization vector of the electromagnetic wave.

[1] B.F. Levine, Journal of Applied Physics, V. 74, pp. R1-R81, (1993).
[2] I.A. Dmitriev, R.A. Suris, Phys. Status Solidi A, Vol. 202, pp.987, (2005).
[3] J. Faist, F. Capasso, D.L. Sivco, Quantum cascade Laser, Science, Vol. 264, pp. 553-556, (1994).
[4] H.T. Grahn, et al., Applied Physics Letters, Vol. 108, No. 19, pp. 191106, (2016).
[5] T.K. Nurubeyli, Inorganic Materials: Applied Research, Vol. 11, p.552-557, (2020).
[6] T.K. Nurubeyli, Technical Physics, Vol. 65, No. 12, pp. 1963–1968, (2020).
[7] G.B. Ibragimov, R.Z. Ibayeva, Advanced Physical Research, Vol. 6, No. 1, pp. 56-62, (2024).
[8] G.B. Ibragimov, R.Z. Ibayeva, Radioelectronics. Nanosystems. Infomation Technologies, Vol. 16, No. 2, pp. 249-254, (2024).
[9] G.B. Ibragimov, R.Z. Ibayeva, Journal Of Surface Investigation: X-Ray, Synchrotron And Neutron Techniques, Vol. 18, No.1, pp. 116-120, (2024).

SYSTEMS WITH STRONG COULOMB AND ELECTRON-PHONON INTERACTION: METHODS OF INVESTIGATING AND RESULTS

I.D. Cebotari*
Institute of Applied Physics, Moldova State University, Chișinău, Republic of Moldova
*E-mail: irina.cebotari@ifa.usm.md

The main useful methods of analysis of strong correlated systems are dynamical mean field theory combined with the density functional theory and the numerical renormalization Group method. The perturbative method for calculating Green's functions and diagrammatic technique is also effective. For weak coupled systems, it is based on the Wick theorem. In the case of strong coupling, the usual Wick theorem is not applicable due to the non-bilinear form of the Hamiltonian of the main approximation, which must include terms responsible for strong interactions. Various solutions to this problem have been proposed: 1) using the Kubo cumulant expansion and the Hubbard operator technique [1-5], 2) based on functional integral formalism and using of Hubbard–Stratonovich transformation [6-8], 3) using the generalized Wick theorem [9, 10]. The role of electron-phonon interaction in systems with both strong electron-phonon coupling and strong Coulomb interaction of electrons is analyzed mainly within the framework of the Hubbard-Holstein model. This model has been investigated by many methods. For example, by the method of equation of motion for retarded Green's functions [11], the density matrix renormalization group method [12], the quantum Monte Carlo method [13], etc., as well as the diagram technique for strong correlated systems (see for example [l4-17]). The last approach uses the canonical Lang-Firsov transformation, which allows one to exclude the terms of the Hamiltonian that are linear in the phonon coordinate and reduces the problem to considering moving polarons. In this case, a new group of average products arises, formed from phonon cloud operators. A generalized Wick theorem has been proposed for this group [14, 15]. The studies of the role of strong electron-phonon interaction in electron processes of Mott metal-insulator transition have demonstrated that, depending on which interaction is dominant in the system and on the filling of the band n in Hubbard-Holstein model, a different physical picture is observed (see for example [12,13]). The system is in the state of an antiferromagnetic Mott insulator in the case where the Coulomb interaction U dominates, or in the so-called bipolaron localized state (or charge density wave state) in the case where the electron-phonon interaction constant g dominates. Concerning the role of the electron-phonon interaction in superconductors in which this coupling is large, theoretical studies demonstrate both effect favoring to superconducting pairing of electrons (see, foe example [18]) and a possible polaron [16, 19] (bipolaron [19] mechanism) of superconductivity.

[1] V.G. Vaks, A.I., Larkin, S.A. Pikin. *JETP* **26** (1968) 188-199[*ЖЭТФ* **53**(1968) 281-299].
[2] Ю. А. Изюмов, Ф. Л. Кассан-оглы, Ю. М. Скрябин. *Полевые методы в теории ферромагнетизма*, М: Наука. (1974) 223 с.
[3] P.M. Slobodyan, I.V., Stasyuk. *ТМФ* **19** (1974), 423-429 [*Theoret. and Math. Phys.***19** (1974)616–620].
[4] R.O. Zaitsev. *JETP* **68** (1975). 207-215 [*ЖЭТФ* **70** (1976)1100-1111].
[5] A. F. Barabanov, K. A. Kikoin, L. A. Maksimov. *Theoret. and Math. Phys*. **25** (1975) 997–1003.
[6] S.Pairault, D.Sénéchal,Y.Trembla. *Eur. Phys. J*. B. **16** (2000) 85-105.
[7] D. Boies, C. Bourbonnais, Y. Trembla. *Phys. Rev. Lett.***74** (1995) 968-971.
[8] S. K Sarker, *J. Phys. C.* **21 (**1988) L667.
[9] W Metzner. *Phys. Rev. B* **43(**1991) 8549-8563.
[10] M.I., Vladimir, V.A. Moskalenko.*Theoret. and Math. Phys*. **82** (1990) 301–308[*ТМФ* **82** (1990), 428–437].
[11] M.L. Kalra, U.N. Upadhyaya, *Nuov Cim B* **41** (2007) 151–175.
[12] M.Tezuka, R.Arita, H. Aoki, *Phys. Rev. B.* **76** (2007) 155114.
[13] S.Karakuzu, F. L. Tocchio, S. Sorella et. al. *Phys. Rev. B*. **96** (2017), 205145.
[14] V.A.Moskalenko, *TMF*. 0**113** (1997) 432–437.[*Theoret. and Math. Phys*. **113** (1997**)** 1559–1563].
[15] V.A Moskalenko, P. Entel, D.F. Digor *Phys. Rev. B.***59** (1999) 619-635. .
[16] V.A. Moskalenko,Entel P, M. Marinaro et. al. *JETP* **97** (2003)632–644 [ЖЭТФ **124** (2003)700-713].
[17] M. Kh. Kharrasova, I.R. Kyzyrgulovb, A. T. Khusainova. *Phys. Met. Metallogr*. **111** (2011)123–132.
[18] B.Yunkyu, *Phys. Rev. B*. **78** (2008) 075116.
[19] A.S.Alexandrov. *Springer Series in Materials Science* **103** (2007) 257–310.

THEORETICAL STUDIES OF PICOSECOND PULSE GENERATION IN GAIN-SWITCHED DFB LASERS

V. Dobrovolschi*, I.Sanduleac, V.Tronciu
Department of Physics, Technical University of Moldova, Chișinău, Republic of Moldova
*E-mail: veronica.dobrovolschi@fiz.utm.md

During recent years, picoseconds optical pulses find different applications in free-space communications, bio-analytics, sensing, distance measurements, material processing, and spectroscopy. Such pulses can be generated by diode lasers. Moreover, diode lasers in addition with other types of lasers as solid state and fibre lasers can improve the pulse energy and peak power of pulses. Therefore, the theoretical and experimental efforts have been performed to improve the performance of pulsed diode lasers [1-3].

We consider in this paper the generation of picosecond pulses by gain-switching of distributed feedback ridge-waveguide laser diode shown in Fig. 1.

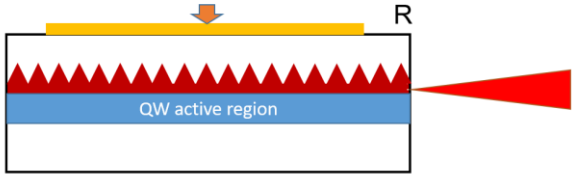

Figure 1. DFB laser.

The model investigated in this paper aims to simulate the mode competition between the Bragg-mode and the residual Fabry-Pérot modes during switch-on of a DFB laser [4]. The rate equation model for Fabry-Perot modes FP and Bragg mode B are treated separately coupled with one equation for charge carriers *n*

$$\frac{dS_B}{dt} = \frac{g_B(n)\Gamma S_B}{1+\varepsilon S_B} - \frac{S_B}{\tau_{S_B}} + K_B n^2, \qquad \frac{dS_{FP}}{dt} = \frac{g_{FP}(n)\Gamma S_{FP}}{1+\varepsilon S_{FP}} - \frac{S_{FP}}{\tau_{S_{FP}}} + K_{FP} n^2,$$

$$\frac{dn}{dt} = J - R - \frac{g_B(n)S_B}{1+\varepsilon S_B} + \frac{g_{FP}(n)S_{FP}}{1+\varepsilon S_{FP}}.$$

We integrate numerically the above equations by studying the influence of different parameters on dynamics of pulses. We investigate the impact of the gain-compression factor on peak power, pulse energy and pulse width. Figure 2 shows a typical temporal behaviour of the optical power at the front facet of laser and the evolution of curriers (black line) under the influence of pulse current (red line).

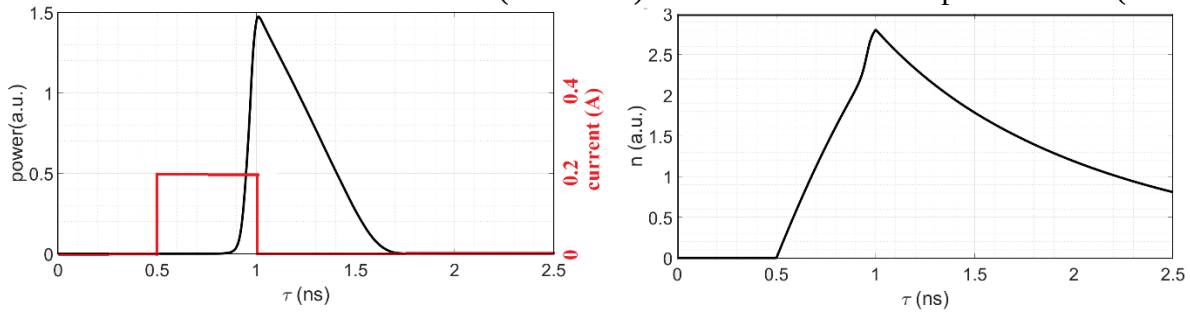

Figure 2. Pulse generation.

[1] H.Wenzel, A. Klehr, S.Schwertfeger, A.Liero, T.Hoffmann, O. Brox, M.Thomas, G.Erbert and G.Tränkle Proc. SPIE 8241 (2012) 82410V
[2] A. Klehr, T.Prziwarka, A.Liero, T.Hoffmann, J.Pohl, J.Fricke, H.J.Wünsche, H.Wenzel, W.Heinrich and G.Erbert G Proc. SPIE 9767 (2016) 976705
[3] V Tronciu, H Wenzel and A Knigge Semicond. Sci. Technol. 35 (2020) 045029 (10pp)
S.Riecke, H.Wenzel, S.Schwertfeger, K. Lauritsen, K. Paschke, R.Erdmann, and G.Erbert IEEE J. of Quantum. Electron., 47(5) (2011) 715.

FEW DIPOLE-DIPOLE INTERACTING TWO-LEVEL EMITTERS IN AN INTENSE LASER FIELD

A. S. Cudreașov*, P. Bardetski, M. A. Macovei
Institute of Applied Physics, Moldova State University, Chișinău, Republic of Moldova
*E-mail: alexandr.cudreasov@ifa.md

The resonance fluorescence (RF) features are widely investigated throughout the scientific community. In the realm of quantum optics, numerous studies have explored both weak and strong atom-field interactions. The collective behavior of closely interacting two-level emitters represents a fundamental area of study. Understanding how these emitters behave under the influence of a moderate laser field, particularly in scenarios where dipole-dipole interactions play a significant role, is crucial for advancing our comprehension of light-matter interactions at the quantum level.

This study employs a combination of theoretical modeling and numerical analysis to investigate the RF patterns of a small number of two-level emitters within the Dicke limit and under moderate laser pumping conditions. The average distance between two-level emitters is close enough that their dipole-dipole interactions play a significant role. It has been discovered that, using a simplified approach, the combined resonance fluorescence spectrum (RFS) of several emitters produces a spectrum with $2N + 1$ distinct lines, where N represents the number of emitters involved. The collective RFS shows $2N$ spectral sidebands symmetrically arranged around the generalized Rabi frequency with respect to the central line at the laser frequency, indicating the number of emitters in the group. These sidebands become noticeable when the dipole-dipole interaction strength surpasses the collective spontaneous decay rate.

[1] P. Bardetski, M. A. Macovei, Dipole-dipole interacting two-level emitters in a moderately intense laser field. arXiv:2403.15193 [quant-ph] (Jun. 2024) (preview available at http://arxiv.org/abs/2403.15193).

PHONON STRUCTURE OF DEFECT BAND AND EXCITON PHOTOLUMINESCENCE SPECTRA IN CdTe AND THE HUANG-RHYS FACTOR

A. A. Cliucanov, A. Varzari*, S. Vatavu
Physics of Semiconductors and Devices Lab, Faculty of Physics and Engineering, Moldova State University, Chisinau, Republic of Moldova
*E-mail: alexandru.varzari@usm.md

In this work, a theoretical analysis of the phonon structure of the exciton and impurity photoluminescence (PL) bands was carried out. The Huang-Rhys (HR) factor for the exciton-phonon interaction in CdTe was calculated by use of PL experimental data for CdTe thin films.

The HR factor cannot be found experimentally in a number of cases due to the self-absorption in PL of the zero-phonon line. The nature of the two exciton peaks in the PL spectrum of CdTe at 4.7 K is due to the radiative annihilation of excitons bound to the acceptor (1.587 eV) and donor (1.592 eV) in the $n = 1$ state. According to experimental data, the phonon replicas of excitons, both free and bound, show weaker than phonon replicas of the 1.45 eV impurity band. Consequently, if the coupling constant in case of 1.45 eV band is greater than unity, then for exciton peaks the number of emitted phonons per photon is less than unity. The calculation of the PL band form-function takes into account multiquantum transitions, the Froehlich interaction of excitons, band electrons, and holes bound to acceptors with LO phonons within the framework of temperature Green's functions. The two-band approximation, the phonon replicas of bound and free excitons are characterized by the matrix element of the Fröhlich interaction $M_{1S}(q) = \langle 1S\left(e^{iqr_h} - e^{iqr_e}\right)1S\rangle$. Here $\psi_{1S}(r) = e^{-r/a_B}(\pi a_B^3)^{-1/2}$. The HR factor of the interaction of the exciton with LO phonons is determined as:

$$N_{1S} = \sum_{q \le q_c} \frac{2\pi e^2 \omega_{LO}^{-1}}{(q^2 + \lambda_D^{-2})} \frac{M_{1S}^2(q)}{\hbar \varepsilon^* V}, M_{1S}(q) = \frac{2\pi}{\pi a_B^3} \int_0^\infty dr \cdot r^2 \int_{-1}^{1} dx \left(e^{iqr\alpha_h} - e^{-iqr\alpha_e}\right) e^{-r\frac{2}{a_B}} \quad (1)$$

The obtained estimate shows that the number of optical phonons emitted by excitons N_{1S} per photon is less than unity, while impurity recombination is characterized by a strong coupling with phonons at $N_A > 1$. In the Fröhlich interaction approximation, N_{1S} is determined by the equation:

$$N_{1S} = \frac{G}{\hbar\omega_{LO}} \frac{5}{8} \frac{m_e + m_h}{m_e} \frac{\varepsilon_0 - \varepsilon_\infty}{\varepsilon_\infty} F(\gamma) = 0.24\left(1 + \gamma - \frac{3.2}{(1-\gamma^2)^2}\left(\gamma^4 + \gamma - \frac{4\gamma^2(\gamma - \gamma^2)}{(1-\gamma^2)}\right)\right) \quad (2)$$

Whereas for the defect band (1.437 eV):

$$N_{eA} = \frac{e^2 \lambda_D}{\pi\hbar\omega_{LO}} \frac{1}{\varepsilon^*} I_A, I_A = \int_0^\infty \frac{x^2}{1+x^2}\left(\frac{1}{(1 + x^2\beta_h^2)^2}\right)^2 dx, \beta_h = \frac{m_h}{m_e + m_h}\frac{a_A}{2\lambda_D}, a_A = \frac{\hbar^2 \varepsilon_0}{m_h e^2} \quad (3)$$

the main contribution is determined by the interaction of holes with polarization arising from crystal vibrations. Taking into account the polarization and $\gamma = \gamma_e/\gamma_h = m_e/m_h = 0.274$, the HR factor is $N_{eA} = 1.85\frac{\varepsilon_0 - \varepsilon_\infty}{\varepsilon_\infty} = 0.74$. The estimations considered a hydrogen equation for the hole binding energy at the acceptor level, which gives $E_A = G \cdot \frac{m_h}{m_e} = 3.65G$ while the experimental value of the binding energy is $E_A = G \cdot \frac{0.2}{0.01}$. HR factor $N_A = 0.74 \cdot \frac{20}{3.65} = 4$. The radius of the acceptor-bound hole state can be calculated in the self-consistent approximation. In (3), Bohr radius of the hole $a_B = \frac{\hbar^2 \varepsilon_0}{m_h e^2} = a_B^{exc} \cdot \frac{m_r}{m_h}$, the HR impurity parameter $N_A = N_{BA} \cdot \frac{a_B}{a_A}$. Here, a_A is the adjustable radius of the acceptor-bound hole state. The parameter N_{BA} is calculated in the approximation of the hydrogen-like state of the hole, and N_A is the experimental adjustable value of the average number of phonons per photon. Considering that $N_{BA} = 0.74, a_B = a_B^{exc}\, m_r/m_h\,, a_A = 0.37 a_B \cong 0.1 a_B^{exc}$, the HR factor $N_{eA} = 2$ was found in accordance with the experiment.

ACKNOWLEDGEMENTS: MEC subprogram 011207

SECTION - GROWTH AND PROPERTIES OF ADVANCED MATERIALS (GPAM)

KEYNOTE LECTURES

EXCITONIC LUMINESCENCE OF IODINE-INTERCALATED HAFNIUM DISULPHIDE

A. Babinski*
Faculty of Physics, University of Warsaw, Warszawa, Poland
*E-mail: babinski@fuw.edu.pl

The ability of layered transition metal dichalchogenides (TMDs) to host intercalating molecules is well known. The TMDs comprise layers of tightly covalently bound layers of atoms separated by van der Waals gaps, in which the intercalants can be placed. In the case of halogen molecules, their large electron affinity results in a short range potential attracting electrons from the TMDs layers. The localized electrons interact with optically excited holes giving rise to bound excitons. The excitonic photoluminescence (PL) was observed in several molybdenum/tungsten sulfides /selenides: systems as eg: MoS_2:Cl_2 [1], WS_2:Br_2 [2], WSe_2:I_2, or WS_2:I_2. [3].

Properties of an excitonic PL from bulk hafnium dislulphide (HfS_2) grown by chemical vapor transport (CVT) method will be reviewed [4] The PL is attributed to the recombination of excitons bound to iodine (I_2) molecules intercalated between layers of HfS_2. The I_2 molecules are introduced to the crystal during the growth as halogen transport agents in the growth process. Their presence in the crystal is confirmed by secondary ion mass spectroscopy.

A series of emission lines was observed at low temperature in the energy range of 1.4–1.5 eV. Classical statistical analysis of their intensities allows to distinguish two groups of transitions in the spectra: main X_1 and X_2 lines followed at lower energies by their replicas involving acoustic and optical phonons.

It is proposed that the X_1 and X_2 emission lines correspond to neutral and charged excitons, respectively. They combine conduction and valence band carriers in HfS_2, which are bound by the iodine molecule potential. Microscopic-scale fluctuations in the unintentionally doped sample may be responsible for the observed quenching of the X_1 emission line, in particular spots of the sample. Notably, while the intensity of the X_1 line fluctuates strongly over the sample area and quenches at some spots, the X_2 line is present in all measured spectra. This may reflect generally intermediate doping of the investigated sample (allowing for the creation of both neutral and charged complexes) with some more heavily doped spots with trions only. Assuming the attribution of the observed excitonic lines to the neutral exciton and trion, one can approximate the binding energy of the latter as $\Delta = 16.3$ meV. The attribution of the PL emission to bound excitons comprising band carriers also explains the apparent effect of the sample thinning on their energy.

It is believed that our results may be of more general importance as similar PL spectra can be observed in several CVT-grown HfS_2 .samples of different origin, including those commercially available. This may suggest their common presence in HfS_2 with its potential effect on electronic transport in that material.

[1] L. Kulyuk, et al., *Phys. Rev. B* **68** (2003) 075314.
[2] L. Kulyuk, et al.,*Phys. Rev. B* **72**, (2005) 075336.
[3] D. Dumchenko, et al, *Thin Solid Films* **495** (2006) 82.
[4] N. Zawadzka et al., *Appl. Phys. Lett.* **122** (2023) 042102).

STUDY OF Tm^{3+} AND Tm^{2+} LUMINESCENCE IN TmF_3-DOPED CaF_2 CRYSTALS

M. Stef[1,*], C. Schornig[1], M. Poienar[2], G. Buse[2], D. Vizman[1], P. Veber[2]
[1]*Faculty of Physics, West University of Timisoara, Timisoara, Romania;*
[2]*Institute for Advanced Environmental Research (ICAM), West University of Timisoara, Romania*
[*]E-mail: marius.stef@e-uvt.ro

Rare-earth doped fluorite crystals have attracted considerable interest due to their exceptional optical properties and potential applications in various fields, including laser technology [1-3]. Among these, TmF_3-doped CaF_2 crystals have emerged as promising candidates owing to their versatile luminescent properties. The goal of this study is to investigate the luminescence of both Tm^{3+} and Tm^{2+} ions doped in CaF_2 crystals grown in our *Crystal Growth Laboratory* using vertical Bridgman technique. The comprehensive Judd-Ofelt analysis of Tm^{3+} ions doped CaF_2 crystals is made in order to elucidate their spectroscopic characteristics and potential applications. The Judd-Ofelt theory offers a robust framework for understanding the optical transitions and spectroscopic parameters of rare-earth ions in crystalline hosts. Applying this analysis to Tm^{3+} ions in CaF_2 crystals, the intensity parameters (Ω_2, Ω_4, and Ω_6) can be calculated. These parameters are crucial for predicting radiative properties such as emission cross-sections, branching ratios, and quantum efficiencies, which are essential for designing efficient laser and optical devices.

Recent advancements in spectroscopic techniques and theoretical models have deepened our understanding of the intricate energy transfer processes and relaxation dynamics of Tm^{3+} ions in CaF_2 matrices [4,5]. By integrating these insights into the Judd-Ofelt analysis, we offer a deeper understanding of the luminescence mechanisms and spectral features of Tm^{3+} ions in CaF_2 crystals, thereby facilitating their optimization for laser applications.

ACKNOWLEDGMENTS: This work was supported by ESCARGOT project founded by the Romania's recovery and resilience plan, PNRR/2022/C9/MCID/i8.[1] Y. Li, Z. Li, H. Zhang, L. Zhang, Optical Materials **120** (2023) 111234.
[2] J. Wang, X. Li, Y. Wang, C. Wang, Q. Zhang, Journal of Luminescence **245** (2023) 118927.
[3] Q. Zhou, S. Yang, Y. Zhang, H. Zhang, X. Li, Journal of Applied Physics **131(2)** (2022) 023101.
[4] M. Liu, Y. Wang, J. Wang, X. Liu, H. Zhang, Optical Materials Express **12(4)** (2022) 4812-4823.
[5] Q. Chen, X. Wu, L. Wang, H. Zhang, Y. Wang, Optics Letters **47(6)** (2022) 1543-1546.

DEFECT STATES IN BI- AND SB- CHALCOGENIDES REVEALED BY COMBINATION OF EXPERIMENTAL TECHNIQUES AND DFT MODELLING

D. Miliaieva[1,*], V. Nadazdy[2], M. Koltsov[1], C. López[3,4], C. Cazorla[3,4], M. Krunks[1], I.O. Acik[1], Nicolae Spalatu[1]

[1]*Department of Materials and Environmental Technology, Tallinn Technical University (Taltech), Tallinn, Estonia;*

[2]*Institute of Physics, Slovak Academy of Sciences, Bratislava, Slovak Republic;*

[3]*Departament de Física, Universitat Politècnica de Catalunya, Barcelona, Spain;*

[4]*Barcelona Research Center in Multiscale Science and Engineering, Universitat Politècnica de Catalunya, Barcelona, Spain*

[*]E-mail: daria.miliaieva@taltech.ee

Understanding the nature of the defects, namely point defects, their formation mechanism and the contribution to the properties is essential for device performance improvement. Shallow-level defects with thermal energy of about k_BT from conduction band minimum (CBM) or valence band maximum (VBM) play the major role in the carrier concentrations and conductivity type determination of the material. In contrast, deep-level defect whose activation energy is much higher than k_BT from CBM or VBM is detrimental to photogenerated carrier lifetime and transport (carrier mobility and diffusion length). These defects result in the trap-assisted Shockley–Read–Hall recombination (dominant non-radiation recombination) in solar cells, which is the primary cause of open-circuit voltage loss [1].

In the center of our interest were lone-pair ns^2 cation chalcogenides such as Bi_2S_3 and Sb_2S_3, and their $(Sb/Bi)_2S_3$ alloys (with 0, 10, 33, 50, 67, 90, 100 at% Sb content). Here we present the chalcogenides' density of states (DOS) obtained experimentally by energy-resolved electrochemical impedance spectroscopy (ER-EIS). The information from DOS includes (but is not limited to) VBM, CBM, and the energy distribution of defect states - all obtained in several minutes with a simple setup and application technique. The DOS showed good agreement with previously reported DFT calculations, as well as experimental characterization of the chalcogenides using UPS, UV-VIS, and Hall effect measurements. Namely (i) VBM position is at ~ 5 eV; (ii) optical bandgap is of 1.3 eV and 1.7 eV for Bi_2S_3 and Sb_2S_3, respectively; (iii) the major charge carrier density in Bi_2S_3 is of the order of 10^{18} cm^{-1}.

Importantly, DOS from ER-EIS directly provides information on the energy distribution of the defect states in the Bi_2S_3, Sb_2S_3 and their alloys. In Bi_2S_3 only shallow defects at CBM were detected. They might be responsible for the well-known n-type conductivity of Bi_2S_3 [2]. In Sb_2S_3, besides shallow defects, ER-EIS also revealed midgap states.

In the series of $(Sb/Bi)_2S_3$ alloys, a gradual transformation of the intraband gap states was observed, namely with increasing Sb:Bi ratio the pronounced DOS band of shallow defects at CBM disappeared, while a distinct peak of midgap states appeared. A comparison between the defect energy distribution and the microstructure was made by comparing the experimental and DFT DOS.

In summary, by combining ER-EIS and DFT calculations it was possible to reveal the energy distribution of the defect states and their nature in Bi_2S_3, Sb_2S_3 and their alloys, which is crucial for their further application in photovoltaics.

[1] W. Lian, C. Jiang, Y. Yin, R. Tang, G. Li, L. Zhang, B. Che, T. Chen, *Nat Commun* **12** (2021), 3260.

[2] A.C. Glatz, V. F. Meikleham. *J. Electrochem. Soc.* **110** (1963), 1231- 1234.

PHASE DIAGRAM OF CUO MULTIFERROIC INVESTIGATED USING PULSED MAGNETIC FIELDS

Y. Skourski*
Helmholtz-Zentrum Dresden-Rossendorf, Dresden, Germany
*E-mail: skourski@hzdr.de

Despite the technical challenges associated with pulsed magnetic fields, this approach enables a range of powerful experimental techniques.To illustrate this we present our results on the multiferroic material CuO. CuO is unique as the only known binary multiferroic compound, and it stands out with its high transition temperature of 230 K into the multiferroic state. By measuring magnetization, pyrocurrent and ultrasound velocity we constructed comprehensive phase diagram. We show that magnetic fields around 50 T can suppress the helical spin modulation in the multiferroic phase and substantially alter the electric polarization. Just below the spontaneous transition from the commensurate (paraelectric) to the incommensurate (ferroelectric) structure at 213 K, even relatively modest magnetic fields induce a transition to the incommensurate structure, which is then suppressed at higher fields. These results reveal the impressive magnetoelectric properties of CuO, highlighting the potential and versatility of pulsed magnetic fields as a research method.

CRYSTAL STRUCTURE OF $Cu_2Zn(Ge_xSi_{1-x})Se_4$ SOLID SOLUTION: THE KESTERITE TO WURZ-KESTERITE STRUCTURAL PHASE TRANSITION

G. Gurieva[1,*], S. Niedenzu[†], A. Manjon Sanz[2], M. Kirkham[2], S. Schorr[1,3]
[1]*Helmholtz-Zentrum Berlin für Materialien und Energie, Berlin, Germany;*
[2]*Neutron Scattering Division, Oak Ridge National Laboratory, Oak Ridge, USA;*
[3]*Freie Universität Berlin, Institute of Geological Sciences, Berlin, Germany*
[*]E-mail: galina.gurieva@helmholtz-berlin.de

The quaternary semiconductors $Cu_2ZnGeSe_4$ (CZGSe) and $Cu_2ZnSiSe_4$ (CZSiSe) belong to the adamantine compound family, contain only earth abundant, non-toxic elements and have drawn wide attention for their potential applications in many fields. For instance, CZGSe is a promising candidate for top cell absorber layers in multi junction solar cells due to its band gap of 1.5 eV [1]. The band gap can be tuned by anion substitution applying different anion ratios such as in the solid solution $Cu_2ZnGe(S_{1-x}Se_x)_4$. However, due to challenges in controlling the anion ratio, cationic substitution like Ge ↔ Si is considered as an alternative method to perform band gap engineering. Thus CZSiSe, which has a band gap of 2.2 eV [2], is discussed to be of interest as material for nonlinear optics [3].

Experimental and theoretical studies show that CZGSe crystallizes in the kesterite type structure (space group $I\bar{4}$) [4]. It was recently shown by multiple-edge anomalous diffraction method (MEAD) that CZSiSe crystallizes in the monoclinic wurtz-kesterite type structure (space group Pn) [5]. But the difference between wurz-kesterite and previously reported wurz-stannite type structures are very small and are impossible to see in the conventional X-ray diffraction (XRD) patterns. According to our XRD studies, the Si-rich mixed crystals $Cu_2Zn(Ge_xSi_{1-x})Se_4$ with x = 0.1 – 0.37 show the orthorhombic wurtz-stannite type structure (space group P$mn2_1$) (or undistinguishable monoclinic wurz-kesterite type structure), whereas the Ge-rich mixed crystals $Cu_2Zn(Ge_xSi_{1-x})Se_4$ with x = 0.59 – 0.9 show the tetragonal kesterite (space group $I\bar{4}$) or stannite type structure (space group $I\bar{4}2m$), also very unlikely to distinguish by conventional XRD. $Cu_2Zn(Ge_xSi_{1-x})Se_4$ with x = 0.45 – 0.55 show a coexistence of both, the monoclinic and the tetragonal phase [6]. A differentiation of Cu^+, Zn^{2+}, and Ge^{4+} is not possible using only XRD since these cations are isoelectronic and have a similar scattering power for X-rays. However, by using neutron diffraction it is possible, since they show different neutron scattering lengths. Thus, neutron diffraction data allows a detailed structural characterization, which enables the differentiation between the stannite and the kesterite type structure as well as between the wurtz-stannite and wurtz-kesterite structure. We already applied neutron diffraction to distinguish between kesterite and stannite type structure and found out that CZGSe adopts the kesterite type structure [4]. For CZSiSe MEAD shows wurz-kesterite to be the ground state structure [5].

In this study we will present a systematic investigation of the full composition range of $Cu_2Zn(Ge_xSi_{1-x})Se_4$ by powder neutron diffraction, will give insights into the composition dependent structural transition from kesterite to wurtz-kesterite type structure and the variation of structural parameters. The study of the crystal structure, focusing on the effect of the cation distribution, will allow us to determine type and concentration of intrinsic point defects which are crucial since it determines the electronic properties and therefore the functionality of the solid material to a high degree. A better understanding of these materials will lead to an improvement of their characteristics and opens the door to new photovoltaic devices.

[1] Q. Guo et al., *Sol. Energy Mater. Sol. Cells*, **105** (2012) 132
[2] Rosmus et al., *Inorg. Chem.* **53** (2014) 7809−7811
[3] G.-Q. Yao et., *Solid State Ionics*, **24** (1987) 249–252
[4] G. Gurieva et al., *J. Phys. Chem. Solids*, **99** (2016) 100-104
[5] D. Többens et al., *Acta Cryst B.*, (2020). **B76**, 1-9
[6] S. Niedenzu et al., *IEEE* (2018), pp. 3290-3293

ANISOTROPIC MAGNETIC AND TRANSPORT PROPERTIES IN KAGOME MAGNETS

L. Prodan[1,2,*], A. Chmeruk[1], I. G. Filippova[2], L. Chioncel[1], V. Tsurkan[1,2]
[1]*Center for Electronic Correlations and Magnetism, Institute of Physics, University of Augsburg, Augsburg, Germany;*
[2]*Institute of Applied Physics, Moldova State University, Chișinău, Republic of Moldova;*
[3]*Department of Inorganic Polymers, "Petru Poni" Institute of Macromolecular Chemistry, Romanian Academy, Iași, Romania*
[*]E-mail: lilian.prodan@uni-a.de

Correlated kagome magnets, extensively investigated as possible candidates of quantum spin-liquid, have recently been recognized as a versatile platform to investigate the interplay between the topology of the electronic band structure and magnetism [1, 2]. The most prominent topological phenomena recently discovered in materials with kagome structure are the topological superconductivity, anomalous Hall effect (AHE) in antiferromagnets, giant anomalous Hall, Nernst and magneto-optical effects in ferromagnets, and skyrmionic bubbles [3, 4]. Recently, it has been suggested that topological-band effects are also responsible for the giant anisotropy of the longitudinal conductivity and off-diagonal Hall resistivity [5].

Here we report the interplay of magnetocristalline anisotropy (MAE) and charge transport in metallic kagome ferromagnet Fe_3Sn. We revealed large anisotropy of the longitudinal resistivity and anomalous Hall resistivity. Our findings show that the anisotropy ratio of Hall resistivity scales linearly with the magnetocrystalline anisotropy constant (K_u) over a broad temperature range ($2\ K \leq T \geq 300\ K$) (Figure 1(a)), indicating that spin-orbit coupling (SOC) is the underlying mechanism driving both the anisotropic transport properties and the MAE. Material-specific *ab-initio* calculations further demonstrate that the magnetic reconstruction of bands near the Fermi level, induced by the spin-orbit coupling, are responsible for the anisotropic behavior of the Berry curvature (Figure 1(b-c)), and, consequently, for the large anomalous Hall effect in Fe_3Sn.

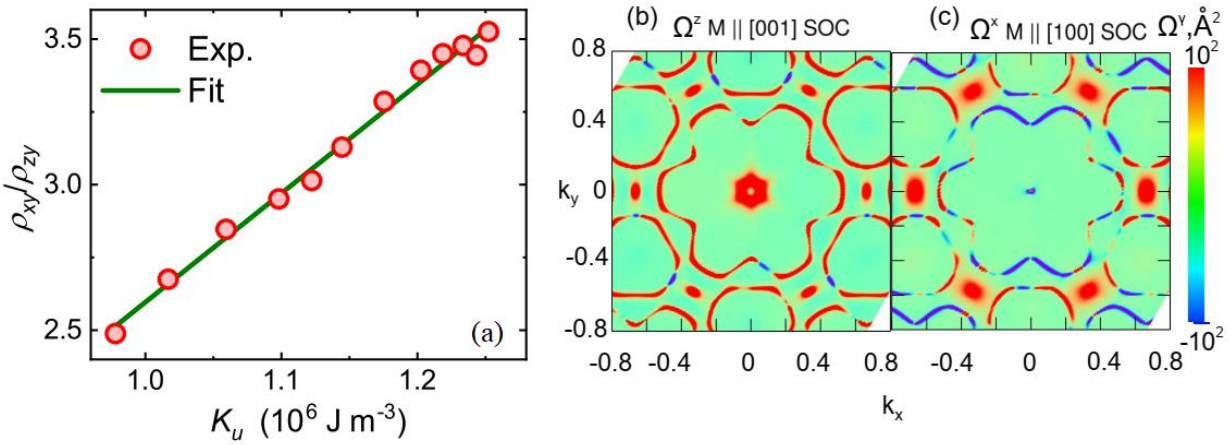

Figure 1. (a) The anisotropy ratio of anomalous Hall resistivity ρ^A_{xy}/ρ^A_{zy} vs uniaxial anisotropy constant Ku. (b) and (c) Calculated Berry curvature for different orientations of magnetization M. Red and blue colors indicate the positive and negative values of the γ-component of the Berry curvature **Ω**γ, respectively.

ACKNOWLEDGEMENTS: This work was supported by the project TRR 360-492547816 and ANCD 20.80009.5007.19.

[1] J.-X. Yin, B. Lian, and M. Z. Hasan, Nature **612** (2022) 647.
[2] L. Prodan, D. M. Evans, S. M. Griffin, et al. Applied Physical Letters **123**, (2023) 10.1063/5.0155295.
[3] M. Altthaler, E. Lysne, E. Roede, L. Prodan, et al. Physical Review Research **3**, (2021) 043191.
[4] F. Schilberth, N. Unglert, L. Prodan, et. al. Physical Review B **106**, (2022) 144404.
[5] H. Huang, L. Zheng, Z. Lin, et al. Phys. Rev. Lett. **128**, 096601 (2022) 096601.

STRUCTURE – PROPERTY RELATIONS OF QUATERNARY ADAMANTINES

Y. Tomm[1,*], G. Gurieva[1], S. Schorr[1,2]
[1]*Helmholtz-Zentrum Berlin, Berlin, Germany;*
[2]*FU Berlin, Institute of Geological Sciences, Berlin, Germany*
[*]E-mail: tomm@helmholtz-berlin.de

The ternary $A^{I}B^{III}X^{VI}_2$ chalcopyrite compound family, which includes the compound semiconductor $Cu(In,Ga)Se_2$ - used as an absorber layer in high-efficiency thin-film solar cells - can be transformed into quaternary adamantines by chemical substitutions while obeying the valence octet rule. Due to added chemical and structural freedom, these quaternary compounds have some novel and exciting properties. One possible substitution would be $A^{I} + B^{III} \leftrightarrow C^{IV} + \square$, resulting in the quaternary semiconductors $A^{I}\square B^{III}C^{IV}X^{VI}_4$ (the symbol $\square$ indicates cation vacancies, i.e., empty cation sites in the crystal structure). These compounds are referred to as defect adamantines [1] and can be considered as potential absorber materials for thin-film solar cell applications.

$A^{I}\square B^{III}C^{IV}X^{VI}_4$ defect adamantines are formed from ternary chalcopyrite-type compounds ($A^{I}B^{III}X^{VI}_2$) by doubling the entire formula unit and replacing one A^{1+} and one B^{3+} cation with one C^{4+} cation. This results in a balanced valency but an unbalanced cation - anion ratio (with respect to the ratio of cation and anion sites in the chalcopyrite-type structure). Accordingly, the structure must be compensated by vacancies ($A^{I} + B^{III} \leftrightarrow$ vacancy + C^{IV}).

Defect adamantines like $Cu\square GaGeS_4$, $Cu\square GaSnS_4$ and $Cu\square AlGeS_4$ can be seen as a compound within the solid solution $(A^{I}B^{III}X^{VI}_2)_{1-x}(C^{IV}X^{VI}_2)_x$ at x = 0.5. These three compounds crystallize in the chalcopyrite type structure which is based on a corner-sharing network of tetrahedra (CuS_4, GaS_4, AlS_4, GeS_4 or $\square S_4$) [2].

$Cu\square GaGeS_4$, $Cu\square GaSnS_4$ and $Cu\square AlGeS_4$ single crystals were grown using the chemical vapor transport technique. The evolved material and the crystals grown were characterized by X-ray diffraction (XRD) at 298K. The diffraction patterns were analysed by a LeBail refinement using the chalcopyrite structure as the structural model. The chemical composition of the crystals was determined by X-ray fluorescence (XRF). The band gap energy of the grown material was determined from diffuse reflectance measured by UV-VIS spectroscopy.

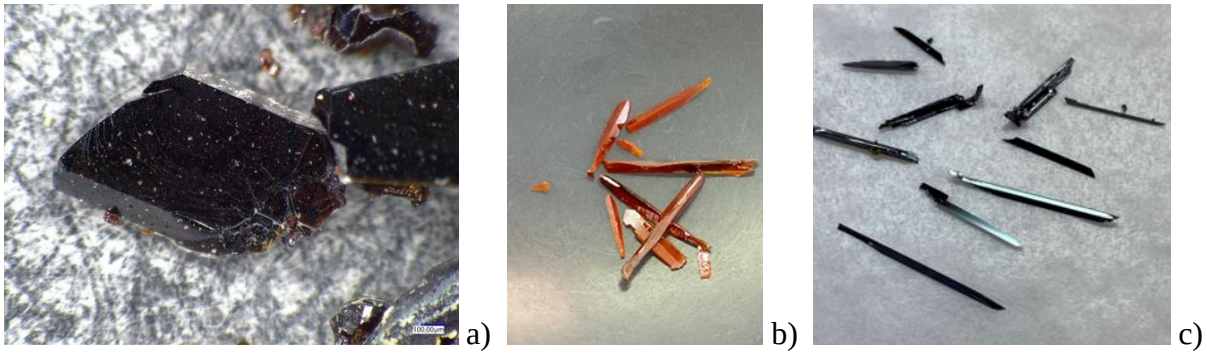
a) b) c)

Figure 1. Single crystals of a) CuAlGeS4, b) CuGaGeS4 and c) $CuGaSnS_4$, grown by chemical vapor transport.

The chemical composition of the grown $Cu\square GaGeS_4$ and $Cu\square AlGeS_4$ crystals was found to vary and deviate significantly from the stoichiometric composition ($A^{I}/(B^{III}+C^{IV}) = C^{IV}/(B^{III}+C^{IV}) = 0.5$). We explain this behaviour by the flexibility of the crystal structure to accept vacancies by keeping the chalcopyrite structure.

Structural and optoelectronic properties were considerably influenced by the cation ratios ($A^{I}/(B^{III}+C^{IV})$ and $C^{IV}/(B^{III}+C^{IV})$, and the number of vacancies.

The band gap energy E_g of the $CuB^{III}C^{IV}X^{VI}_4$ mixed crystals varies between 1.6 and 2.4 eV. Thus, such defect adamantines are interesting materials for photovoltaic applications.

[1] B. Pamplin, *Prog. Cryst. Growth Charact.* **3** (1981) 179–192.
[2] Y. Tomm, D.M. Többens, G. Gurieva, S. Schorr, *Crystals*, **13** (2023) 1545.

HIGH QUANTUM YIELD POLYMER COMPOSITE NANOMATERIAL $[Eu(\mu_2\text{-}OC_2H_5)(btfa)(NO_3)(phen)]_2 \cdot phen/PEPC$

V. Verlan[1], I. Culeac[1,*], V. Ghenea[1,2], I. Bulhac[3], I. Cojocaru[1], M. Enachescu[4]
[1]*Institute of Applied Physics, Moldova State University, Chişinău, Republic of Moldova;*
[2]*Technical University of Moldova, Chişinău, Republic of Moldova;*
[3]*Institute of Chemistry, Moldova State University, Chişinău, Republic of Moldova;*
[4]*Center for Surface Science and Nanotechnology, National University of Science and Technology POLITEHNICA Bucharest, Romania*
[*]E-mail: ion.culeac@ifa.usm.md

Lanthanide complexes possess a number of unique properties, which make them attractive for practical applications in optoelectronics. Particularly, Eu^{3+}-based complexes display strong emission upon UV or blue-light irradiation owing to the sensitization of lanthanide ions by the coordinating ligands. For various applications in optoelectronics there is a need of materials with high thermo-stability and high emission efficiency. One of possible ways to meet these needs is to incorporate the lanthanide complex into a polymer matrix in order to obtain more stable composite material. In the present communication we report a luminescent nanocomposite (NC) made of Eu^{3+}-based coordination compound $[Eu(\mu_2\text{-}OC_2H_5)(btfa)(NO_3)(phen)]_2 \cdot phen$ and an oligomer matrix of poly-N-epoxypropylcarbazole (PEPC). The nanocomposite shows good PL efficiency along with improved thermal stability.

The nanocomposite $[Eu(\mu_2\text{-}OC_2H_5)(btfa)(NO_3)(phen)]_2 \cdot phen/PEPC$ was obtained from chemical solutions at different molar ratios of coordination compound into polymer matrix. Deposition of the nanocomposite films on quartz substrates was performed applying the spin-coating method. Photoluminescence (PL) spectra of the NC (Fig. 1) reveal characteristic atomic-like narrow emission bands associated with internal 4f-4f radiative transitions of Eu^{3+} ion, $^5D_{0,1} \rightarrow {}^7F_J$ (J = 0–4). The excitation spectrum (Fig. 2) contains a broad band (≈ 300–500 nm) related to the matrix, as well as a number of narrow excitation bands, determined by the internal transitions within the Eu^{3+} ion.

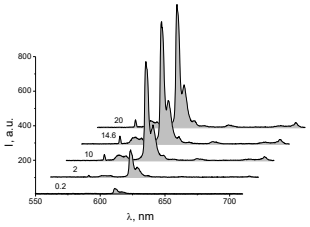

Figure 1. Emission spectra of the of the NC for different concentrations of the Eu^{3+} complex.

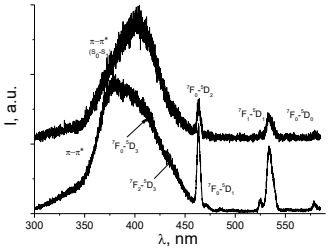

Figure 2. Excitation spectrum of the Eu^{3+} complex (down) and of NC sample 20% (up).

Variation in the PL emission intensity with Eu^{3+} complex concentration shows that PL quenching appears at concentration of about 10%, as expected based on literature data. The broad band in the excitation spectrum of the nanocomposite is shifted to infrared, from ~375 to ~402 nm, compared to coordination compound [1]. The intrinsic quantum yield of the NC, evaluated from PL decay profile, is found to be 32.7%. The radiative parameters of the NC are comparable with corresponding values of the original Eu $^{3+}$ complex [1] and demonstrates a good potential for practical applications.

ACKNOWLEDGEMENTS: This research was funded by the Ministry of Education and Research of the Republic of Moldova (subprograms 011201, 010602).

[1] I.P. Culeac et all. *Nanomaterials* **12**, 2788 (2022).

PHYSICAL PROPERTIES OF CdS/ZnTe HETEROSTRUCTURES

I. Lungu[1,*], T. Potlog[1], V. Suman[2], D. Untila[1], I. Gadiac[2]
[1]*Organic/Inorganic Materials in Optoelectronics, Moldova State University, Chişinău, Republic of Moldova;*
[2]*Doctoral School "Natural Sciences" Moldova State University, Chisinau, Republic of Moldova*
[*]E-mail: ionlungu.usm@gmail.com

CdS/ZnTe heterostructures are studied in materials physics due to their distinct semiconductor properties and potential applications in photovoltaics [1]. Their properties can be adjusted by modifying the layer thicknesses and doping to optimize light absorption and conversion efficiency [2].

In this study, we studied the current transport across CdS/ZnTe heterojunctions fabricated using the CSS method. Transparent front contacts were deposited on glass substrates via DC magnetron sputtering from a ZnO:Al:Cl target. CdS and ZnTe powders, with 4N purity, were purchased from Merck. For synthesizing CdS and ZnTe thin films, we developed the CSS method, selecting deposition temperatures to prevent re-evaporation of the CdS thin films. CdS and ZnTe thin films, with thicknesses of approximately 234 nm and 3.07 μm, respectively, were grown on conductive ZnO substrates, with Ag paste used as the back contact.

We employed conventional current-voltage (I–V) and capacitance-voltage (C-V) measurements, along with impedance spectroscopy, utilizing appropriate equivalent circuit models. The current-voltage (I-V) characteristics in the dark were recorded over a temperature range of 220-350 K. We observed that the barrier height changes from 0.69 eV at 220 K to 1.01 eV at 290 K, while the ideality factor n varied from 20.78 to 10.95, respectively, indicating temperature-dependent inhomogeneity in the barrier height. These changes suggest that different recombination current losses, such as interfacial and bulk recombination, impact the heterostructure's performance. Capacitance-voltage (C-V) measurements at various frequencies (10 kHz, 100 kHz, 1 MHz) showed cyclic variation or hysteresis in the C-V curve. These measurements allowed us to estimate the space charge region thickness, which varied with frequency from 2.16 μm at 10 kHz to 4.33 μm at 1 MHz. Across the temperature range, the built-in potential V_b was around 1.2 V. The acceptor state density (N_A), estimated from the linear slope of C^{-2}=f(V) plots, was $0.81 \cdot 10^{17}$ cm^{-3} at 350 K, $1.22 \cdot 10^{17}$ cm^{-3} at 300 K, and $3.23 \cdot 10^{14}$ cm^{-3} at 220 K. The frequency dependence of the real (Z') and imaginary (Z") components of complex impedance at different AC voltages indicated that Z' and Z" values increased with applied AC voltage at lower frequencies. The capacitance showed a relaxation maximum near 1 kHz, followed by a monotonic decrease with increasing frequency. The loss trend exhibited high values at low frequencies below 1 kHz and high frequencies above 1 MHz, with subunit values in the intermediate region. Nyquist plots revealed bulk and grain boundary effects, with each semicircle representing an RC circuit corresponding to individual material components. For this structure we obtained the following characteristics: an open-circuit voltage (V_{OC}) of 0.84 V, a short-circuit current density (J_{SC}) of 0.25 mA/cm², a fill factor (FF) of 38.6%, and the conversion efficiency (η) of 0.12%.

By analyzing DC current-voltage characteristics and impedance spectroscopy, we investigated the transport mechanism in the respective heterojunction, which exhibits both DC and AC conductivity.

[1] O. Skhouni, A. El Manouni, B. Mari, H. Ullah. *The European Physical Journal Applied Physics* **74(2)** (2016) 24602.
[2] W. Wang, A. Lin, J. Phillips. *Applied Physics Letters* **95(1)** (2009) 011103.

HOPPING CONDUCTIVITY IN $Cu_2Zn_{1-x}Cd_xSnS_4$

V. Batîr[1,*], E. Hajdeu-Chicarosh[1], I. A. Viktorov[3], E. Lähderanta[2],
K. G. Lisunov[1,2], E. Arushanov[1]
[1]*Institute of Applied Physics, Moldova State University, Chișinău, Republic of Moldova;*
[2]*Lappeenranta University of Technology, Lappeenranta, Finland;*
[3]*Scientific and Practical Materials Research Center of NAS of Belarus, Minsk, Belarus*
[*]E-mail: batir.valentin@usm.md

Interest in kesterite-type compounds, such as $Cu_2Zn_{1-x}Cd_xSnS_4$, results from their promising photovoltaic properties. However, their applicability is limited by the high concentration of deep intrinsic defects, mainly Cu_{Zn} antisites [1], which generate a defect acceptor band within the band gap. Incorporating Cd into Cu_2ZnSnS_4 has been proposed as a method to reduce these defects [1].

Here, we investigate resistivity, ρ (T), of the $Cu_2Zn_{1-x}Cd_xSnS_4$ single crystals between x = 0 – 0.7 within a temperature range of T ~ 20 – 300 K. It is worth mentioning, that this compound has been already investigated previously, but using another set of samples within a more narrow interval of x ≈ 0.15 – 0.25 [2]. Other important difference between the two sets of samples is non-stoichiometry of Cu. Namely, our samples has the deficient Cu content of ~ 18 – 22 at. %, whereas samples in Ref. [2] have been characterized by the Cu excess of ~ 26 – 27 at. %.

The resistivity of our samples exhibits an activated character. Inside the intervals of $\Delta T_M \approx$ 139 – 72 K, 95 – 56 K, 135 – 100 K and 110 – 84 K for x = 0, 0.3, 0.5 and 0.7, respectively, it follows the Mott law of the variable-range hopping (VRH), $\ln(\rho T^{-1/4}) \propto (T_0/T)^{1/4}$ [3]. Here, T_0 is the characteristic temperature, T_0 = (1.12, 0.52, 3.42 and 2.53)×10^5 K for x = 0, 0.3, 0.5 and 0.7, respectively. Within $\Delta T_n \approx$ 180 – 225 K, 109 – 151 K, 150 -167 K and 170 – 192 K for x = 0, 0.3, 0.5 and 0,7, respectively, the resistivity obeys the law $\ln(\rho/T) \propto E_a/(k_BT)$ of the nearest-neighbor hopping (NNH) [3], where E_a = 34, 25, 32 and 68 meV is the activation energy, for x = 0, 0.3, 0.5 and 0.7, respectively.

Width of the density of the localized states (DOS), $W \approx$ 32, 20, 41 and 58 meV for x = 0, 0.3, 0.5 and 0.7, respectively, has been found with the VRH data above. In addition, the acceptor concentration, $N/N_c \approx$ 0.59, 0.63, 0.49 and 0.27 (in units of the critical concentration N_c of the metal-insulator transition, MIT) and the ratio of $a/a_0 \approx$ 2.5, 2.7, 2.0 and 1.4, are obtained for x = 0, 0.3, 0.5 and 0.7, respectively, in the rectangular approximation of DOS. Here, a is the localization radius of the holes and a_0 is its value far from the MIT.

It can be seen that $E_a \approx W$ for x = 0 with an error of ~ 5 %, supporting a good NNH regime. For x = 0.3, 0.5 and 0.7, the deviations ~ 15 - 30 % of E_a from W suggest rather a crossover between the VRH and the NNH conduction regimes within ΔT_n. The data of N/N_c ~ 0.59 – 0.63 and a/a_0 ~ 2.5 – 2.7 for our samples between x = 0 – 0.3 are comparable with those of Ref. 2, $N/N_c \approx$ 0.61 – 0.82 and $a/a_0 \approx$ 2.7 – 5.9 (having similar x around 0.2), but lie somewhat lower. Such shift from the MIT in our samples with respect to Ref. [2] can be explained by the deficit of Cu in our samples and excess of Cu in Ref. [2] (see above). This influences generation of Cu_{Zn} defects, responsible for N in the corresponding sets of samples, in an opposite ways. Finally, the average DOS values, g_{av} ~ (0.9 – 1.5)×10^{18} $meV^{-1}cm^{-3}$, evaluated for our samples with x = 0 – 0.3 by taking the value of $N_c \approx 9.4\times10^{18}$ cm^{-3} [2], lie very close to g_{av} ~ (0.6 – 2.4)×10^{18} $meV^{-1}cm^{-3}$ for samples from Ref. [2].

[1] M. He, C. Yan, J. Li, M. P. Suryawanshi, J. Kim, M.A. Green, X. Hao. *Adv. Science* **8** (2021) 2004313.
[2] E. Lähderanta, E. Hajdeu-Chicarosh, V. Kravtsov, M. A. Shakhov, V. N. Stamov, I. V. Bodnar, E. Arushanov, K. G. Lisunov. *New J. Phys.* **24** (2022) 093008.
[3] B. I. Shklovskii & A. L. Efros, Electronic properties of doped semiconductors (Springer, Berlin, 1984).

DE HAAS VAN ALPHEN EFFECT IN TPHREE-DIMENTIONAL DIRAC SEMIMETAL Cd_3As_2 DOPED BY Fe

A. Nateprov[1,*], L. Konopko[2], V. Fritsch[3]
[1]*Institute of Applied Physics, Moldova State University, Chișinău, Republic of Moldova;*
[2]*Technical University of Moldova, D.Ghitu Institute of Electronic Engineering and Nanotechnologies, Chișinău, Republic of Moldova*;
[3]*University of Augsburg, Augsburg, Germany*
[*]E-mail: alexandr.nateprov@ifa.usm.md

Despite a large number of studies devoted to Cd_3As_2, the canonical 3D Dirac material, the effect of iron doping on the properties of that compound has not been investigated so far. This is why the effect of iron impurity on the electrical and magnetic properties of Cd_3As_2 have been investigated for the first time. The unoriented monocrystalline Cd_3As_2:Fe samples were cut from the ingots obtained by the modified Bridgman method. The X-ray phase analysis confirmed the correspondence of the obtained samples to the low-temperature α–phase Cd_3As_2, space group I41cd, with the lattice parameters a=b= 1.2628(13) nm, and c=2.544(5) nm. The energy dispersive analysis (EDA) showed low iron solubility of up to 1 mol% in the studied samples and the presence of small inclusions with more iron. The samples retain metallic conductivity with high electron mobility (μ_H=3.2∗10^4 cm^2/V*sec) at 12 K, ρ_{295}/ρ_{10}=20, with the electron concentration n=2.8*10^{18}cm^{-3}. At the same time, the iron-doped samples are paramagnetic, unlike undoped cadmium arsenide which is diamagnetic [1]. At the temperature dependence of magnetic susceptibility (2-300 K), no signs of a transition to a magnetically ordered state have been established. There was noticed a marked difference in magnetic susceptibility for the case of sample cooling in the presence of a magnetic field (fc) and a zero magnetic field (zfc) in the temperature range studied. This may be due to the influence of inclusions of iron – arsenic compounds in the samples. A slight hysteresis was observed on the dependence of magnetization χ at the low magnetic field B at a temperature of 2 K. In the fields B>2 T, oscillations of magnetization are clearly visible (de Haas van Alphen (dHvA) effect). The oscillation frequencies after a fast Fourier transform found from the dHvA effect were 51.0 T and 54.6 T. The presence of two frequencies in the oscillation spectrum indicates the splitting of the Fermi surface of electrons in the samples studied. The splitting of the Fermi surface of electrons was previously established elsewhere for pure Cd_3As_2 [2]. From the Landau index n plotted against 1/B for the dHvA oscillation, two intercepts at 0.46 and 0.73 were found due to the presence of two frequencies. This result clearly demonstrates a nontrivial Berry's phase in the samples Cd_3As_2 doped by Fe.

[1] A. Pariari, P. Dutta, and P. Mandal, Probing the Fermi surface of three-dimensional Dirac semimetal Cd_3As_2 through the de Haas–van Alphen technique, *Phys. Rev. B* **91**,(2015) 155139
[2] W. Desrat, S. S. Krishtopenko, B. A. Piot, M. Orlita, C. Consejo, S. Ruffenach, W. Knap, A. Nateprov, E. Arushanov, and F. Teppe, Band splitting in Cd_3As_2 measured by magnetotransport, *Phys. Rev. B*,**97**, (2018) p. 245203

CVT SINTERING OF HIGHLY CONDUCTIVE ZnS_xO_{1-x} ALLOYS

G. V. Colibaba[1,*], D. Rusnac[1], N. Spalatu[2]
[1]*Institute of Applied Physics, Moldova State University, Chișinău, Republic of Moldova;*
[2]*Tallinn University of Technology, Tallinn, Estonia*
[*]E-mail: gkolibaba@yandex.ru

ZnO thin films have broad prospects for light-emitting and photoconductive devices, gas sensors, and piezoelectric transducers [1]. ZnS_xO_{1-x} alloys can have special chemical properties and broader application prospect for photovoltaic cells [2]. Magnetron sputtering is a relatively simple and cost-effective method to produce thin films, but ceramic targets with high uniformity and density are required for this technology. Chemical vapor transport (CVT) is used for obtaining bulk oxides and chalcogenides [3, 4]. Recently, this technology has been successfully extended to sintering ZnO ceramics [5]. CVT ZnO ceramic targets are easily doped [6] and can be operated at high magnetron power, contributing to high structural perfection and conductivity of thin films [7]. The development of CVT technology for ZnS_xO_{1-x} ceramics and thin films with controllable electrical properties is of great interest.

The sintering of ZnS_xO_{1-x} alloys (x = 0 – 50 %) by the CVT method using ZnO:Ga + ZnS mixed micropowders and HCl + H_2 as a transport agent has been developed. CVT ceramics were sintered in sealed quartz chambers at 1050 °C for 24 h. For comparative analyses, classical ceramic samples sintered in a vacuum under the same conditions were also obtained. Thin films of the investigated compounds were deposited by DC magnetron sputtering using Ar as the working gas.

The advantages of the proposed sintering method are as follows: (i) low sintering temperature and cost-effective equipment; (ii) the use of simple and cost-effective micropowders as a source of material; (iii) minimal losses of the sintered material, especially chalcogenides; (iv) minimal deviation of the ceramics diameter; (iv) higher density and hardness of the obtained material, larger crystallite size and structural perfection; (v) higher conductivity (by 1–2 orders of magnitude) due to Ga impurity and stoichiometric deviation; (vi) CVT ceramics can be used as targets for high-power magnetron sputtering, increasing the structural perfection of the deposited thin films. The use of ZnS_xO_{1-x} CVT ceramic targets instead of classical targets decreases the resistivity of thin films by 1 order of magnitude to 10^{-3} Ω·cm and promotes an increase in transparency in a visible spectral range to 75 % at x = 0.25.

ACKNOWLEDGEMENTS: This work was supported by the Ministry of Education, Culture and Research of Moldova under the project No. 011201 (Functional 2D and 3D oxychalcogenic materials, metals and polymers with advanced magnetic, photoelectric, optical and bioactive properties for applications in spintronics, optoelectronics and biomedicine) in collaboration with Estonian Research Council projects PSG689 and COST Action project CA21148 (RENEW-PV)

[1] K. Ellmer, A. Klein, B. Rech. *Springer-Verlag Berlin Heidelberg* (2008)
[2] S. Polivtseva et al. *ACS Appl. Energy Mater.* 1 (2018) 6505
[3] G.V. Colibaba. *Journal of Solid State Chemistry* **266** (2018) 166
[4] G.V. Colibaba. *Glass Physics and Chemistry* **48** (2022) 547
[5] G.V. Colibaba, D. Rusnac, N. Costriucova, O. Shikimaka, E.V. Monaico. *J Mater Sci: Mater Electron* **34** (2023) 82
[6] G.V. Colibaba. *Solid State Sciences* **97** (2019) 105944
[7] G.V. Colibaba, D. Rusnac, V. Fedorov, E.I. Monaico. *J Mater Sci: Mater Electron* **32** (2021) 18291

THE EFFECT OF LINE BROADENING ON THE PROPERTIES OF REFRACTIVE INDEX GRATINGS PRODUCED BY E-BEAM RECORDING

S. Sergeev, A. Meshalkin, E. Kanarovskii, I. Cojocaru*
Institute of Applied Physics, Moldova State University, Chişinău, Republic of Moldova
*E-mail: ion.cojocaru@ifa.usm.md

It is well known, that a change of physical and chemical properties occurs in chalcogenide films under electron-beam irradiation. A single line is formed on amorphous As_xS_{1-x} film due to induced increment of refractive index Δn under e-beam irradiation along raster line. The latter has a Gauss distribution of Δn across the line with maximum value Δn_0 (height of Gaussian line profile) along its center region and can be characterized by halfwidth (FWHM) w of Gaussian line profile. A refractive index diffraction grating (DG) is produced by alternate e-beam recording of m lines. The profile of this grating is formed by space modulation of Δn and, in the case of constant grating period Λ, it can be calculated as sum of Gaussian lines:

$$\Delta n(x) = \sum_m \Delta n_0 \cdot \exp\left[-4 \ln 2 \cdot \frac{(x - m\Lambda)^2}{w^2} \right] \qquad (1)$$

Diffraction grating with non-sinusoidal profile may be represented by Fourier transform as a set of sinusoidal subgratings, which determine the diffraction properties of recorded grating, particularly, the first order diffraction efficiency.

The modelling of grating profile (m=5) according to the formula (1) followed by Fourier analysis was used for studying of influence of halfwidth w on the first Fourier harmonic amplitude a_1. In all calculations the Gaussian height value was taken equal to 1. The w value was varied from 0.2 to 0.9 μm, in according with the range value of electron beam diameter which was measured at different electron beam currents and energies as well. Calculations were carried out for grating periods Λ equal to 0.8 μm, 1.0 μm, 1.6 μm and 2.0 μm. The corresponding curves $a_1(w)$ are shown in Fig. 1. The calculated dependences $a_1(w)$ have non-monotonic form with maximum a_1 value, followed by decline section. Increasing of w value causes the overlapping of tails of Gaussian lines. The Δn minimum value of periodic grating profile increases as a result. Due to this effect the decline section on the curve $a_1(w)$ is more pronounced for smaller values of grating period (curves 1 and 2 in Fig. 1). According to calculated curves $a_1(w)$, the maximum value of amplitude a_1 corresponds to w/Λ value approximately equal to 0.4.

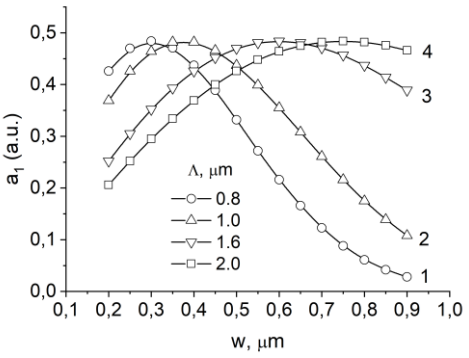

Figure 1. Dependences $a_1(w)$ for different Λ values

For DG with Λ=0.8 μm and Λ=1.0 μm, recorded on amorphous $As_{40}S_{60}$ and $As_{25}S_{75}$ films respectively, the dependences of diffractive index modulation depth n_1 on dose of electron-beam irradiation q were obtained. The n_1 values were obtained from the experimental values of the first order diffraction efficiencies. The course of the curve $n_1(q)$ turned out to be similar to one of the $a_1(w)$. It is reasonable to assume, that the $n_1(q)$ dependence can be explained by the broadening of the region of interaction of the electron beam with the amorphous film with increasing electron irradiation dose. It should be noted, that increasing of Δn_o with q influences the course of the curve $n_1(q)$ as well. Nevertheless, it seems, that the dose broadening of Gaussian line plays the main role.

ACKNOWLEDGEMENTS: This research was funded by the Ministry of Education and Research of the Republic of Moldova (subprogram 011201).

EFFECT OF STOICHIOMETRIC DEVIATION ON PROPERTIES OF ZnO:Ga:Cl THIN FILMS

D. Rusnac[1], M.A. Koltsov[2], N. Spalatu[2], G.V. Colibaba[1,*]
[1]*Institute of Applied Physics, Moldova State University, Chișinău, Republic of Moldova;*
[2]*Tallinn University of Technology, Tallinn, Estonia*
[*]E-mail: gkolibaba@yandex.ru

ZnO thin films have broad prospects [1]. Magnetron sputtering is a relatively simple method to produce these films. Co-doping with III-valence metals and halogens is one of the most promising approaches to achieve high conductivity in ZnO thin films [2, 3]. Recently, chemical vapor transport (CVT) has been proposed as a new sintering method to produce metal-halogen co-doped ZnO ceramic targets [3, 4]. CVT ceramic targets are easily doped [5] and can be operated at high magnetron power, contributing to high structural perfection and conductivity of thin films [6].

ZnO thin films co-doped with Ga and Cl are an object of great interest [6]. To analyze the effect of the interaction between Ga_2O_3, chlorine and Zn during the film growth, we can consider four samples obtained using different targets. The first sample is a film obtained by sputtering of a classical target ZnO:Ga (6 at. % Ga) sintered in air. The (Zn) sample was obtained by sputtering of the same classical target, additionally annealed in an atmosphere of saturated Zn vapor. To obtain the (Cl) sample, the CVT target ZnO:Ga:Cl was obtained using HCl (2 atm) and then annealed in air to remove any Zn excess. Finally, a (Cl+Zn) sample was obtained by sputtering a CVT target with the same level of Ga doping and Zn excess.

For the classical film, the value of resistivity (ρ) is 5.7×10^{-4} Ω·cm and the sheet resistance (R_{sh}) and figure of merit (FM) are about 10 Ω/sq and 15 $k\Omega^{-1}$, respectively. A moderate excess of zinc slightly increases the concentration of current carriers, which may be due to an increase in donor defects such as oxygen vacancies. At a higher stoichiometric deviation due to the partial loss of the main Ga impurity, deterioration in the crystallinity of the films, an increase in ρ to 6.9×10^{-4} Ω·cm, an increase in R_{sh} to 13 Ω/sq and decrease in FM to 13 $k\Omega^{-1}$ are observed.

According to thermodynamic estimates, $ZnCl_2$ vapor interactions with Ga_2O_3 are too weak. Consequently, Cl co-doping does not have a significant effect on the solubility of the main impurity and the value of ρ. On the contrary, at co-doping Cl+Zn, the Ga impurity is better incorporated into the ZnO crystal lattice as donor defects, increasing the concentration of current carriers. It also increases the structural perfection of films and the mobility of free electrons. As a consequence, ρ and R_{sh} decrease by more than 40% to a value of 3.3×10^{-4} Ω·cm and 5.5 Ω/sq, respectively, and FM increases to 21 $k\Omega^{-1}$.

ACKNOWLEDGEMENTS: This work was supported by the Ministry of Education, Culture and Research of Moldova under the project No. 011201 (Functional 2D and 3D oxychalcogenic materials, metals and polymers with advanced magnetic, photoelectric, optical and bioactive properties for applications in spintronics, optoelectronics and biomedicine) in collaboration with Estonian Centre of Excellence project TK141 (TAR16016EK) and COST Action project CA21148 (RENEW-PV)

[1] K. Ellmer, A. Klein, B. Rech. *Springer-Verlag Berlin Heidelberg* (2008)
[2] Fang-Hsing Wang, Chiao-Lu Chang. *Applied Surface Science* **370** (2016**)** 83
[3] G.V. Colibaba et al. *Journal of the European Ceramic Society* **41** (2021) 443
[4] G.V. Colibaba, D. Rusnac, N. Costriucova, O. Shikimaka, E.V. Monaico. *J Mater Sci: Mater Electron* **34** (2023) 82
[5] G.V. Colibaba. *Journal of Solid State Chemistry* **266** (2018) 166
[6] G.V. Colibaba, D. Rusnac, V. Fedorov, E.I. Monaico. *J Mater Sci: Mater Electron* **32** (2021) 18291

EDGE PHOTOLUMINESCENCE OF CdSe SINGLE CRYSTALS IN THE TEMPERATURE RANGE BETWEEN 15 AND 200 K

K. Sushkevich[1], N. Siminel[2], N. Nedeoglo[1,*], A. Siminel[2], T. Iurieva[1], D. Nedeoglo[1]
[1]*Faculty of Physics and Engineering, Moldova State University, Chisinau, Moldova;*
[2]*Institute of Applied Physics, Moldova State University, Chișinău, Republic of Moldova*
[*]E-mail: natalia.nedeoglo@usm.md

Photoluminescence (PL) spectra of CdSe single crystals grown by the Bridgman technique were investigated between 640 nm (1.9375 eV) and 760 nm (1.6316 eV) at temperatures between 15 and 200 K under excitation with laser radiation of 447 nm. The X-ray diffraction (XRD) analysis exhibited a single-phase hexagonal CdSe of high structural quality.

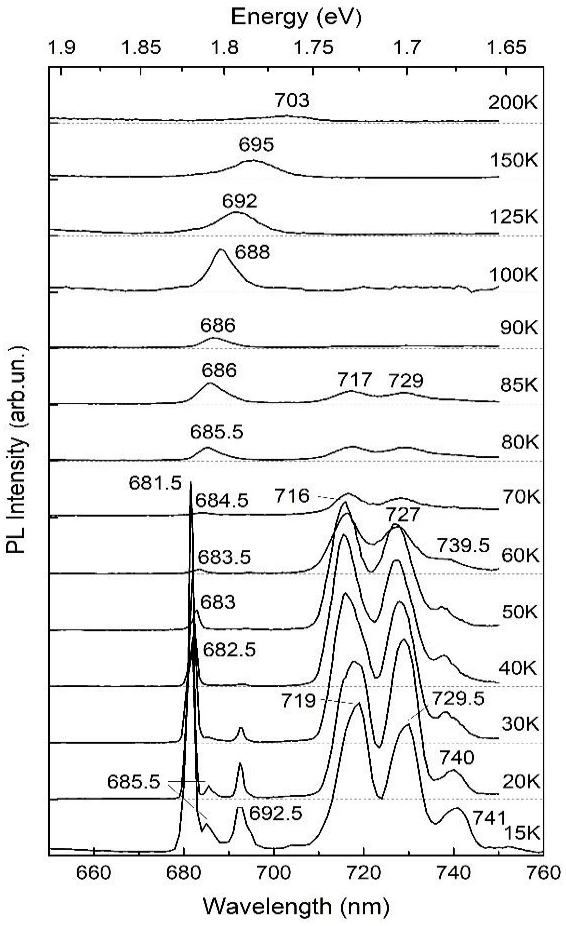

Figure 1. Temperature evolution of the edge PL for CdSe single crystal.

Temperature evolution of PL spectrum for as-grown CdSe single crystal is shown in Fig. 1. At temperature of 15 K, a narrow PL band with full width at half maximum (FWHM) of 3.5 meV is observed at 681.5 nm (1.8195 eV), as well as less intensive bands are found at 685.5 nm (1.8089 eV) and 692.5 nm (1.7906 eV). The long-wavelength region of the spectrum consists of a wide (FWHM is equal to 19.4 meV) PL band with the main maximum at 719 nm (1.7246 eV) accompanied by PL bands at 729.5 nm (1.6998 eV) and 741 nm (1.6734 eV), the distance between the adjacent maxima being 0.0264 eV in both cases.

A narrow short-wavelength PL band is attributed to free exciton annihilation. As the temperature increases, the PL band decreases in intensity, broadens and shifts towards low energies, following the band gap energy variation. The full exciton energy, including the kinetic energy, is weakly dependent on temperature with increasing temperature to 70 K, and then increases linearly up to the value of 38 meV at 200 K.

The long-wavelength PL band with LO-phonon replica is attributed to donor-acceptor pair recombination at low temperatures (below 50 K). The LO-phonon energy is estimated to be (25.6 ± 0.8) meV. As temperature increases, shallow donors become ionized and the PL band is attributed to free-to-bound transitions involving the acceptor level of 117 meV energy depth.

The long-term thermal treatment of CdSe single crystals in Cd + 0.25 mass % $CrCl_3$ melt partially quenches excitonic luminescence and completely quenches the long-wavelength PL bands. At the same time, a new PL band with maximum at 1.9165 eV, the value that exceeds the band gap energy for CdSe, appears. As the PL band position is independent on temperature, it may be attributed to intra-center transtitions within the ions of background impurity, probably Mn.

ACKNOWLEDGEMENTS: This work was carried out in the framework of projects 011207 and 011201 by National Agency for Research and Development of the Republic of Moldova.

Zn-SUBSTITUTION EFFECT IN MULTIFERROIC $Fe_2Mo_3O_8$

L. Prodan[1,2,*], D. Croitori[2], I. G. Filippova[2], M. Roman[2], S. Shova[3], V. Tsurkan[1,2]
[1]*Center for Electronic Correlations and Magnetism, Institute of Physics, University of Augsburg, Augsburg, Germany;*
[2]*Institute of Applied Physics, Moldova State University, Chișinău, Republic of Moldova;*
[3]*Department of Inorganic Polymers, "Petru Poni" Institute of Macromolecular Chemistry, Romanian Academy, Iași, Romania*
[*]E-mail: dorinacroitori@gmail.com

Antiferromagnetic materials hold great promise for the design of ultra-fast and energy-efficient spintronic devices. Therefore, understanding the robustness of crystals, their magnetic structures, and their manipulation is of high importance. Here, we report the effect of site-selective substitution of Zn^{2+} for Fe^{2+} ions on the crystal structure, magnetic and thermodynamic properties of the multiferroic $Fe_2Mo_3O_8$. This compound is known as mineral *kamiokite*, which adopts the hexagonal unit cell of the polar space group $P6_3mc$ with lattice constants a = 5.777 Å and c = 10.057 Å. The Fe^{2+} ions occupy two different positions with tetrahedral and octahedral oxygen coordination forming honeycomb-like layers in the *ab* plane separated by the breathing kagome layers of molybdenum octahedra (Figure 1, left panel). The Mo ions do not contribute to the magnetic properties due to the spin-singlet state of Mo_3O_{13} clusters [1]. Undoped $Fe_2Mo_3O_8$ exhibits a collinear antiferromagnetic (AFM) order of the iron ions below the Néel temperature T_N = 60 K [1].

Our recent study of lightly Zn-doped $Fe_2Mo_3O_8$ has demonstrated the unconventional magnetization reversal in the field-induced ferrimagnetic (FiM) state [2] that motivated further investigations for higher Zn concentrations.

We found the strong preference of Zn to occupy the tetragonal positions for substitution concentrations 0 < x <1.3. This contrasts the previously reported results for related system $Co_{2-x}Zn_xMo_3O_8$ [3] where for low doping regime (x < 0.2) the Zn^{2+} ions occupy the octahedral coordinated sites, although at higher doping level they also show a clear preference for the tetrahedral sites.

Site-selective substitution affects the magnetic phase diagram of $Fe_2Mo_3O_8$ influencing both the intra and inter-layer exchange interactions. This leads to the stabilization of the FiM phase for x > 0.2 and to the decrease of T_C with increasing the Zn content (Figure 1, right panel).

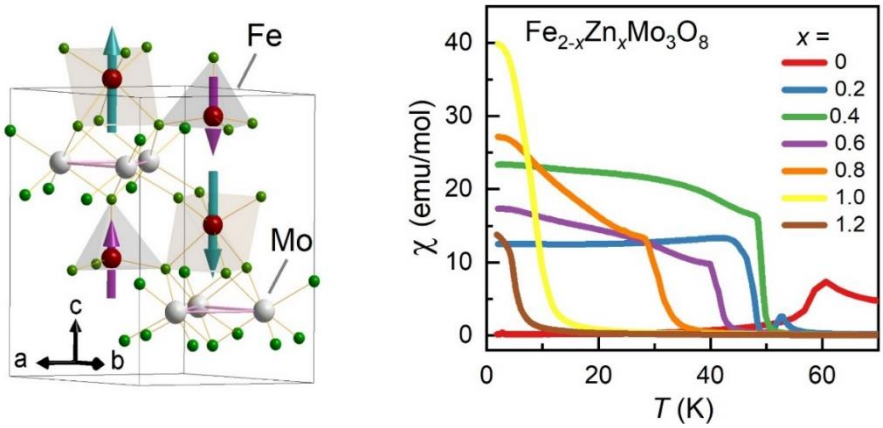

Figure 1. Left panel: Crystal and magnetic structures of $Fe_2Mo_3O_8$. The Fe honeycomb planes are separated by the nonmagnetic Mo_3O_{13} clusters. Right panel: Temperature dependence of the magnetic susceptibility measured in 10 mT applied along the c-axis, revealing the T_N (T_c) transitions for varying Zn content.

ACKNOWLEDGEMENTS: This work was supported by the Young Research Project 23.70105.5007.15T, DFG German Research Foundation TRR 360-492547816, and Project No. ANCD 20.80009.5007.19.

[1] S. Reschke, A. A. Tsirlin, *et.al*. Physical. Rev. B **102**, (2020) 094307.
[2] S. Ghara, E. Barts, *et al*. Nature Communications **14** (2023) 5174.
[3] L. Prodan, I. Filippova, *et al*. Phys Rev **B 106** (2022) 174421.

OPTICAL INVESTIGATION OF THE As-S-Se:Sn THIN FILMS

O. Iaseniuc*, A. Prisacar, V. Verlan
Institute of Applied Physics, Moldova State University, Chișinău, Republic of Moldova
*E-mail: oxana.iaseniuc@ifa.usm.md

Semiconductor chalcogenide alloys based on (Ge, Sn, As) and (S, Se, Te) are still of interest for research due to their physical and optical properties, which change under the influence of external factors (irradiation with light and heating [1]).

The present study is devoted to the As-S-Se:Sn_x (x=1-10%) thin films (thickness d≈1μm) deposited onto a glass substrate. The effect of light irradiation with laser (λ=532 nm, P=140 mW) and UV lamp (λ=254 nm, P=15 W) at the room temperature, as well as heat treatment (t≈100 C°) on the shift of the optical absorption edge of the thin films was investigated.

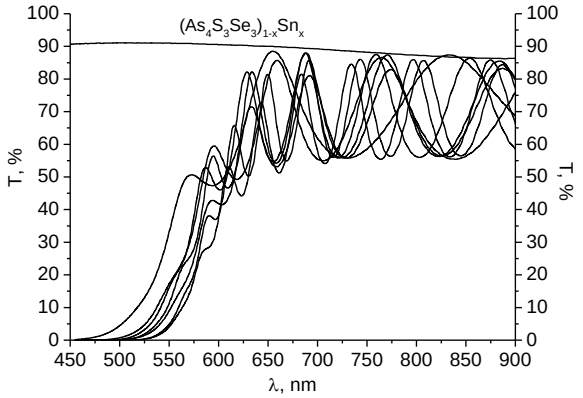

Figure 1. Optical transmission spectra of the As-S-Se:Sn_x (x=1-10%) thin films before light exposure.

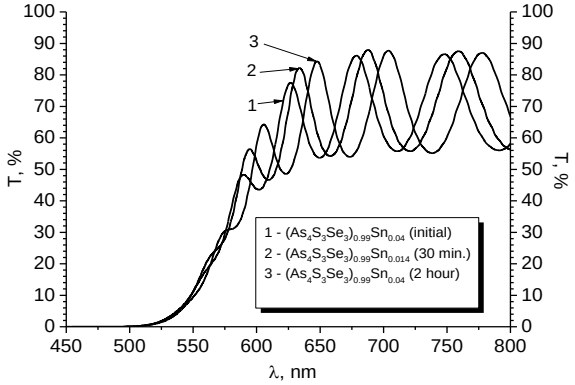

Figure 2. Optical transmission spectra of the $(As_4S_3Se_3)_{0.96}Sn_{0.04}$ thin films before and after light exposure with UV lamp.

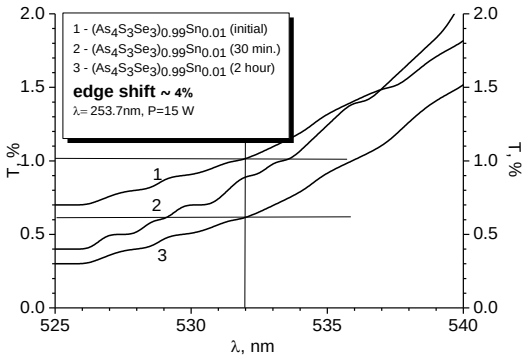

Figure 3. Optical transmission spectra of the $(As_4S_3Se_3)_{0.99}Sn_{0.01}$ thin films at different illumination times (λ=254 nm).

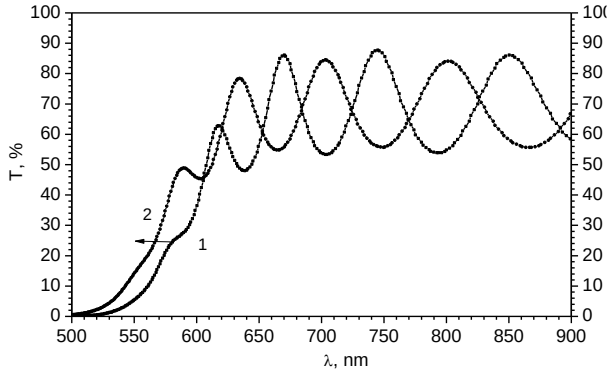

Figure 4. Optical transmission spectra of the $(As_4S_3Se_3)_{0.96}Sn_{0.04}$ thin films after light illumination with Uv lamp (1) and after heat treatment at the glass transition temperature (t≈100 C°).

As a result, the film shows a red shift of the optical absorption edge by ~ 15 nm and at the same time the photodarkening occurs by ~ 10 % at the λ=532 nm which corresponds to the band gap energy of the studied material. According to [1] after light illumination of the film takes place the polymerization reaction: $As_4S_4 + S_n \rightarrow^{h\nu} As_2S_3$. The effect of polymerization leads to a sharp change in the etching rate of the thin film with alkaline solutions [1, 2]. In that case the photo polymerization is considered to be the main mechanism leading to these changes [3].

[1] H. Jain, M. Vlcek, *J. Non-Cryst. Solids* **354** (2005) 1401-1406.
[2] V. Lyubin, *Phys. Status Solidi (b)*, **246 (**2009**)**. 1758-1767.
[3] J.P. De Neufville, S.C.Moss, S.R Ovshinsky, *J. Non-Cryst.* Solids, **13** (1974) 191-223.

LOW-TEMPERATURE CVT SINTERING OF In_2O_3:Sn CERAMICS

D. Rusnac[1], P. Bulimaga[1], E. V. Monaico[2], N. Spalatu[3], G. V. Colibaba[1,*]
[1]*Institute of Applied Physics, Moldova State University, Chișinău, Republic of Moldova;*
[2]*Technical University of Moldova, Chișinău, Republic of Moldova;*
[3]*Tallinn University of Technology, Tallinn, Estonia*
[*]E-mail: gkolibaba@yandex.ru

Highly conductive In_2O_3:Sn (ITO) thin films have broad prospects for light-emitting and photoconductive devices [1]. Magnetron sputtering is a relatively simple and cost-effective method for producing thin films, but this technology requires ceramic targets with high uniformity and density. The classical sintering method of ITO requires very high temperature 1500–1600 °C and special equipment [2]. The chemical vapor transport (CVT) is used for growth of indium oxide crystals at low temperatures [3]. CVT materials are easily doped [3, 4]. Recently, a new ceramic sintering method based on CVT has been proposed for ZnO [5, 6]. The development of CVT technology for ITO ceramics and thin films is of great interest.

The sintering of ITO ceramics ([Sn] = 0, 5, 10 %) by the CVT method using a In_2O_3 + SnO_2 mixed micropowders and Cl_2 as a transport agent has been developed. CVT ceramics were sintered in sealed quartz chambers at 800 °C for 12 h. For comparative analyses, classical ceramic samples sintered in air were also obtained. ITO thin films were deposited by DC magnetron sputtering with Ar as the working gas.

The advantages of the proposed sintering method are as follows: (i) low sintering temperature and cost-effective equipment including quartz as a crucible material; (ii) the use of simple and cost-effective micropowders as a material source; (iii) minimal loss of the sintered material and deviations in diameter of ceramics; (iv) higher density, hardness and conductivity; (vi) CVT ceramics can be used as targets for high-power magnetron sputtering at a current density of 40 mA/cm^2.

The presence of Cl impurity enhances the structural quality of the deposited ITO thin films. At the same, the interaction between residual Cl and the main Sn impurity is relatively weak: co-doping with Cl+Sn does not significant affect the optical and electrical properties of the films. This is explained by the low stoichiometric deviation of the obtained ceramics and low concentration of Sn halides in the thin film growth medium.

ACKNOWLEDGEMENTS: This work was supported by the Ministry of Education, Culture and Research of Moldova under the project No. 011201 (Functional 2D and 3D oxychalcogenic materials, metals and polymers with advanced magnetic, photoelectric, optical and bioactive properties for applications in spintronics, optoelectronics and biomedicine) in collaboration with Estonian Research Council projects PSG689 and COST Action project CA21148 (RENEW-PV)

[1] M. Sawada, M. Higuchi, S. Kondo, H. Saka. Jpn. *J. Appl. Phys.* **40** (2001) 3332
[2] F. Mei, T. Yuan, R. Li, K. Qin. *J Mater Sci: Mater Electron* **28** (2017) 15996
[3] G.V. Colibaba. *Glass Physics and Chemistry* **48** (2022) 547
[4] G.V. Colibaba. *Solid State Sciences* **97** (2019) 105944
[5] G.V. Colibaba et al. *Journal of the European Ceramic Society* **41** (2021) 443
[6] G.V. Colibaba, D. Rusnac, N. Costriucova, O. Shikimaka, E.V. Monaico. *J Mater Sci: Mater Electron* **34** (2023) 82

RAMAN ANALYSIS OF $Cu_2Zn_{1-x}Cd_xGeS_4$ AND $Cu_2CdSn_{1-x}Ge_xS_4$ SOLID SOLUTIONS

V. Batîr[1,*], S. Aazou[2,3], L. Dermenji[1], N. Curmei[1], Z. Sekkat[2,3], E. Arushanov[1], M. Guc[4]
[1]*Institute of Applied Physics, Moldova State University, Chișinău, Republic of Moldova;*
[2]*Department of Chemistry, Faculty of Sciences, Mohammed V University in Rabat, Morocco;*
[3]*Optics and Photonics Center, Moroccan Foundation for Advanced Science & Innovation & Research, MAScIR-University Mohammed VI Polytechnic UM6P, Rabat, Morocco;*
[4]*Catalonia Institute for Energy Research (IREC), Barcelona, Spain;*
[*]E-mail: batir.valentin@usm.md

For further advancement of solar cells based on quaternary compounds, tandem structures are recommended. In these structures, the top cell has a larger band gap, enhancing the spectral sensitivity range of a single-junction solar cell towards higher photon energies. This makes $Cu_2Zn_{1-x}Cd_xGeS_4$ (CZCGS) and $Cu_2CdSn_{1-x}Ge_xS_4$ (CCTGS) solid solutions attractive candidates for such applications. However, a deeper understanding of the fundamental material properties of these compounds is required before estimating their appropriate applications.

In line with this goal, the main aim of the present study is to investigate the vibrational properties of CZCGS and CCTGS solid solutions, and to present Raman spectra for these solid solutions. For this purpose, thin films of above mentioned compounds were obtained by spray pyrolysis deposition in a carbon dioxide atmosphere at temperatures of 270-280 °C. Furthermore, room temperature Raman spectra were measured using 785 nm laser and a LabRam spectrometer from Horiba.

As a result of Raman analysis of the previously mentioned solid solutions, the Cu_2ZnGeS_4 compound showed the highest intensity mode (A mode) at 359 cm^{-1}, which is in good accordance with previously published study [1]. This A mode corresponds to "breathing" of sulfur atoms around Ge, or stretching of Ge-S bonds. For the Cu_2CdGeS_4 compound, the most intense peak was at 357 cm^{-1}, also in accordance with the value reported in literature [2]. Additionally, for Cu_2CdSnS_4, the most intense peak was observed at 334 cm^{-1}, as demonstrated by M. Pilvet et al. [3].

With increasing Cd/(Zn+Cd) ratio in CZCGS solid solutions, the position of main peak shifted to lower wavenumbers (from 359 cm^{-1} to 357 cm^{-1}). Meanwhile with increasing Ge/(Sn+Ge) ratio in CCTGS solid solutions, the position of main peak shifted to higher wavenumbers (from 334 cm^{-1} to 357 cm^{-1}), which is expected behavior taking into account the nature of vibrations of main peak.

Besides, for CZCGS solid solutions, with increasing Cd/(Zn+Cd) ratio, FWHM of the main peak decreases. While for CCTGS solid solutions, with increasing of Ge/(Sn+Ge) ratio, FWHM of the main peak increases.

In addition to primary phase, the secondary phases GeS_2 and GeS were observed in CZCGS solid solutions. Similarly, in CCTGS solid solutions, identified secondary phases included SnS and GeS.

[1] M. Guc, A. P. Litvinchuk, S. Levcenko, M. Ya. Valakh, I. V. Bodnar, V. M. Dzhagan, V. Izquierdo-Roca, E. Arushanov, and A. Pérez-Rodríguez. *RSC Adv.* **6**, (2016) 13278.
[2] J. Krustok, T. Raadik, X. Li, M. Kauk-Kuusik, K. Timmo, S. Oueslati, and M. Grossberg. *J. Phys. D: Appl. Phys.* **53**, (2020) 275102.
[3] M. Pilvet, M. Kauk-Kuusik, M. Grossberg, T. Raadik, V. Mikli, R. Traksmaa, J. Raudoja, K. Timmo, and J. Krustok. *Journal of Alloys and Compounds* **723**, (2017) 820.

THE INFLUENCE OF THE SYNTHESIS ATMOSPHERE ON THE QUALITY OF THIN LAYERS OF $(Ag_xCu_{1-x})_2ZnSnS_4$

L.V. Dermenji[1,*], N.N. Curmei[1], L.I. Bruk[1], M. Franckevičius[2], V. Pakštas[2]
[1]*Institute of Applied Physics, Moldova State University, Chișinău, Republic of Moldova;*
[2]*Center for Physical Sciences and Technology, Vilnius, Lithuania;*
[*]E-mail: lazari.dermenji@ifa.usm.md

The quality of kesterite thin films is determined to a large extent by the optimal technological conditions of production. Selection of unsuitable conditions for obtaining thin films can lead to the formation of structural defects, e.g. antisite defects, bulk defects and secondary phases. These problems are solved by partially reducing Cu, Zn and Sn by substituting Ag, Cd and Ge. We believe that the most appropriate way to reduce defects in thin kesterite layers, given its low toxicity and distribution in the earth's crust, is the partial replacement of Cu by Ag.

Another factor influencing the quality of the thin films is the oxygen present when obtaining the kesterite layers by pyrolysis. The higher the oxygen content in the thin film, the smaller the average grain size. In order to analyze the influence of oxygen on the thin layers, they were obtained using the spray-pyrolysis technique in a volume isolated from the normal atmosphere. This allowed, to obtain two samples of $(Ag_xCu_{1-x})_2ZnSnSnS_4$ thin films with substitution of Cu with 0, 5, 10 and 15 mol % of Ag under different atmospheric conditions. Initially nitrogen (N_2) was used to form the atmosphere. Later it was replaced with carbon dioxide (CO_2) because the density of CO_2 is higher than the density of oxygen and the diffusion of residual oxygen molecules into the synthesis zone is quite difficult. In the second case the samples were obtained in normal air pressure atmosphere and compressed air was used as carrier gas. In both cases the $(Ag_xCu_{1-x})_2ZnSnS_4$ layers were obtained on glass support heated at 315°C, subsequently the obtained layers were heat treated in a similar way at ~520°C for 30 min in sulfur atmosphere.

The Raman spectra obtained for $(Ag_xCu_{1-x})_2ZnSnS_4$, show that the quality of the thin films obtained in CO_2 is higher than in thin films synthesized in ordinary atmosphere. This is observed from the dependence of FWHM on the Ag concentration in the thin films. From which we observe, that the maximum of the Raman spectra, is narrower in the case of the layers synthesized in CO_2 atmosphere with Cu substitution with Ag in the proportion of 5-10%. Cross-sectional analysis of the $(Ag_xCu_{1-x})_2ZnSnS_4$ thin films, produced in air atmosphere, showed that with increasing Ag concentration the size of the crystallites increases, but the space between the crystallites increases and the obtained films become porous. We assume that, the abundant pore density is due to pulse sputtering and this shortcoming can be avoided by continuous deposition of kesterite layers. The ratio of conglomerated crystallites to pore density was found to be most suitable when Cu is substituted with Ag in the proportion of 10% and the thin layers are obtained in CO_2 atmosphere. Substitution of copper with Ag in 0 and 5% proportions contributes almost not at all to crystallite conglomeration, and substitution of copper with silver in 15% proportions leads to the formation of an exaggeratedly high pore density.

Analysis of the $(Ag_xCu_{1-x})_2ZnSnS4$ thin films synthesized in CO_2 atmosphere showed an advantage over the thin films synthesized in ordinary atmosphere. Analysis of the obtained layers using Raman microscopy and scanning electron microscopy suggests that for obtaining higher quality $(Ag_xCu_{1-x})_2ZnSnS_4$ sputter layers it is necessary to obtain them in inert atmosphere and the Cu to Ag substitution should be 5-10%.

ACKNOWLEDGMENTS: This work was supported by NARD through the national project for young researchers 23.70105.5007.14T.

CVT SINTERING OF CONDUCTIVE $Fe_2O_3 \cdot (ZnO)_k$ ALLOYS

G. V. Colibaba[1,*], D. Rusnac[1], V. Fedorov[1], V. Suman[2], D. Topal[1],
E. V. Monaico[2], N. Spalatu[3], A. Sidorenko[2], O. Shikimaka[1]
[1]*Institute of Applied Physics, Moldova State University, Chișinău, Republic of Moldova;*
[2]*Technical University of Moldova, Chișinău, Republic of Moldova;*
[3]*Tallinn University of Technology, Tallinn, Estonia*
[*]E-mail: gkolibaba@yandex.ru

Thin films of $Fe_2O_3 \cdot (ZnO)_k$ alloys have diverse application prospects. Depending on the composition (k), these alloys can have different chemical, electrical and optical properties. For example, the alloy with k = 1 ($ZnFe_2O_4$) has wide applicability for use as chemical sensors [1]. Magnetron sputtering of ceramic targets is a relatively simple and cost-effective method for producing thin films, but this technology requires ceramic targets with high uniformity and density. Recently, a new ceramic sintering method based on chemical vapor transport (CVT) has been developed for ZnO [2, 3]. CVT ZnO ceramic targets are easily doped and can be operated at high magnetron power, promoting to high structural perfection and conductivity of thin films [4, 5].

The sintering of $Fe_2O_3 \cdot (ZnO)_k$ alloys (k = 0.5 – 7) by the CVT method using a HCl + H_2 gas mixture as a transport agent has been developed. Fe_2O_3 + kZnO mixed micropowders were axially compressed (25 MPa) and loaded onto the flat bottom of chambers. Before loading the transport agent, the sintering chamber and the material were purified by annealing in a dynamic vacuum. CVT ceramics were sintered in sealed quartz chambers at 1050 °C for 24 h. For comparative analyses, classical ceramic samples were also sintered in air under the same conditions.

The advantages of the proposed sintering method are the following: (i) low sintering temperature and cost-effective equipment; (ii) the use of simple and cost-effective micropowders as a source of material; (iii) higher density (relative density 91 %) and higher hardness (1.66 GPa) of the obtained ceramics, higher crystallite size (60 mkm) and structural perfection; (iv) high electron conductivity variable in a wide range due to Cl impurity and controllable stoichiometric deviation; (v) CVT ceramics, which have high electrical and thermal conductivity, can be used as targets for high-power magnetron sputtering, increasing the structural perfection of deposited thin films with different chemical composition, electrical and optical properties.

ACKNOWLEDGEMENTS: This work was supported by the Ministry of Education, Culture and Research of Moldova under the projects No. 011201 and 020201 in collaboration with Estonian Research Council projects PSG689 and COST Action project CA21148 (RENEW-PV)

[1] A.C. Ulpe et al. *De Gruyter, Z. Phys. Chem.* (2019)
[2] G.V. Colibaba et al. *Journal of the European Ceramic Society* **41** (2021) 443
[3] G.V. Colibaba, D. Rusnac, N. Costriucova, O. Shikimaka, E.V. Monaico. *J Mater Sci: Mater Electron* **34** (2023) 82
[4] G.V. Colibaba, D. Rusnac, V. Fedorov, E.I. Monaico. *J Mater Sci: Mater Electron* **32** (2021) 18291
[5] G.V. Colibaba. *Solid State Sciences* **97** (2019) 105944

THE STUDY OF DISTRIBUTION OF THULIUM IONS IN CaF_2: TmF_3 CRYSTALS

C. Schörnig[1,*], M. Ștef[1], P Veber[1], D. Vizman[1,2], M. Poienar[2], Gabriel Bușe[2]
[1]*Faculty of Physics, West University of Timisoara, Timisoara, Romania*
[2]*ICAM, West University of Timisoara, Timisoara, Romania*
[*]E-mail: carla.schornig76@e-uvt.ro

Rare-earth doped fluorite crystals are known for their excellent optical properties, making them integral to the majority of solid-state lasers in use today. Specifically, CaF_2 crystals doped with TmF_3 have gained significant attention due to their outstanding spectroscopic properties and potential applications in lasers, amplifiers, and quantum memory devices. The distribution of dopants within these crystals can influence their luminescence properties, making it crucial to understand the segregation coefficient for the laser-active centers in the host material [1].

This study aims to investigate the distribution of Tm^{3+} and Tm^{2+} ions in CaF_2 crystals and determine the segregation coefficient using the optical absorption method.

The crystals were grown in our Crystal Growth Laboratory using the vertical Bridgman method. Crushed CaF_2 optical UV-VIS windows (Crystran Ltd. UK) and supra-pure grade (Merck) TmF_3 were used as raw materials. The resulting crystals, which were colorless and transparent, were grown in a graphite crucible under vacuum (~10^-3 Torr) using a shaped graphite furnace [2]. The obtained crystals were transparent, 10 mm in diameter, and 5-6 cm in length, free of visible inclusions or cracks. The segregation coefficient values obtained indicate high-quality crystals suitable for laser materials.

To study the distribution of the dopant in TmF_3-doped CaF_2 crystals with various concentrations, the segregation coefficient of Thulium(Tm^{3+} and Tm^{2+}) ions was determined [3]. The characteristic segregation coefficients for Tm^{3+} ions are around unity, indicating a relatively homogeneous distribution of Tm^{3+} ions in the studied crystals. For Tm^{2+} ions, the segregation coefficient for the CaF_2:1 mol% TmF_3 crystal is 1.03, suggesting a slightly higher dopant concentration at the beginning of the crystal. In the case of the CaF_2:5 mol% TmF_3 crystal, the segregation coefficient is less than one, indicating that these impurities accumulate towards the end of the crystal.

[1] D.R. Taikar, R.N. Taikar, K.R. Nagde, S.R. Sarve, *Macromol. Symp.* **400** (2021), 2100019
[2] D. Nicoara and I. Nicoara, *Mater. Sci. Eng.* **A 102** L1 (1988)
[3] I. Nicoara, M. Stef, G. Buse, A. Racu, *Journal of Crystal Growth* **547** (2020) 125817

KEYNOTE LECTURES

SYNTHESIS–STRUCTURE–PROPRETIES CORRELATION OF HYDROXYAPATITE BASED BIOCOMPOSITES

O. Shikimaka[1,*], M. Bivol[1], D. Grabco[1], D. Topal[1], C. Pyrtsac[2], A. Prisacaru[1,2], V. Cobzac[3], V. Nacu[3], B. A. Sava[4], M. Dumitru[4], C. Tardei[5], B. G. Sbarcea[5]
[1]*Institute of Applied Physics, Moldova State University, Chișinău, Republic of Moldova*;
[2]*Technical University of Moldova, Chișinău, Republic of Moldova;*
[3]*"Nicolae Testemitanu" State University of Medicine and Pharmacy, Chișinău, Republic of Moldova;*
[4]*National Institute for Laser, Plasma and Radiation Physics, Bucharest, Romania;*
[5]*National Institute for R&D in Electrical Engineering, Bucharest, Romania*
[*]E-mail: olga.shikimaka@ifa.usm.md

Bioceramics based on hydroxyapatite (HA) and bioglass (BG) are of increasing interest due to their potential using in the treatment, regeneration or replacement of bone tissue. In this work, biocomposites based on hydroxyapatite obtained by two different routes - chemical precipitation (HAP) and sol-gel (HAG) - were investigated. The bioglass of an original boro-silico-phosphate composition was introduced into bioceramics in two different proportions of 5 and 10%. In addition, different temperatures covering the range of 1100-1250°C were used for the biocomposites sintering. A comparative analysis of the influence of each of these conditions on the structure, porosity, mechanical behavior (hardness, plasticity, fragility) and biological properties (bioactivity, cell viability) of the composites was performed.

The results showed that HAG-based composites had higher porosity in comparison with HAP ones (Fig 1. a, b). Higher glass content and higher sintering temperature (T_s) promoted the decomposition of the hydroxyapatite into tricalcium phosphate. This in turn influences the mechanical and biological properties [1]. HAP-based composites demonstrated higher hardness and at the same time higher fragility as opposed to HAG-based ones. The optimal T_s was found to be 1200°C and the optimal glass content 5% for better mechanical properties. Concerning the bioactivity, HAG-based composites were more active during the first days of SBF (simulated body fluid) testing due to higher porosity and solubility showing earlier formation of carbonated hydroxyapatite (CHA) layer on its surface (Fig. c). But after longer period of 10-15 days there were no differences between HAP and HAG based composites, both of them showing a dense layer of CHA important for osteoconduction and osteointegration of the implant material. The MTT test of biocompatibility demonstrated 94-99% of cell viability for HAP-based composites and some lower values for HAG ones due to higher dissolution rate inducing an increased ion concentration in the surrounding biological environment.

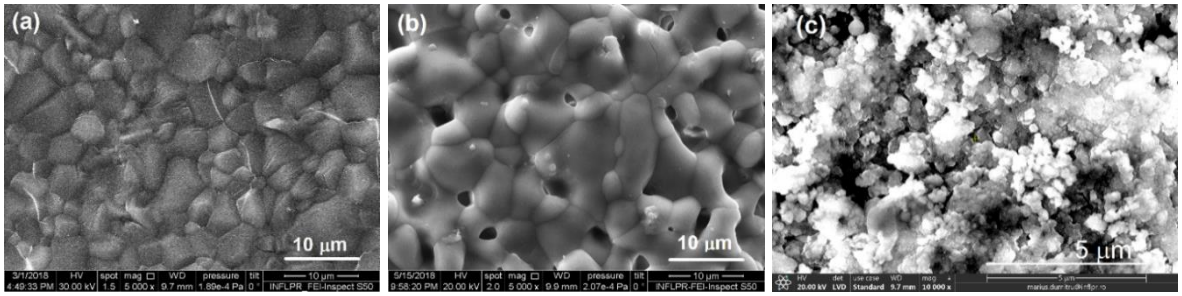

Figure 1. SEM images of HAP (a) and HAG (b) based composites with 5% of BG sintered at 1250°C. HAG-5%BG-1200°C after 3 days of soaking in SBF (c).

[1] O. Shikimaka, M. Bivol, B. A. Sava, M. Dumitru, et al. *Beilstein J. Nanotechnol.* **13** (2022) 1490–1504.

NON MASK E-BEAM LITHOGRAPHY OF TESCAN VEGA FOR DIRECT RECORDING OF DIFFRACTION OPTICAL ELEMENTS: PART 1 – LINES RECORDING

V. Abaskin*, E. Achimova, S. Moldovanu, C. Losmanschii
[1]*Institute of Applied Physics, Moldova State University, Chișinău, Republic of Moldova*
*E-mail: vabaskin48@yahoo.com

In recent years, diffractive optical elements (DOEs) have been widely used for applications to optical disc pickup, array generators, spectrum filtering, wavelength division/multiplexing, and many others. E-beam direct recording of DOE is a more universal method in comparison with holography. For example, free-form optical elements can be created. This technique of DOE recording is based on e-beam scanning and sensitive film. In our presentation, nanomultilayers from As2S3-Se chalcogenide glasses are used. It is very important to emphasize that the use of the above nanomultilayers allows direct obtaining of a relief diffraction element without subsequent etching. Thus, the image resulted by the e-beam recording will remain unchanged, unlike in the etching process. The electron-beam writer TESCAN VEGA with an acceleration voltage of 30 kV and a beam diameter of 3 nm was applied for the line writing of DOE. The dose of the electron beam and backscattering determines the transverse profile of the elementary component of the DOE, which is a line. The e-beam scanning speed will be taken into account. The dependence of line height and its profile from e-beam doze is studied. ASM microscope is used for this purpose. As for DOE working in the vision range of the spectra, the line width must be in diapason 3–6 μm. Lines with a stepped profile in the transverse direction of the line were made.

ESTIMATION OF TWO MODALITIES OF DHM FOR QUANTITATIVE MEASUREMENTS OF MICROSPHERES AS SIZE STANDARDS

V. Abaskin[1], E. Achimova[1,*], A. Prisacar[1], A. Meshalkin[1], M. F. Toy[2]
[1]*Institute of Applied Physics, Moldova State University, Chișinău, Republic of Moldova;*
[2]*Department of Electrical and Electronics Engineering, Istanbul Medipol University, Turkey*
[*]E-mail: eachimova@yahoo.com

Digital Holographic Microscopy (DHM) is a quantitative phase imaging method that relies on optical interferometry to record holograms and numerical reconstruction procedures to retrieve amplitude and phase information from micrometric specimens [1]. DHM provides quantitative information on the complex fields, i.e., amplitude and phase. This is advantageous in the context of real-time live quantitative imaging, digital depth focusing, 3D, and label-free nondestructive imaging. Therefore, DHM has proven to be a powerful metrological tool when non-invasive imaging is desired across various fields and applications: in biology, it has been applied to study cells and tissues; in material science, to study the microstructure and mechanical properties of materials; and in particle analysis in liquids and suspensions, allowing for the determination of particle size, shape, and concentration.

Different DHM schemes have been developed, and significant among them are off-axis and phase-shifting. These DHM configurations can be distinguished depending on the angle between the reference and object beams, the number of recorded holograms, and the numerical reconstruction algorithm. The off-axis configuration enables the reconstruction of the information using a single hologram acquisition [2]. The phase-shifting configuration implies in-line acquisition (the angle value between the reference and object rays is close to 0) of multiple, typically four holograms, with the reference beam phase-shift equal to $\pi/2$ via a retarder [3]. The phase-shifting DHM is offers higher space bandwidth product (larger field of view at the same level of Nyquist-Shannon rate matched optical resolution) compared to its off-axis counterpart, as it employs the entire pixel count along with high-quality reconstruction of the object phase achieved thanks to the twin image and zero-order terms removal, but it requires multiple hologram acquisitions in contrast to the single snap in the off-axis setup. Off-axis DHM, on the other hand, is more robust against the environmental disturbances thanks to its single shot nature, in expense of the reconstructed field's reduced spatial sampling.

In this work, the sizes of 1 and 5 μm of SiO_2 microspheres were studied by two DHM methods to compare the figures of merit of each method. Figure 1 shows the developed phase-shifting and off-axis configurations of the DHM.

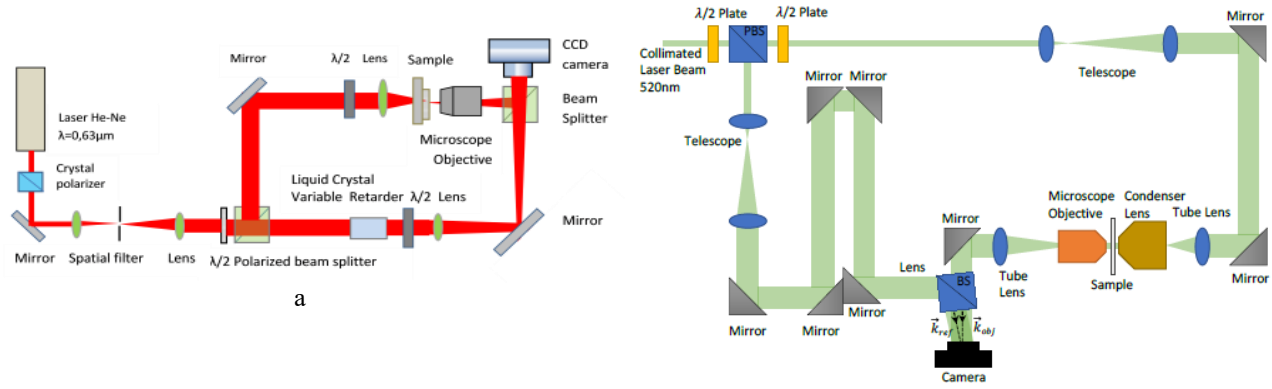

Figure 1. The phase-shifting (a) and off-axis (b) configurations of the DHM.

[1] Kim M. K., Digital Holographic Microscopy: Principles, Techniques and Applications, Springer, 2011.
[2] Sánchez-Ortiga E., Doblas A., Saavedra G. et al, Off-axis digital holographic microscopy: practical design parameters for operating at diffraction limit. J. Applied Optics, 2014, vol. 53, nr. 10, pp. 2058-2066.
[3] Yamaguchi I., Phase-Shifting Digital Holography. In: Digital Holography and Three-Dimensional Display [online]. Boston; Massachusetts: Springer New York, 2006.

CCD

SYNTHESIS AND CHARACTERIZATION OF NEW POLYFUNCTIONAL CONDUCTIVE NANO-SIZED OLIGO AND CO-OLIGOMERS OF 2-METHYL ANILINE AND RESORCINOL

R. Rzayev[1,2,3,*], N. Sucman[1], B.A. Mammadov[2], E. İbadov[2], F. Macaev[1]
[1]*Laboratory of Organic Synthesis, Institute of Chemistry of the Moldova State University, Chișinău, Republic of Moldova;*
[2]*Institute of Polymer Materials, Azerbaijan National Academy of Sciences, Azerbaijan Republic;*
[3]*Department of Chemical Engineering, Baku Engineering University, Baku, Azerbaijan.*
[*]Email: ramilrzayev81@gmail.com

Conductive polymers (CPs), such as polyacetylene, polyaniline (PANI), polypyrrole, polythiophene, and many PANI derivatives, have attracted particular academic and manufacturing interest due to their physical and chemical properties and application opportunities. These polymers possess various valuable physical and chemical properties (exceptional electrical and optical properties, thermal and environmental stability, enhanced conductivity, doping capacity, etc.).

Aromatic amines, especially anilines, and their derivatives have attracted particular academic and manufacturing interest due to their physical and chemical properties and application opportunities.[1, 7] One of the most important derivatives of aromatic amines is 2-methyl aniline (or o-toluidine). Applications range from the use in supercapacitors and secondary batteries, sensors, to corrosion protection.[11] Poly-*o*-toluidine and its copolymers can be prepared by electro-polymerization and oxidative chemical polymerization.

In this regard, nanoparticle polymers of 1,3-benzenediol (1,3-BD) with 2-methylaniline (2-MeAn) were synthesized using potassium persulfate ($K_2S_2O_8$) as an oxidant. Since these combined polymers have a polyfunctional aromatic bonding system that retains amine and hydroxyl groups, their compositions with thermoplastics, epoxy resins, and elastomers have been obtained, and their properties have been studied.

Co-polymers of 2-MeAn with 1,3-BD in nano sizes were synthesized under ultrasonic waves in an HCl medium. Potassium persulfate ($K_2S_2O_8$) has been used as an oxidation agent. The reaction was carried out for 4 hours at a temperature of 273K. Reaction products consist of homo (oligo-1,3-BD and oligo-2-MeAn) and co-oligomers (2-MeAn-co-1,3-BD). The amount of homo and co-oligomers in the reaction products also depends on the mol ratio of oxidizing agent in the single oligomer, the ratio of 2-MeAn:1,3-BD (mol), and the temperature. The obtained copolymer product yields 50 ÷ 70%, depending on the conditions. The element, chemical, and spectral analysis methods determined the composition and structure of the synthesized co-oligomers.

In the FTIR spectrum, the N–H bond stretching vibrations from an aromatic amine were observed at a wavenumber of 3227 cm^{-1}. The stretching vibrations of the C-H bond (2920 cm^{-1}) were detected within the -CH_3 group. We observed prominent peaks within the benzene ring in the 1633 to 1554 cm^{-1} range, attributed to stretching vibrations of benzenoid (C=C) structures. The absorption bands observed in the 1459–1498 cm^{-1} wavenumber range result from stretching the phenol group's C–O-H bond. The UV-Vis spectra showed strong absorption bands at 280 and 435 nm, associated with $\pi \rightarrow \pi^*$ and $n \rightarrow \pi^*$ transitions, respectively. Electron Paramagnetic Resonance (EPR) detected the presence of radicals in the polymer chain and established their position on the nitrogen atom. The XRD analysis has proved the semi-crystalline structure of synthesized oligomers. Furthermore, the micro-morphology (SEM) study revealed that oligomers consist of nano-size fibers (100 – 400 nm).

Additionally, itthermogravimetric analysis was demonstrated that the nanopolymers are thermally stable up to 320°C.

The synthesized compounds are black powder, soluble in polar organic solvents. They exhibit paramagnetic properties and are high-density semiconductors.

DESIGN AND STRUCTURAL CHARACTERIZATION OF MULTINUCLEAR Fe-Ln CLUSTERS BASED ON PIVALATE AND POLYALCOHOL LIGANDS

D. Podgornii*
Institute of Applied Physics, Moldova State University, Chișinău, Republic of Moldova
*E-mail: daniel.podgornii@ifa.usm.md

The development of mixed metal Fe-Ln coordination clusters has become a highly active area of research due to the intriguing magnetic properties that these materials can exhibit, for example such as single molecule magnets (SMMs) behaviour. Among the various strategies for the preparation of Fe-Ln polynuclear clusters, the use of carboxylate and polyalcohol ligands has proved to be one of the most successful. The employment of pivalic acid in the synthesis of heterometallic polynuclear assemblies is driven by the diverse coordination modes exhibited by this ligand and its impact on the topology, size, solubility, and reactivity of the final clusters. Moreover, from a design perspective, the presence of a bulky hydrophobic *tert*-butyl fragment in this ligand may prevent the formation of a polymeric structure and facilitate the formation of discrete assemblies. Polyalcohols also provide multiple coordination sites but assembly the metal ions in another manner, enhancing the stability and functionality of the clusters and represent a variable component for producing different heterometallic clusters with desirable properties. In addition to the chosen ligands our effective strategy for obtaining heterometallic clusters is based on the using of small trinuclear iron cluster as a starting material. The advantages of this approach include the ability to predict and control the atomic arrangement in larger clusters, and the high stability of small assemblies that can be transferred to the larger structures they form. In addition, combining small polynuclear assemblies with other metallic ions and ligands can lead to synergistic effects in the larger clusters, improving their overall properties. The synthesis of a series of tetranuclear $\{Fe_2Ln_2\}$, hexanuclear $\{Fe_4Ln_2\}$, nonanuclear $\{Fe_5Ln_4\}$, and tetracosanuclear $\{Fe_{18}Ln_6\}$ clusters was achieved by employing a trinuclear iron(III) pivalate cluster, $[Fe_3O(piv)_6(H_2O)_3]piv \cdot Hpiv$, in conjunction with lanthanide salts and polyalcohol ligands (Fig. 1). The structural features of the prepared materials will be discussed.

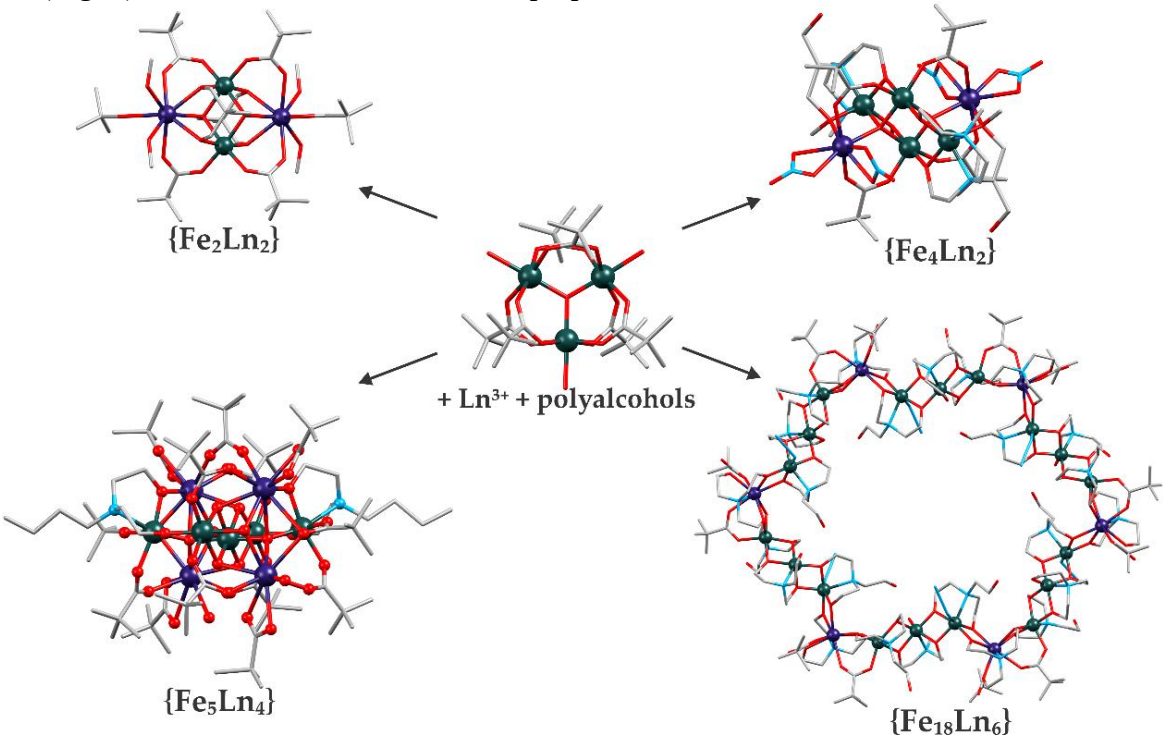

Figure 1. Evolution of nuclearity in the multinuclear Fe-Ln heterometallic coordination clusters.

ACKNOWLEDGMENTS: The author is grateful for the subprogram financed by the Ministry of Education and Research of R. Moldova 011202.

THE KINETICS OF POLARIMETRY OF DIFFRACTION EFFICIENCY OF GRATING RECORDED ON AZOPOLIMERIC NANOCOMPOSITE PEPC-SY3:AUNP

C. Losmanschii*, E. Achimova, V. Abaskin, A. Meshalkin
Institute of Applied Physics, Moldova State University, Chişinău, Moldova
*E-mail: constantin.losmanschii@ifa.usm.md

Azopolymers represent a class of materials that exhibit photoinduced anisotropy, allowing for the direct holographic recording of diffraction gratings with selective polarization [1]. Additionally, doping the polymer matrix with nanoparticles induces changes in the nanocomposite's properties, one of which is the enhancement of photoinduced birefringence, leading to increased diffraction efficiency values [2]. On the other hand, azopolymer nanocomposites demonstrate selectivity towards the probe beam. This behavior can be explained by the formation of chiral structures during illumination with the recording beams [3]. Non-actinic laser light and its different polarization states were used as probe beams.

In this paper, the results of the study on the kinetics of diffraction efficiency and polarimetric parameters, specifically azimuth and ellipticity, are presented. The study was conducted on thin films of the nanocomposite poly-n-epoxypropylcarbazole-Solvent Yellow 3 doped with Au nanoparticles (PEPC-SY3:Au). The PEPC-SY3 nanocomposite thin films were obtained by mechanically mixing AuNP in toluene with the azopolymer PEPC-SY3, with an SY3 concentration of 30 wt%. To understand the influence of nanoparticles on diffraction efficiency and polarimetric parameters, nanoparticle concentrations of 0, 2, 4, 6, 8, and 10 μg/ml were selected. The average thickness of the films is 1 μm ± 10 nm. Diffraction efficiencies and the temporal dependencies of ellipticity and azimuth were obtained through direct holographic recording in polarized beams. The polarization states of the recording beams were selected as PP, ±45°, and LCP:RCP. Additionally, considering that the azopolymeric nanocomposite exhibits photoinduced anisotropy, the control of the I^{st} diffraction order was achieved using the PAX1000 polarimeter with high dynamic range of 70 dB.

The analysis of the maximum diffraction efficiency values in relation to nanoparticle concentration and probe beam polarization indicates that the azopolymeric nanocomposite exhibits pronounced photoanisotropy. Additionally, the analysis of the ellipticity and azimuth curves before, during, and after holographic recording shows changes in the values of azimuth and ellipticity angles, thereby indicating a variation in the refractive index of the azopolymer layer. These changes are a consequence of the periodic structures formed on the surface of the azopolymer film, which induce local variations in the refractive index and photoinduced anisotropy.

In the result, the azimuth of the beam in the first diffraction order is modified. The variation, decrease, or increase in azimuth angles after the completion of holographic recording to values significantly lower than the initial ones can be attributed to the surface azopolymer molecules, where they have sufficient space to isomerize into a thermodynamically favorable isomer. However, as the depth within the polymer structure increases, the azo dye molecules suffer spatial constraints and lacks sufficient space for isomerization.

[1] Meshalkin, Alexei, et al. *Adv. Phys. Res 1* **2** (2019) pp.86-98.
[2] R. Falcione, et al. *Optical Materials* **115 (**2021) p.111015, ISSN 0925-3467,
[3] Lian Nedelchev, et al. *Optics Communications* **461 (**2020) p.125269, ISSN 0030-4018.

EPR STUDIES OF ANTIFERROMAGNETIC EXCHANGE INTERACTION IN A BINUCLEAR COPPER(II) COMPOUND WITH ISOTHIOSEMICARBAZONE

Ion Geru[1,*], Nicolae Gaiu[2], Tudor Jovmir[1], Vasile Lozan[1]
[1]*Institute of Chemistry, Moldova State University, Chișinău, Republic of Moldova;*
[2] *Department of Theoretical Physics, Moldova State University, Chișinău, Republic of Moldova*
[*]E-mail: iongeru@gmail.com

Earlier it has been found an antiferromagnetic interaction between copper centers in the complex $Cu_2(H_2L)Cl_3 \cdot H_2O$ (**1**), where L stands for the mono deprotonated bis-isothiosemicarbazone of 2,6-diformyl-4-methylphenol [1] (Fig. 1).

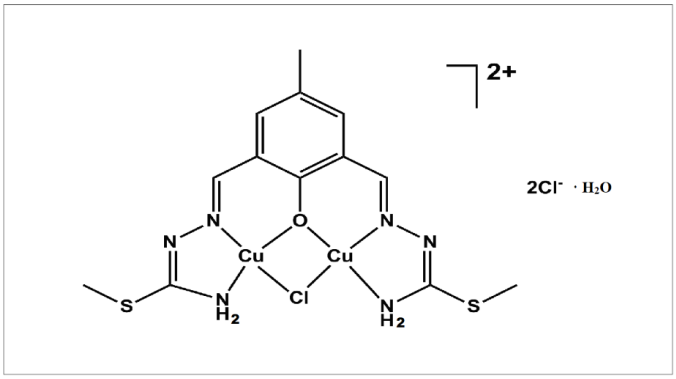

Figure 1. Molecular structure of the compound **1**.

In this work, we are studying the EPR spectrum of the compound **1** at a temperature of 300 K. In the absence of a magnetic field, the ground state of the dimer formed by ions with spin $S_1 = S_2 = 1/2$ is the singlet state (S= 0). Despite this, the EPR spectrum can be recorded at T=300 K since the thermal energy of 210 cm^{-1} exceed the singlet-triplet splitting (148 ± 1) cm^{-1} [1]. The EPR spectrum contains one asymmetric line with g = 4.34 ± 0.02 and a group of seven lines of hyperfine structure (Fig 2), the g-factor of the central component of which is g = 2.006 ± 0.001. The hyperfine interaction constant is A = (126.9 ± 0.2) •10^{-4} cm^{-1}.

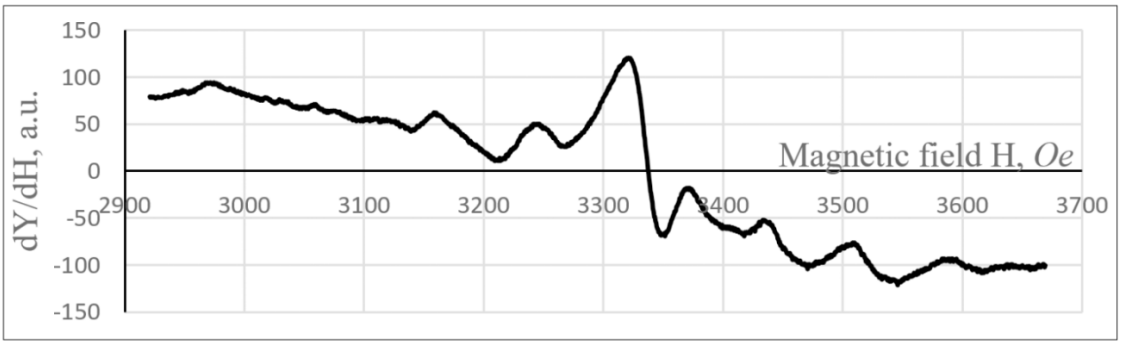

Figure 2. Hyperfine structure of the EPR spectrum of binuclear clusters containing Cu(II) ions in coordination compound **1** at T= 300 K.

The seven components of the hyperfine structure of the EPR spectrum indicate an intradimer antiferromagnetic exchange interaction in the compound 1.

[1]. N.V. Gerbeleu, M.D. Revenco, T.C. Jovmir. *J. Inorg. Chem.* **21** (1986) 2017-2022.

HUMAN CARBONIC ANHYDRASE II – A NEW TOOL FOR THE SYNTHESIS OF VALUABLE ORGANIC MATERIALS

L.-E. Barabás*, C. Paizs, M. Toșa
Babeş-Bolyai University, Faculty of Chemistry and Chemical Engineering, Enzymology and Applied Biocatalysis Research Center, Cluj-Napoca, Romania
*E-mail: laura.barabas@ubbcluj.ro

In nature, or more precisely in the structure of naturally occurring substances, vicinal diol motifs can be found in the most diverse forms (one of the most striking examples is the group of alkaloids). And, of course, nature is true to itself, and among these natural products, the stereochemistry of the 1,2-diol motif deserves more attention. Given the stereospecificity of these compounds and the processes occurring in nature, it is not surprising that these vicinal diols can be associated with biological activity. However, these *anti*- or *syn*-1,2-diols can also be important intermediates for a number of industrially relevant products, as the hydroxyl group is a relatively easily substitutable substituent.

We present here a new enzymatic procedure for the synthesis of enantiopure *anti*- and *syn*-1,2-diols from 1-phenylpropane-1,2-diones mediated by human carbonic anhydrase II in the presence of phenylsilane as hydride donor. The reduction biotransformation reactions were also performed in the case of enantiomerically pure 1-hydroxy-1-phenylpropan-2-one and 2-hydroxy-1-phenylpropan-1-one, which were also enzymatically synthesized using AK lipase.

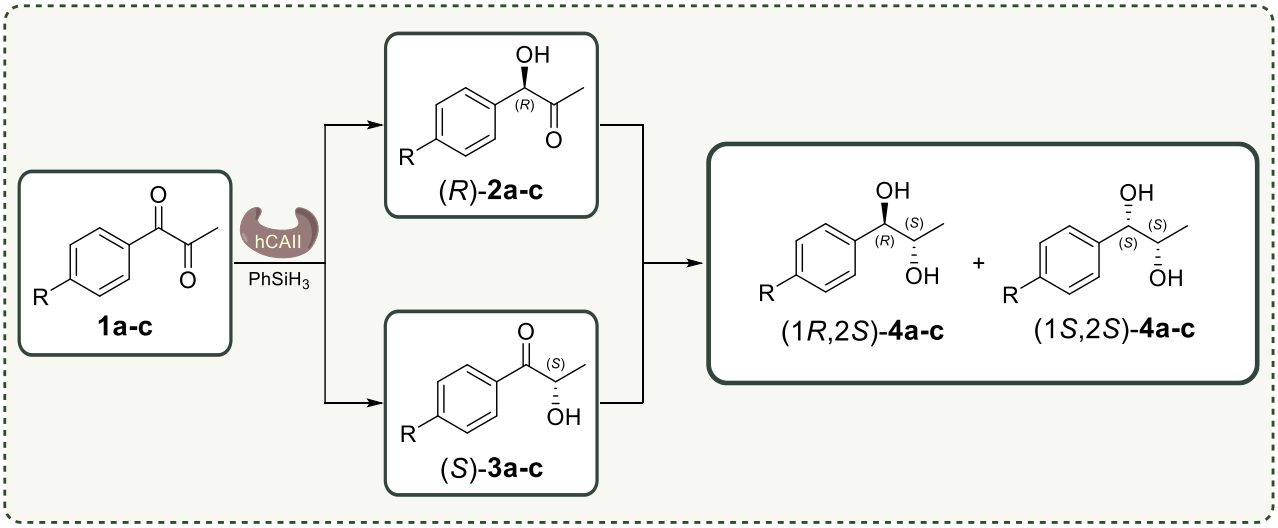

Figure 2: Synthesis of (S)-1-hydroxy-1-phenylpropan-2-one and (R)-1-hydroxy-1-phenylpropan-2-one

The developed detection methods used to identify and characterize the formed diols are also presented.

ACKNOWLEDGEMENTS: This work was supported by PNRR-III-C9-2022-I8-ASPIRE/PNRR2022, through the Romanian Ministry of Research, Innovation and Digitalization, within Component 9, Investment I8.

[1] J. Pengfei, P. Jeeyoung, G. Yang, S. C. Douglas, F. H. John, *Nature Chemistry* **13** (2021) 312–318.

HETEROMETALLIC TETRANUCLEAR {Co(III)$_2$Ln(III)$_2$} COORDINATION COMPLEXES BASED ON PIVALATE AND *N*-BUTYLDIETHANOLAMINE LIGANDS

E. Beleaev*, V. Ch. Kravtsov, S. G. Baca
Institute of Applied Physics, Moldova State University, Chișinău, Republic of Moldova
*E-mail: ecaterina.beleaev@ifa.usm.md

Polynuclear heterometallic 3d-4f complexes are of great interest due to their diverse structures and fascinating properties that make them attractive for applications as catalytic, magnetic, porous and conductive materials. These properties depend on the nature of the metal ions involved and the ligands attached to the metals, as well as the configuration of the compounds, so the design and synthesis of new compounds with a novel metal skeleton is of great importance. A series of five heterometallic tetranuclear cluster compounds with the general formula $[Co_2Ln_2(\mu_3\text{-}OCH_3)_2(piv)_4(bdea)_2(NO_3)_2]$ (Ln = Dy (**1**), Ho (**2**), Nd (**3**), Er (**4**), and Yb (**5**)) were prepared by ultrasonic treatment of cobalt(II) pivalate (Hpiv = pivalic acid) with $Ln(NO_3)_3{\cdot}xH_2O$ and *N*-butyldiethanolamine (H_2bdea) in CH_3OH. X-ray structural analysis shows that compounds **1**-**5** are isomorphic and isostructurally identical and crystallise in the monoclinic space group $P2_1/n$. The compounds contain a tetranuclear heterometallic $\{Co_2Ln_2(\mu_3\text{-}OCH_3)_2\}^{10+}$ core with "butterfly" topology in which two Ln(III) ions acting as "body atoms" and two Co(III) ions acting as "wing atoms" are connected by two bridging μ_3-OCH_3 groups. The clusters are located on the inversion center, thus having C_i molecular symmetry, and all metal atoms are in a common plane. Peripheral binding of the metal atoms are provided by two bdea2 and four piv ligands. Two NO_3 groups are coordinated to lanthanide atoms in chelate mode, completing the triangular dodecahedral O_8 coordination sphere of the Ln(III) ions, while the cobalt atom resides in an octahedral N_1O_5 environment (Fig. 1a). Hirshfeld surface analysis and fingerprint plots were used to decipher the intermolecular interactions in **1**-**5** (Fig. 1b) and to assess the fine differences in the intermolecular interactions due to the different Ln(III) centres.

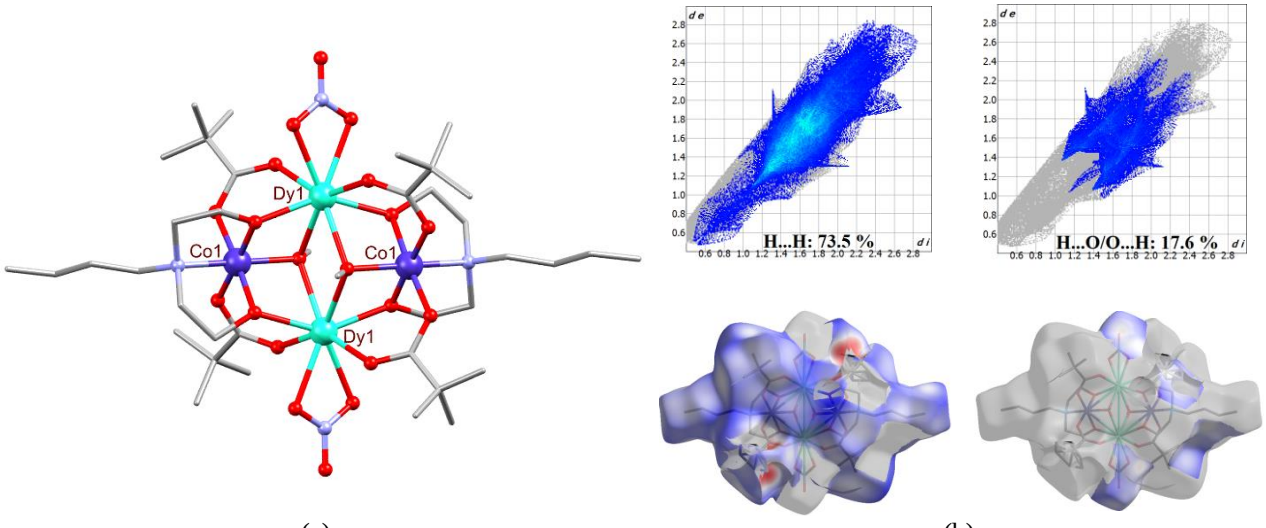

(a) (b)

Figure 1. (a) Structure of the $[Co_2^{III}Dy_2^{III}(\mu_3\text{-}OCH_3)_2(NO_3)_2(piv)_4(bdea)_2]$ (**1**) cluster; (b) HS analysis over d_{norm} and 2D fingerprint plots in **1**.

ACKNOWLEDGMENTS: The authors are grateful for the subprogram financed by the Ministry of Education and Research of R. Moldova 011202.

DINUCLEAR Co(II) COMPLEX WITH PIVALATE AND ISONICOTINAMIDE LIGANDS: SYNTHESIS, CRYSTAL STRUCTURE AND HIRSHFELD SURFACE ANALYSIS

E. Beleaev*, V. Ch. Kravtsov, S. G. Baca
Institute of Applied Physics, Moldova State University, Chișinău, Republic of Moldova
*E-mail: ecaterina.beleaev@ifa.usm.md

The non-covalent interactions, encompassing hydrogen bonding and π-π stacking, exert a profound influence on the structural and compositional properties of coordination compounds, facilitating the design of materials with both predictable structures and desirable properties. A new dinuclear Co(II) compound with the formula $[Co_2(H_2O)(piv)_4(Hpiv)(ina)_2]$ (**1**) (where Hpiv = pivalic acid, ina = isonicotinamide) has been prepared and characterized by X-ray structural analysis. Compound **1** crystalizes in the monoclinic *I2/a* space group, with the unit cell parameters: a = 24.7492(14), b = 11.8842(6), c = 33.3877(19) Å; β = 97.665(5); $\alpha = \gamma$ = 90 º; V = 9732.4(9) Å^3. In **1**, two cobalt atoms (Co1 and Co2) are bridged by a water molecule and two pivalates. The coordination sphere of metal ions is completed by the addition of isonicotinamide and pivalic acid molecules (Fig. 1a). One of the pivalate ligands is coordinated to the Co1 atom in a chelate mode, while the other pivalate and pivalic acid are coordinated to the Co2 atom in monodentate fashion. The pivalic acid participates in the formation of an intramolecular O–H···O hydrogen bond of 2.654(8) Å with the neighboring pivalate. Furthermore, the aforementioned monodentate pivalate forms a strong intramolecular O–H···O hydrogen bond of 2.593(5) Å with the coordinated water molecule. In the crystal the N-H···O and O-H···O hydrogen bonds and π-π stacking interactions unite the **1** in the supramolecular layer parallel to (*bc*) crystallographic plane (Fig. 1b). The theoretical computational analysis of the Hirshfeld surface (HS) and fingerprint plots has been used to analyze the contribution of the different intermolecular interactions, including O–H···O, N–H···O, and π-π stacking, on the stabilization of the crystal structure in **1** (Fig. 1c).

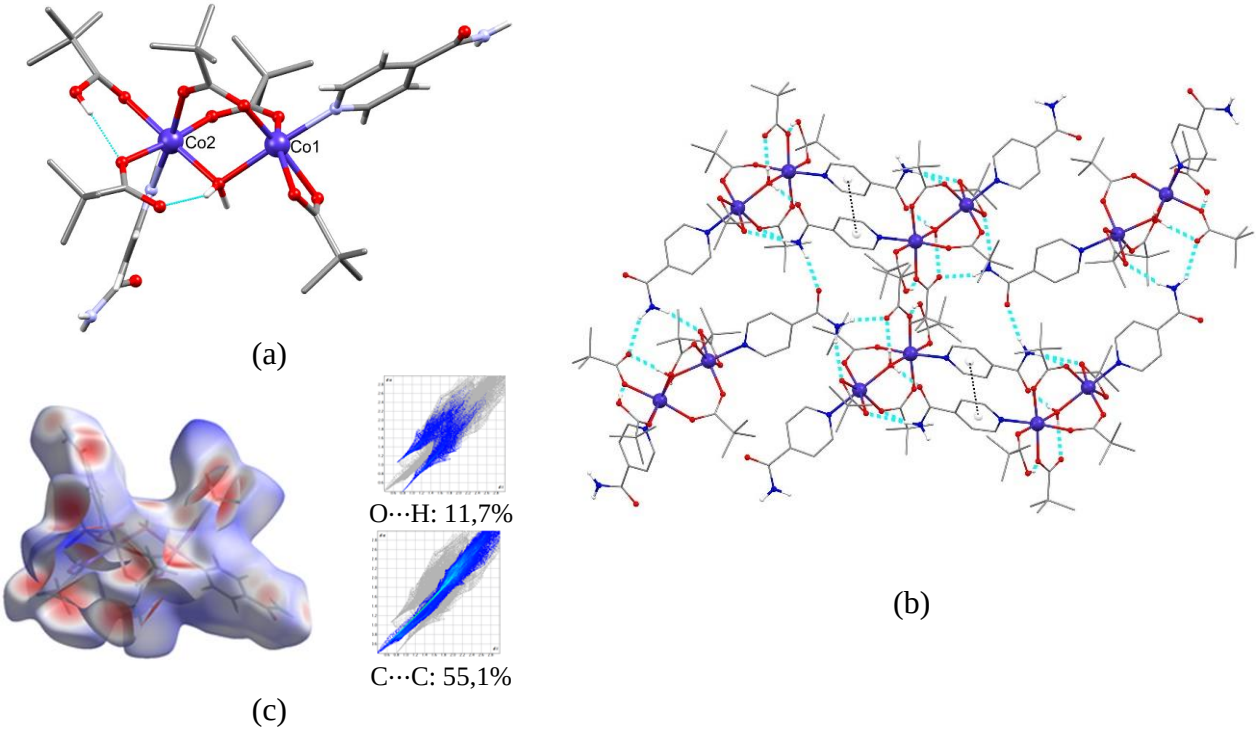

Figure 1. Structure (a), the HS over d_{norm} and 2D fingerprint plots (b), and fragment of crystal packing illustrates the H-bonds patern and π-π stacking interactions in the crystal of **1** (c).

ACKNOWLEDGMENTS: The authors are grateful for the subprogram financed by the Ministry of Education and Research of R. Moldova 011202.

THEORETICAL STUDY OF BINDING ENERGIES IN COMPOUNDS CONTAINING HEXAAMMINECOBALT(III) CATIONS AND AROMATIC SULFONIC ACID DERIVATIVES

E. Beleaev*, Y.M. Chumakov, S. G. Baca
Institute of Applied Physics, Moldova State University, Chișinău, Republic of Moldova
*E-mail: ecaterina.beleaev@ifa.usm.md

In living organisms, cobalt plays a role in the formation or activation of enzymes, vitamins, and hormones, as well as in the regulation of metabolism. In this context, the synthesis and study of new cobalt compounds, which have the theoretical potential to be utilized in the development and investigation of biological systems, are of significance in the advancement of scientific knowledge. As part of our ongoing research on the development of novel innovative multicomponent solids with biological properties [1,2], we present the synthesis of a new series of compounds comprising the $[Co(NH_3)_6]^{3+}$ cation and aromatic sulfonic acid derivatives. The series includes $[Co(NH_3)_6](pys)_3 \cdot Hpys$ (**1**), $[Co(NH_3)_6](pys)_2Cl \cdot 2CH_3CN$ (**2**), $\{K_2[Co(NH_3)_6](4\text{-}sb)_2Cl\}n$ (**3**), $[Co(NH_3)_6](3\text{-}sb)Cl \cdot H_2O$ (**4**), $[Co(NH_3)_6](3\text{-}sb)(SO_4)Cl_2 \cdot 7H_2O$ (**5**), $\{Na[Co(NH_3)_6](3\text{-}sb)Cl_2\}n$ (**6**), and $[Co(NH_3)_6](Hssz)(ssz) \cdot 2H_2O$ (**7**) (where Hpys = 3-pyridinesulfonic acid, H_2sb = 3-/4-sulfobenzoic acid; H_2ssz = sulfasalazine). An energy decomposition analysis of the intermolecular interaction energy (E_{int}) for hydrogen-bonded pairs of complex cations and anions was performed to investigate the non-covalent interactions of $[Co(NH_3)_6]^{3+}$ cations with anions in these compounds **(Fig. 1**). The calculated binding energy for compound **1** was found to be minimal (absolute values of E_{int} decrease in the order E**1**>E**2**>E**7**>E**3**>E**4**>E**6**>E**5**). In selected pairs of **1-2**, the electrostatic term dominates in the calculated binding energy followed by induction interaction, whereas for **3** it is observed the inverse order. In **1**, both the cation and the anion have the potential to influence the biological activity, as indicated by the minimum binding energy observed for the compounds.

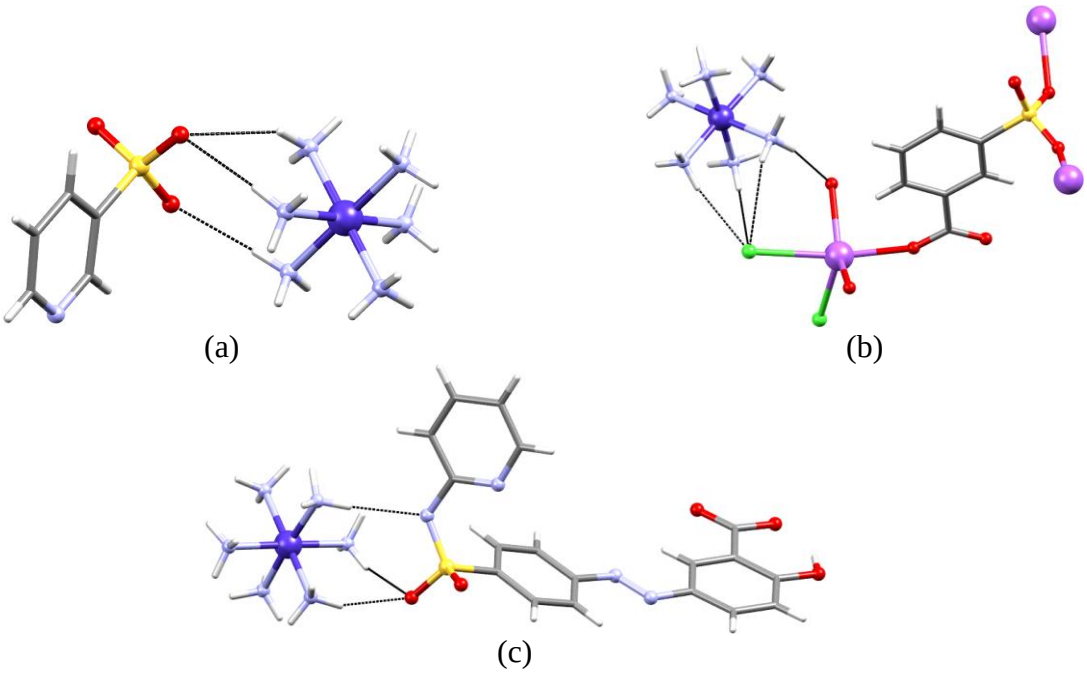

Figure 1. Selected hydrogen-bonded pairs in **2** (a), **6** (b), and **7** (c).

ACKNOWLEDGMENTS: The authors are grateful for the subprogram financed by the Ministry of Education and Research of R. Moldova 011202.

[1] M Darii, E. S. Beleaev, V. C. Kravtsov, P. Bourosh, Y. Chumakov, J. Hauser, S. Decurtins, S.-X. Liu, O. Sultanova, S. G. Baca. *New Journal of Chemistry* **46** (2022) 11404.
[2] S. Baca, O. Sultanova, M. Darii, P. Bouroș. Patent MD 4725 C1, BOPI 06/2021.

SUPRAMOLECULAR ISOMERISM IN Cu(II) PYRAZINECARBOXYLATE COORDINATION COMPOUNDS

O. Capbătut*, V. Ch. Kravtsov, S. G. Baca
Institute of Applied Physics, Moldova State University, Chișinău, Republic of Moldova
*E-mail: olga.capbatut@ifa.usm.md

A plethora of crystalline materials are capable of forming distinct crystalline forms with the objective of reducing the lattice energy under specific thermodynamic conditions. Despite the chemical composition remaining unaltered, there can be notable differences in the physical properties exhibited by polymorphs and supramolecular isomers [1] that result from the assembly of identical components. The formation of different polymorphs and supramolecular isomers is contingent upon a multitude of variables, including the composition of the solvents, the synthetic methodology, the temperature at which crystallization occurs, and the temperature at which cooling occurs, among others.

A new coordination polymer with the structural formula $[Cu(pyca)_2]_n$ (**1**) (where pycaH = pyrazinecarboxylic acid) was obtained and its structural characteristics were elucidated. The compound crystallizes in the monoclinic $P2_1/n$ space group, with the unit cell parameters a = 9.4706(6), b = 7.4120(3), c = 8.0169(5) Å, β = 108.029(5)°, and V = 535.12(4) Å^3. In the crystal the planar $[Cu(pyca)_2]$ monomeric units extended in a two-dimensional coordination polymer structure due to weak coordination of second oxygen atom of the carboxylic group from two neighboring monomeric units resulting in square-bipyramidal coordination polyhedron $[CuN_2O_4]$ (Fig. 1a). The Cu1–O1 and Cu1-N1 distances in the base of bipyramid equal 1.951(2) and 1.977(2) Å, respectively, while Co1–O2 equals to 2.534 Å. This compound represents a novel supramolecular isomer compared to another one documented in the Cambridge Structural Database under the code BEYPUQ [2], where the same monomeric units are linked to a one-dimensional polymer by weaker Cu–O = 2.723 Å coordination bonds (Fig. 1b). In both supramolecular isomers, copper(II) atoms occupy a position in the crystallographic inversion center.

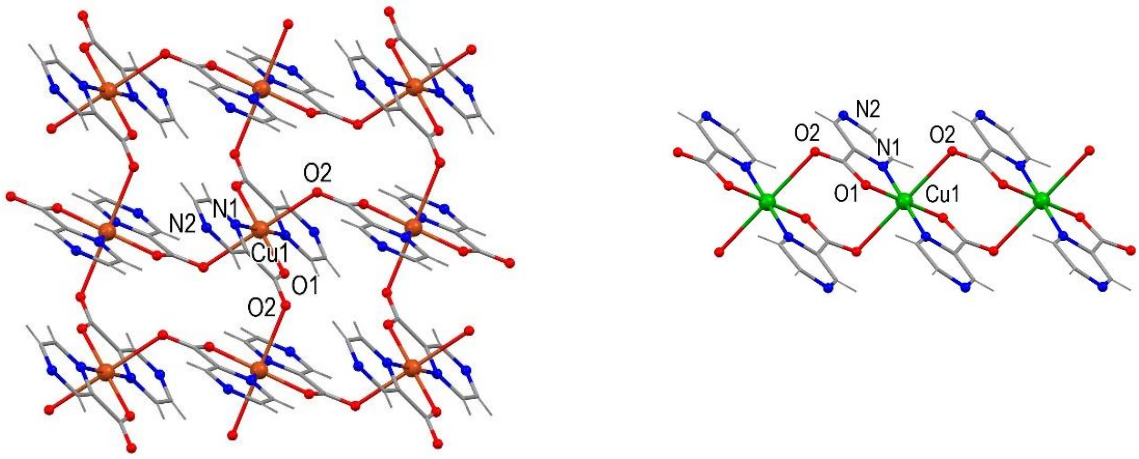

(a) (b)

Figure 1. Crystal structure of the two supramolecular isomers of $[Cu(pyca)_2]_n$: (a) 2D coordination polymer (**1**) and (b) 1D coordination polymer [2].

ACKNOWLEDGMENTS: The authors are grateful for the subprogram financed by the Ministry of Education and Research of R. Moldova 011202.

[1] H. Abourahma, B. Moulton, V. Kravtsov, M. J. Zaworotko, *J. Am. Chem. Soc.* **124** (2002) 9990.
[2] C. L. Klein, R. J. Majeste, L. M. Trefonas, C. J. O'Connor. *Inorg.Chem.* **21** (1982) 1891.

SYNTHESIS OF 4-(3-HYDROXYPHENYL)-3,4-DIHYDROPYRIMIDIN-2-ONES (THIONES) VIA B-CYCLODEXTRIN AND LOW-ESTERIFIED PECTIN CATALYZED APPROACH

N. Gh. Ciobanu*, F. Z. Macaev
Laboratory of Organic Synthesis, Institute of Chemistry, Moldova State University, Chişinău, Republic of Moldova
*E-mail: karakuianat@mail.ru

3,4-Dihydropyrimidin-2-ones (thiones) motifs have gained a great deal of pharmacological interest over the years. There 3-hydroxyphenyl substituted derivatives are present in many biologically active molecules, ranging from naturally antiviral to synthetically produced antineoplasic.

We chose to synthesise the 3,4-dihydropyrimidine containing cycle, which would provide a template for the combinatorial chemistry. We envisaged 4-(3-hydroxyphenyl)-3,4-dihydropyrimidin-2-one (thiones) **1** to be an excellent scaffolds for elaboration, thereby providing a host of derivatised polycycles **2** and 3 as well for biological testing.

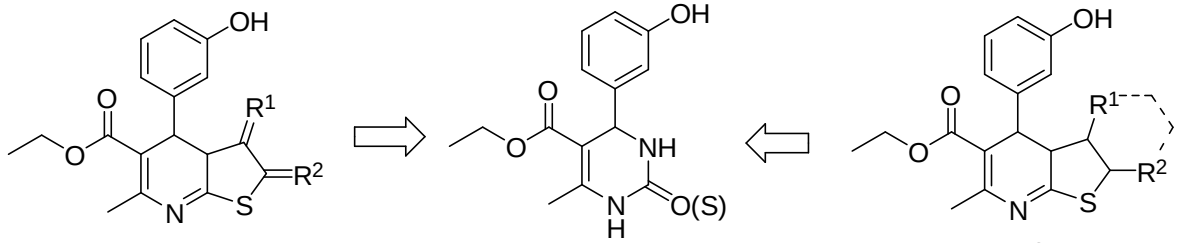

2 **1** **3**

Currently, we are developing conditions for multistep – one pot reaction which allow the selective formation of targets compounds by using β-cyclodextrin and low-esterified pectin as catalysts. This technique from the point of view of "green chemistry" provides quick and efficient access to diverse range of substrates, which are close analogues of Monastrol and Oxymonastrol [1-4]

The advantages of the proposed method are: availability of the reagents used, simplicity of the synthesis method and the method of purifying the final product by crystallization, compliance with the linear relationship of the theoretical principles of green chemistry with practical experience of application, features that allow to get as close as possible to eco-friendly catalytic conditions. The structures of the compounds are confirmed by elemental analysis data, IR and NMR spectral data.

ACKNOWLEDGMENTS: This study was supported by the research subprogram 010601 funded by Ministry of Education and Research of the Republic of Moldova.

[1] Kulakov I.V., Talipov S.A., Shulgau Z.T., Seilkhanov T.M. Synthesis, structure and antiradical activity of new derivatives of methano[1,3]thiazolo-[2,3-d][1,3,5]benzoxadiazocine. Chemistry of heterocyclic compounds, 2014, 10, 1604–1613.
[2] Mayer T.U., Kapoor T. M., Haggarty S. J., King R. W., Schreiber S. L,
Mitchison T. J. Small molecule inhibitor of mitotic spindle bipolarity identified in a phenotype-based screen. Science, 1999, 286, 971.
[3] Macaev F. Green chemistry protocols: specific ionic liquids as recyclable reagents, catalysts, solvents and extractors. Environmental Security Assessment and Management of Obsolete Pesticides in Southeast Europe. SPRINGER Science&Business media, 2013, 313-331.
[4] Kurbanova M. M. Synthesis and intramolecular conversion of substituted 2-methyl-11-nitro-5,6-dihydro-2H-2,6-methanobenzo[g][1,3,5] oxadiazocin-4(3H)-ones in different solvents. Org. Chem., 2010, 46, 599.

SYNTHESIS AND CRYSTAL STRUCTURE OF *BIS[TRIS*(1,10-PHENANTHROLINE)-CADMIUM(II)] TETRAKIS(PERCHLORATE) 4,4'-(ETHANE-1,2-DIYL)DIANILINE ACETONITRILE SOLVATE

N. Craciun[1,*], D. Chisca[2], E. Melnic[1], M.S. Fonari[1]
[1]*Institute of Applied Physics, Moldova State University, Chișinău, Republic of Moldova;*
[2] *"Ion Creangă" State Pedagogical University of Chișinău, Chișinău, Republic of Moldova*
[*]E-mail: nicoleta.craciun@ifa.usm.md

Extending our previous research [1] we synthesised new compound, $[Cd(phen)_3]_2(ClO_4)_4(dadpe)(CH_3CN)$ by reaction of cadmium(II) perchlorate hexahydrate salt with aromatic ditopic ligands, 4,4′-diaminodiphenylethane (dadpe) and 1,10-phenanthroline (phen) in an EtOH/MeCN solvent mixture. The title ionic compound crystallizes in the centrosymmetric triclinic space group *P*-1: *a*= 13.0433(9), *b*= 13.0998(9), *c*= 13.5835(9) Å; α= 89.028(5), β= 75.710(6), γ= 74.084(6)°, *V* = 2159.7 Å^3, Z=1. The crystal is built of mononuclear cations, $[Cd(phen)_3]^{2+}$, perchlorate anions and dadpe and MeCN outersphere molecules. The Cd(II) atom takes an octahedral N_6-coordination geometry from three bidentate-chelate phen ligands, Cd-N distances are in a narrow range, 2.330(6) - 2.379(6) Å. The three-blade propeller shaped Cd(II) cations by two phen blades provide cavities for entrapping dadpe molecules, and by the third blade they participate in the homomeric π-π stacking (Fig. 1). The crystal is stabilised by the interplay of NH...O(ClO_4^-) hydrogen bonds and weak intermolecular interactions.

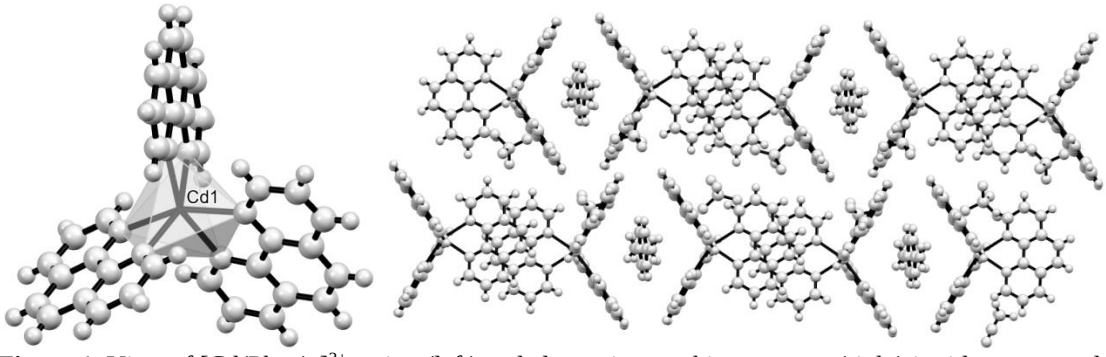

Figure 1. View of $[Cd(Phen)_3]^{2+}$ cation (left) and alternating stacking patterns (right) in title compound.

Competition between 1,10-phen and dadpe resulted in coordination to Cd(II) of phen as a stronger N-base. The architecture of the three-blade cation $[Cd(phen)_3]^{2+}$ resembles $[Cd(2,2'\text{-bpy})_3]^{2+}$ in $[Cd(2,2'\text{-bpy})_3](ClO_4)_2]_2(dadpe)(4,4'\text{-bpy})$ analogue [1].

ACKNOWLEDGMENTS: The authors are grateful for the subprograms financed by the Ministry of Education and Research of R. Moldova 011202.

[1] N. Craciun, D. Chisca, E. Melnic, M.S. Fonari, *Crystals* (2023), **13**, 289.

SYNTHESIS AND CHARACTERISATION OF A NOVEL Cu(II) SEBACATE

O. Cuzan[1,*], V. Gorinchoy[1], S. Shova[2], V. Lozan[1]
[1]*Institute of Chemistry, Moldova State University, Chișinău, Republic of Moldova;*
[2]*"Petru Poni" Institute of Macromolecular Chemistry, Iași, Romania*
[*]E-mail: olesea_cuzan@yahoo.com

Coordination polymers represent a widely investigated class of compounds due to their use as building blocks in polymeric systems and the ability to manifest a broad range of properties such as sorption, catalytic and magnetic properties [1].

The 3D polymer with the composition $[Cu_2(C_{10}H_{16}O_4)_2(C_{12}H_{12}N_2)_2]_n$, where $\{C_{10}H_{16}O_4\}^{2-}$ is the sebacic dianion, and $C_{12}H_{12}N_2$ is 4,4′-dimethyl-2,2′-bipyridine has been synthesized and fully characterized. The compound crystalizes in the triclinic *P*-1 group with the unit cell parameters *a*= 12.4451(5), *b*= 13.6855(6), *c*= 15.5450(6) Å, *α*= 77.513(3), *β*= 70.573(4), *γ*= 88.045(3)°. The Cu(II) ions have a five coordinated geometry provided by two nitrogen atoms from 4,4′-dimethyl-2,2′-bipyridine ligand and three oxygen atoms from three different sebacate dianions, thus generating a N_2O_3 slightly distorted tetragonal pyramid environment (Figure 1). For each Cu(II) atom the Cu-N distances of the pyramid base, where within the range of 0.981-0.999 Å, the Cu-O distances are of 1.935-1.968 Å. The apical position is occupied by the oxygen atom of the monodentate carboxylate group at Cu-O bond distances of 2.256 and 2.275 Å respectively.

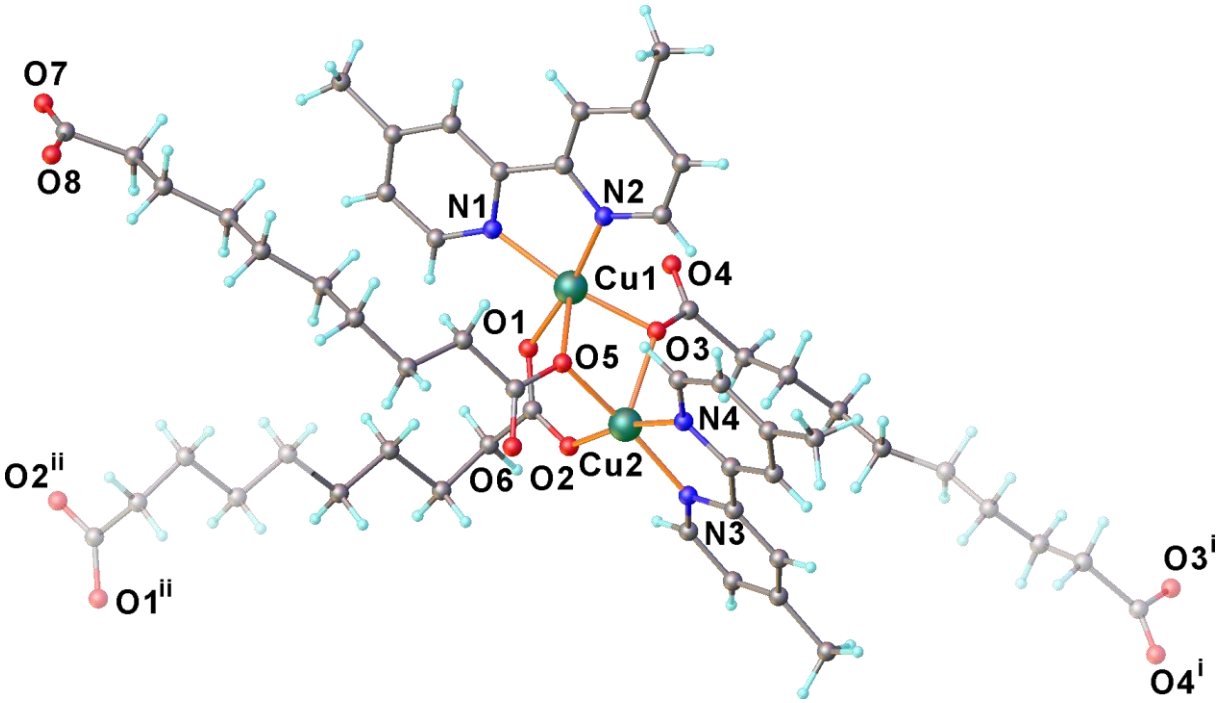

Figure 1. Crystal structure of the compound $[Cu_2(seb)_2(dimetil\text{-}dipy)_2]_n$.

ACKNOWLEDGEMENTS: This work was funded by the research subprogram SSMCCLP (code 010602).

[1] O. Cuzan, S. Shova, G. Novitchi, V. Lozan. *Inorganica Chimica Acta* **553** (2023) 121526.

SYNTHESIS, STRUCTURES AND PROPERTIES OF Fe(III) COMPLEXES WITH DIHYDRAZONE LIGAND

O. Danilescu[1,3], I. Bulhac[1], O. Kulikova[2], Yu. Chumakov[2], M. Cocu[1], P. Bourosh[2]
[1]*Institute of Chemistry, Moldova State University, Chișinău, Republic of Moldova;*
[2]*Institute of Applied Physics, Moldova State University, Chișinău, Republic of Moldova;*
[3]*Technical University of Moldova, Chișinău, Republic of Moldova*
[*]E-mail: olgadanilescu@gmail.com

The pentadentate N_3O_2 Schiff base ligand, H_2L = 2,6-diacetylpyridine bis(picolinoylhydrazone), has been used for the synthesis of two mononuclear iron(III) complexes: $[Fe(H_2L)(H_2O)_2](NO_3)_3{\cdot}2.5H_2O$ (**1**) and $[Fe(H_2L)(H_2O)_2](ClO_4)_3{\cdot}2.5H_2O$ (**2**), which were characterized by IR spectroscopy and X-ray diffraction. The crystal structures of these complexes contain mononuclear cations - $[Fe(H_2L)(H_2O)_2]^{3+}$, NO_3^- /ClO_4^- anions, and water molecules. The Schiff base ligand in both compounds is coordinated in the form of a double zwitterions [1]. It was found that in cation complex of **1** and **2** there are protons transfer from the N atoms of the amide groups to N atoms of the pyridine rings. This migration of protons was confirmed by IR spectroscopy. The band ν(NH), observed in the free ligand at 3324 cm^{-1}, is absent in the IR spectra of complexes **1** and **2.** The broad absorption in the region of 3650-2600 cm^{-1} could be explained by the joining of hydrogen bonds due to their lengths into several groups and the broad bands of weak intensity might be PyH^+ oscillations.

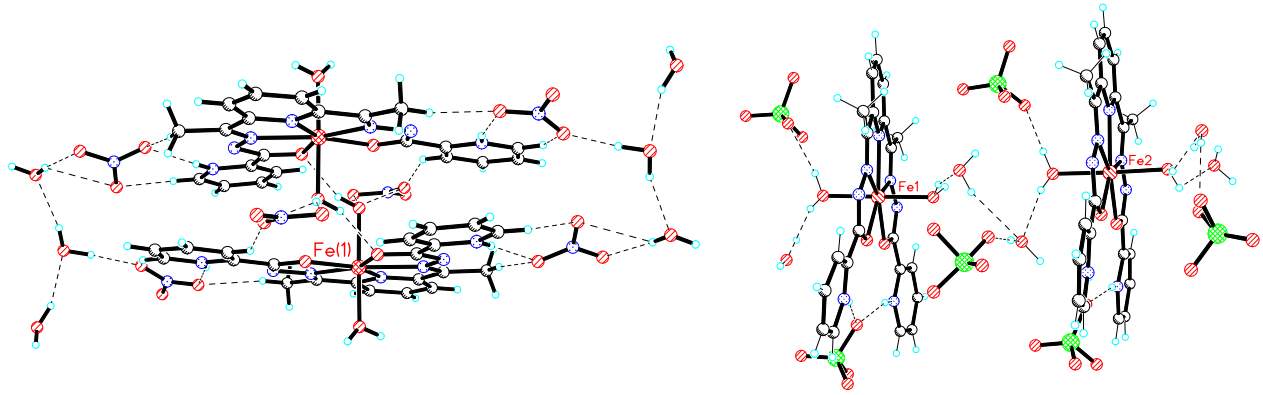

a *b*

Figure 1. Fragments of crystal packings in **1**(a) and **2**(b)

The crystal structures of compounds **1** and **2** are stabilized by hydrogen bonding that give rise to a supramolecular *3D*-networks *via* coordinated and crystallization water molecules, NO_3^- or ClO_4^- anions and NH^+ (PyH^+) (Figure 1).

The hydrogen bond mediated intermolecular magnetic couplings in mononuclear high spin iron(III) Schiff base complexes have been studied by **TB2J** python package used for calculating the magnetic interaction parameters in Heisenberg models from Density Functional Theory [2].

The photoluminescence study was performed on both samples and luminescence excitation was carried out by pulse nitrogen laser (337.1 nm) at a temperature of 300 K. The weak photoluminescence was observed in the 350 - 750 nm spectral range with maxima in the red (1.9 eV), yellow (2.1 eV) and blue (2.6 eV) spectral regions.

ACKNOWLEDGEMENTS: The authors are grateful for the research subprograms 011201, 011202 and 010602, financed by the Ministry of Education and Research of R. Moldova.

[1] O. DANILESCU, I. BULHAC, P.N. BOUROSH, L. CROITOR. Anion-assisted Fe(III)-coordination supramolecular systems based on 2,6-diacetylpyridine dihydrazone. *Polyhedron*. **2022**, volume 215, page 115679.
[2] X. HE, N. HELBIG, M.J. VERSTRAETE, E. BOUSQUET. TB2J: a python package for computing magnetic interaction parameters. *Computer Physics Communications*. **2021**, page 107938.

PHARMACEUTICAL AND NON-LINEAR OPTICAL PROPERTIES OF NEW PHENOTHIAZINYL PORPHYRINS

Emese Gal*, Balazs Brem, Luiza Ioana Gaina
Babes-Bolyai University, Faculty of Chemistry and Chemical Engineering, Cluj-Napoca, Romania
*E-mail: emese.gal@ubbcluj.ro

The systems with extended conjugation are of interest and have therefore been the subject of intensive study recently due to their electronic properties, which have led to applications in material science and medicine. Many of these systems are designed to take advantage of synergistic interactions between fragments and molecules that are already prone to conjugation. As phenothiazines and porphyrins make excellent candidates for extended conjugation systems, in this research work present the synthesis, structural characterization, optical properties and biological activities of some new phenothiazinyl-porphyrin derivatives.

The synthesis of *meso*-cross-coupling products were carried out using A_4-, A_3B- and A_2B_2-type bromo porphyrins and (hetero)aryl boronic acid derivatives. This process leads to functionalized *meso*-phenothiazinyl-porphyrins in high yield, under mild conditions.

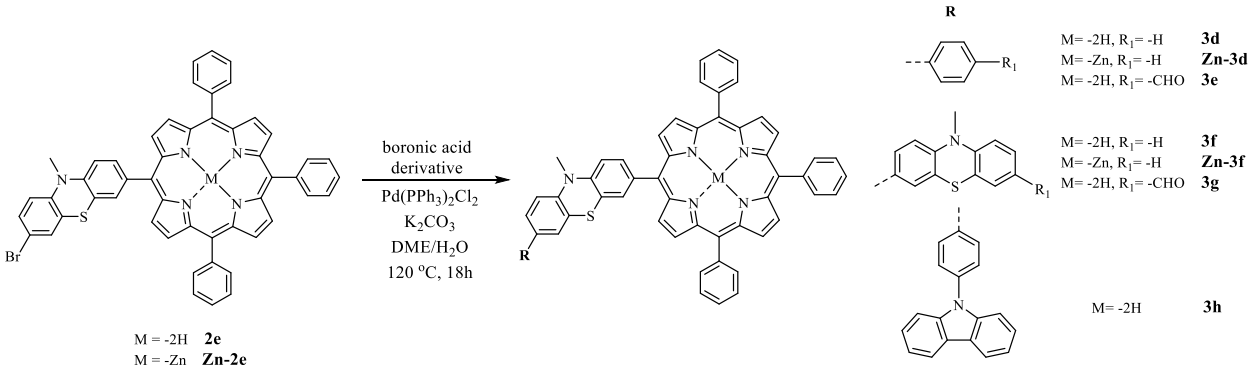

[1] E. Gal, B. Brem, I. Pereteanu, L. Gaina, T. Lovasz, M. Perde-Schrepler, C. Cristea, L. Silaghi-Dumitrescu, *Dyes Pigments*, **2013**, 99, 144.
[2] B. Brem, E. Gal, L. Găină, C. Cristea, A. M. Găbudean, S. Aştilean, L. Silaghi-Dumitrescu, *Dyes Pigments*, **2015**, 123, 386.
[3] E. Molnar, E. Gal, L. Gaina, C. Cristea, E. Fischer-Fodor, M. Perde-Schrepler, P. Achimas-Cadariu, M. Focsan, L. Silaghi-Dumitrescu, *International Journal of Molecular Sciences*, **2020**, 21, 3178.

AMMONIUM HEXAFLUOROSILICATES AS POTENTIAL ANTI-CARIES AGENTS: SYNTHESIS, STRUCTURES, SOLUBILITY, BIOLOGICAL ACTIVITY

V. O. Gelmboldt[1,*], I. O. Shyshkin[1], I. V. Lytvynchuk[1], L. M. Khromagina[2], M. S. Fonari[3], V. Ch. Kravtsov[3]
[1]*Odesa National Medical University, Odesa, Ukraine;*
[2]*Institute of Stomatology and Maxill-Facial Surgery, National Academy of Medical Sciences of Ukraine, Odesa, Ukraine;*
[3]*Institute of Applied Physics, Moldova State University, Chișinău, Republic of Moldova*
[*]E-mail: vgelmboldt@te.net.ua

Ammonium hexafluorosilicates (AHFS) are a class of inorganic compounds widely used in modern technological practice and laboratory research [1, 2]. In recent years, AHFS have been actively studied as promising caries-preventive agents because of their certain advantages over traditional fluoride drugs. In the present communication the synthesis, structural characteristics, properties and biological activity of AHFS with heterocyclic and phenylammonium cations as potential anti-caries agents are discussed.

The crystalline salts with the composition $(LH)_2[SiF_6]$ (L^{1-3} = 2-, 3-, 4-carboxypyridine, **I-III**; L^{4-6} = 2-, 3-, 4-carboxymethylpyridine, **IV-VI**; L^{7-9} = 2-, 3-, 4-carboxyethylpyridine, **VII-IX**; L^{10} = 3-hydroxymethylpyridine, **X** (monohydrate); L^{11} = 4-hydroxymethylpyridine, **XI**; L^{12} = 2-amino-4,6-dihydroxypyrimidine, **XII**) were obtained by the interaction of hexafluorosilicic acid (45 %) with methanol solution of corresponding ammonium chlorides (LH)Cl or free base L. The amorphous salts $(L^{13})[SiF_6]$ (L^{13} = octenidine, **XIII**) and $(LH)_2[SiF_6]$ (L^{14-16} = 2-, 3-, 4-aminophenylacetic acid, **XIV-XVI**; L^{17-19} = 3-(3-aminophenyl)propionic, 3-(4-aminophenyl)propionic, 2-amino-2-phenylbutyric acid, **XVII-XIX**) were obtained in a similar way. All compounds were characterized by elemental analysis, ^1H, ^{19}F NMR, IR, mass-spectrometry, solubility data, and **III-XII** by X-ray crystallography. Based on X-ray diffraction data, interionic H-bonds are the main structure-organizing and stabilizing factor in the formation of structures of AHFS. The involvement of fluoride-ligands of the $[SiF_6]^{2-}$ anion in systems of inter-ionic H-bonds NH···F, H···F, OH···O and CH···F contacts of various strengths leads to a noticeable redistribution of the Si–F bond lengths. Analysis of XRD data allows us to underline the general tendency: as a rule, in the N–H···F–Si structural fragments, the Si–F and N···F distances are in the antibate dependence. Judging from the results of Hirschfeld surface analysis for complexes **VII-IX**, the dominant intermolecular contacts are H···F/F···H, H···H, H···O/O···H with percentages 33.3-34.5 %, 26.4-30.0 % and 16.0-21.8 % [3].

Assessment of solubility in water and organic solvents is a mandatory procedure for all drug candidates. The observed general tendency for a significant decrease in solubility of ionic AHFS when moving from solutions in highly polar water and DMSO solvents to less polar alcoholic media is generally to be expected, and the decrease in solubility of these salts in ethanol compared to methanol and water may reflect the relative “lipophilization" of the medium.

According to biological experiments (Wistar rats), all AHFS exhibit noticeable anti-caries activity with the simultaneous significant improvement in the biochemical parameters of dental pulp and the absence of hepatotoxic effects in a given dosing (with the exception of **XII**) [1-3]. Among the studied AHFS, complexes **VI** and **XII** exhibits the highest caries-preventive efficacy, which exceeds the analogous indicators for the reference drug, NaF, by 5 times. The results of determining the characteristics of acute toxicity of salts **VI** (LD_{50} = 481.28 mg/kg) and **XIII** (LD_{50} = 555.05 mg/kg) by the oral route of administration make it possible to classify this compounds as moderately toxic and slightly toxic compounds (hazard class III and IV, respectively).

ACKNOWLEDGMENTS: MSF and VCK are grateful for the sub-program funded by the Ministry of Education and Research of R. Moldova 011202.

[1] V. O. Gelmboldt, V. Ch. Kravtsov, M. S. Fonari. *J. Fluorine Chem*. **221** (2019) 91-102.
[2] A. Ouasri, A. Rhandour. *Russ. J. Coord. Chem*. **47** (2021) 502-517.
[3] V. O. Gelmboldt, I. V. Lytvynchuk, I. O. Shyshkin et al. *Arch. Pharm*. **355** (2022) 2200074.

Eu^{3+} AS A LUMINESCENT PROBE FOR LOCAL SITE SYMMETRY IN Eu(III) COORDINATION COMPOUNDS

V. Ghenea[1,2,*], I. Culeac[1], A. Buzdugan[2]
[1]*Institute of Applied Physics, Moldova State University, Chișinău, Republic of Moldova;*
[2]*Technical University of Moldova, Chișinău, Republic of Moldova*
[*]E-mail: vladislav.ghenea@ifa.usm.md

Eu(III) coordination compounds attract a lot of interest because of their excellent properties, both from the application point of view as well as from the pure theoretical aspects [1,3]. Usually under the UV or blue-light excitation the Eu^{3+} complex exhibits a bright-red luminescence with narrow atomic-like emission bands. Because of relatively small number of ^7F_J components in the PL emission spectrum the Eu(III) ion is convenient when analysing the PL spectra, drawing information and making conclusions vs the symmetry properties of the specific complex. The topic of this paper encompasses the use of Eu(III) ion as a site symmetry probe in lanthanide coordination compounds.

We discuss a number of important aspects on the use of tripositive ion Eu^{3+} for evaluation of local symmetry in europium(III) coordination compounds. When examining these aspects, we bring both the literature data as well as our own experimental results [2]. As one of example we discuss the PL spectra on the binuclear complex $[Eu(\mu_2\text{-}OC_2H_5)(NO)_3(phen)]_2phen$ [3]. In general, the character of PL bands splitting is directly related to the symmetry of the complex, and Table 1 taken from [4] illustrates this aspect.

Table 1. Stark-level splitting for specific crystal field symmetries vs the total angular momentum J [4].

Local Symmetry	**Triclinic (C_1, C_i)**	**Monoclinic (C_s, C_2, C_{2h})**	**Rhombic (C_{2v}, D_2, D_{2h})**
J = 0	1	1	1
J = 1	3	3	3
J = 2	5	5	5
J = 3	7	7	7

One of the very interesting features of Eu^{3+} PL spectra is the emission band at ca 580 nm, associated with the transition $^5D_0 \rightarrow {}^7F_0$. Because both $^5D_0$ and $^7F_0$ levels are non-degenerate, the number of components related to this band indicates on the number of different Eu(III) sites in the coordination compound. Figure 1 illustrates two components of the transition $^5D_0 \rightarrow {}^7F_0$ for the binuclear complex $[Eu(\mu_2\text{-}OC_2H_5)(NO)_3(phen)]_2phen$. Registration of two components in this transition indicates on two emission sites of this complex. One has to be careful when drawing conclusions based on PL spectra, and excellent reviews on these aspects are presented by K. Binnemans [5] and P. Tanner [6]. Actually, the final assignment of the point group symmetry can be made on the basis of XRD measurements.

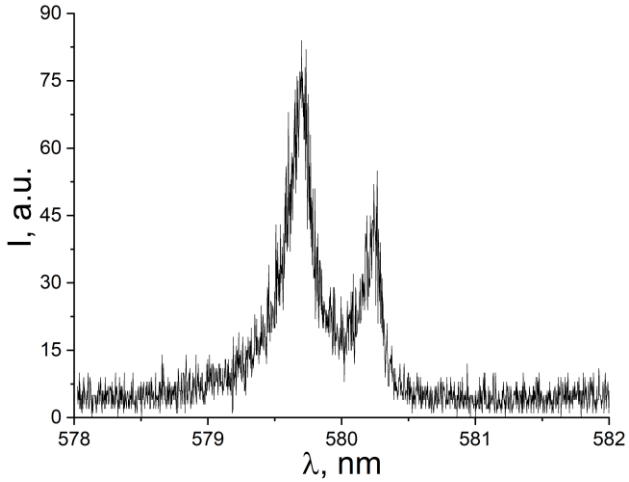

[1] P. Serna-Gallen et al. *Ceramics International* **49** (2023) 41078-41089.
[2] V. Ghenea et al. *Journal of Engineering Science* (2024) – to be published.
[3] I. Culeac et al. *Nanomaterials* **12** (2022) 2788.
[4] T.N.L. Tran et al. *Materials* **15** (2022) 1847.
[5] K. Binnemans. *Coordination Chemistry Reviews* **295** (2015) 1 – 45.
[6] A.P. Tanner al. *Royal Society of Chemistry* **42** (2013) 5090 – 5101.

ANTIMICROBIAL, ANTIPROLIFERATIVE AND DNA-INTERACTING PROPERTIES OF 6-(2,4-DICHLOROBENZOYL)-7-(2,4-DICHLOROPHENYL)INDOLO[3,4-*jk*]PHENANTHRIDIN-5(4*H*)-ONE

E. Gorincioi[1], V. Pogrebnoi[1], D. Iunac[2], G. Balan[2], A. Rotaru[3], N. Sucman[1], F. Macaev[1]
[1]*Institute of Chemistry, Moldova State University, Chișinău, Republic of Moldova;*
[2]*"Nicolae Testemitanu" State University of Medicine and Pharmacy, Chișinău, Republic of Moldova;*
[3]*"Petru Poni" Institute of Macromolecular Chemistry, Iași, Romania*
[*]E-mail: elena.gorincioi@sti.usm.md

The successful development of oxindole chemistry in recent years is inextricably linked to numerous studies on the synthesis of new compounds within this group and the search for physiologically active substances among them [1]. Research conducted in this direction has led to the creation of new effective drugs, which have been incorporated into the treatment of various pathological conditions [2]. Therefore, studies aimed at developing efficient synthetic methods for the selective production of polyfunctionalized oxindoles and investigating the "structure-bioactivity" relationship are highly relevant and of practical interest.

This paper presents the results of studying some of biological properties of the title compound **2**, its synthesis being performed from compound **1** by using a described protocol [3] (Figure 1).

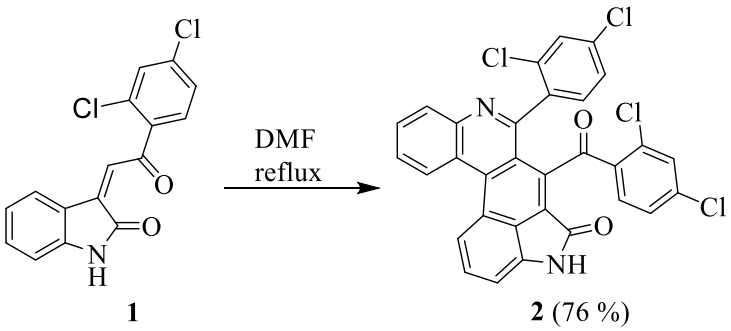

1 **2** (76 %)

Figure 1. A. *Scheme for the synthesis of compound **2**.*

The results of estimating the antimicrobial activity of compound **2** have showed that it exhibits moderate antibacterial (MIC = 0.68 and 1.37 mg/mL on *Bacillus cereus* ATCC 11778 and *Escherichia coli* ATCC 25922) and antifungal (MIC = 0.68 mg/mL on *Candida albicans* ATCC 10231) effects. Assays on eight tumor cell lines have demonstrated its higher anticancer properties on Glioblastoma LN229 and Lung Carcinoma NCI-H460 cells, the found CC_{50} values of 12.9 and 16.6 μM being comparable with that of reference compound Etoposide.

Compound **2** has been studied as a model to mimic duplex DNA–protein interaction. The results of circular dichroism (CD) titration experiments employing the 24 mer palindromic sequence of the Drew-Dickerson Dodecamer (DDD) argue that compound **2** perturbs the secondary structure of duplex DNA, causing a loss of helicity, while having a minimal impact on base pair stacking interactions [4]. This is indicative of a groove-binding (minor groove) rather than a base pair intercalative binding mode of the title compound [5].

[1] F. Macaev, A. Geronikaki, N. Sucman. In: „Targets in heterocyclic systems. Chemistry and Properties". Ed. O. A. Attanasi and D. Spinelli. Italian Chemical Society (2011), nr. 15, 294-326.
[2] Y. M. Khetmalis, M. Shivani, M. Sankaranarayanan, K. V. G. Chandra Sekhar. *Biomedicine & Pharmacotherapy*, **141** (2021), 111842.
[3] V. Pogrebnoi. Synthesis of substituted oxindoles based on isatines. PhD thesis, Institute of Chemistry of the ASM, 2017, 147 pag.
[4] Z. Molphy, D. Montagner, S. S. Bhat, et al. *Nucleic Acids Research*, **46**, (2018), 9918–9931.
[5] A. Kellett, Z. Molphy, C. Slator et al. *Chemical Society Reviews*, **48** (2019), 971 – 988.

NMR STUDIES OF THE DUPLEX DNA-LIGAND INTERACTIONS BY USING ANTICANCER ACTIVE PRIMARY AMINE IONIC LIQUIDS

E. Gorincioi[1,*], E. Stîngaci[1], P. Sket[2], J. Plavec[2-4], F. Macaev[1]
[1]*Institute of Chemistry, Moldova State University, Chișinău, Republic of Moldova;*
[2]*Slovenian NMR Centre, National Institute of Chemistry, Ljubljana, Slovenia;*
[3]*Faculty of Chemistry and Chemical Technology, University of Ljubljana, Ljubljana, Slovenia;*
[4]*EN-FIST, Center of Excellence, Ljubljana, Slovenia*
[*]E-mail: elena.gorincioi@sti.usm.md

Small synthetic ligands have been reported as therapeutics to either block, or in some cases, mimic a duplex DNA–protein interaction, by which they may be used as models in the study of various diseases, including cancer biogenesis [1]. NMR spectroscopy has gained a prominent position amongst the direct molecular methods for identification of the non-covalent nucleic acid recognition [2,3]. Accordingly, search for the novel bioactive ligands with high potential for targeting the DNA by using NMR may open new promising avenues in the identification of the DNA binders endowed with significant therapeutic benefit.This paper showcases the two room temperature ionic liquids **1** and **2**, acting as efficient anticancer agents against HeLa cell line and showing low cytotoxicity at Vero cells [4]. For duplex DNA model the Dickerson−Drew dodecamer (DDD) has been employed that is one of the most studied prototypic B-DNA molecules, with the d-[CGCGAATTCGCG]2 oligonucleotide sequence.

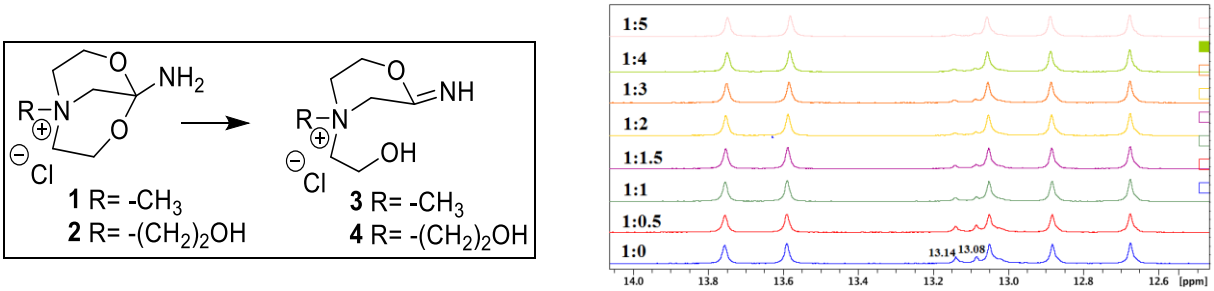

Figure 10. Chemical structures of the used ligands **1,2** and their half-closed structures **3,4** [4] and imino- region of the ^{1}H NMR titration spectra of DDD in 10 mM KPi (pH 7.0), 10 % D_2O (25 °C, 600 MHz). For conformity, the DDD-**1** case is illustrated; the DDD-**1** ratio is shown at the left side of the spectra.

The data of ^{1}H NMR experiments employing the DDD DNA sequence have demonstrated that **1** and **2** do not recognize the major homodimeric form of DDD, as both chemical shift and shape of signals for the representative imino- protons do not vary upon titration (Figure 1). At the same time, changes were noticed regarding the presence of minor DDD conformers in solutions, attested by small peaks at δ 13.08 and 13.14 ppm. Based on broadening of these signals upon ^{1}H NMR titrations one can conclude about the occurrence of weak nonspecific interactions between compounds **1** / **2** and the minor conformers of the model DNA.

ACKNOWLEDGEMENTS: E.G, E.S. and F.M. thank the subprogram 010601. E.G. acknowledges the CERIC for the access to experimental facilities of Slovenian NMR Centre for NMR studies on DNA.

[1] S. Bhaduri, N. Ranjan, D.P. Arya, *Beilstein J. Org. Chem*., **14** (2018), 1051–1086.
[2] H. M. Al-Hashimi. *J. Magn. Reson*. **237** (2013), 191–204.
[3] M. Marušič, M. Toplishek, J. Plavec. *Curr. Opin. Struct. Biol*., **79** (2023), 102532.
[4] D. Prodius, H. Shah, J. Iqbal et al. *Chem. Commun.*, **50**, (2014), 4888-4890.

FULL ^{1}H, ^{13}C and ^{15}N NMR CHARACTERISATION OF DIOXOINDOLINONE ENDOWED WITH ANTIDEPRESSANT PROPERTIES

E. Gorincioi[1,*], T. Ștefăneț[2], E. Stîngaci[1], V. Valica[2], F. Macaev[1]
[1]*Institute of Chemistry, Moldova State University, Chișinău, Republic of Moldova;*
[2]*"Nicolae Testemițanu" State University of Medicine and Pharmacy, Chișinău, Republic of Moldova*
[*]E-mail: elena.gorincioi@sti.usm.md

Currently the power of nuclear magnetic resonance (NMR) spectroscopy is well acknowledged as one of the superior tools for fast and accurate quality control of active constituents in drugs, which provides detailed quality-related information [1,2]. Particularly challenging NMR applications in the pharmaceutical industry are aspects with respect to determining the purity of drug substance, drug product and establishing the identity of impurities and its level.

In continuation of our studies focused on compounds expressing the anxiolytic and antidepressive properties [3], the results of detailed NMR identification for ^{1}H, ^{13}C and ^{15}N nuclei in 1-(2-oxopropyl)spiro[[1,3]indoline-3,2'-[1,3]dioxolan-2-one **1**, conventionally named dioxoindolinone are herein presented. The title compound represents a derivative of indolin-2,3-dione **2 (**isatin) that is a potent endogene monoamine oxidase inhibitor (MAOI) [4]. It should be mentioned that the key roles played by MAO isoforms in neurodegenerative disorders, make it an important drug target [5]. Especially, as a part of polypharmacological approach to the treatment of depression, the use of MAOI has demonstrated efficacy [6].

Studies regarding the properties of dioxoindolinone **1** itself and related compounds are of great interest, as these compounds may be advanced for further biological testing and preclinical development, or used as possible lead compounds for the future design of MAO inhibitors.

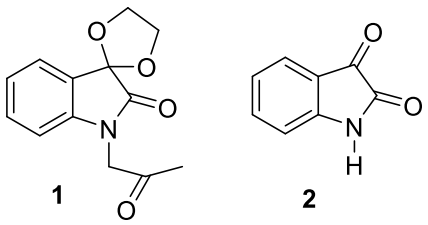

Figure 1. Chemical structures of compounds **1** and **2**

For the first time, the exhaustive spectral ^{1}H, ^{13}C and ^{15}N NMR individual characteristics for dioxoindolinone **1** will be presented. The undoubteful assignment of all ^{1}H, ^{13}C and ^{15}N signals in the spectra have been obtained on the basis of the 1D (^{1}H, ^{13}C, DEPT-135) and 2D homo- ($^{1}H/^{1}H$ COSY-45) and heteronuclear ($^{1}H/^{13}C$ HSQC, $^{1}H/^{13}C$ HMBC and $^{1}H/^{15}N$ HMBC) correlation spectra.

ACKNOWLEDGEMENTS: This study was supported by the research subprogram 010601 funded by Ministry of Education and Research of the Republic of Moldova.

[1] Khalil, A., Kashif, M. *Critical Reviews in Analytical Chemistry*, **53** (2023), 997-1011.
[2] Holzgrabe, U., Wawer, I., Diehl, B. NMR Spectroscopy in Pharmaceutical Analysis, Elsevier, Amsterdam, 2008, 528 p.
[3] Ştefaneţ, T., Stîngaci, E., Vîslouh, O., Valica, V., Macaev, F. *Akademos*, **55** (2019), 52-56 (in Roumanian).
[4] Zhunghietu, G. *Revue Roumaine de Chimie*, **46** (2001), 517-520.
[5] Naoi, M., Maruyama, W., Inaba-Hasegawa, K. *Current Topics in Medicinal Chemistry*, **12** (2012), 2177-88.
[6] Ebert, T.J. In: „Pharmacology and Physiology for Anesthesia" 2nd ed. Philadelphia, PA: Elsevier; 2019, 282-299.

TWO-DIMENSIONAL Cd(II) COORDINATION POLYMER DERIVED FROM A 1,2,3-TRIAZOLE-BASED TRICARBOXYLATE LIGAND

V.V. Gorinchoy[1,*], G. Roman[2], S.G. Shova[2], V.I. Lozan[1]
[1]*Institute of Chemistry, Moldova State University, Chișinău, Republic of Moldova;*
[2]*"Petru Poni" Institute of Macromolecular Chemistry, Iași, Romania*
[*]E-mail: viorina.gorincioi@sti.usm.md, oviorina@gmail.com

Coordinative polymers are entities assembled from metal ions with organic ligands through coordinative bonds or supramolecular interactions by forming very well-ordered structures as 1, 2 or 3 dimensional polymeric networks. In the present communication, we report the synthesis, IR characterization and crystal structure of a 2D polymeric complex with formula $\{[Cd_3L_2(H_2O)_6]\cdot 1.5H_2O\}_n$ (where, L=5-(4-carboxy-5-methyl-1H-1,2,3-triazol-1-yl)isophthalic acid (H_3L)). The transition metal polymeric complex was prepared by the reaction of H_3L[1] with cadmium nitrate tetrahydrate, in a mixture of dimethylacetamide and water. In a few days pale-beige crystals were isolated and characterized by physical methods. In the IR spectrum the bands between 3382 and 3238 cm^{-1} correspond to O–H stretching vibrations of coordinated water molecules. The characteristic vibration modes $\nu(_{C\text{-}H})$ of the methyl group appear at 3069 cm^{-1}. The peaks at 1605 and 1358 cm^{-1} are the characteristic absorbtions for the asymmetric $\nu_{as}(COO^-)$ and symmetric stretching $\nu_s(COO^-)$ vibrations of C=O bond. The absorbtion band appearing at 1371 cm^{-1} confirms the presence of the triazole ring in the structure of the polymeric compound. The peak at 1074 cm^{-1} belongs to the stretching vibration of $\nu(_{C–N})$, and the peak at 1046 cm^{-1} belongs to the stretching vibration of $\nu(_{C–O})$.

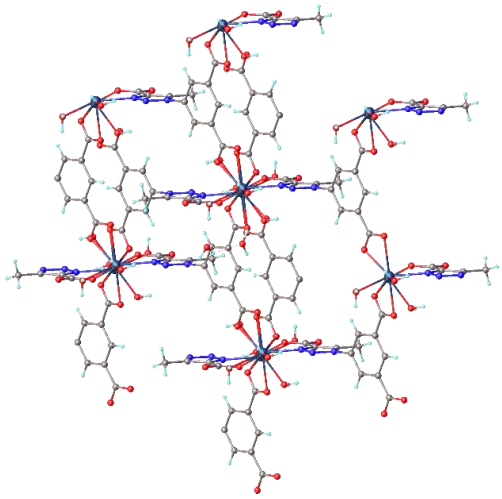

Figure 1. Crystal structure of $\{[Cd_3L_2(H_2O)_6]\cdot 1.5H_2O\}_n$.

The X-ray diffraction study has shown that the investigated compound represents a trinuclear coordination polymer (Figure 1), where one Cd ion is hexa- coordinated and other two Cd ions are octa-coordinated. The compound crystallizes in the triclinic space group P–1, with unit cell parameters: a=9.0286(6), b=10.1274(7), c=10.5441(7) Å, α=117.448(7), β=93.767(6), γ=99.033(6)°. The Cd1 ion is surrounded by six oxygen atoms provided by tetra carboxylate functions and two water molecules, the Cd2 and $Cd2^i$ ions are octa-coordinated by four oxygen atoms provided by bidentate carboxylate group, one oxygen atom from monodentate (COO^-) and one nitrogen atom from the H_3L ligands. The 2D networks are linked by H-bonding into 3D supramolecular network, where the H_3L behaves as $\eta^1{:}\eta^1$ bidentate chelate, $\mu_2{:}\eta^2{:}\eta^1$ tridentate chelate and $\mu_2{:}\ \eta^1{:}\eta^1$ bridging ligand.

ACKNOWLEDGEMENTS: We thank the research subprogram SSMCCLP (code 010602) for the financial support of this work.

[1] M. Dascălu, A.-L. Chibac-Scutaru, G. Roman. Journal of Molecular Liquids **386** (2023) 122457.

SYNTHESIS, CRYSTAL STRUCTURE AND SPECTROSCOPIC PROPERTIES OF HETERO COORDINATION POLYMER $\{[CuBa_2(5\text{-}MeSal)_2(5\text{-}MeSalH)_2(DMA)_4]\}_n$ DERIVED FROM A 5-METHYLSALICYLIC ACID

V.V. Gorinchoy[1,*], O.I. Cuzan[1], S.G. Shova[2], V.I. Lozan[1]
[1]*Institute of Chemistry, Moldova State University, Chișinău, Republic of Moldova;*
[2] *"Petru Poni" Institute of Macromolecular Chemistry, Iași, Romania*
[*]E-mail: oviorina@gmail.com, viorina.gorincioi@sti.usm.md

New copper(II) complex with 5-Methylsalicylic acid was obtained and characterized by X-ray diffraction and IR spectroscopy. Single crystal X-ray diffraction analysis indicates that crystalline compound with formula $\{[CuBa_2(5\text{-}MeSal)_2(5\text{-}MeSalH)_2(DMA)_4]\}_n$ (1) belongs to the monoclinic space group $P2_1/c$, with unit cell parameters: a=9.19983(16), b=19.0948(3), c=14.9232(3), β=90.3147(16) and Z=2. The X-ray diffraction study has showed that compound **1** represents a heteronuclear one-dimensional coordination polymer (Figure 1), where the Ba(II) ions are octa-coordinated and the Cu(II) ion is tetra- coordinated.

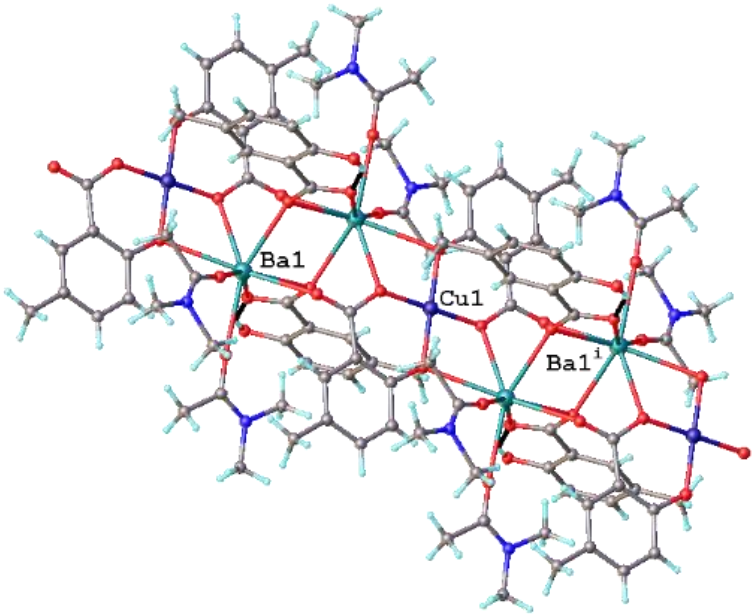

Figure 1. Crystal structure of $\{[CuBa_2(5\text{-}MeSal)_2(5\text{-}MeSalH)_2(DMA)_4]\}_n$.

The Cu(II) ion is surrounded by four oxygen atoms provided by two carboxylate functions and two hydroxyl groups, the Ba1 and Ba2 ions are octa- coordinated by six oxygen atoms provided by mono- and bidentate carboxylate groups and two oxygen atoms from two DMA molecules. The carboxylate and hydroxyl groups form bridges between metal ions. The carboxylate anions coordinate in several ways: η^1:η^1 bidentate bridging, μ_2:η^2:η^1 tridentate chelate-bridging mode and μ_3: η^1:η^2: η^1 tridentate bridging mode.

The IR study of the polymeric compound indicates the presence of carboxylic groups, phenolic ring and DMA solvent. The attribution of the observed bands was made in accordance with the data from the specialized literature [1]. The valence oscillations $\nu_{as(COO^-)}$ and $\nu_{s(COO^-)}$ are found as two intense absorption bands in the regions 1569 cm^{-1} and 1355 cm^{-1}, respectively.

ACKNOWLEDGEMENTS: We thank the research subprogram SSMCCLP (code 010602) for the financial support of this work.

[1] K. Nakamoto. Infrared and Raman Spectra of Inorganic and Coordination Compounds. Part B: Applications in Coordination, Organometallic, and Bioinorganic Chemistry. John Wiley & Sons, New Jersey, 2009; 416 p.

INDIVIDUAL K(I) COORDINATION POLYMERS WITH DIFFERENTLY SUBSTITUTED CHLORONITROBENZOATES

A. Gorobet*, M.E. Crisan, P.N. Bourosh, O.V. Kulikova, L. Croitor
Institute of Applied Physics, Moldova State University, Chișinău, Republic of Moldova
*E-mail: nasteagorobet@gmail.com

Chloronitrobenzoic acid derivatives have a variety of uses in medicinal chemistry. The presence of chloro and nitro groups in their structure boosts their biological activity, making them useful for developing drugs against diseases like viral infections and cancer. In this study, we selected differently substituted chloronitrobenzoates, 2-chloro-4-nitrobenzoic acid ($2Cl_4NBH$) and 2-chloro-5-nitrobenzoic acid ($2C_{l5}NBH$), due to their ability to generate diverse stable coordination polymers (CP), resulting in different properties. Consequently, the examination of how the position of the nitro group affects the formation of two distinct CP, each with unique luminescent properties, will be undertaken. The reaction of KI with $2C_{l4}NBH$ and $2C_{l5}NBH$ have led to two CPs (figure). CP 1 has three different K(I) ions in the asymmetric unit: K(1) is 6-coordinated, K(2) is 8-coordinated, and K(3) is 7-coordinated. The carboxylate groups exhibit tetradentate and chelate-pentadentate coordination modes, while the nitro groups show monodentate and chelate-bidentate coordination modes. CP 2 represents a 2D layer formed by $K(H_2O)^+$ cationic moieties linked by $2C_{l5}NB$ anions, where each K ion is 9-coordinated. In this compound, the carboxylate acts as chelate-tetradentate ligand, the nitro group coordinates in a monodentate way, and the Cl atom show a bidentate type of coordination, in contrasts with CP 1, where the Cl atom remains inactive. The solid-state luminescent properties of both CPs, carried out at room temperature, present distinct behaviours that reflect the structural differences between the compounds.

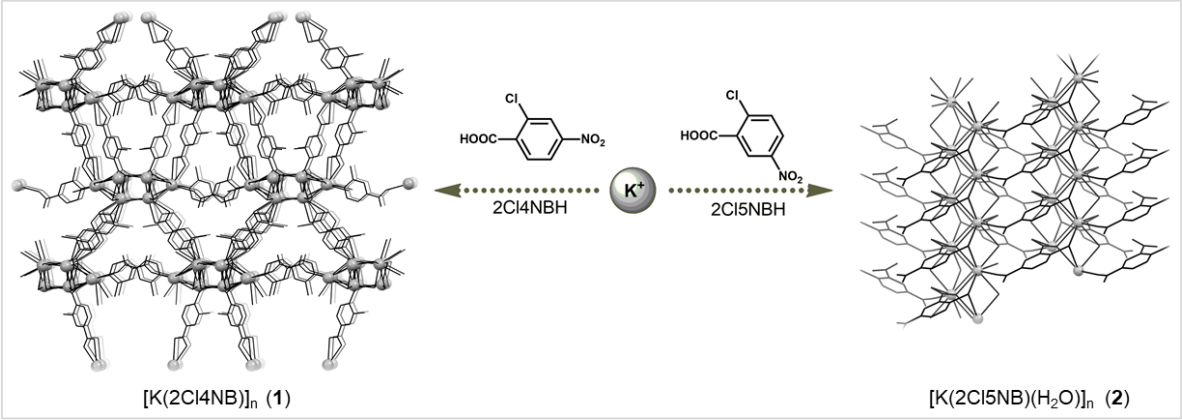

Figure 1. Schematic representation of K(I) CPs preparation

ACKNOWLEDGMENTS: The authors from RM are grateful for the subprograms financed by the Ministry of Education and Research of R. Moldova 011201 and 011202.

INFLUENCE OF STRUCTURAL POLYMORPHISM ON LUMINESCENT PROPERTIES

A. Gorobet[1,*], O. Danilescu[2], E. Melnic[1], Y.M. Chumakov[1],
O.V. Kulikova[1], V.Ch. Kravtsov[1], L. Croitor[1]
[1]*Institute of Applied Physics, Moldova State University, Chişinău, Republic of Moldova;*
[2]*Institute of Chemistry, Moldova State University, Chişinău, Republic of Moldova*
[*]E-mail: anastasia.gorobet@ifa.usm.md

Polymorphism is the phenomenon where by the same chemical compound can have different crystal structures, and crystals of different polymorphs can have different physical properties. Polymorphism can therefore have a direct impact on its functional properties and thus on its technological applications. [1]. This study shows the relationship between the crystal structures and photoluminescent properties for two polymorphs (**α** and **β**) of (*E*)–4-amino–*N*′–(1–(3–aminophenyl)ethylidene)benzohydrazide, obtained from 3′–aminoacetophenone (3–AAP) and 4-aminobenzoic acid hydrazide (4–ABAH) (Scheme 1), known for their antibacterial and therapeutic properties, respectively.

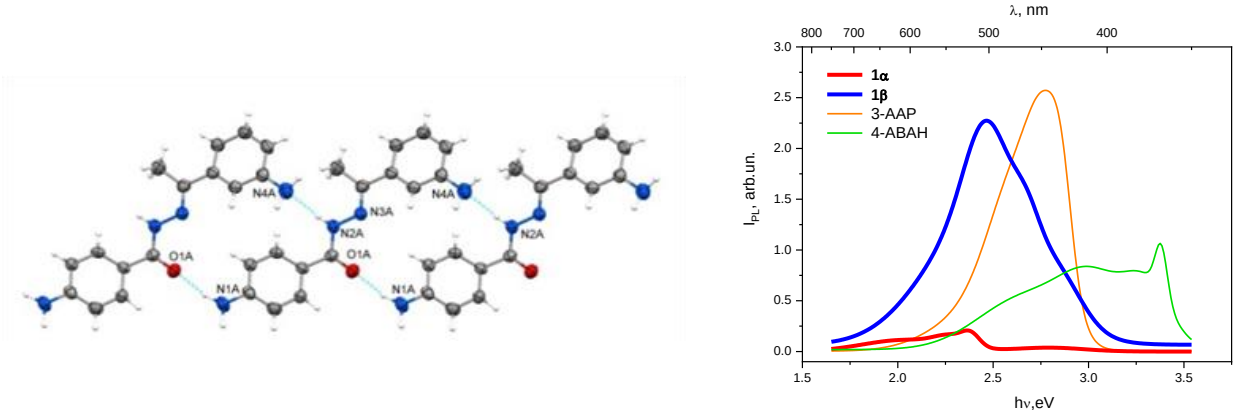

Figure 1. View of the supramolecular chain observed in both polymorphs and PL emission spectra at room temperature for 1α and 1β and 3-AAP and 4-ABAH ligands.

Both polymorphs crystallize in the monoclinic crystal system, **α** in $P2_1/c$ symmetric space group (a=20.9842(19), b=8.2564(7), c=16.6938(16) Å, β=113.344(11)°), while the polymorph **β** in *Cc* non-centrosymmetric space group (a=28.473(2), b=8.2365(4), c=18.0369(13) Å, β=107.262(5)°). The asymmetric unit of **α** contains two identical molecules (A and B), while **β** comprises three identical molecules (A, B and C). Both polymorphs feature the same supramolecular building block, namely mono chains of molecules connected by hydrogen bonds in a head-to-tail manner, Fig.1. Further aggregation in crystals is different: in **α** two parallel and symmetrically related chains H-bonded into double chains, while in **β** symmetry independent chains united by H-bonds and N-H···π interactions into triple chains, in which one of the symmetry independent chain, namely B, is antiparallel to two others, A and C.

The photoluminescent (PL) studies of the polymorphs revealed that PL intensity of **β** in two orders of magnitude higher than that of **α**. The density of states (DOS) of **α** and **β**, were calculated using Siesta software to get insight on difference of their PL spectra. It was found that the number of DOS near the top of the valence band and the bottom of the conduction band in **β** is almost in two times higher than in **α**, which could lead to a higher PL intensity in polymorph β compared to **α**. In both compounds the maximum peaks of photoluminescence emission originate from the recombination of electrons and holes at the edges of the conduction and valence bands.

ACKNOWLEDGMENTS: The authors are grateful for the subprograms financed by the Ministry of Education and Research of R. Moldova 011202, 011201 and 010602.

[1] D.Gentili, M.Gazzano, M.Melucci, D.Jones, M.Cavallini. *Chem Soc Rev* **48** (2019) 2502–2517.

TEMPERATURE FIELD CHANGE ASSESSMENT IN ZIRCONIUM ALLOY Zr1.0%Nb DURING ECAP PROCESS USING FINITE ELEMENT MODELING

Hanan Alsheikh, D.Z. Grabco*, O.A. Shikimaka
Institute of Applied Physics, State University of Moldova, Chişinău, Republic of Moldova
*E-mail: daria.grabco@ifa.usm.md

Zirconium alloys have high performance characteristics, such as melting point, radiation resistance, physical and mechanical properties. Thereby, Zr based alloys find wide applications in various fields, in particular, as implants in dentistry and bone surgery [1]. For an effective use in medicine, the material mechanical characteristics (strength, hardness, plasticity) are very important. Significant improvement of these characteristics can be achieved, for example, by obtaining an ultrafine-grained structure of the workpiece using the equal-channel angular pressing (ECAP) method [2]. However, ECAP is a rather complex technology and requires a large number of experiments. Therefore, to facilitate the solution of research problems, the computer modeling method is used.

In this work, the temperature changes in different zones of a workpiece of Zr1.0%Nb alloy during ECAP processing was investigated applying finite element modeling by using QFORM metal forming simulation software. The initial data for computational modeling included the geometric parameters of workpiece and ECAP die, the chemical composition and physical characteristics of Zr1.0%Nb alloy, as well as, the conditions of severe plastic deformation: temperature, pressing force, number of ECAP passes and other necessary data. The temperature values of workpiece, corresponding to 25, 50 and 75% of the workpiece length passed through the intersection plane of die channels are determined (Fig. 1).

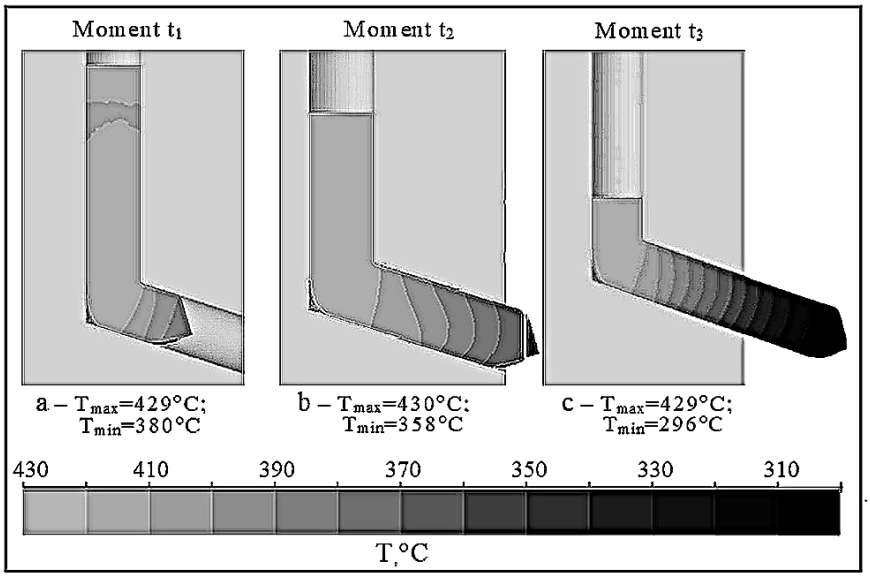

Figure 1. Temperature distribution along the longitudinal section of the workpiece

It was shown that the temperature gradient exists both in the longitudinal and transverse sections of the workpiece. The maximum temperature of the workpiece was achieved in the zone of maximum deformation and exceeded the initial heating by approximately 10ºC, which is a sufficiently small value and should not have a significant effect on the processes of deformation and phase transformations.

ACKNOWLEDGMENTS: This study was supported by research Subprogram **011201** of the Institute of Applied Physics, Moldova State University, funded by the Ministry of Education and Research of Moldova Republic

[1]. L. Saldaña, L. Jiang, M. Multigner, et al. *Biomaterials*, 2007, **28**, pp. 4343 – 4354.
[2]. S.A. Nikulin, A.B. Rozhnov, S.O. Rogachev, et al. *Materials Letters*. 2016, **169**, pp. 223 – 226.

CRYSTAL STRUCTURES OF *N*-(4-METHOXYPHENYL)-2-[2-(PROP-2-EN-1-YLCARBAMOTHIOYL)HYDRAZINYLIDENE]PROPANAMIDE AND ITS COPPER(II) COMPLEX

E. I. Melnic[1], P. N. Bourosh[1], I. I. Graur[2,*], V. O. Graur[2],
O. S. Garbuz[3], V. I. Tsapkov[2], A. P. Gulea[2]
[1]*Institute of Applied Physics, Moldova State University, Chișinău, Republic of Moldova;*
[2]*Laboratory of Advanced Materials in Biopharmaceutics and Technics, Institute of Chemistry, Moldova State University, Chișinău, Republic of Moldova;*
[3]*Laboratory of Systematics and Molecular Phylogenetics, Institute of Zoology, Moldova State University, Chișinău, Republic of Moldova*
[*]E-mail: ulchina.ianina@usm.md

Thiosemicarbazones are versatile ligands which can coordinate as neutral ligands or in their deprotonated form. Nitrogen and sulfur atoms of thiosemicarbazone act as donor atoms for binding with different metal atoms. Thiosemicarbazones of various pyruvic acid amides have been scarcely studied and are rarely described in the literature. Therefore, it is of interest to investigate their mode of coordination to metal atoms, using the copper(II) complex as an example.

The aim of this work is to determine the structural properties of *N*-(4-methoxyphenyl)-2-[2-(prop-2-en-1-ylcarbamothioyl)hydrazinylidene]propanamide (**HL**) and its copper(II) complex $[Cu(L)(Cl_2CHCOO)]_2$ (**I**). Compound (**HL**) crystallizes in the monoclinic space group $P2_1/c$ with unit cell parameters: a = 9.2947(2), b = 4.93970(10), c = 33.8742(9) Å, β = 97.151(2)°, whereas compound **I** crystallizes in the triclinic system, P-1 space group with unit cell parameters: a = 9.2521(8), b = 9.7926(6), c = 12.4632(10) Å, α = 100.663(6), β = 106.344(8), γ = 106.206(7)°. The X-ray study of the crystals of these compounds revealed the conformational change of the basic thiosemicarbazide fragment of the ligand, allowing it to coordinate with Cu(II) through the set of ONS donor atoms to the metal atom. In the crystal, the organic molecules **HL** are linked by N–H···S hydrogen bonds into a centrosymmetric dimer, forming the $R_2^2(8)$ supramolecular synthon, Figure 1a. These dimers are linked by N–H···O hydrogen bonds, forming supramolecular layers.

In the structure **I**, the dichloroacetate anion exhibits the chelate-bridging function resulting in the formation of a centrosymmetric dimer, Figure 1b. The coordination polyhedron of the metal atoms is formed by the set of O4NS donor atoms in the vertices of the distorted tetragonal bipyramid. The Cu...Cu distance in the dimers is 3.436 Å.

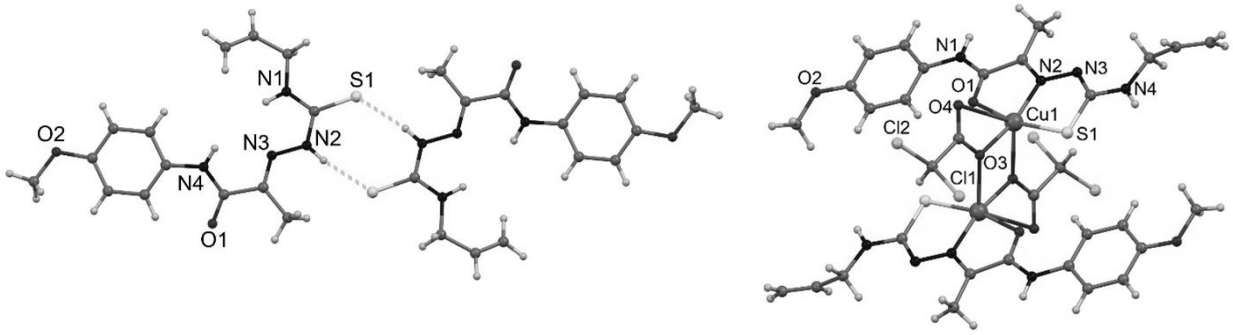

a b

Figure 1. The supramolecular dimer in **HL(a)** and molecular structure of **I (b)**

The antioxidant activity of these substances towards $ABTS^{\bullet+}$ cation radicals was studied. The results of the study showed that both **HL** and complex **I** manifest antiradical activity. Their IC_{50} values towards $ABTS^{\bullet+}$ are 68.6 and 78.6 μM, respectively.

ACKNOWLEDGMENTS: This work was fulfilled with the financial support of the subprograms 010602, 010701, and 011202 of the institutional projects.

CRYSTAL STRUCTURE OF COPPER(II) COORDINATION COMPOUND WITH *N*-(PROP-2-EN-1-YL)-2-(PYRIDIN-2-YLMETHYL)HYDRAZINECARBOTHIOAMIDE

P. N. Bourosh[1], V. O. Graur[2,*], I. S. Usataia[2], C.S. Lozan-Tirsu[3], A.P. Gulea[2]
[1]*Institute of Applied Physics, Moldova State University, Chișinău, Republic of Moldova;*
[2]*Laboratory of Advanced Materials in Biopharmaceutics and Technics, Institute of Chemistry, Moldova State University, Chișinău, Republic of Moldova;*
[3]*State University of Medicine and Pharmacy "Nicolae Testemitanu",Chișinău, Republic of Moldova*
[*]E-mail: vasilii.graur@usm.md

A sub-class of thiosemicarbazones is that one derived from condensation of thiosemicarbazones with 2-formylpyridine. In these ligands, the pyridine nitrogen atom is able to coordinate metals inducing extra-stability to the final complexes by forming two fused five-membered rings. Besides this, interesting biological activities have been reported for 2-formylpyridine thiosemicarbazone (Triapine), one of the most studied thiosemicarbazones for cancer chemotherapy. In order to understand the origin of a substance's activity, it is necessary to study its structure.

The aim of this work is the determination of crystal structure of copper(II) coordination compoud with *N*-(prop-2-en-1-yl)-2-(pyridin-2-ylmethyl)hydrazinecarbothioamide $[Cu(L)(Cl_2CHCOO)]_2$. The X-ray study showed there is a centrosymmetric dimer in the crystal, formed by monodeprotonated L^- ligands with a bridging function. The carbothioamide ligand L^- in the dimeric compound is a tetradentate ligand. The coordination polyhedron of the metal atoms takes the form of a tetragonal bipyramid, formed by the coordination set $N_2O_2S_2$, of which N_2S belongs to one ligand L^-, one S atom belongs to the neighbouring ligand L^-, and the two O atoms belong to one monodeprotonated chelate ligand Cl_2CHCOO^-. The Cu...Cu interatomic distance in the dimer is equal to 3.482 Å. The bond distances in the coordination polyhedron Cu(1)-O(1), Cu(1)-O(2), Cu(1)-S(1), Cu(1)-N(3), Cu(1)-N(4), and Cu(1)-S(1)* equal 1.950(2), 2.863(3), 2.262(2), 1.961(5), 2.006(5) and 2.820(2) Å, respectively.

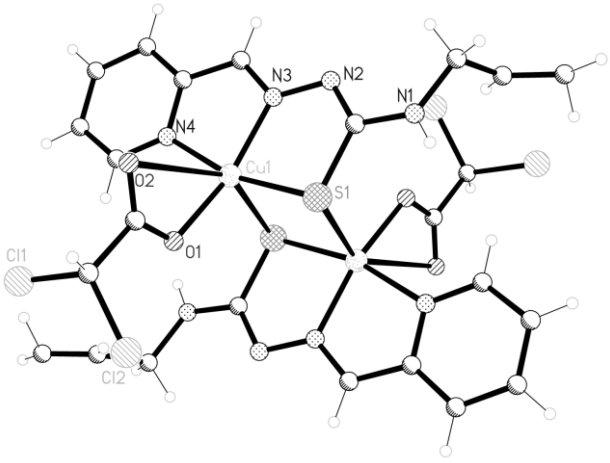

Figure 1. The crystal structure of $[Cu(L)(Cl_2CHCOO)]$.

The antibacterial activity of this complex against Gram-positive microorganisms *Staphylococcus aureus* ATCC 25923 and *Bacillus cereus* ATCC 11778 was studied. The complex showed the following results towards *Staphylococcus aureus*: MIC 0.488 $\mu g \cdot mL^{-1}$ and MBC 0.977 $\mu g \cdot mL^{-1}$, towards *Bacillus cereus*: MIC 0.488 $\mu g \cdot mL^{-1}$ and MBC 0.488 $\mu g \cdot mL^{-1}$.

ACKNOWLEDGMENTS: This work was fulfilled with the financial support of the subprograms 010602 and 011202 of institutional projects.

STRUCTURES OF *N*-(BICYCLO[2.2.1]HEPT-2-YL)-2-[PHENYL(PYRIDIN-2-YL)METHYLIDENE]HYDRAZINECARBOTHIOAMIDE AND ITS COPPER(II) COORDINATION COMPOUND

E. I. Melnic[1], V. Ch. Kravtsov[1], V. O. Graur[2,*], I. I. Dvorschi[2], I. I. Graur[2], I. S. Usataia[2], G. G. Balan[3], A. P. Gulea[2]

[1]*Institute of Applied Physics, Moldova State University, Chișinău, Republic of Moldova;*

[2]*Laboratory of Advanced Materials in Biopharmaceutics and Technics, Institute of Chemistry, Moldova State University, Chișinău, Republic of Moldova;*

[3]*State University of Medicine and Pharmacy "Nicolae Testemitanu", Chișinău, Republic of Moldova*

[*]E-mail: vasilii.graur@usm.md

Thiosemicarbazones with a bicyclic substituent in the fourth position are not well known. According to the literature, the presence of bicyclo[2.2.1]heptane fragment in the composition of substances can affect their properties, including biological ones, such as antiallergic, antagonistic, and anticancer activities. Therefore, it is important to study the mode of coordination of such thiosemicarbazones, as this may affect their properties.

The aim of this work is the determination of the mode of coordination of *N*-(bicyclo[2.2.1]hept-2-yl)-2-[phenyl(pyridin-2-yl)methylidene]hydrazinecarbothioamide (**HL**) and structural properties of its copper(II) coordination compound (**I**).

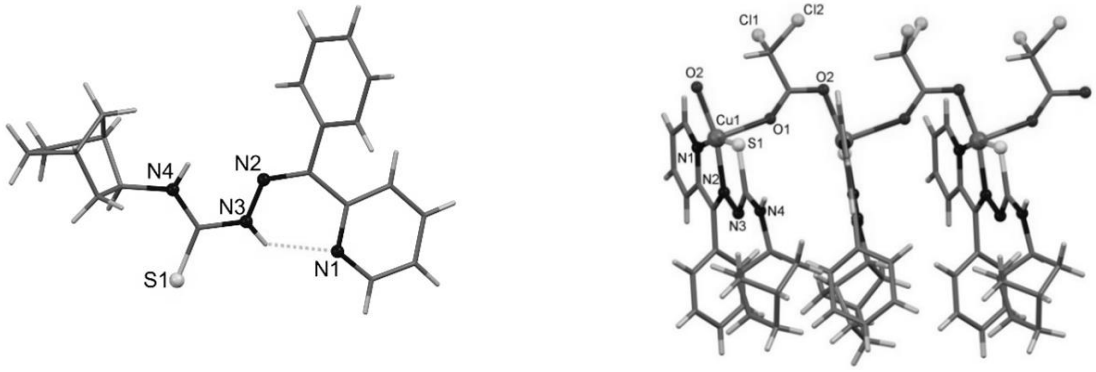

(a) (b)

Figure 1. The molecular structure of **HL(a)** and fragment of polymeric chain in **I(b)**.

The crystal structures of these compounds have been studied by single crystal X-ray diffraction method, which shows that **HL** and **I** crystalize in monoclinic $P2_1/n$ and $P2_1/c$ space groups with unit cell parameters: a = 6.0721(3), b = 18.5106(11), c = 16.7437(10) Å, β = 92.964(5)° and a = 14.2885(7), b = 18.4380(11), c = 9.5574(5)Å, β= 106.981(5)°, respectively. The structure of **HL** shows its *E*-configuration and the mutual arrangement of thiosemicarbazide and pyridine fragments stabilized by strong intramolecular N-H···N hydrogen bond, Figure 1a. The structure of **I** reveals the 1D polymer $\{[Cu(L)(Cl_2CHCOO)]\}_n$ in which planar CuL moieties are linked in the chain by the bridging function of dichloroacetate anions, resulting in the square pyramidal SN2O2 Cu(II) surrounding, Figure 1b.

Antibacterial activity against Gram-positive (*Staphylococcus aureus* ATCC 25923, *Bacillus cereus* ATCC 11778) and Gram-negative (*Acinetobacter baumannii* BAA-747) microorganisms was studied for these substances. Thiosemicarbazone (**HL**) showed no activity at all, while its complex **I** showed results against *Staphylococcus aureus with MIC* 1.95 $\mu g \cdot mL^{-1}$, *Bacillus cereus with MIC* 0.977 $\mu g \cdot mL^{-1}$, and *Acinetobacter baumannii with MIC* 62.5 $\mu g \cdot mL^{-1}$. The coordination of **HL** to copper(II) atom led to an increase in antibacterial activity.

ACKNOWLEDGMENTS: This work was fulfilled with the financial support of the ANCD project 24.80012.5007.14TC and of the subprogram 011202 of institutional project.

ABSORPTION OF THE MONONUCLEAR Fe(III) COORDINATION COMPOUNDS

O. Kulikova[1,*], O. Danilescu[2,3], P. Bourosh[1], I. Bulhac[2], Y. Chumakov[1], M. Cocu[2]
[1]*Institute of Applied Physics, Moldova State University, Chișinău, Republic of Moldova;*
[2]*Institute of Chemistry, Moldova State University, Chișinău, Republic of Moldova;*
[3]*Technical University of Moldova, Chișinău, Republic of Moldova*
[*]E-mail: olkulikova@rambler.ru

This paper presents the study of wide-gap semiconductors in the form of two new Fe(III) mononuclear coordination compounds ($[Fe(H_2L)(H_2O)_2]\cdot X_2\cdot 2.5H_2O$, where $X=NO_3^-$, ClO_4^-) based on the 2,6-diacetylpyridine bis(picolinoylhydrazone) (H_2L).

Optical absorption spectra were measured using **UV-Vis Spectrophotometer (PerkinElmer Lambda 25)** at 300 K in the wavelength range 200-500 nm measured. The UV-vis spectral titration of H_2L with Fe^{3+} were carried out by gradually increasing the amount of Fe^{3+} (10-100 μL) in the ethanol media of ligand. The spectra of three concentrations of Fe^{3+} (Fig.1) represent a series of curves characterized by the position of the absorption maxima at the same wavelength and differing only in their intensities. Upon successive addition of Fe^{3+} the absorbance bands gradually decreases in intensity, accompanied by the appearance of shoulder peaks in the region of 250-400 nm.

To estimate the band gap E_g, Tauc coordinates were used [1]: $\boldsymbol{(\alpha\cdot h\nu)^{1/n} = h\nu - E_g}$, where α is the absorption coefficient, E_g is the band gap, n is a constant depending on the type of electronic transition in the material.

An analysis of the optical absorption spectra under the assumption of direct allowed transitions (n=1/2) is presented in the inset to figure 2a. Approximation of the intrinsic absorption edge constructed in coordinates $(\alpha h\nu)^2$ from $(h\nu)$ gives the value of the direct band gap (E_g^{dir}).Approximation of the intrinsic absorption edge plotted in coordinates $(\alpha h\nu)^{1/2}$ from $(h\nu)$, which corresponds to allowed indirect transitions, shows the value of the indirect band gap (E_g^{indir}) (Fig. 2b).

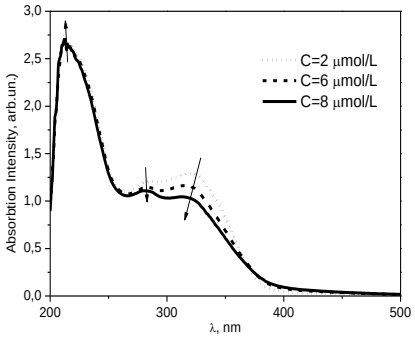

Figure 1. Absorption spectra at various concentration s(C)

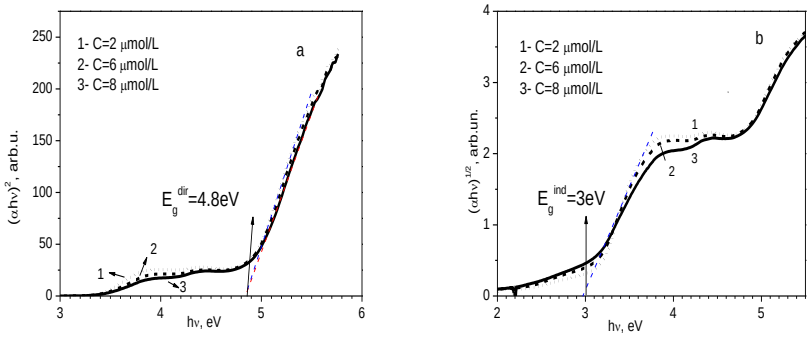

Figure 2. The edge of the optical absorption band in the Tauc coordinates of the sample for three concentrations

Approximations of the curves of the intrinsic absorption edge taken for different concentrations converge at one point and give the exact value of the width of the direct (E_g^{dir}= 4.8 eV) and indirect (E_g^{indir}=3.0 eV) band gap.

These values agree well with those theoretically calculated from the band structure.

ACKNOWLEDGEMENTS: The authors are grateful for the subprograms financed by the Ministry of Education and Research of R. Moldova: 011201, 011202 and 010602.

[1] Tauc J. Optical Properties and Electronic Structure of Amorphous Germanium /J.Tauc, R.Grigorovici, A.Vancu. *Physica status solidi*. 1966. Vol. 2, I. 15. P. 627–637.

SYNTHESIS AND STUDY OF NEW Cd(II) AND Zn(II) METAL-ORGANIC FRAMEWORKS

S. Melnic[1,2,*], V. Druta[1], S. Shova[3], V. Lozan[1]
[1]*Institute of Chemistry, Moldova State University, Chișinău, Republic of Moldova;*
[2]*"Nicolae Testemitanu" State University of Medicine and Pharmacy, Chișinău, Republic of Moldova;*
[3]*"Petru Poni" Institute of Macromolecular Chemistry, Iași, Romania*
[*]E-mail: silvia.melnic@usmf.md

Coordination polymers, commonly known as metal-organic frameworks (MOFs), have emerged at the forefront of scientific research and public interest. Their potential for neutral guest bonding, particularly in gas storage and separation, has garnered significant attention. MOFs are composed of rigid organic linkers with coordinating functional groups, connected by inorganic nodes. This unique structure endows MOFs with a wide range of applications, including gas storage, catalysis, luminescence, chemical sensing, drug delivery, solar energy, and biomedicine. The considerable porosity, high surface area, and versatile properties of MOFs have made them a key focus for synthetic chemists.

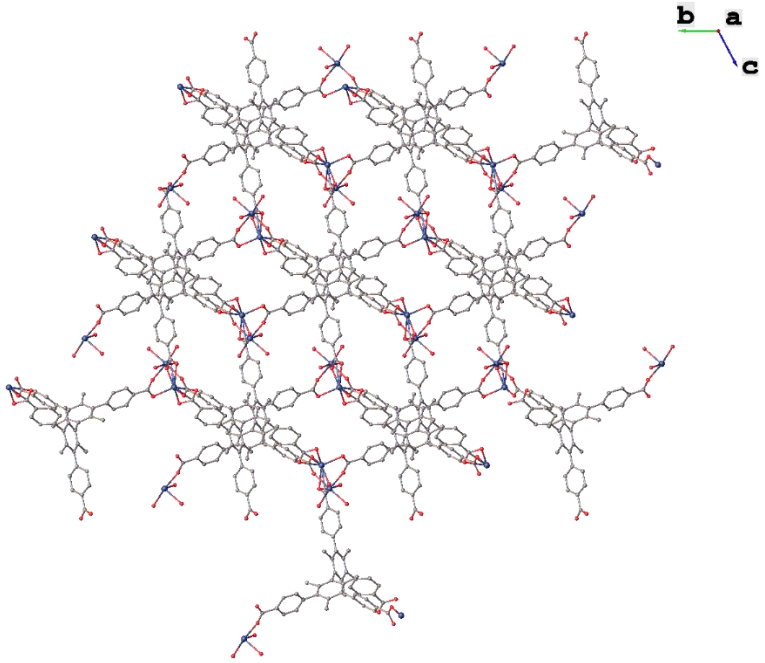

Figure 1. Metal-organic framework of 3,3',5,5'-tetrakis(4-carboxyphenyl)-2,2',4,4',6,6'-hexamethyl-1,1-biphenyl with Cd(II)

Two new coordination polymers have been synthesized using the rigid ligand 3,3',5,5'-tetrakis(4-carboxyphenyl)-2,2',4,4',6,6'-hexamethyl-1,1-biphenyl (H_4L), $Cd(NO_3)_2$ and $Zn(NO_3)_2$ under solvothermal conditions. Single-crystal X-ray diffraction revealed that in its deprotonated form, H_4L acts as a tetradentate ligand, coordinating with metal ions to form a three-dimensional metal-organic network (Fig. 1). The coordination polymers of Cd(II) and Zn(II) are isostructural and crystallize in the triclinic space group P-1. To assess the robustness of their coordination architecture, thermogravimetric analysis was conducted on the crystalline material, demonstrating that both complexes exhibit excellent thermal stability. Further characterization of Cd(II) and Zn(II) coordination polymers was achieved using IR spectroscopy and elemental analysis.

ACKNOWLEDGMENTS: This work was supported by Moldova State University, Institute of Chemistry, subprogram SSMCCLP code 010602**.** 010602.

POLYMERIC COMPOUND Cd(II) WITH 5-(4-CARBOXYPHENYL)1-PHENYL-1H-PYRAZOLE-3-CARBOXYLIC ACID

E. Neguta[1,*], G. Roman[2], S. Shova[2], V. Lozan[1]
[1]*Institute of Chemistry, Moldova State University, Chișinău, Republic of Moldova;*
[2]*"Petru Poni" Institute of Macromolecular Chemistry, Iași, Romania*
[*]E-mail: elena.neguta@sti.usm.md, neguta26elena@gmail.com

Metal-organic frameworks (MOFs) for hydrogen storage have continued to receive intense interest over the past decade. MOFs are a class of organic-inorganic hybrid crystalline materials consisting of metallic moieties that are linked by strong coordination bonds to organic ligands. They exhibit a great structural diversity and possess low weight, exceptionally high surface areas, large free volumes, and tunable pore sizes and functionalities, making them extremely attractive for a variety of applications. For these reasons MOFs have been extensively studied [1,2].

In this work, the synthesis of a polymeric compound of Cd(II) with 5-(4-carboxyphenyl)1-phenyl-1H-pyrazole-3-carboxylic acid (H_2L) is presented. The polymeric complex was prepared by the reaction of H_2L [3] with cadmium nitrate tetrahydrate, by solvothermal method in dimethylformamide and water. According to X-ray crystallography is a three-dimensional coordination polymer $\{[Cd_2L_2(H_2O)_2]\cdot 1.5H_2O\}_n$ (**1**) which crystallizes in the *Pnn*2 space group of the orthorombic system, with the unit cell parameters: a=8.8527(3); b=19.2171(7); c=19.812(8) Å. As shown in Figure 1, the asymmetric part of the structure consists of two Cd atoms, two L^{2-} molecules and two interstitial water molecules. The hexacoordinated Cd1 atom has a slightly distorted tetragonal bipyramid coordination polyhedron. The base of the coordination polyhedron is formed by the N1, O1, $O1^{ii}$ atoms of the ligand and an oxygen atom O3 of water molecule. While in apical positions are situated the oxygen atom $O3^{ii}$ of the water molecule and the nitrogen atom $N1^{ii}$. The Cd2 atom has the coordination number eight, being surrounded by four chelated carboxylate groups of H_2L.

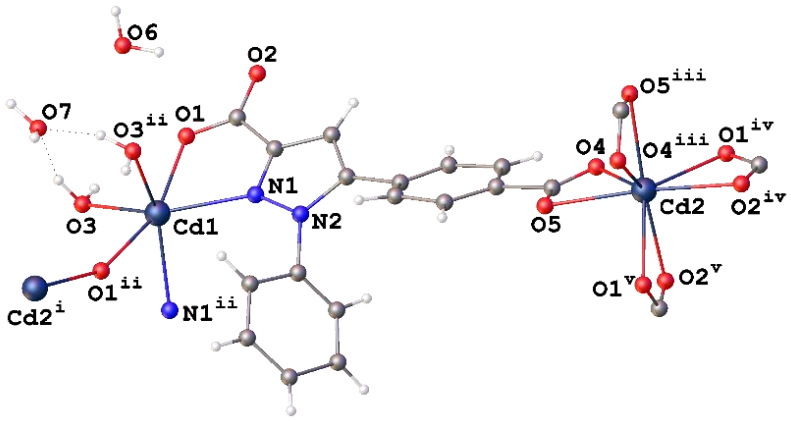

Figure 1. The crystal structure of the compound $\{[Cd_2L_2(H_2O)_2]\cdot 1.5H_2O\}_n$

ACKNOWLEDGEMENTS: This work was funded by the Research Subprogram SSMCCLP (code 010602).

1. H.W. Langmi, J. Ren, B. North, M. Mathe, D. Bessarabov. *Electrochim. Acta* **128** (2014) 368-392.
2. Y. Lin, C. Kong, Q. Zhang, L. Chen. *Adv. Energy Mater.* **7** (2017) 1601296.
4. B.-I. Bratanovici, A. Nicolescu, S. Shova, I.-A. Dascălu, R. Ardeleanu, V. Lozan, G. Roman. *Research on Chemical Intermediates* (2019) 1-25.

3D COORDINATION POLYMER OF Eu(III) AND 5-(4-CARBOXYPHENYL)-1-PHENYL-1H-PYRAZOLE-3-CARBOXYLIC ACID

E. Neguta[1,*], G. Roman[2], S. Shova[2], V. Lozan[1]
[1]*Institute of Chemistry, Moldova State University, Chișinău, Republic of Moldova;*
[2] *"Petru Poni" Institute of Macromolecular Chemistry, Iași, Romania;*
[*]E-mail: elena.neguta@sti.usm.md, neguta26elena@gmail.com

Metal-organic frameworks (MOFs) have attracted considerable attention as emerging nanomaterials. Based on their tunable size, high porosity, and large specific surface area, MOFs have a wide range of applications in the fields of chemistry, energy, and biomedicine. However, the MOF materials obtained from lanthanides with a unique electronic configuration as inorganic building units have unique properties such as optics, magnetism, and radioactivity [1,2].

A three-dimensional coordination polymer of Eu(III) with 5-(4-carboxyphenyl)-1-phenyl-1H-pyrazole-3-carboxylic acid (H_2L) was synthesized using the solvothermal method. The obtained compound was characterized by single-crystal X-ray diffraction, IR spectroscopy, elemental and thermal analysis, and luminescence. The compound $\{[Eu(HL)(L)]\cdot 20H_2O\}_n$ **(1)** crystallized in a tetragonal system with space group $P\bar{4}n2$, with the unit cell parameters: a=16.5239(3); b=16.5239(3); c=19.5872(3) Å. The ligand coordinates in a tridentate fashion, with carboxylate groups onechelating and the other bridging. The free nitrogen atom does not participate in coordination bonding. The coordination number of metal ion is eight, generated by oxygen atoms from the carboxylate groups of four ligand molecules, resulting in a three-dimensional coordination network. In the IR spectrum of **1** the broad bands at 3448 cm^{-1} correspond to the asymmetric and symmetric O-H stretching vibrations of water molecules. The strong absorption peaks at 1690–1650 and 1450–1440 cm^{-1} are attributed to the asymmetric and symmetric vibrations of carboxylate groups. The bands in the range 1597–1537 cm^{-1} are assigned to the characteristic stretching vibrations of phenyl rings and the absorption bands appearing between 1353 and 1265 cm^{-1} are associated with the pyrazole ring.

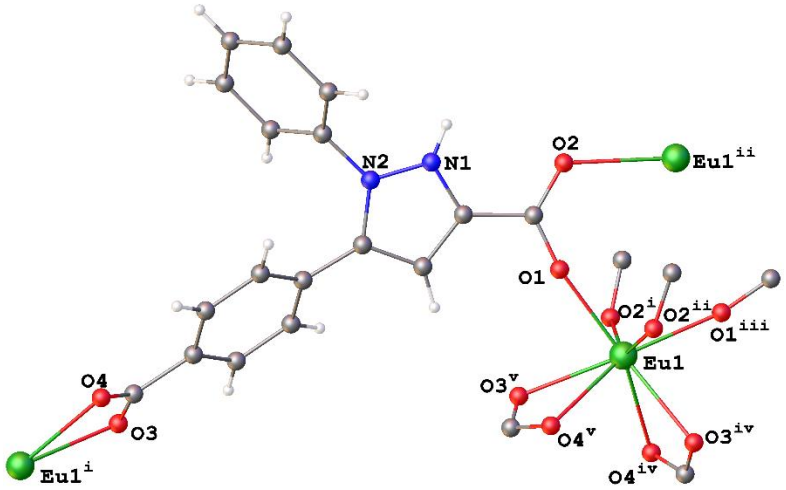

Figure 1. The crystal structure of the compound $\{[Eu(HL)(L)]\cdot 20H_2O\}_n$

ACKNOWLEDGEMENTS: This work was funded by the Research Subprogram SSMCCLP (code 010602).

[1] S. Sun, Y. Zhao, J. Wang, R. Pei. *J. Mater. Chem. B* **10** (2022) 9535-9564
[2] Y. Zhang, S. Liu, Z.-S. Zhao, Z. Wang, R. Zhang, L. Liu, Z.-B. Han. *Inorg. Chem. Front.* **8** (2021) 590-619

IMMOBILIZATION OF LIPASE B FROM *CANDIDA ANTARCTICA* ON VARIOUS SUPPORTS. ACTIVITY AND SELECTIVITY TESTING IN CONTINUOUS FLOW MICROFLUIDIC SYSTEM

M. Pap*, M.- E. László, C. Paizs, G. Katona
Enzymology and Applied Biocatalysis Research Center, Babeș-Bolyai University, Faculty of Chemistry and Chemical Engineering, Cluj-Napoca, Romania
*E-mail: matild.pap@ubbcluj.ro

Present research is focused on the activity and the selectivity testing of immobilized Lipase B from *Candida antarctica* yeast (CaL-B) in continuous flow microfluidic system using a self-designed and CNC / laser engraving technique manufactured microchip as biocatalyst holder.

For the immobilization of the enzyme 3 different carriers were used: Immobead T2-150 (as purchased), magnetite [1] and sol-gel [2], both freshly synthesized before used.

The microchip inner channels were filled with the prepared biocatalysts, the substrate and acylating agent were dosed *via* the microfluidic device, which facilitates reactions and enables precise control over parameter optimization [3], such as substrate concentration, temperature or flow rate.

The biocatalysts activity and selectivity was investigated upon the acylation reaction of (*R*,*S*)-1-phenylethanol with vinyl acetate, since it is known that CaL-B being an *R*-selective lipase [4], catalyzes the formation of (*R*)-1-phenylethyl acetate product, which can be easily identified using high pressure liquid chromatography (HPLC) or gas chromatography (GC) analysis. The immobilization rate and the synthetic activity of the prepared biocatalysts were determined by UV-Vis spectroscopy.

Upon optimization it was found that lower flow rate values return higher conversion rates and controllable parameters such substrate/acylating agent ratio significantly influence the efficiency of the continuous flow microfluidic system.

[1] S. Melhi. *Crystals*. **13** (2023), 1301.
[2] A. I. Dudu, M. A. Lăcătuș, L. C. Bencze, C. Paizs, M. I. Toșa. *ACS Sustainable Chemistry & Engineering*. **9** (2021), 5461-5469
[3] J. Coloma, Y. Guiavarc'h, P.- L. Hagedoorn, U. Hanefeld. *Chem. Commun*. **57** (2021), 11416-11420.
[4] M. Z. Habulin. *Journal of Molecular Catalysis B: Enzymatic*. **58** (2009), 24-28.

SYNTHESIS AND CHARACTERIZATION OF DINUCLEAR Gd(III) COMPLEX BASED ON N-(PYRIDIN-2-YLMETHYLENE)PICOLINHYDRAZONE

D. Podgornii[1,*], F. M. Amombo Noa[2], L. Öhrström[2], S. G. Baca[1]
[1]*Institute of Applied Physics, Moldova State University, Chișinău, Republic of Moldova;*
[2]*Chemistry and Biochemistry, Department of Chemistry and Chemical Engineering, Chalmers University of Technology, Gothenburg, Sweden*
[*]E-mail: daniel.podgornii@ifa.usm.md

The fascinating optical and magnetic properties of the lanthanides, which can be exploited in a wide range of technological applications, have generated considerable interest in the fabrication of novel lanthanide complexes. Multidentate pyridine acylhydrazones exert a profound influence on the structural, electronic and magnetic properties of the lanthanides, forming stable complexes due to nitrogen coordination. A new dinuclear complex, $[Gd_2(pphz)_2(NO_3)_4(H_2O)]\cdot MeCN$ (**1**) (where $pphz^-$ = *N*-(pyridin-2-ylmethylene)picolinhydrazonate), has been synthesized by the ultrasonic treatment of Gd(III) nitrate salt with 3,6-bis(2-pyridyl)-1,2,4,5-tetrazine (bptz) and *N*,*N*,*N*′,*N*′-tetrakis(2-hydroxyethyl)ethylenediamine ligands in acetonitrile. X-ray structural analysis revealed that **1** crystallizes in the monoclinic $P2_1/n$ space group with unit cell parameters: a = 12.1189(6), b = 23.6819(12), c = 12.5156(6) Å; β = 91.910(2)°, V = 3589.9 Å^3. The resulting complex consists of two Gd(III) atoms (Gd1 and Gd2), two $pphz^-$ ligands, four nitrate anions, a coordinated water molecule, and the solvate acetonitrile (Fig. 1). It is interesting to note that the reaction of Gd(III) nitrate with the heterocyclic bptz in acetonitrile resulted in the opening of its tetrazine ring to give an asymmetric product $pphz^-$, which then coordinated to the metal ions.

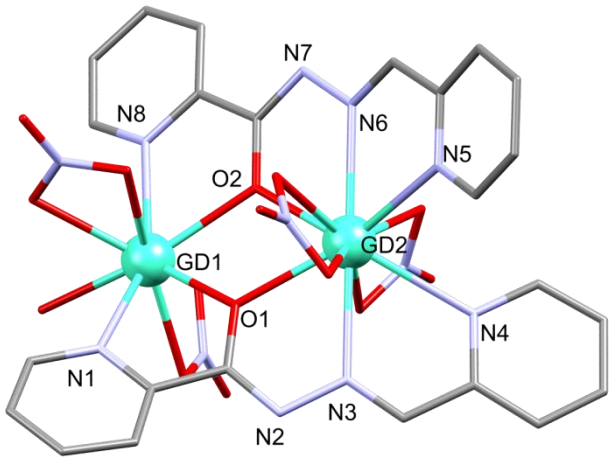

Figure 1. The structure of $[Gd_2(pphz)_2(NO_3)_4(H_2O)]$ in **1**.
Hydrogen atoms and solvate acetonitrile molecule are omitted for clarity.

In **1**, the two metal ions have different coordination environments. Gd1 has an N_2O_7 donor set formed by two nitrogen atoms and the two bridging hydrazonic oxygen atoms from the two $pphz^-$ ligands, as well as four oxygen atoms from the two chelated nitrates and a water molecule. The N_4O_6 coordination sphere of Gd2 is completed by four nitrogen atoms and two oxygen atoms of $phzp^-$ moieties and four oxygen atoms from the two chelated nitrates. The Gd–N distances are between 2.53 and 2.63 Å, and the Gd–O distances are between 2.32 and 2.49 Å. The solid-state structure of **1** is stabilized through a combination of O–H···O, O–H···N, and C–H···N interactions. Hirshfeld surface analysis was calculated to establish the contributions of the different intermolecular interactions in the crystal packing motif of **1**.

ACKNOWLEDGMENTS: The authors from R. Moldova are grateful for the subprogram financed by the Ministry of Education and Research of R. Moldova 011202.

CRYSTALLOGRAPHIC CHARACTERIZATION OF TETRANUCLEAR {Fe_2M_2} (M = Y, Ln) CLUSTERS

D. Podgornii*, V. Ch. Kravtsov, S.G. Baca
Institute of Applied Physics, Moldova State University, Chișinău, Republic of Moldova
*E-mail: daniel.podgornii@ifa.usm.md

New series of tetranuclear {$Fe^{III}_2M^{III}_2$} clusters: $[Fe_2M_2(piv)_6(thme)_2(MeOH)_4]\cdot n(MeOH)$ (n =0: M^{III} = Y(**1**), Pr (**2**), Nd (**3**), Gd (**4**), Tb (**5**); n = 3: M^{III} = Dy (**6**)) and $[Fe_2M_2(piv)_6(thmp)_2(MeOH)_4]\cdot n(MeOH)$ (n =0: M^{III} = Gd (**7**); n = 1: M^{III} = Tb (**8**), Dy (**9**) ; Ho (**10**)) were obtained by reaction of trinuclear $[Fe_3O(piv)_6(H_2O)_3](piv)\cdot$Hpiv cluster (Hpiv = pivalic acid), $M(NO_3)_3\cdot xH_2O$ (M^{III} = Y, Ln) with 1,1-tris(hydroxymethyl)ethane (H_3thme) or 1,1,1-tris(hydroxymethyl)propane (H_3thmp). Single-crystal X-ray diffraction analysis revealed that compounds **1-10** feature a tetranuclear heterometallic {$Fe^{III}_2M^{III}_2$} core with a "butterfly" topology. This structure results in a planar Fe_2M_2 rhombus. All the clusters in the crystal are located on a crystallographic inversion center, thus having C_i molecular symmetry. The asymmetric unit contains one half of the cluster, including a unique Fe1 and Y1 or Ln1 ion, along with solvent methanol molecules in compounds **6** and **8-10**. The triply deprotonated polyalcohol ligands, $thme^{3-}$ and $thmp^{3-}$, adopt a $\eta^2{:}\eta^2{:}\eta^3{:}\mu^4$ bridging mode, while four pivalate ligands bind to the Fe-M edge in a $\eta^1{:}\eta^1{:}\mu^2$ mode. The other two pivalates coordinate to Y/Ln ions in two ways: as monodentate ligands in compounds **1, 5, 6**, and **8-10**, forming type **I** clusters (Fig. 1a), or in a chelating (η^2) mode in compounds **2-4** and **7**, forming type **II** clusters (Fig. 1b). In all clusters, Y/Ln atom coordinates with two methanol molecules, completing the coordination sphere to O_8 in type **I** clusters and O_9 in type **II** clusters. The coordination environment of the lanthanide atoms correlates with their ionic radius: smaller lanthanides than Gd form type **I** clusters, while Gd and larger lanthanides form type **II** clusters. The coordinated and solvent methanol molecules in crystal structures **1-10** participate in O–H···O hydrogen bonds. In type **I** clusters, one coordinated MeOH molecule forms intramolecular O–H···O bonds, stabilizing the monodentate pivalate ligand. The other MeOH molecule forms intermolecular H-bonds with neighbouring clusters in **1**, **5**, and **8-10**, or via bridging methanol in **6**, linking them into H-bonded chains. In solvent-free type **II** clusters, the two coordinated MeOH molecules form intermolecular O–H···O bonds with pivalate ligands on neighbouring clusters, bridging them into H-bonded chains.

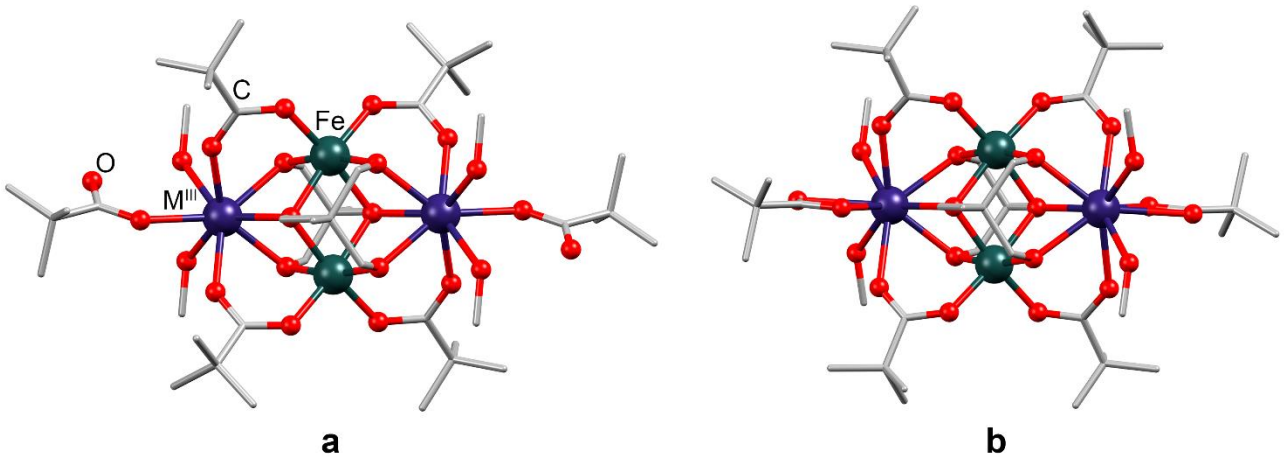

Figure 1. (a) View of cluster **5** as a representative example of type **I** clusters (**1, 5, 6**, and **8-10**).
(b) View of cluster **2** as a representative example of type **II** clusters (**2-4** and **7**).

ACKNOWLEDGMENTS: The authors are grateful for the subprogram financed by the Ministry of Education and Research of R. Moldova 011202.

SYNTHESIS OF NEW THIOSEMICARBAZONES CONTAINING "PARACETAMOL" FRAGMENT

R. Rusnac*, A. Gulea
Moldova State University, Chișinău, Republic of Moldova
*E-mail: roman.rusnac@usm.md

In recent years there has been an increase in studies in the cytostatic field. Thus in the foreground appear the compounds of a coordinative nature based on which a central ion is located, usually from the 3*d*-5*d* series, which are based on the research of cisplatin and its derivatives. Organic molecules with a thiosemicarbazone fragment with different electron-donor or electron-acceptor substituents are increasingly found as ligands.

Metallodrugs are the most promising in the coming years, according to a very pertinent index such as: the selectivity index and the possibility that drugs will become a paradox of personalized treatment in the near future. A disadvantage of cisplatin is its adverse effect, together with problems of tumor recurrence especially in breast, lung and bladder cancer [1].

The inclusion in the thiosemicarbazide skeleton in the position of the nitrogen atom (4) of the fragment derived from the hypothetical "*paracetamol*" could contribute to reducing the toxicity of the synthesized compounds and could increase the selectivity of the final compounds towards biological targets.

The aim of this work is the synthesis of thiosemicarbazones (H_2L^1 and H_2L^2) based on salicylic aldehyde derivatives with increase electron density (positive mesomeric effect +M) and electron-accepting (negative inductive effect -I) groups, in order to determine the biological properties.

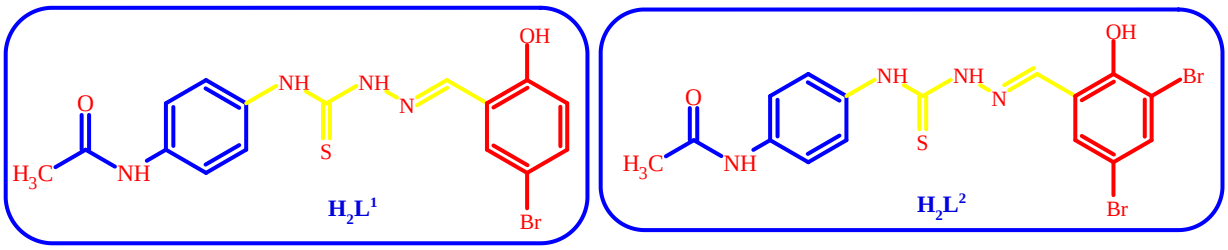

Figure 1. Structural formulas of the thiosemicarbazones H_2L^1 and H_2L^2.

IUPAC name:

H_2L^1- ***N*-[4-({(2*E*)-2-[(5-bromo-2-hydroxyphenyl)methylidene]hydrazinecarbothioyl}amino)phenyl]acetamide**

H_2L^2- ***N*-[4-({(2*E*)-2-[(3,5-dibromo-2-hydroxyphenyl)methylidene]hydrazinecarbothioyl}amino)phenyl]acetamide**

The synthesis of N-(4-isothiocyanatophenyl)acetamide is carried out according to the procedure described in [2], subsequently following a reaction with hydrazine monohydrate in THF, thiosemicarbazide is obtained. Following the elimination addition reaction between N-{4-[(hydrazinecarbothioyl)amino]phenyl}acetamide and 5-bromo-2-hydroxybenzaldehyde or 3,5-dibromo-2-hydroxybenzaldehyde, thiosemicarbazones H_2L^1 and H_2L^2 are obtained. The structural formulas for thiosemicarbazones have been investigated using modern research methods such as: NMR and FTIR.

ACKNOWLEDGMENTS: This work was fulfilled with the financial support of the "young researchers 2024-2025" project 24.80012.5007.14TC, and subprogram 010602 of the institutional project.

[1] V. Palakkeezhillam, V.Namboothiri, et al. *Organometallics*, vol.43.3, 2024, pages: 242-260.
[2] R.Rusnac, O. Garbuz, et al. *Inorganics*, vol. 11.10, 2023, page 408.

DESIGN AND SYNTHESIS OF N-CYCLOHEXYL-2-(9*H*-FLUOREN-9-YLIDENE)HYDRAZINE-1-CARBOTHIOAMIDE

R. Rusnac[1,*], I. Bulimestru[1], A. Ciursin[1], L. I. Gaina[2]
[1]*Faculty of Chemistry and Chemical Technology, State University of Moldova, Chișinău, Republic of Moldova;*
[2]*Faculty of Chemistry and Chemical Engineering, Babeș-Bolyai University, Cluj-Napoca, Romania*
[*]E-mail: roman.rusnac@usm.md

Fluorenone-based thiosemicarbazones in recent years have attracted special attention due to its structural and molecular architecture. Their biological relevance is particularly interesting, due to a wide spectrum of pharmacophore groups, thiosemicarbazones exhibit a series of essential properties such as: antiviral, antimalarial, anticancer as well as antibacterial [1].

In this study it was proposed to functionalized cyclohexylamine in thiosemicarbazide fragment then followed by azomethine condensation between fluorenone and N-cyclohexylhydrazinecarbothioamide in a molar ratio of 1:1 followed by acid catalysis (Figure).

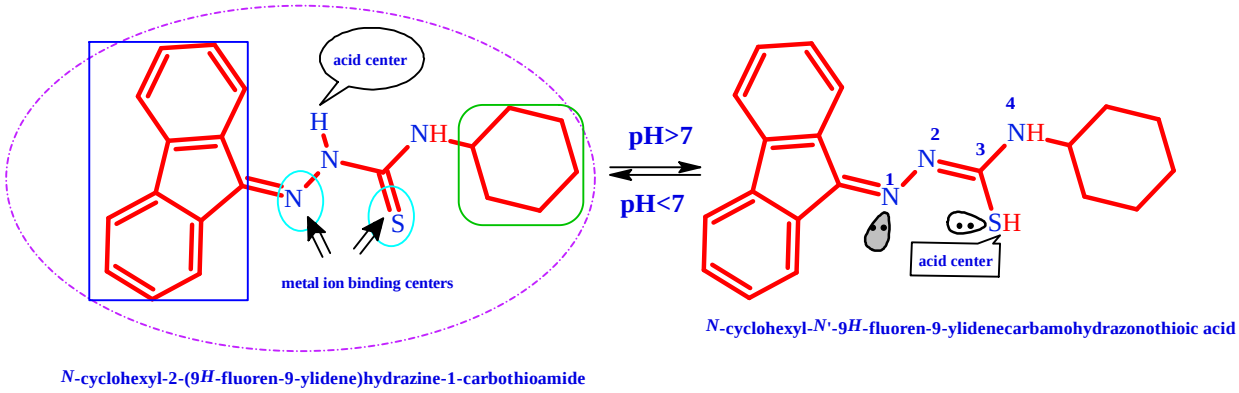

Figure 1. Tautomeric forms of N-cyclohexyl-2-(9*H*-fluoren-9-ylidene)hydrazine-1-carbothioamide.

N-cyclohexyl-2-(9H-fluoren-9-ylidene)hydrazine-1-carbothioamide was structurally confirmed by NMR analysis: 1.14-2.15 ppm cyclohexane ring (10 H); 4.38 ppm $CH_{(ring)}$-N; 7.33-8.40 ppm $CH_{(Fluorene)}$; 8.50 ppm NH(4); 9.98 ppm N-H $_{hydrazinic}$.

ACKNOWLEDGMENTS: This work was fulfilled with the financial support of the AUF-ECO 2023 - Soutien aux Equipes de recherche SER-ECO. Projet: "Synthèse et analyse de dérivés organiques à base de fluorénone pour des applications en biologie".

[1] N.C.Giffert L., et al. *Journal of Organometallic Chemistry*, vol. 957, 2022, page 122148.

PENTANUCLEAR $\{Co^{III}_3Ln^{III}_2\}$ (Ln = Pr, Nd, Sm) ISOBUTYRATE CLUSTERS WITH N-BUTYLDIETHANOLAMINE

D. D. Stati[1,*], J. van Leusen[2], V. Ch. Kravtsov[1], Y. Chumakov[1], P. Kögerler[2], S. G. Baca[1]
[1]*Institute of Applied Physics, Moldova State University, Chișinău, Republic of Moldova;*
[2]*Institute of Inorganic Chemistry, RWTH Aachen University, Aachen, Germany*
[*]E-mail: dumitru.stati@ifa.usm.md

Heterometallic d-f coordination clusters are of current interest in chemistry and material science because of their magnetic properties and potentials for high-density information storage devices, quantum computing, spintronics, and magnetocaloric materials. As part of our ongoing research in the development of 3d-4f complexes [1], three new heterometallic $[Co_3Ln_2(OH)(ib)_5(bdea)_3(NO_3)_3]\cdot n$MeCN ($Ln^{III}$ = Pr (**1**), Nd (**2**), Sm (**3**)) clusters have been synthesized by the reaction of cobalt(II) isobutyrate (Hib = isobutyric acid) and $Ln(NO_3)_3\cdot 6H_2O$ with N-butyldiethanolamine (H_2bdea) in the MeCN solution. The compounds were characterized by IR spectroscopy, ESI mass spectrometry, thermogravimetric analysis, and their structures were determined by single crystal X-ray diffraction. Clusters **1-3** are isostructural and isomorphous, crystallizing in the *P*-1 space group and possessing a robust and unusual of $\{Co^{III}_3Ln^{III}_2\}$ core topology, previously unseen in Co/Ln chemistry. This topology comprises three non-coplanar triangles ($\{CoLn_2(\mu_3\text{-}OH)\}$, $\{CoLn_2(\mu_3\text{-}O_{bdea})\}$, and $\{Co_2Ln(\mu_3\text{-}O_{bdea})\}$) that share a common Ln^{III} site, as shown in Figure 1. The cluster core in **1-3** can also be described as a heterometallic $\{CoLn_2(OH)\}$ unit decorated with an additional $\{Co_2\}$ unit. The metal atoms in the $\{CoLn_2\}$ triangle are additionally linked by two ib^- and three O atoms of two $bdea^{2-}$ ligands. The $\{Co_2\}$ moiety binds to the trinuclear $\{CoLn_2(OH)\}$ moiety through two bridging ib^- ligands and two O-bridges from two $bdea^{2-}$ units. The ib^- and O atoms of two $bdea^{2-}$ additionally bridge two Co atoms in the dimeric unit. Magnetic studies reveal non-interacting or very weakly interacting Ln^{III} centers and low spin Co^{III} centres. The DFT-TB2J approach has been applied to estimate the magnetic anisotropy energy of compounds **1-3** and to calculate the exchange coupling between lanthanides.

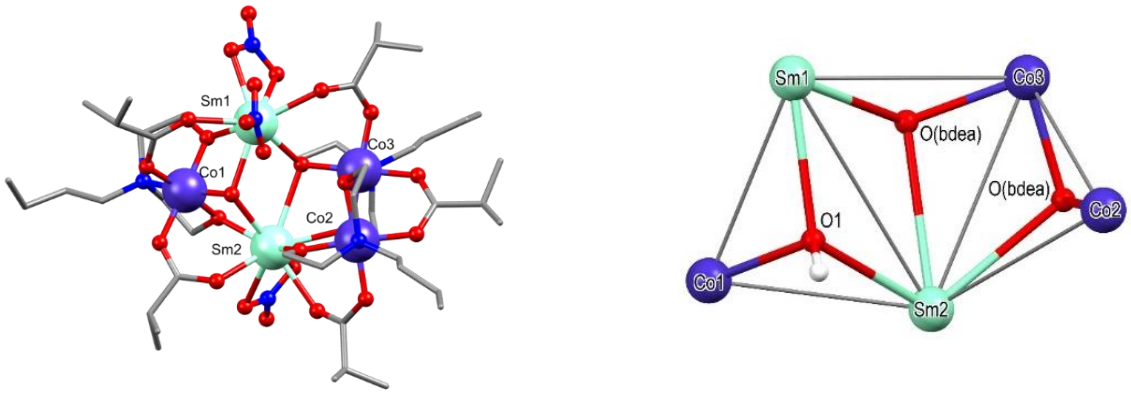

(a) (b)

Figure 1. Structure of the $[Co_3Sm_2(OH)(ib)_5(bdea)_3(NO_3)_3]$ cluster (a) and view of $\{Co_3Sm_2O_7\}$ core (b) in **3**.

ACKNOWLEDGMENTS: DS, VCK, YC, and SB are grateful for the subprogram financed by the Ministry of Education and Research of R. Moldova 011202. The authors thank the National Initiatives for Open Science in Europe for granting 'MAGNANO' and the provided access to the e-infrastructure purchased under the National Roadmap for RI, financially coordinated by the MES of the Republic of Bulgaria (grant No D01-325/01.12.2023). DS thanks the World Federation of Scientists for the excellence scholarship.

[1] M. Darii, J. van Leusen, V.Ch. Kravtsov, Y. Chumakov, K. Krämer, S. Decurtins,; S.-X. Liu, P. Kögerler, S.G. Baca. *Cryst. Growth Des.* **23** (2023) 6944; D. Stati, J. van Leusen, N. Ahmed, V.Ch. Kravtsov, P. Kögerler, S.G. Baca. *Cryst. Growth Des.* **23** (2023) 395; M. Darii, V.Ch. Kravtsov, K. Krämer, J. Hauser, S. Decurtins, S.-X. Liu, M. Affronte, S.G. Baca. *Cryst. Growth Des.* **20** (2020) 33.

THERMOGRAVIMETRIC ANALYSIS OF ISATIN β-ETHYLENEKETALS: IMPLICATIONS FOR PSYCHOTROPIC DRUG DEVELOPMENT

E.P. Stingaci[1], O. Petuhov[1,2], N.S.Sucman[1,*], T. Ștefaneț[3], V. Valica[3], F.Z.Macaev[1,3]
[1]*Institute of Chemistry, Moldova State University, Chișinău, Republic of Moldova;*
[2]*Research Center of Thermal Analysis in Environmental Problems, West University of Timisoara, Timișoara, România;*
[3]*Scientific Center for Drug Research, "Nicolae Testemitanu" State University of Medicine and Pharmacy, Chișinău, Republic of Moldova*
[*]E-mail: natalia_sucman@yahoo.com

Depression is associated with a deficiency of neurotransmitters like norepinephrine and serotonin. This has led to two main types of antidepressants: those inhibiting monoamine oxidase (MAO) and those preventing neurotransmitter reuptake. MAO inhibitors enhance adrenergic signalling by preventing the inactivation of norepinephrine and serotonin. Isatin and its β-ethyleneketals have shown potent MAO inhibitory activity and notable antidepressive effects, with some compounds also displaying significant sedative properties. Among them, isatin β-ethyleneketals exhibit notable antidepressive activity, with some compounds also showing significant sedative effects [1,2]. For instance, the β-ethyleneketal of N-acetonylisatin (Fig.1(a)) demonstrated a marked activity at a dose of 60 mg/kg, affecting various behavioural parameters. Given its promising psychotropic properties and moderate toxicity (LD50 value is 600 mg/kg), this study aimed to further research their stability for broader pharmacological potential. In this work, the thermal stability of the sample was analyzed using thermogravimetry (TG). The TG results indicated that decomposition begins at 300°C, with an 90% mass loss (DTG data) over a short temperature range due to the decomposition of organic matter (see Fig.1(b)). Additionally, the DTA data revealed that phase transitions at 128.33 °C occur in the analyte corresponding to the compound's melting. Therefore, as a result of this study, it is recommended that temperatures above 128°C should not be used in the technological process of creating β-ethyleneketal of N-acetonylisatin-based medical products.

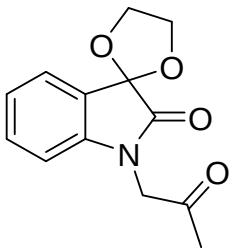

1'-(2-oxopropyl)spiro[[1,3]dioxolane-2,3'-indolin]-2'-one

(a)

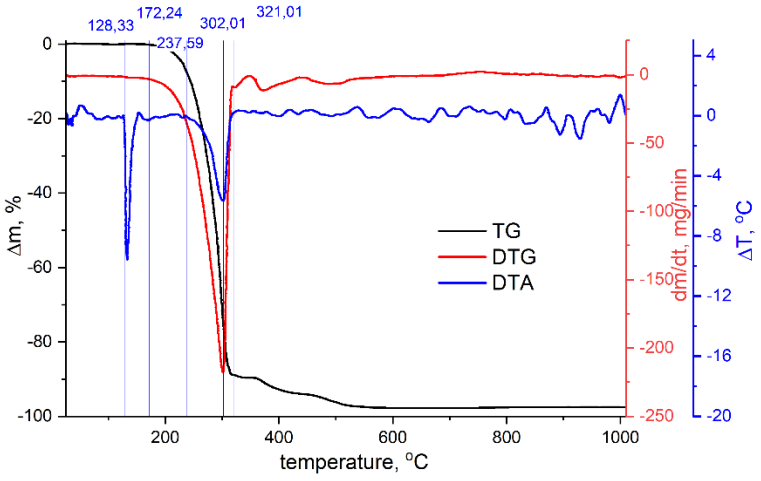

(b)

Figure 1. The structure and IUPAC name of the studied ketal (a) and its thermogravimetric data (b).

[1] T. Ștefaneț, E. Stîngaci, O. Vîslouh, V. Valica, F. Macaev. Akademos, 4 (54) (2019) 24-28.
[2] G. Zhunghietu. Revue Roumaine de Chimie 46 (2001) 517–520.

DIANYLINEGLYOXIME AND ISOPHTHALIC DIANION IN THE SYNTHESIS OF BINUCLEAR COMPLEXES WITH OCTAHEDRAL GEOMETRY

D. Ureche[1,*], P. Bourosh[2], I. Bulhac[1]
[1]*Institute of Chemistry, Moldova State University, Chișinău, Republic of Moldova;*
[2]*Institute of Applied Physics, Moldova State University, Chișinău, Republic of Moldova*
[*]E-mail: d.ureche@yahoo.com

The *vic*-dioximes obtained in recent years are successfully used to obtain compounds with increased nuclearity, including coordination polymers [1]. An effecient method for obtaining the latter involves the use of additional bridging ligands. The reported complexes were synthetized by interaction of a mixture of ligands consisting of dianylineglyoxime ($DAnH_2$) and isophthalic acid (1,3-H_2bdc) with manganese acetate tetrahydrate in a molar ratio of 2:2:1, respectively. The reaction was carried out in a mixture of ethanol and DMSO in a ratio of 3:1 (vol/vol).

Previously, under similar conditions, a series of Zn(II) and Mn(II) complexes were synthesized, using methanol, DMF or DMSO as solvents, which proved to be binuclear and whose octahedral polyhedra were completed with solvent molecules [2, 3].

The new obtained compound was investigated by IR spectroscopy (4000-400 cm^{-1}) and single crystal X-ray diffraction. The crystallographic study reported the creation of a binuclear compound similar to those from [2, 3] with the molecular formula $[Mn_2(DAnH_2)_2(1,3\text{-bdc})_2(DMSO)_4]$ (Figure *a* and *b*).

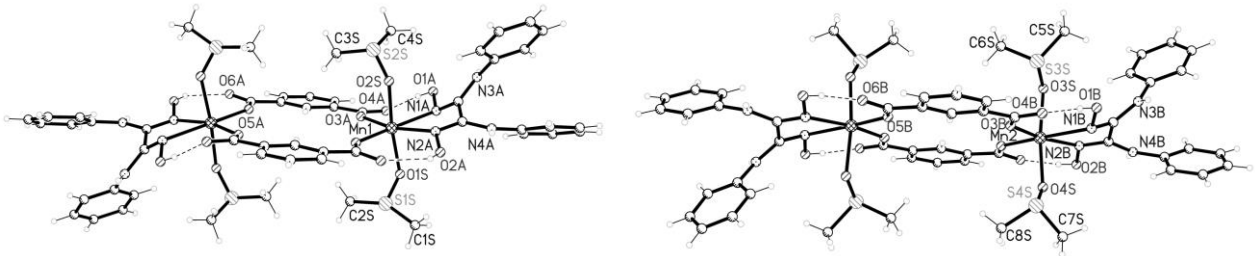

(a) (b)

Figure 1. Molecular structure of complexes $[Mn_2(DAnH_2)_2(1,3\text{-bdc})_2(DMSO)_4]$ (*a*,*b*).

The IR spectrum of the Mn(II) complex, includes several characteristic absorption bands for reported compound. Among these can be mentioned the signals that confirm the presence of the functional group ν(NH) at 3201 cm^{-1} and ν(OH) at 2600 cm^{-1}. The highest intensity band at 1012 cm^{-1} is attributed to ν(S=O) oscillations of coordinated DMSO and for the 1,3-substituted aromatic ring, intense bands between 746-693 cm^{-1} are attributed to $\delta_{nonpl.}(CH)_{arom.}$ [4].

The XRD analysis proved that binuclear complex $[Mn_2(DAnH_2)_2(1,3\text{-bdc})_2(DMSO)_4]$ crystallizes in the triclinic space group $P\bar{1}$. As a result, two crystallographically independent centrosymmetric binuclear molecular complexes (A and B) are formed in the crystal. The asymmetric part of the unit cell of the crystal contains two crystallographically independent Mn^{2+} cations, two neutral $DAnH_2$ ligands, two diprotonated dicarboxylate anions $(1,3\text{-bdc})^{2-}$ and four DMSO molecules. The octahedral coordination polyhedron of each metal atom is formed by the N_2O_4 donor atoms, in which one $DAnH_2$ ligand coordinates as bidentate-chelate *via* nitrogen atoms, two $(1,3\text{-bdc})^{2-}$ exo-ligands *via* one O-atom and two ligands DMSO *via* O-atom.

ACKNOWLEDGMENTS: The results reported in this paper were obtained within two research subprograms entitled: "*Synthesis and studies of new materials based on complex combinations with polyfunctional ligands and having useful application in medicine, biology and technology*" (code: 010602) and "*Design and fabrication of intelligent materials with advanced magnetic, adsorption, luminescent and biologically active properties*" (code 011202).

[1] D. Ureche, A. Rija, I. Bulhac, et al. *Russ. J. Inorg. Chem.,* **65(12),** (2020), 1838-1847.
[2] D. Ureche, I. Bulhac, A. Rija, et al. *Russ. J. Coord. Chem.,* **45(12),** (2019), 843-855.
[3] D. Ureche, I. Bulhac, S. Shova, P. Bourosh. *Chem. J. Mold.*, **17(2),** (2022), 62-72.
[4] L.J. Bellamy. Infrared spectra of complex molecules. New York, USA. Wiley, (1958), 426 p.

Ni(II) *TRIS*-DIOXIMATE CONTAINING A NOVEL *BIS-p*-TOLUIDINEGLYOXIME LIGAND

D. Ureche[1,*], I. Bulhac[1], P. Bourosh[2]
[1]*Institute of Chemistry, Moldova State University, Chișinău, Republic of Moldova;*
[2]*Institute of Applied Physics, Moldova State University, Chișinău, Republic of Moldova*
[*]E-mail: d.ureche@yahoo.com

An impressive number of Ni(II) *tris*-dioximates containting different *vic*-dioximes have been described so far [1, 2]. In addition to Ni(II) *tris*-dioximates, Cu(II) *tris*-dioximates containing disulfanilamideglyoxime and dianylineglyoxime have recently been synthesized and described [3]. The reported nickel(II) complex was obtained for the first time by synthesis methods described in the specialized literature, but using a new dioximic ligand *bis-p*-toluidineglyoxime ($DpatH_2$), terephthalic acid and nickel(II) sulfate hexahydrate. The structure of reported compound was confirmed by means of IR spectroscopy (4000-400 cm^{-1}) and single crystal X-ray diffraction. Crystallographic study established that the Ni(II) compound has the molecular formula $[Ni(DpatH_2)_3]SO_4 \cdot 1,4\text{-}H_2bdc \cdot 2.5DMF \cdot H_2O$ (Figure).

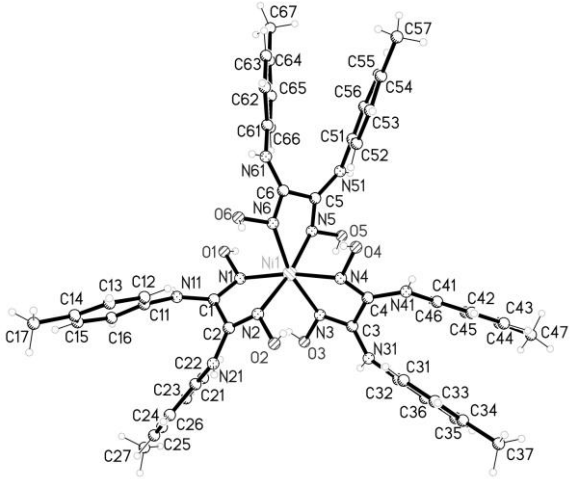

Figure 1. Molecular structure of the complex cation $[Ni(DpatH_2)_3]^{2+}$.

The IR spectra of compound is quite complex and includes many common absorption bands. The broad bands at 3174 cm^{-1} and 2511 cm^{-1} can be attributed to the associated ν(NH) and ν(OH) oscillations, respectively. Also, in the spectrum of the title compound, the frequencies of $\nu(C{=}O)_{DMF}$ at 1654 cm^{-1} and of the SO_4^{2-} anion are observed: 1180, 1097, 1050, 973, 629, 605, 590 and 494 cm^{-1} [4]. The presence of 1,4-substitution type in the aromatic rings of the ligand is confirmed by the intensive band at 813 cm^{-1} [4].

According to XRD data, the mononuclear compound crystallizes in orthorhombic space group $P2_12_12_1$. This is an ionic compound and consists of the complex cation $[Ni(DpatH_2)_3]^{2+}$, SO_4^{2-} anion, one 1,4-H_2bdc molecule, DMF molecules and one water molecule in the external sphere. The octahedral coordination polyhedron of the nickel atom is formed by donor N_6 atoms belonging to three oxime ligands $DpatH_2$, which are coordinated to the metal atom in a chelate-bidentate manner in a neutral form through/via the nitrogen atoms of the oxime groups.

ACKNOWLEDGMENTS: The results reported in this abstract were obtained within two research subprograms entitled: "*Synthesis and studies of new materials based on complex combinations with polyfunctional ligands and having useful application in medicine, biology and technology*" (code: 010602) and "*Design and fabrication of intelligent materials with advanced magnetic, adsorption, luminescent and biologically active properties*" (code 011202).

[1] E.B. Coropceanu, D. Ureche, A.P. Rija, et al. *Russ. J. Coord. Chem.,* **47(1),** (2021), 17-25.
[2] F. Yuksel, A.G. Gürek, M. Durmuş, et al. *Inorg. Chim. Acta,* **361,** (2008), 2225-2235.
[3] P.N. Bourosh, E.B. Coropceanu, A.P. Rija, et al. *Russ. J. Coord. Chem.,* **48(1),** (2022), 41-51.
[4] L.J. Bellamy. Infrared spectra of complex molecules. New York, USA. Wiley, (1958), 426 p.

STACKING PATTERNS IN CRYSTALS OF CYCLIC TRIIMIDAZOLES REGULATED BY THE NUMBER OF NITRILE GROUPS

V. Lozovan[1,2,*], V. Ch. Kravtsov[1], E. Cariati[3,4], M. S. Fonari[1]
[1]*Institute of Applied Physics, Moldova State University, Chișinău, Republic of Moldova;*
[2]*"Raluca Ripan" Institute for Research in Chemistry, Babes-Bolyai University, Cluj-Napoca, Romania;*
[3]*Department of Chemistry Università degli Studi di Milano,* [4]*INSTM Research Unit of Milano, Milano, Italy*
[*]E-mail: vasile.lozovan@ubbcluj.ro

Triazine and its derivatives are in great demands nowadays for numerous applications [1-3]. The nitrile monomers are the source of the nitrogen-rich covalent triazine frameworks (CTFs) that are among the promising functional materials due to their high specific surface area, adjustable pore size, suitable physicochemical stability and designable surface-active site [1,2]. Moreover, the nitrogen-rich electron-deficient triazine skeletons provide a number of intermolecular interactions such as hydrogen bonding, metal chelation and π-π interactions which can influence its properties. Since π-π stacking arrangements are strongly associated with high mobility, they affect the spin diffusion length in organic single-crystal layers. Finding ways to regulate stacking arrangements is crucial for the construction of highly efficient spintronic devices based on organic semiconductor single crystals (OSSCs) [3]. We report here the stacking patterns in three nitrile derivatives of cyclic triimidazole, triimidazo[1,2-*a*:1',2'-*c*:1",2"-*e*][1,3,5]triazine (**TT**). In the two-step synthetic protocol, the **TT** was first subjected to halogenation to obtain iodinated compounds **TT-I$_x$**. (x=1-3). In the next step the iodinated compounds were treated with cuprous cyanide resulting in the targeted nitrile compounds, **TT-CN$_x$**. (x=1-3, **1-3**). All compounds belong to the monoclinic crystal system and crystallize in the $P2_1/c$ (*a* 8.3343(12), *b* 16.3430(16), *c* 7.3667(11) Å, *β* 109.502(17) ˚ **1**; *a* 5.8554(4), *b* 11.0086(5), *c* 15.6784(13) Å, *β* 90.709(7) ˚ **2**), and $P2_1/n$ (*a* 7.0104(4), *b* 11.7770(6), *c* 13.8283(8) Å, *β* 91.133(5) ˚ **3**) space groups with *Z*=4. The crystal packing in **1** and **2** is governed by the CH…N edge-to-edge short contacts that combine molecules **1** and **2** in the planar layers, and π-π stacking interactions between the molecules in adjacent layers that provide slipped-stack stacking with one-dimensional π-π overlap in **1**, and the brick-wall stacking motif with two-dimensional π-π overlap in **2**. The significant rearrangement of intermolecular contacts in **3** resulted in the herringbone stacking motif with face-to-face π-π overlap (Fig. 1).

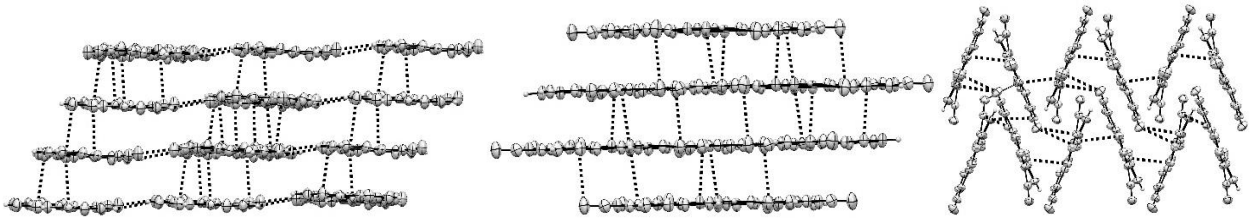

Figure 1. Stacking patterns in **1** (left), **2** (middle) and **3** (right) with short contacts shown by dotted lines.

Thus, this series of mono-, di-, and tri-nitrile substituted triimidazoles gives a beautiful example of how modification of molecular structure and intermolecular interactions allow to regulate the packing patterns in monocomponent crystals.

ACKNOWLEDGEMENTS: The authors from Moldova thank the subprogram 011202 for support.

[1] P. Katekomol, J. Roeser, M. Bojdys, J. Weber, A. Thomas. *Chem. Mater.* **25** (2013) 1542-1548.
[2] R. Luo, W. Xu, M. Chen, X. Liu, Y. Fang, H. Ji. *ChemSusChem* **13**, (2020) 6509–6522.
[3] M. Ding, X. Gu, L. Guo, R. Zhang, X. Zhu, R. Li, X. Zhang, W. Hua, X. Sun *J. Mater. Chem.* C, **10 (**2022) 2507–2515.

SYNTHESIS AND STRUCTURE OF TWO NEW COORDINATION POLYMERS BASED ON 3,4-PYRIDINEDICARBOXYLATE AND 4,4'-BIS(1H-IMIDAZOL-1-YL)METHYL-1,1'-BIPHENYL

I. Voda[1,*], V. Druta[1], S. Shova[2], V. Lozan[1]
[1]*Institute of Chemistry, Moldova State University, Chișinău, Republic of Moldova;*
[2] *"Petru Poni" Institute of Macromolecular Chemistry, Iași, Romania*
[*]E-mail: iravoda@gmail.com, irina.voda@sti.usm.md

The coordination chemistry and functions of imidazole-based MOFs provide a basis for designing new metal–organic cages with various host–guest combinations and manipulating key structural features with new functions (e.g. host–guest chemistry, luminescence, magnetism, catalysis, proton conductivity and biology applications) that are crucial to the advancement of this field.

Two new coordination polymers $\{[Co_2(Im_2CH_2Ph_2)(3,4\text{-}PyDC)_2]\cdot 2H_2O\}_n$ and $\{[Zn_2(Im_2CH_2Ph_2)(3,4\text{-}PyDC)_2]\cdot 3H_2O\}_n$, where $Im_2CH_2Ph_2$ - 4,4'-bis((1H-imidazol-1-yl)methyl-1,1'-biphenyl and 3,4-PyDC - 3,4-pyridinedicarboxylic acid, were synthesized and spectroscopically analysed by various physico-chemical methods (elemental analysis, IR, thermogravimetry, X-ray diffraction). The number of water molecules was determined through thermal analysis, the compounds beeing stable up to 200 and 310°C, respectively, after solvent removal. The carboxylic groups coordinate monodentately and provide bands at $\nu_{asim}(COO^-)$ - 1587 and 1597 cm^{-1}, $\nu_{sim}(COO^-)$ - 1389 and 1378 cm^{-1}, respectively.

X-ray diffraction analysis on single crystals showed that the coordination number of both metal ions Co(II) and Zn(II) is 4, the metal coordination nodes represent tetrahedral N_2O_2 environment created by a nitrogen atom from $Im_2CH_2Ph_2$ ligand, one from the 3,4-pyridinedicarboxylic acid and two oxygen atoms from different carboxylic groups of the acid. The compounds are isostructural one-dimensional polymers.

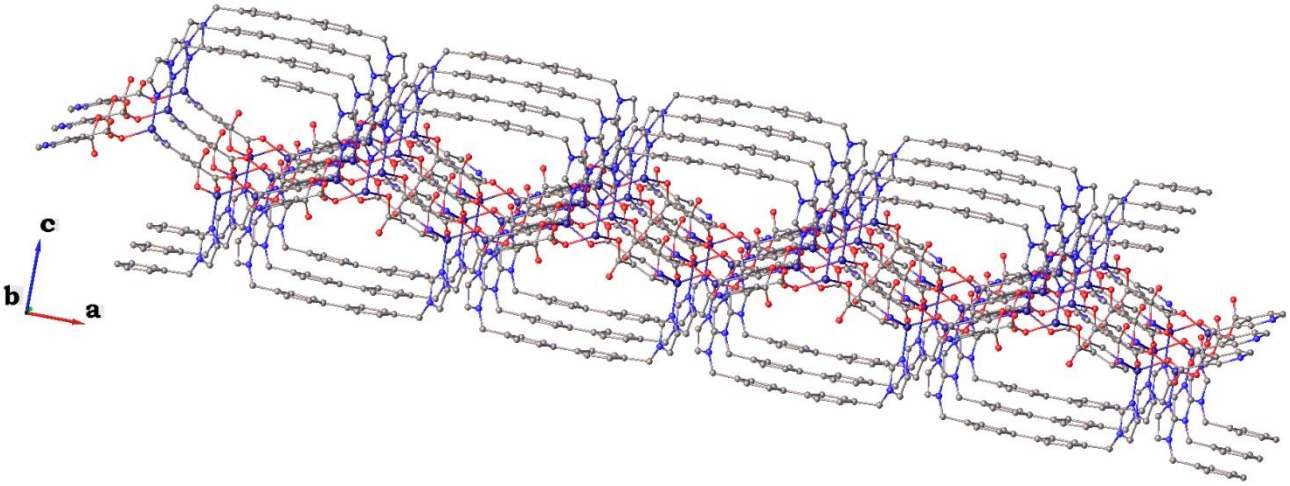

Figure 1. Graphical representation of 1D-$\{[Co_2(Im_2CH_2Ph_2)(3,4\text{-}PyDC)_2]\cdot 2H_2O\}_n$ polymer

ACKNOWLEDGEMENTS: This work was funded by the Research Subprogram SSMCCLP (code 010602).

SYNTHESIS AND STRUCTURE OF A NEW COORDINATION POLYMER CONTAINING 2,4-PYRIDINEDICARBOXYLATE AND IMIDAZOLE-BASED SPACER

I. Voda[1,*], S. Shova[2], V. Lozan[1]
[1]*Institute of Chemistry, Moldova State University, Chișinău, Republic of Moldova;*
[2] *"Petru Poni" Institute of Macromolecular Chemistry, Iași, Romania*
[*]E-mail: iravoda@gmail.com, irina.voda@sti.usm.md

Rational design and synthesis of coordination polymers with tailor-made structures have been one of the most attractive areas in crystal engineering and supramolecular chemistry. Great progress and developments have been made in the construction of diverse architectures, the prediction of the precise solid-state structures or the control of structural dimensionality of coordination polymers remains a long-term challenge in the field of crystal engineering.

The aim of this work was the synthesis, structure, composition and properties determination of zinc polymer with mixed ligands. Utilizing hydrothermal technique, using zinc(II) salt, 2,4-pyridinedicarboxylic acid (2,4-PyDC) and 4,4'-bis((1H-imidazol-1-yl)methyl-1,1'-biphenyl (Lig), a new one-dimensional coordination polymer with $\{[Zn(Lig)(2,4\text{-}PyDC)]\cdot 2H_2O\}_n$ composition was obtained. Single X-ray diffraction analysis has shown that the compound crystallizes in orthorhombic space group *Pnma* with following cell parameters: a= 31.4540(14) Å, b= 17.8850(13) Å, c= 9.5555(7) Å. Zinc (II) ion is four-coordinated with a tetrahedron geometry, the 2,4-PyDC acid is double deprotonated and coordinates to zinc ions through nitrogen atom and both carboxylic groups giving rise to a chain. Semi rigid imidazolate ligand has a conformation that blocks polymer growth (see the figure).

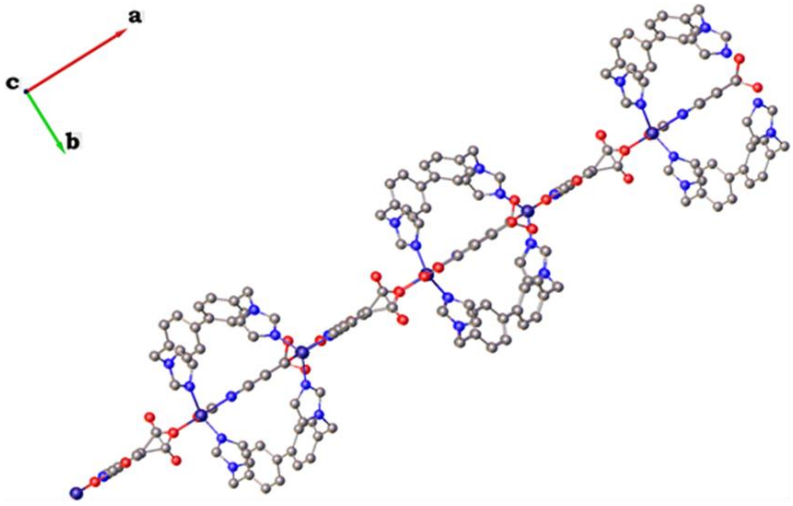

Figure 1. Graphical representation of 1D-$\{[Zn(Lig)(2,4\text{-}PyDC)]\cdot 2H_2O\}_n$ polymer

Thermogravimetric analysis of the compound showed two water molecules (6,2% weight) in the external sphere that are eliminated before 200°C. In the absence of the guest molecules the compound is thermally stable up to 320°C. In the IR spectrum there are bands of $\nu_{asim,sim}(OH)$ between 3700 – 2600 cm^{-1} and $\delta(H_2O)$ at 1624 cm^{-1}. The carboxylic group coordinates monodentately and provides bands at $\nu_{asim}(COO^-)$ -1606 cm^{-1} and $\nu_{sim}(COO^-)$ - 1348 cm^{-1}.

ACKNOWLEDGEMENTS: This work was funded by the Research Subprogram SSMCCLP (code 010602).

PHOTOPHYSICAL PROPERTIES OF SOME PHTHALOCYANINE DERIVATIVES

I.R. Tigoianu[1,*], A. Airinei[1], C. Gherasim[1], I. Lungu[2], V. Suman[2], T. Potlog[2]
[1]*Petru Poni Institute of Macromolecular Chemistry, Laboratory of Physical Chemistry of Polymers, Iasi, Romania*
[2]*Moldova State University, Laboratory of Organic/Inorganic Materials for Optoelectronics, Chisinau, Republic of Moldova*
[*]E-mail: tigoianu.radu@icmpp.ro

Transient absorption (**TA**) spectroscopy, steady state, and time-resolved fluorescence spectroscopy were used to investigate and characterize the tetra- and octa- carboxy zinc phthalocyanine derivatives with applications in medicine. For this purpose, new compounds were been synthesized in order to have a good emission, stability and sensitivity. We chose the investigation of some phthalocyanine derivatives for the theoretical information and applications resulting from this study, and to develop new technological innovations for the health sciences, a new pathway for the treatment of cancer.

From the transient absorption map for phthalocyanine derivatives, it can be observed ground state bleaching bands (**GBS**), absorption in excited state (**ESA**) and more than one excited state ($\mathbf{S_n}$>1). At longer wavelengths stimulated emission (**SE**), and other stimulated emissions can appear ascribed to the triplet manifold, confirmed by time-resolved experiments to be phosphorescence. Also, the triplet excited state absorption can occur.

The values of the fluorescence lifetimes vary between 1.0 and 10.0 ns, whereas the phosphorescence lifetimes are in the range of 0.9 to 9.0 μs. Also, emission quantum yields under 15% were determinated.

ACKNOWLEDGMENTS: This work was supported by a grant of the **Ministry of Research, Innovation, and Digitization**, **CNCS-UEFISCDI**, contract no. **20ROMD/2024**, project **PN-IV-P8-8.3-ROMD-2023-0048 (DSUPRAMED),** within **PNCDI IV.**

EXPLORING SPIN DIFFUSION OF EXCITONS IN ORGANIC-INORGANIC LEAD HALIDE PEROVSKITES

S. Anghel[1,*], A. V. Poshakinskiy[2], D. R. Yakovlev[1,2], E. Kirstein[1], N. E. Kopteva[1], M. Bayer[1], M. Betz[1]
[1]*Experimentelle Physik 2, Technische Universität Dortmund, Dortmund, Germany*
[2]*Ioffe Institute, Russian Academy of Sciences, St. Petersburg, Russian Federation*
[*]E-mail: sergiu.anghel@tu-dortmund.de

In recent years, hybrid lead-halide organic-inorganic perovskites have garnered significant attention due to their structural and chemical design flexibility. This flexibility holds promise for enhancing device performance and stability. These materials have achieved efficiencies exceeding 28% in solar cells and are also used in high-efficiency light-emitting diodes and various optoelectronic applications. A key process intimately linked to these properties is the diffusion of excitons, which is crucial for understanding exciton structure and the spatial energy landscape. Exciton transport is one of the most critical parameters determining the efficiency limits of optoelectronic devices, including both light-harvesting and light-emitting applications.

Recent studies have focused on exciton diffusion in both bulk and two-dimensional perovskites, revealing that the exciton diffusion coefficient (D) varies widely depending on the specific perovskite material. However, while exciton transport properties have been extensively studied, research on their spin transport properties remains limited. Currently, significant efforts are being made to develop effective methods for generating and detecting spin-polarized carriers, and it is crucial to identify new materials that can maintain spin polarization during charge transport. Perovskite materials appear to be promising candidates in this area, as indicated by initial investigations of their local spin properties [1,2].

In this study, we investigate the diffusion of spin-polarized excitons in $FA_{0.9}Cs_{0.1}PbI_{2.8}Br_{0.2}$ bulk lead halide perovskite crystals at cryogenic temperatures [3]. We use temporally and spatially resolved magneto-optical Kerr microscopy, where a circularly polarized pump creates excitons with a specific spin orientation, and a linearly polarized probe measures their subsequent spatial and temporal evolution. Our findings reveal a surprisingly high spin diffusion coefficient ($D_s \sim 100\ \mathrm{cm}^2/\mathrm{s}$), a significant deviation from recent results obtained for bulk or two-dimensional perovskites, where the exciton diffusion coefficient is at least two orders of magnitude lower [4]. Additionally, the spin polarization signal exhibits a complex dependence on pump power: beyond a certain threshold, we observe an anomalous, nonlinear spatial and temporal behavior. These unusual results can be modeled within the framework of kinetic theory and are explained by a memory effect, specifically, it was found that a spatial and temporal temperature variation induced by the pump pulse leads to a corresponding variation in spin lifetimes.

[1] E. Kirstein, D. R. Yakovlev, M. M. Glazov, E. Evers, E. A. Zhukov, V. V. Belykh, N. E. Kopteva, D. Kudlacik, O. Nazarenko, D. N. Dirin *et al.*, Adv. Mater. **34**, 2105263 (2022).
[2] E. Kirstein, D. R. Yakovlev, E. A. Zhukov, J. Höcker, V. Dyakonov, and M. Bayer, ACS Photonics **9**, 1375 (2022).
[3] S. Anghel, A. V. Poshakinskiy, D. R. Yakovlev, E. Kirstein, N. E. Kopteva, O. Hordiichuk, M. V. Kovalenko, M. Bayer, and M. Betz, ACS Photonics **10**, 4169 (2023).
[4] I. Dursun and B. Guzelturk, Light. Sci. Appl. **10**, 39 (2021)

HYSTERESIS LOOP IN SPR STRUCTURES CONTAINING THIN AMORPHOUS As_2S_3 FILMS

A.A Popescu*, D. Savastru
National R&D Institute for Optoelectronics INOE 2000, Magurele, Ilfov, Romania
*E-mail: apopescu@inoe.ro

The amorphous films show photoinduced changes of transmission. However, the changes of optical constants are too small for optoelectronic applications. In this report we consider amorphous As_2S_3 thin films placed in surface plasmon resonance (SPR) structure. Theoretical and experimental study of nonlinear phenomenon occurring were done. The light coupling was carried out by using BK7 prism with angular interrogation. As As_2S_3 shows photoinduced modifications, the characteristic resonance angle becomes function of the incident intensity. It was found that the magnitude and time-response of these optical modifications depend on the total number of photons absorbed per unit area, and thus depend on the fluence (exposure) of radiation.

For many chalcogenides amorphous materials used for information recording the needed exposure for optical modifications to occur were demonstrated to be of the order of 1-2 J/cm^2 [1]. SPR structures were irradiated with CW laser radiation of 514 nm wavelengths and of low intensity (JDS Uniphase argon laser of 50 mW power). The wavelength is near the optical band-gap of the As_2S_3. The resonance coupling angle of SPR structure was analyzed as a function of the incident power in vicinity of the resonance angle.

The SPR configuration consisted of four layers and is presented in Fig. 1a.

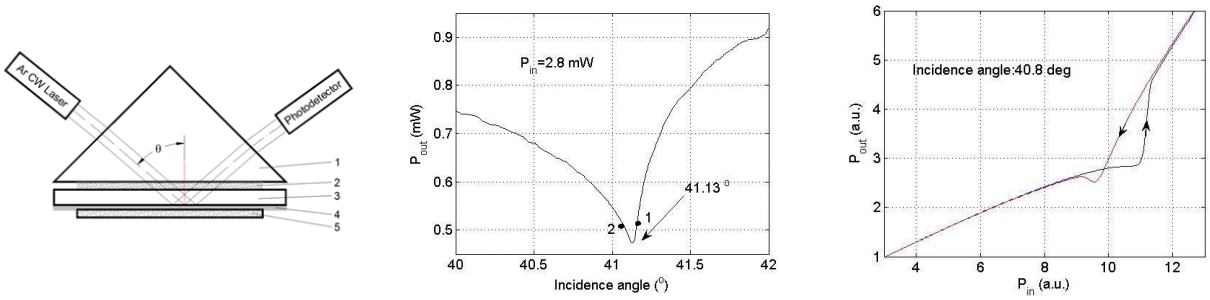

a) b) c)

Figure 1. a) Experimental setup: 1-prism of BK7 glass; 2-immersion oil; 3-substrate glass slide; 4-gold film; 5- As_2S_3 amorphous film; b) SPR resonance curve; c) Hysteresis loop behavior for $P_{out} = F(P_{in})$

The system of Helmholtz equations for four layers are solved numerically in MATLAB in order to obtain the curves of resonance, and the reflected wave power was measured relative to the incident power. The amorphous chalcogenide As_2S_3 films were deposited on top of the gold film by thermal evaporation in vacuum of $6.6 \cdot 10^{-4}$ Pa using direct resistive heating of crucible made of tantalum, and are prepared in IFA Labs. The gold films of 50 nm thickness are obtained by electron sputtering, and are commercial ones. The polarization of the laser was set in the plane of incidence, so that TM modes were coupled. The incident laser power was varied between 1 and 20 mW. The output power vs input is shown in Fig. 1c. Large nonlinear change of reflectivity was observed near 10-11.5 mW power.

Hysteresis was only detected when the angle was set below the resonant dip. (point 2 on Fig. 1b). SPR structure is very sensitive to small changes of the chalcogenide layer optical properties. The self-induced changes of the optical constants lead to different shape of optical hysteresis loop which depends strongly on the set incident angle. The structure is promising for photonic applications.

[1]. Abdulhalim I., Gelbaor M., Klebanov M., and Lyubin V. *Opt. Mater. Express* **1**, (2011), 1192.

ZnO AS A BASIS FOR FABRICATION OF NANOCOMPOSITE MATERIALS FOR SENSOR APPLICATIONS

V.V. Ursaki[1,2,*], V. Morari[3], E.V. Rusu[3], T. Braniste[1], I. M. Tiginyanu[1,2]
[1]*National Center for Materials Study and Testing, Technical University of Moldova, Chișinău, Republic of Moldova;*
[2]*Academy of Sciences of Moldova, Chișinău, Republic of Moldova;*
[3]*Technical University of Moldova, D.Ghitu Institute of Electronic Engineering and Nanotechnologies, Chișinău, Republic of Moldova*
[*]E-mail: vvursaki@gmail.com

Zinc oxide is an abundant multifunctional material with unique physical and chemical properties making it suitable for applications in various branches of industry, such as rubber, pharmaceutical, biomedical, cosmetics, agriculture, textile, photocatalysis, electronic and electrotechnology [1]. It provides conditions for the formation of a rich diversity of micro/nanostructure due to the possibility of multiple and switchable growth directions of the wurtzite structure and the high ionicity of its polar surfaces [2], in addition to various nanoparticles [3] and thin films forms [4]. From the point of view of optoelectronic applications, ZnO is an important material for use in blue and ultraviolet optical devices due to its wide bandgap of 3.36 eV at room temperature and large exciton binding energy of 60 meV [5].

This report is focused on the review of two areas of ZnO applications, namely as microstructured sacrificial templates for the preparation of a wide variety of composite nanomaterials and as nanostructured thin films for UV radiation detectors.

Microstructured sacrificial ZnO templates assembled from various microstructures such as microrods, tetrapods or multipods can be produced by different technologies such as chemical bath deposition, hydrothermal synthesis, carbothermal reduction processes, and chemical vapor deposition. Among these technologies, a flame transport synthesis approach for the production of flexible 3D interconnected ZnO networks, based on the direct transformation of metal precursor particles into nano-microstructures of different shapes, proved to feature versatility, simplicity, productivity, and suitability for mass production [6]. Such sacrificial ZnO templates are widely used for the preparation of an ultra-lightweight carbon microtube material called Aerographite (AG) through converting the sacrificial template to graphitic shells in a one-step chemical vapor deposition (CVD) process with toluene or acetylene as carbon source [7]. The AG material has been further used for the preparation of a variety of nanocomposite materials such as AG-GaN, AG-InP, AG-ZnO, AG-CdTe, AG-CdS, etc. The semiconductor nanocrystalline component of these nanocomposites has been grown by hydride vapor phase epitaxy (HVPE) synthesis or magnetron sputtering. The produced nanocomposite materials have been characterized from the point of view of their applications in strain, pressure, photo-, or gas sensors.

The second subject of this report is related to the production and characterization of nanostructured ZnMgO films for UV radiation detectors applications. Alloying of ZnO with MgO ensures a wider range of photodetector wavelength tunability in the UV spectral region (3.4 – 7.8) eV as compared to the GaAlN system (3.4 – 6.0) eV.

[1] A. Kolodziejczak-Radzimska, T. Jesionoski. *Materials (Basel)* **7** (2014) 2833-2881.
[2] V.V. Ursaki, et al, *Nanotechnology* **18** (2007) 215705.
[3] A. Singh, J. Das, P. C. Sil. *Advances in Colloidal and Interface Science* **286** (2020) 102317.
[4] S. Vyas. *Johnson Matthey Technology Review* **64** (2020) 202-218.
[5] U. Ozgur, et al. *J. Appl. Phys*. **98** (2005) 041301.
[6] Y.K. Mishra, *et al. Part. Part. Syst. Charact*. **30** (2013) 775–783.
[7] M. Mecklenburg, *et al. Adv. Mater.* **24** (2012) 3486–3490.

Au_{25} AND $Au_{24}Pt$ THIOL-PROTECTED CLUSTERS AS NANOCATALYSTS FOR CONVERTION OF H_2O_2

K. Zdunek*, A. Więckowska
Faculty of Chemistry, University of Warsaw, Warsaw, Poland
*E-mail: k.zdunek10@student.uw.edu.pl

Metal clusters of defined stoichiometry attract the attention of scientists due to their unique optical, electrical, and electrochemical properties [1, 2]. Replacing one metal atom in the core with another one significantly changes the properties of the cluster while maintaining the same structure. The detailed characterization of the electrocatalytic properties of $Au_{24}Pt$ clusters protected by n-butanothiol is still lacking. The platinum atom within the $Au_{12}Pt$ gold core, surrounded by delocalized electrons, displays different behavior compared to atoms in pure platinum nanoparticles.

In this research, we confirm this unique behavior by demonstrating a pronounced electrocatalytic effect for the electrooxidation and electroreduction of H_2O_2. This effect was observed using a gold working electrode modified with a Nafion-suspended product containing $Au_{24}Pt$ clusters. The measured currents at constant potentials of ±0.5 V versus an Ag/AgCl reference electrode, with H_2O_2 molarities ranging from 1 to 10 mM, exhibited a strong linear dependence with a correlation coefficient as high as 0.999. The modified electrodes' durability in aqueous solutions and the reproducibility of the results suggest that this technique is promising for H_2O_2 detection in biological samples without causing damage, as long as the potential range remains stable.

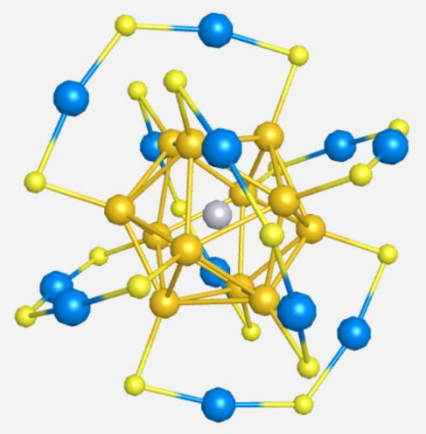

Figure 1. The geometric structure of the $Au_{24}Pt$

[1] H. Qian, D. Jiang, G. Li, C. Gayathri, A. Das, R.R. Gil, R. Jin. *J. Am. Chem. Soc.* **134** (2012) 16159−16162.
[2] W. Fei, S. Antonello, T. Dainese, A. Dolmella, M. Lahtinen, K. Rissanen, A. Venzo, F. Maran. J. *Am. Chem. Soc.* **141** (2019) 16033−16045.

CARRIER SPIN COHERENCE IN INAS/INALGAAS QUANTUM DOTS EMITTING IN THE TELECOM RANGE

E. Evers[1], N. E. Copteva[1], V. Nedelea[1,*], A. Kors[2], R. Kaur[2],
J. P. Reithmaier[2], M. Benyoucef[2], M. Bayer[1], A. Greilich[1]
[1]*Experimentelle Physik 2, Technische Universität Dortmund, Dortmund, Germany*
[2]*Institute of Nanostructure Technologies and Analytics (INA), University of Kassel, Germany*
[*]E-mail: vitalie.nedelea@tu-dortmund.de

The coherence properties of quantum systems are essential for the advancement of quantum communication, in particular for enabling long-distance transmission via quantum repeaters (QR) [1]. QR rely heavily on the ability to maintain quantum coherence over extended distances. This study focuses on the carrier spin coherence in quantum dots (QDs), which are promising candidates for entanglement with an emitted photon as well as entanglement of two remote spins induced by measuring of two indistinguishable photons [2].

The Samples were grown by molecular beam epitaxy and consist of 5.5nm InAs monolayers separated by InAlGaAs barriers. The bottom barrier contains a Si δ-doped layer, at a distance of 15 nm from the QD layer, in order to provide resident electrons. Differential transmission (ΔT/T), (fig. 1) reveals a double exponential decay behaviour, with a short exciton decay time of *0.5ns* and the long indirect molecular exciton decay time of *2ns*. Consequently, the dependence of the Larmor frequencies on the transversal magnetic field (B_V) gives us information about the carrier *g-factor*, $|g_e| = 1.88$ for the electron and $|g_h|=0.6$ for the hole. The hole spin dephasing saturates at a higher value of $T_2^*=1.4ns$ than the electron $T_2^*=0.6ns$, which could be explained by the weaker hyperfine coupling of the hole.

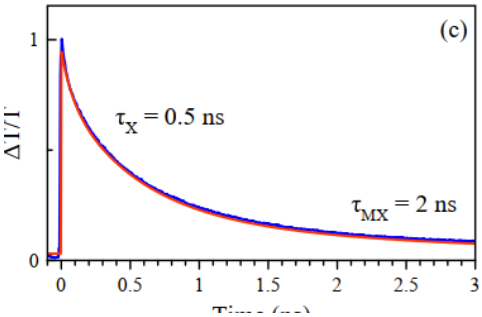

Figure 1. ΔT /T dynamics.

For the longitudinal spin lifetime T_S and the spin relaxation time T_1 we employ the spin inertia technique, where the pump helicity is modulated between $\sigma+$ and $\sigma-$ at the frequency f_m. When the modulation period becomes shorter than the spin lifetime T_S, the averaged signal amplitude starts to decrease. The decay of the FR signal as a function of f_m gives $T_S=0.3\mu s$. Extrapolating the power dependence to zero gives the spin relaxation time $T_1=0.5\mu s$. The wide spread of g-factors and long spin relaxation times are promising candidates for the spin mode locking (SML) [4] effect (fig. 2) that we show for the holes in the QDs ensemble. The resident hole spin polarisation is created by the trion excitation mechanism in the pump-probe Faraday rotation [5]. After the action of an infinite number of pulses with a repetition period of TR, the spin polarisation accumulates for the carriers with $T_2>T_R$. In the inhomogeneous ensemble of QDs, the sum of the multiple oscillating signals with Larmor frequencies corresponding to ω_R contributes to the SML. We measure the dependence of the SML on the BV and conclude from the g-factor values that the signal is related to the hole spins. Since each optical pulse changes the spin polarisation proportional to the pump pulse area, we also consider the range of pulse areas with $\Theta= 0.6\pi$, leading to the maximum $T_2 = 400$ *ns*, and the $\Theta= \pi$ with the minimum possible $T_2=20ns$.

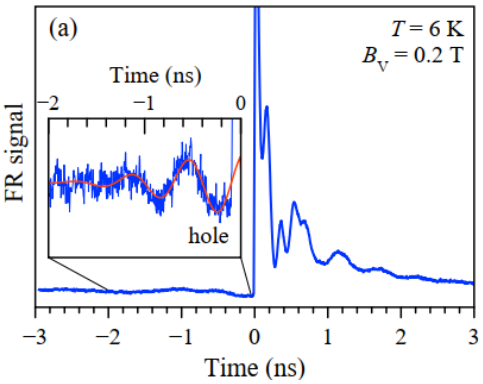

Figure 2. SML at negative time delays.

[1] H.-J. Briegel, W. Dür, J. I. Cirac, and P. Zoller, *Phys. Rev. Lett.* **81**, 5932 (1998).
[2] R. Stockill, M. J. Stanley, L. Huthmacher, et al., *Phys. Rev. Lett.* **119**, 010503 (2017).
[3] V. V. Belykh, A. Greilich, D. R. Yakovlev, et al., *Phys. Rev. B* **92**, 165307 (2015).
[4] A. Greilich, D. R. Yakovlev, A. Shabaev, et al., *Science* **313**, 341 (2006).
[5] I. A. Yugova, M. M. Glazov, E. L. Ivchenko, and A. L. Efros, *Phys. Rev. B* **80**, 104436 (2009).

EFFECT OF AlGaN INTERLAYER ON PERFORMANCE OF InGaN-BASED RED LIGHT EMITTING DEVICES

V. P. Sirkeli*, I. B. Boris, D. L. Nika
Faculty of Physics and Engineering, Moldova State University, Chișinău, Republic of Moldova
*E-mail: vadim.sirkeli@gmail.com

InGaN-based light-emitting diodes (LEDs) have attracted attention of researchers as a promising candidate for many applications, including general lighting, direct view full color LED displays, and LED micro-displays. To date, most of blue and green LEDs are based on InGaN/GaN structures and have achieved a high wall-plug efficiency (WPE) of 81% and 56%, respectively [1]. Most of the red LEDs are based on AlGaInP material and have WPE of ~ 50%. However, AlGaInP-based red LEDs are very sensitive to operation temperature, and high operation temperature will cause a significant carrier leakage through red LEDs, leading to the efficiency thermal droop. Hwang et al. [2] reported on a successful fabrication of InGaN-based red LED grown on c-plane sapphire substrate with external quantum efficiency of 2.9% with wavelength of 629 nm. In order to improve efficiency of LED devices different approaches could be used such as p-i-n-doping, inserting interlayers and others [1-3]. In this work, we have numerically studied the effect of AlGaN interlayer on the efficiency of InGaN-based red LEDs. As shown in Fig. 1(a) the active region of red LEDs consists of a 3 nm thick $In_{0.40}Ga_{0.60}N$ quantum well and a 10 nm thick $In_{0.08}Ga_{0.92}N$ quantum barriers. A 2 nm thick $Al_xGa_{1-x}N$ interlayer is inserted between the quantum well and the upper quantum barrier. Fig. 1(b) demonstrates the internal quantum efficiency (IQE) versus current density for red InGaN-based LEDs with different Al content in AlGaN interlayers. It is found that among different red LEDs, the maximum IQE of ~ 66.5% at 636 nm corresponds to the LED device with $Al_{0.2}Ga_{0.8}N$ interlayer. The mechanisms of IQE enhancing for InGaN-based red LEDs with AlGaN interlayer are discussed.

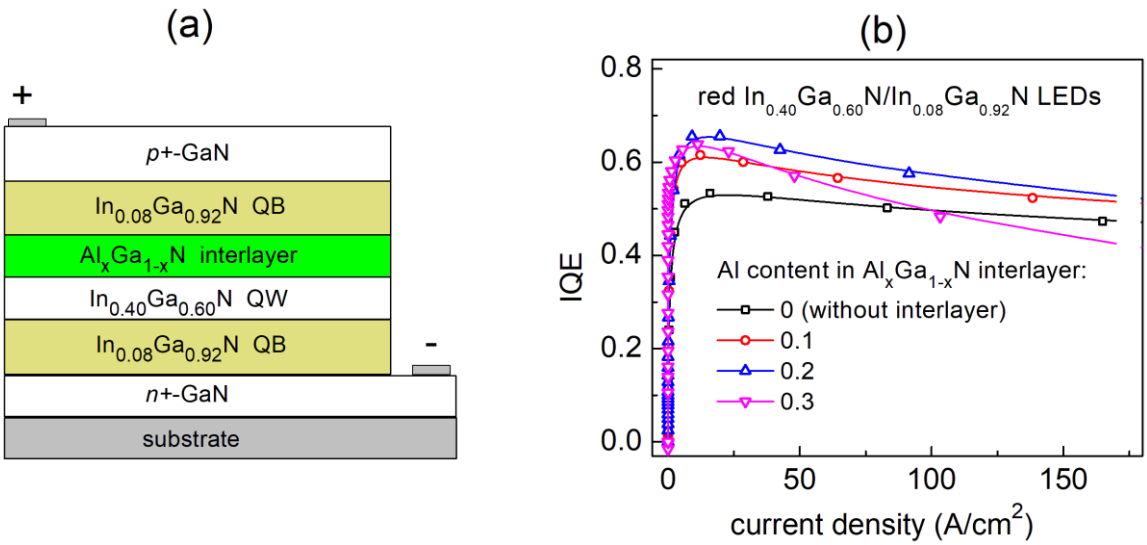

Figure 1. (a) Schematic structure of InGaN-based red LED device with $Al_xGa_{1-x}N$ interlayer. (b) Effect of Al content in $Al_xGa_{1-x}N$ interlayer on IQE of InGaN-based red LEDs.

ACKNOWLEDGEMENTS. V.P.S., I.B.B, and D.L.N. acknowledge the financial support from the Ministry of Education and Research of the Republic of Moldova (research program no. 011208).

[1] V. P. Sirkeli, O. Yilmazoglu, F. Küppers, H. L. Hartnagel. *Semicond. Sci. Technol.* **30** (2015) 065005.
[2] J.-I. Hwang et al. *Appl. Phys. Express* **7** (2014) 071003.
[3] V. P. Sirkeli et al. *J. Phys. D: Appl. Phys.* **50** (2017) 035108.

DECAY KINETICS OF EXCITONS BOUND AT IODINE MOLECULES IN $MoSe_2$:I_2 LAYERED CRYSTALS

N. Siminel*, C. Slobodeniuc, A. Micu, A. Siminel, L. Kulyuk
Institute of Applied Physics, Moldova State University, Chișinău, Republic of Moldova
*E-mail: nikita.siminel@ifa.usm.md

Molybdenum diselenide $MoSe_2$ belongs to the family of transition metal dichalcogenides (TMDs), which are layered semiconductor compounds with remarcable optoelectronic properties, due to which the interest of researchers in these materials has rapidly increased in the last decade. The bulk samples of these compounds, are attributed to semiconductors with an indirect band gap [1], while in the form of an atomic monolayer they exhibit a direct band gap and radiative properties due to efficient excitonic recombination [2, and references therein]. In addition, the layered structure of DMT ensures the possibility of changing the physico-chemical properties of these materials by means of intercalation of some species (atoms, molecules) into the van der Waals [3]. In particular the intercalation of diatomic halogen molecules provide a bright luminescence of TMDs compounds at low temperatures due to the bound excitons recombination.

This paper presents the results of the investigation of the temporal characteristics of the radiative recombination of excitons bound to iodine molecules in $MoSe_2$:I_2 bulk crystals. The relatively high intensity of bound excitons luminescence and, in contrast to MoS_2:I_2 and WS_2:I_2 [4], a sufficiently large energy gap between the components *A* (E_A = 1.0360 eV) and *B* (E_B = 1.0416 eV) of the excitonic spectral doublet, made it possible, for the first time, to measure the kinetics of the luminescence decay for each spectral line separately. This, in turn, made it possible to show that at temperatures lower than 20K the excitonic states involved in radiative recombination are not in thermodynamic equilibrium conditions. This was manifested by the fact that the decay times of the *A* and *B* spectral components differ considerably (almost two times at T=12K) in the temperature range up to 20K.

From the analysis of the experimental results of time-resolved measurements, taking into account the temperature evolution of the intensities of the *A* and *B* components observed in the steady-state luminescence spectra [5], were estimated the probabilities $W_{AB}(T)$ and W_{BA} of nonradiative transitions between levels *A* and *B* ($W_{AB} = W_{BA} \exp(-\Delta_{BA}/k_B T)$, Δ_{BA} = 5.6 meV), which determine the rate of reaching thermal equilibrium for *A*-*B* excitonic states. The value of W_{BA} obtained as a result of calculations is 0.9 μs, which is in good agreement with the values of a similar parameter found for bound excitons in silicon [6].

The nature of non-radiative processes leading, first, to the temperature ignition of exciton luminescence, then, at temperatures above 40 K, to its attenuation and, finally, to its very rapid thermal quenching is also discussed.

ACKNOWLEDGEMENTS: Authors acknowledge the financial support provided by the MEC, subprogram 011201

[1] R. Coehoorn *et al.*, *Phys. Rev.* B **35**, (1987) 6195.
[2] Saju Joseph *et al., Materials Chemistry and Physics*, **297**, (2023) 127332.
[3] Jiajing Wu *et al., Advanced Materials*, 34 (2022) 2200425.
[4] A. Colev, C. Gherman, V. Mirovitskii, L. Kulyuk, E. Fortin, *J. Luminescence*, **129** (2009) 1945.
[5] N. Siminel, K. Sushkevich, S. Aazou, A. Micu, A. Siminel, Z. Sekkat, L. Kulyuk, *Optical Materials Express*, **13**, (2023) 887.
[6] G. Bohnert, K. Weronek, A. Hangleiter, *Phys.Rev.* **B48** (1993), 14973.

REDUCTION OF THE LATTICE THERMAL CONDUCTIVITY IN SI-BASED NANOWIRES AND NANOTUBES

C. I. Isacova[1,*], A. I. Cocemasov[1], D. L. Nika[1]
[1]*Department of Physics and Engineering, Moldova State University, Chișinău, Republic of Moldova*
[*]E-mail: isacova.calina@gmail.com

The continuous miniaturization of electronic devices creates a new challenge in effectively controlling their electronic and thermal properties. One such approach is phonon engineering [1], which allows for modification of the electronic and thermal properties of semiconductor nanomaterials by altering their phonon characteristics. It is known that thermal conductivity in nanomaterials is lower than that of the corresponding bulk materials [2-3]. The quantum size effect along with the increased influence of surface scattering, results in a significant reduction in lattice thermal conductivity. Here we report on the theoretical investigation of phonon properties and thermal transport in Si/Ge nanowires as well as in Si/SiO_2 nanotubes.

The calculation of the phonon spectrum was carried out within the framework of the face-centered cubic cell (FCC) model of lattice vibrations. The lattice thermal conductivity was calculated using a formula derived from the Boltzmann transport equation, taking into account the one-dimensional phonon density of states:

$$\kappa_{ph} = \frac{1}{2\pi k_B T^2} \sum_s \int_0^{q_{z,max}} \left[\hbar\omega_s(q_z) v_{z,s}(q_z)\right]^2 \tau_{tot,s}(q_z) \frac{\exp\left(\frac{\hbar\omega_S(q_Z)}{k_B T}\right)}{\left[\exp\left(\frac{\hbar\omega_S(q_Z)}{k_B T}\right)-1\right]^2} dq_z \quad (1)$$

where s is the number of phonon branches, k_B is the Boltzmann constant, $\hbar$ is the Planck constant, T is the absolute temperature, and τ_{tot} is the total phonon relaxation time, calculated according to Matthiessen's rule. The following phonon scattering mechanisms were considered: Umklapp scattering, impurity scattering, and boundary scattering.

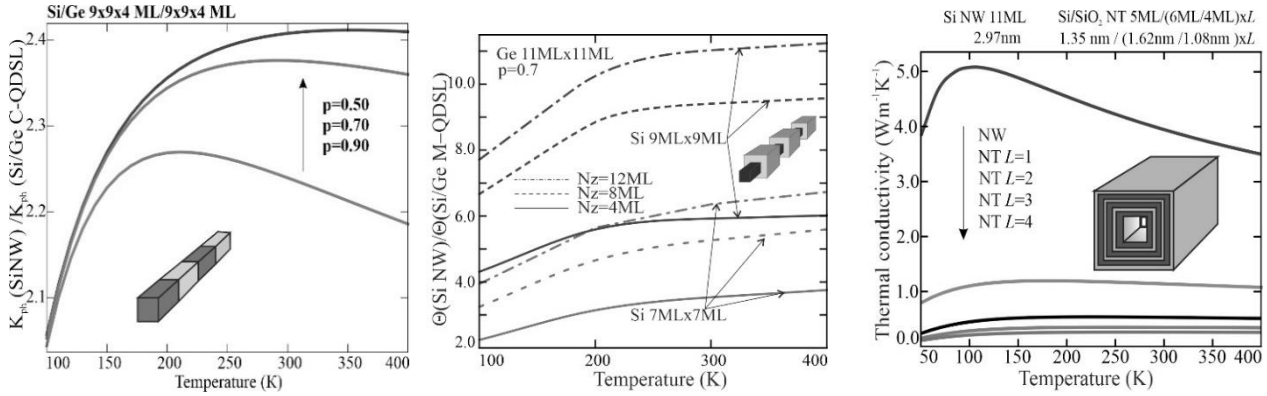

(a) (b) (c)

Figure 1. The decrease in the thermal conductivity/heat flow in Si/Ge nanowires with constant (a) and variable cross-sections (b), as well as in nanotubes (NT), compared to smooth Si nanowires (NW) (c).

Figure 1 illustrates the decrease in the thermal conductivity/heat flow in Si/Ge nanowires with constant (a) and variable cross-sections (b), as well as in nanotubes (NT), compared to smooth Si nanowires (NW). At T = 300 K, the thermal conductivity of segmented Si/Ge [3] nanowires decreases by 2-10 times compared to generic Si NWs. The reduction in thermal conductivity of NTs depends on the number of NT layers and can reach 3 to 4 times near the room temperature [4].

ACKNOWLEDGEMENTS: Authors acknowledge financial support from the Ministry of Education and Research of the Republic of Moldova (research subprogram no. 011208).

[1] A.A. Balandin. *J. Nanosci. Nanotechnol* **5** (2005) 1015-1022.
[2] N. Zincenco, D. Nika, E. Pokatilov, et al. *Journal of Physics: Conference Series*. **92** (2007) 012086-1–012086-4.
[3] C.I. Isacova, N.D. Zincenco, I.B. Boris, D.L. Nika. *Physics of the Solid State* 65, 89-105 (2023).
[4] C. Isacova, A. Cocemasov, D.L. Nika, V.M. Fomin. *Applied Science* **11** (2021) 3419.

ANISOTROPIC THERMOELECTRIC DEVICES BASED ON SINGLE-CRYSTAL Bi MICROWIRES AND FILMS

L. A. Konopko[1,*], A. A. Nikolaeva[1], T. E. Huber[2], D. Shiversky[1]
[1]*Technical University of Moldova, "D.Ghitu" Institute of Electronic Engineering and Nanotechnologies, Chișinău, Republic of Moldova;*
[2]*Howard University, Washington, DC, USA*
[*]E-mail: leonid.konopko@iien.utm.md

Here, we present a demonstration of an unconventional thermoelectric energy conversion that is based on a single element made of an anisotropic material. In such materials, a heat flow generates a transverse thermoelectric electric field lying across the heat flow. A feature of anisotropic thermoelectrics is that the thermoelectric voltage is proportional to the element length and inversely proportional to the effective thickness. We have prepared an experimental sample consisting of a 10-m-long glass-insulated single-crystal tin-doped bismuth microwire (D=20 μm, d=4 μm) [1,2]. Crucial for this experiment is the ability to grow the microwire as a single-crystal using a technique of recrystallization with laser heating and under a strong electric field. The sample was wound as a spiral, bonded to a copper disk, and used in various experiments. The sensitivity of the sample to heat flow is as high as 10^{-2} V/W with a time constant s of about 0.5 s. Polycrystalline Bi films with a thickness of 2-5 μm were deposited on the mica support by the vacuum thermal evaporation method. Experimental samples of heat flux sensors were made on the basis of recrystallized Bi films under laser heating and in a strong electric field.

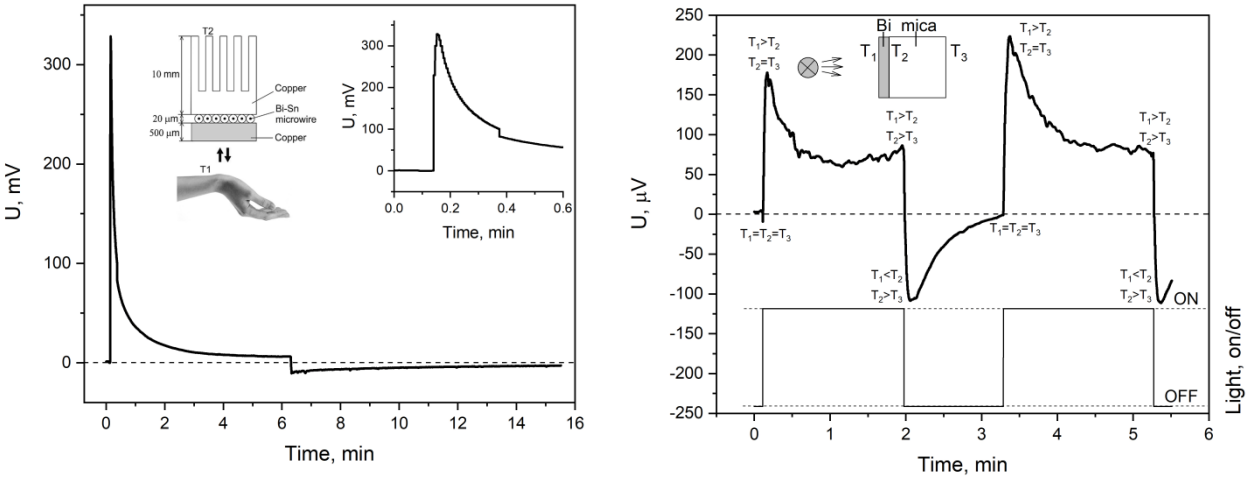

(a) (b)

Figure 1. (a) Dependence of the output voltage of the heat flux sensor based on 10-m-long glass-insulated single-crystal Bi–0.05 at % Sn microwire (D=20 μm, d=4 μm) on the time of contact with a human hand; (b). Dependence of the output voltage of the heat flux sensor based on the recrystallized Bi film (d=3 μm) deposited on a mica substrate on the time of illumination with an MBS-9 illuminator.

The dynamics of voltage changes at the output of the developed heat flux sensors during the registration of modulated heat fluxes (see Fig. 1) can be explained in the limit of the theory of an anisotropic thermoelement.

ACKNOWLEDGMENTS: This work was supported by the Ministry of Education and Research of R. Moldova within the program no. 020201 in Moldova. In the U.S., the work was sponsored by the U.S. National Science Foundation STC Center for Integrated Quantum Materials, Grant 1231319, The Boeing Company, and the Keck Foundation.

[1] L. Konopko, A. Nikolaeva, A. Kobylianskaya, T. Huber. *J. Electron. Mater.* **47** (2018) 3171-3176.
[2] L. Konopko, A. Nikolaeva, T. Huber, A. Kobylianskaya. *Semiconductors* **53** (2019) 662–666.

APPLICATIONS OF MAGNETIC MICRO- AND NANOWIRES AS A CODE LABELS

S. Baranov, O. Yaltychenko*, E. Kanarovskii
Institute of Applied Physics, Moldova State University, Chișinău, Republic of Moldova
*E-mail: olga.ialticenco@ifa.usm.md

This paper evaluates the feasibility for code labels applications of short segments of bi-stable micro- and nanowires, such as glass-coated amorphous magnetic micro- and nanowires produced by the Taylor-Ulitovsky method. Bistable micro- and nanowires can be used for applications in code labels for goods, car parts, valuables, documents, securities, and money, as well as for the creation of informational files, for the remote control of actuating mechanisms, and for the creation of sensitive elements (sensors) in measuring equipment. They also find application in medicine for distinguishing affected organs or observations of transport process of medicinal preparations (with magnetic labels) in organisms. Note that this transport process could be controlled by an external magnetic field.

The obtained experimental and theoretical results testify that labels made from magnetic micro- and nanowires can be used only at small distances from the recording units (at distances of ~ (0.1–1) m) depending on the micro- and nanowires' diameter. In this aspect, they are not competitive for the known radio-frequency identification (RFID) systems. However, if the location of the label and the use of the label in environments absorbing radio waves are necessary or the priority of using the label is not the reading distance but, e.g., confidentiality, the use of the magnetic label made from micro- and nanowires can become preferable. In addition to the Barkhausen effect, the bistable micro- and nanowires labels also possess natural ferromagnetic resonance (NFMR), which can also be used as an additional property for identification.

The critical length of the short segments sections at which the bistable effect is preserved is about a millimeter, being at least ten (or more) times smaller than bistable tapes and wires obtained by other methods. The magnetization reversal rate of the microwire is higher than those of its analogs.

MODELING AND PARAMETRIC CONTROL OF A SINGLE-ELECTRON TUNNELING OF THE "NANOOBJECT-ELECTRODE" TYPE USING THE EXAMPLE OF A TRIMER NANOCLUSTER

O. Yaltychenko*, E. Kanarovskii
Institute of Applied Physics, Moldova State University, Chișinău, Republic of Moldova
*E-mail: olga.ialticenco@ifa.usm.md

Advancement of the technology for manufacturing electronic circuits in the sub-10 nm region and their further miniaturization within the framework of a traditional planar structure leads to the complication and significant increase in cost of the technological process. In addition, in electronic devices with characteristic dimensions on the order of several nanometers, quantum effects arise, some of which are "parasitic." The transition to single-electron elements and devices using the transport of single electrons and built on the basis of molecular-scale nanostructures seems very promising. In this regard, the use of single molecular objects a few nanometers in size as components of such electronic nanodevices are of great interest. It has been shown that it is possible to both implement logical digital operations using single-electron transistors based on nanoparticles and create single-molecule memory. At the same time, by parameterizing single-electron devices based on these nanoobjects, it is possible to simplify the modeling of electron transport.

In this work, the object of study is a single-electron trinuclear nanocluster in a ligand shell located in an external electromagnetic field. This nanocluster as a nanoobject can also be placed as a central island in a nanogap and form two tunnel transitions of the "nanoobject-electrode" type with metal electrodes.

Essentially, two conducting electrodes are separated by a thin layer of dielectric (on the order of one nanometer). On the other hand, this dielectric is in some way a ligand shell for the nanotrimer. The probability of electron tunneling through this dielectric with the built-in nanotrimer is investigated and the possibility of parametric control of the process is studied. Conditions have been identified under which tunneling will occur predominantly in one direction.

HETEROGENOUS INTEGRATIONS ON 3D INTEGRATED CIRCUITS

I.-M. Pletea*, V. Șontea
Technical University of Moldova, D.Ghitu Institute of Electronic Engineering and Nanotechnologies, Chișinău, Republic of Moldova
*E-mail: ipletea@etti.tuiasi.ro

The strongest value of an Integrated Circuit is the integration of many functions in one device. This is and will remain the most important driver of Moore's Law because by integrating functions into one Integrated Circuit we achieve orders of magnitude benefits in power, speed, costs and reliability [1]. 3D Integrated Circuit enables far more than an alternative for increased integration. It provides another dimension of design flexibility [2]. A well-known aspect of this flexibility is the ability to split the design into layers which could be processed and operated independently, and still be tightly interconnected – especially for monolithic 3D [3].

The most important market for semiconductor products is smart mobility. For this market the System on Chip device needs to integrate many functions. In most cases the pure high-performance logic would be about 25% of the die area, 50% would be memories and the rest would be analog functions such as I/O. In 2D they all need to be processed together and bear the same manufacturing costs and limitations. In a monolithic 3D-IC stack using heterogeneous integration each stratum is processed in an optimized flow, allowing for a significant cost reduction and increased functionality [4,5].

The function itself could be constructed better using heterogeneous integration. In many cases only portion of the logic needs to be high performance while other portion could be better and cheaper done using older process node. Other scenarios could include designing different strata with different supply voltages for power savings, different number of metal interconnect layers, or other variations of the semiconductor manufacturing space [6].

3D monolithic device would be a good fit to platform-based designs wherein some part of the device is used by all customers and others are tailored to a specific customer segment. Although there are EDA tools for 3D IC on the market, built on existing 2D tools by adding 3D awareness capabilities, no EDA tools for monolithic 3D exist. There is a need for monolithic 3D EDA Tools with 3D routing, placement, and floor planning tools that work Inter-Layer Vias close to minimum lithography feature size and support both block-level and gate-level partitioning [7].

[1] G.E. Moore. *Solid-State Circuits Society Newsletter* **11** (2006), 33-35
[2] H.B. Muhibul. *SEU Journal of Science and Engineering* **11** (2017), 28-42.
[3] Y. Xie, J. Cong, S. Sapatnekar. Three-Dimensional Integrated Circuit Design. *Springer (*2010)
[4] S. Bobba, A. Chakraborty, O. Thomas, P. Batude, T. Ernst, O. Faynot, G. Micheli. *Asia and South Pacific Design Automation Conference* (2011), 337-343.
[5] C. Chiang, S. Sinha. *Asia and South Pacific Design Automation Conference (*2009), 429-436.
[6] D.H. Kim, S.K. Lim. *Interconnect Technology Conference, IEEE (*2011)
[7] I. Pletea, Z.E. Wurman, Z. Or-Bach. Monolithic 3D layout using 2D EDA for embedded memory-rich designs. *IEEE*. (2015), 1–2.

SURFACE PLASMON-WAVEGUIDE RESONANCES IN STRUTURES WITH AMORPHOUS As_2S_3 FILMS

D. Savastru, A. A. Popescu*
National R&D Institute for Optoelectronics INOE 2000, Magurele, Ilfov Romania
*E-mail: apopescu@inoe.ro

In the amorphous chalcogenide materials (ACM) changes of the optical constants arise under the action of light with the photon energy exceeding the band gap. However, the changes of the refractive index in chalcogenide films are small. An inspired way to amplify the phenomenon would be the insertion of films in a resonance structure. The surface plasmon resonance (SPR) structure with prism coupling can be appropriate. Conventional three layers configuration was proposed by Kretschmann. It consists of a metallic thin film deposited on prism base.

Four layers configurations we developed [1] contains an additional thin film made of ACM deposited over the metal film. As the chalcogenide materials have high refractive index value of the (2.45-2.30), these films constitute planar waveguides. The resonance mode spectrum and changes due to film refractive index modification was studied numerically (Fig.1).

Software for numerical SPR calculations of four layers structure was developed by using transfer matrix formalism. The shown here calculations of the reflectivity were performed for a four-layer system made up of a GaP prism, a 50 nm silver layer, a ACM layer with variable thickness and air. Two different thicknesses for As_2S_3 layer were considered: d_{ACM} = 50 nm and d_{ACM} = 250 nm. Gallium phosphide is an optically isotropic material with the refractive index n_{pr}=3,31 and it is transparent to the wavelength of 633 nm. We used such prism earlier for the characterization of planar chalcogenide waveguides [2]. An average refractive index value for As_2S_3 films was taken to be 2,47. The results are presented in Figure 1.

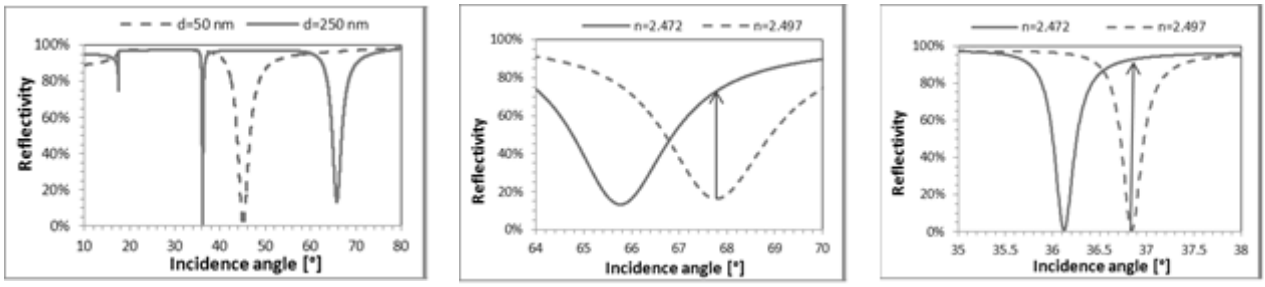

(a) (b) (c)

Figure 1. a) Reflectance spectrum for two As_2S_3 thicknesses; b) Curve's shape and shifting for basic plasmonic wave; c) The same as b), but for coupling with waveguide mode.

As can be seen for the left image, only one pick (dashed line) exists for small thickness corresponding to true plasmon-polariton interaction. While for thicknesses of 250 nm, besides the plasmonic peak at 65^0, an additional pick at 36^0 appears, corresponding to bound plasmon-planar waveguide mode. Please note that mode coupled resonances are sharper than plasmon-polariton modes, which indicates to greater sensitivity. As conclusion, the ACM films can have applications for plasmonic optical modulators or optical storage devices.

[1] Popescu A., Savastru D., Stafe M., Puscas N., *Materials*, **16** (18), (2023), Article no.6110.
[2] A. A. Popescu, D. Savastru, S. Miclos, *J. Optoelectron. Adv. Mater.*, **12**(5), (2010), 1012.

MODIFICATION IN REDOX POTENTIAL DURING ELECTROLYSIS OF MILK WHEY

I. Vutcariova*, G. Balan
Institute of Applied Physics, Moldova State University, Chișinău, Republic of Moldova
*E-mail: irinavutkareva@yahoo.com

Whey contains several chemical compounds that can be easily oxidized and reduced. The redox system of whey is formed by lactic acid, tocopherols, riboflavin, cysteine, oxidoreductases, oxygen, and other easily reducing and oxidizing substances. A change in the ratio of reducing and oxidizing agents in serum (during heat treatment, microbial development, etc.) causes a change in the redox potential. The decrease in the redox potential of serum is affected by the products of microorganisms.

The redox system of serum includes various components, for example: ascorbic acid - dehydroascorbic acid; lactic acid - pyruvic acid. The objective was to identify the causes of changes in redox potential during the electrolytic production of organic acids from whey. Any change in the concentration of the contained oxidizing and reducing agents can cause a change in the redox potential. For example, heating leads to volatilization of soluble oxygen. Electrolysis at a controlled potential allows selective oxidation of certain functional groups to produce a mixture of acids and alcohol, as well as the production of pure lactic acid.

Pasteurized milk whey produced by Chișinău dairy plant was used as an object of research. The whey was thickened to a dry matter content of 12 and 13 %. Further the whey was electro-processed in a diaphragm electrolyzer. The advantage of the electrolysis method of processing over the reagent method is that electro-processing avoids contamination of the environment and research objects with extraneous substances. The electrolysis unit includes a cathode, an anode, and a semipermeable diaphragm (partition)-membrane. During electro-processing whey is placed in the cathode chamber, in the anode chamber - a weak solution of soda NaHCO3. Electro treatment in the optimal mode was carried out under the following parameters: current strength - 1-0.2 A, voltage - 29 V, temperature - 20-35°C, duration - 40-60 minutes. Both fresh and fermented whey were processed.

To achieve this goal, the yeast strain Saccharomyces cerevisiae cultured on milk whey was used, the activity (productivity) of the strain: up to 6.2% of ethyl alcohol formation. The alcohol-forming activity of Saccharomyces cerevisiae strain was determined by pycnometer method. Optimal conditions and composition of the medium for fermentation - temperature 28-30°C; unsalted whey containing at least 4.5% lactose. We study the process in the cathodic and anodic chamber of the electrolyzer with fermented and unfermented whey to show the influence of the degree of fermentation on the process of redox potential modifications. In the case of fermented whey, we note a sharp decrease in the redox potential in the cathode chamber of the electrolyzer as a result of microorganism's activity. Subsequently, up to 50% water was evaporated from the whey at temperature of 45 °C, to reduce the loss of lactic acid. The whey was then fermented and treated in an electrolysis device. As a result of thickening, the dry matter content of the whey changed from 6.6 % to 11-13.1 %. It was necessary to find out what changes the modification in the degree of concentration entails on the passage of the electrolysis process. An increase in the current was observed in the electrolysis of more concentrated serum from 0.6 to 1.6 A. According to the results obtained, in the cathode chamber of the electrolyzer, in the case of fermentable whey, a slightly acidic and neutral environment is maintained longer, as in the case of more concentrated whey, which has a positive effect on the process of lactic acid production.

Studies have established that the optimum concentration of solids in whey intended for electrolysis treatment for the separation of various components is 12%. In the cathodic chamber with more concentrated whey a smooth transition to the alkaline zone is observed, it is in all cases a concentration chamber.

Studies of these processes allow to improve the quality, simplify the process of electro treatment and electrolyzer design, and expand the range of study parameters.

PHOTOPHYSICAL PROPERTIES of $ZnPc(SO_3H)_4$/CHITOSAN/AgNPs SYSTEMS

V. Suman[1,*], T. Potlog[2], D. Untila[2], I. Lungu[1], E. Stratulat[2], M. Diru[2]
[1]*Doctoral School "Natural Sciences" Moldova State University, Chișinău, Republic of Moldova;*
[2]*Organic/Inorganic Materials in Optoelectronics, Moldova State University, Chișinău, Republic of Moldova*
[*]E-mail: victor.suman@iien.utm.md

Silver nanoparticles (AgNPs) have attracted significant attention in the fields of materials science and nanotechnology due to their unique properties and universal applications. By changing dimensions of these nanoparticles, on the nanometer scale, they exhibit distinct behavior compared to macroscopic forms of silver, owing to quantum effects and surface interactions. The optical, electrical, and antimicrobial properties of silver nanoparticles make them crucial in various domains, ranging from modern medicine and water purification to advanced electronics and chemical catalysis [1].

Silver nanoparticles (AgNPs) were synthesized using sodium citrate ($C_6H_5O_7Na_3$) as a reducing agent. In this reaction, silver ions (Ag^+) are reduced to metallic silver (Ag^0) by sodium citrate, which is oxidized to citric acid ($C_6H_5O_7H_3$). During the formation of AgNPs, citrate ions encapsulate the particles to prevent their aggregation. The size and properties of nanoparticles depend on the capping and stabilizing agent, which is used in chemical synthesis. The functionalization of AgNPs with chitosan was carried out as follows: 0.2 g of chitosan was dissolved in 98 ml of water in a vessel. Then, 2 ml of acetic acid (99.99% concentration) and 1 ml of hydrogen peroxide (10% concentration) were added. The resulting mixture was stirred for 3 hours at 60 °C using a magnetic stirrer.

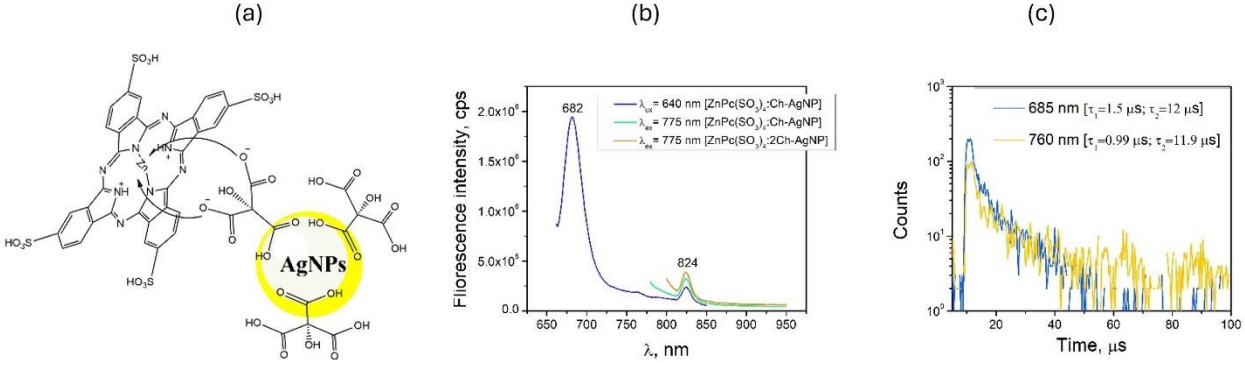

Figure 1. Scheme of $ZnPc(SO_3H)_4$/Chitosan/AgNP system (a), fluorescence emission spectrum at different excitation wavelengths of λ_{ex}=640 nm and λ_{ex}=775 nm (b), and the triplet state lifetime (c) of $ZnPc(SO_3H)_4$/Chitosan/AgNP.

Finally, $ZnPc(SO_3H)_4$ was dissolved in DMSO and then mechanically mixed with chitosan-coated AgNPs in a 1:1 ratio. With the increase in AgNP concentration in the DMSO/H_2O solution, the emission peak intensity at 825 nm increases. The fluorescence quantum yield (Φ_F) values either decreased or remained unchanged with the increase in the number of (SO_3) groups in $ZnPc(SO_3H)_4$/Chitosan/AgNP system. For system with $ZnPc(SO_3H)_4$ quantum yield of the fluorescence Φ_F=0.16, for $ZnPc(SO_3H)_3$ equals Φ_F=0.12, while for $ZnPc(SO_3H)$ (Φ_F=0.07). The low Φ_F value for $ZnPc(SO_3H)_4$ could be due to aggregation. The lifetime of excited states of the system depends on the value of λ_{ex}.

ACKNOWLEDGMENTS: This research paper was financially supported by the Ministry of Education and Research of the Republic of Moldova, Moldova State University, subprogram "Design of supramolecular architectures based on metal phthalocyanine derivatives – functionalized nanoparticles for medicine", #011209.

[1] Q. Tran, A. Le, A. (2013). *Advances in natural sciences: nanoscience and nanotechnology* **4(3)** (2013) 033001.

INNOVATIVE 3D MICROFLUIDIC SYNTHESIS OF MAGNETIC NANOPARTICLE-ENHANCED SILICA AEROGEL COMPOSITES FOR EFFICIENT PESTICIDE REMOVAL FROM WATER

A.-G. Niculescu[1,2,*], A.C. Bîrcă[1], D.I. Tudorache[1], A. M. Holban[2,3], A. Hudiță[2,4], R.D. Trușcă[1], O.M. Munteanu (Mihaiescu)[1], B.Ș. Vasile[1], M. Rădulescu[5], T. Hadibarata[1,6], A.M. Grumezescu[1,2]
[1]*Department of Science and Engineering of Oxide Materials and Nanomaterials, National University of Science and Technology Politehnica Bucharest, Bucharest, Romania;*
[2]*Research Institute of the University of Bucharest-ICUB, University of Bucharest, Romania;*
[3]*Department of Microbiology, Faculty of Biology, University of Bucharest, Bucharest, Romania;*
[4]*Department of Biochemistry and Molecular Biology, Faculty of Biology, University of Bucharest, Bucharest, Romania;*
[5]*Department of Inorganic Chemistry, Physical Chemistry and Electrochemistry, National University of Science and Technology Politehnica Bucharest, Bucharest, Romania;*
[6]*Department of Environmental Engineering, Faculty of Engineering and Science, Curtin University Malaysia, Miri, Malaysia*
[*]E-mail: adelina.niculescu@upb.ro

This work focused on developing and implementing a novel 3D microfluidic platform for the high-productivity synthesis of nanostructured silica aerogel-based composites. The produced materials integrate microfluidically obtained magnetic nanoparticles (Fe_3O_4) and active carbon, aiming to efficiently extract pesticides from water samples. The innovative microfluidic system was constructed from PMMA sheets obtained by laser cutting and further mounted in the microfluidic assembly involving reagents, pumps, valves, and control devices (Figure 1a). The multilayered device allowed adaptive liquid flow pathways and tight control over reaction parameters for the production of almost monodisperse core-shell nanoparticles, also enabling the synthesis of Fe_3O_4 cores and their in-situ shell functionalization with salicylic acid in a single step [1-3]. These functionalized nanoparticles were further incorporated into on-chip-synthesized aerogel formulations, endowing the material with magnetic properties. XRD, FT-IR, DLS, RAMAN, SEM, and TEM characterization techniques confirmed the successful production of salicylic acid-functionalized iron oxide nanoparticles and the resultant aerogel-based nanocomposites (Figure 1b). The designed material was tested by studying its ability to remove pesticides from an aqueous environment [4], exploiting its magnetic nature for easy separation. This research underscores the potential of 3D microfluidic systems for scalable, high-efficiency production of functional nanomaterials, with significant implications for water decontamination technologies.

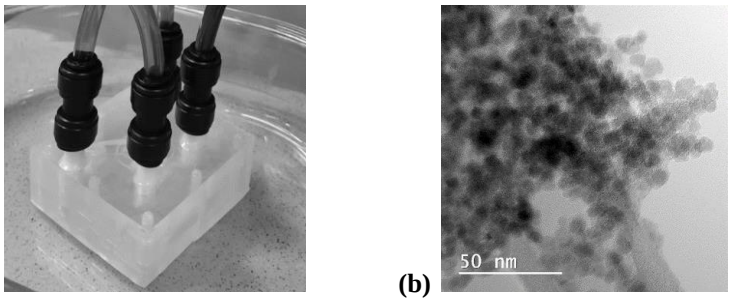

Figure 1. (a) 3D microfluidic device assembled and connected to the experimental set-up. (b) TEM micrograph of the aerogel-based nanocomposite.

[1] A.G. Niculescu, O.M. Munteanu, A.C. Bîrcă, A. Moroșan, B. Purcăreanu, B.Ș. Vasile, D. Istrati, D.E. Mihaiescu, T. Hadibarata, A.M. Grumezescu. *Nanomaterials* **14** (2024) 902.
[2] A.G. Niculescu, C. Chircov, A.C. Bîrcă, A.M. Grumezescu. *Nanomaterials* **11** (2021) 864.
[3] A.G. Niculescu, D.E. Mihaiescu, A.M. Grumezescu. *International Journal of Molecular Sciences* **23** (2022) 8923.
[4] A.G. Niculescu, B. Mihaiescu, A.C. Bîrcă, A. Moroșan, O.M. Munteanu, B.Ș. Vasile, T. Hadibarata, D. Istrati, D.E. Mihaiescu, A.M. Grumezescu. *Gels* **10** (2024) 394.

DEVELOPMENT OF FUNCTIONALIZED SILICA AEROGEL NANOCOMPOSITES FOR SOLID PHASE EXTRACTION IN ENVIRONMENTAL MONITORING

A.-G. Niculescu[1,2], A.C. Bîrcă[1], D.I. Tudorache[1], A. M. Holban[2,3], A. Hudiță[2,4], R.D. Trușcă[1], D. Istrati[5], B.Ș. Vasile[1], T. Hadibarata[1,6], A.M. Grumezescu[1,2], D.E. Mihaiescu[5,*]

[1]*Department of Science and Engineering of Oxide Materials and Nanomaterials, National University of Science and Technology Politehnica Bucharest, Bucharest, Romania;*

[2]*Research Institute of the University of Bucharest, University of Bucharest, Bucharest, Romania;*

[3]*Department of Microbiology, Faculty of Biology, University of Bucharest, Bucharest, Romania;*

[4]*Department of Biochemistry and Molecular Biology, Faculty of Biology, University of Bucharest, Bucharest, Romania;*

[5]*Department of Organic Chemistry, National University of Science and Technology Politehnica Bucharest, Bucharest, Romania;*

[6]*Department of Environmental Engineering, Faculty of Engineering and Science, Curtin University Malaysia, Miri, Malaysia*

*E-mail: danedmih@gmail.com

Solid phase extraction (SPE) represents an extensively used advanced sample preparation technique that offers high adsorption capacity, good reproducibility, and significant cost mitigation in sample preparation. Recent scientific efforts have focused on developing new SPE materials with enhanced surface areas and specific polarity to extract various organic compounds effectively. The latest literature trends recommend different aerogel types—such as carbon, silica, metal-oxide, metal-organic, and inorganic-organic hybrids—for SPE due to their large surface areas, high porosities, and low densities [1,2]. Given the increasing environmental pollution, driven by industrialization and urbanization, and widespread utilization of pesticides, high concentrations of persistent contaminants accumulate in surface waters [3]. In this context, this study aimed to develop new silica-based aerogels and explore their potential for surface water sample preparation and high-resolution mass spectrometry (HR-MS) analyses. Our research has enabled the production of functionalized silica aerogel nanocomposites with high surface areas integrated into microfluidic devices for on-site water sampling. The fabricated aerogels have been thoroughly characterized using physicochemical techniques, including X-ray diffraction (XRD), Fourier-transform infrared spectroscopy (FT-IR), Raman spectroscopy, scanning electron microscopy (SEM), transmission electron microscopy (TEM), Brunauer-Emmett-Teller (BET) surface area analysis, and Fourier-transform ion cyclotron resonance HR-MS (FT-ICR HR-MS). The experimental results demonstrate the efficacy of these materials, recommending them as promising new alternatives for SPE in environmental monitoring applications.

[1] T. Feng, X. Ye, Y. Zhao, Z. Zhao, S. Hou, N. Liang, L. Zhao. *New Journal of Chemistry* **43** (2019) 5159-5166.

[2] A.G. Niculescu, D.I. Tudorache, M. Bocioagă, D.E. Mihaiescu, T. Hadibarata, A.M. Grumezescu. *Nanomaterials* **14** (2024) 469.

[3] A.G. Niculescu, B. Mihaiescu, A.C. Bîrcă, A. Moroșan, O.M. Munteanu, B.Ș. Vasile, T. Hadibarata, D. Istrati, D.E. Mihaiescu, A.M. Grumezescu. *Gels* **10** (2024) 394.

MORPHOLOGY AND OPTICAL PROPERTIES OF $ZnFe_2O_4$ THIN FILMS GROWN BY RF-MAGNETRON SPUTTERING

T. D. Gutsul[1,*], S. N. Zavrajnii[1], S. A. Moldovanu[2], M. C. Lupu[1], V. M. Fedorov[1]
[1]*Technical University of Moldova, "D.Ghitu" Institute of Electronic Engineering and Nanotechnologies, Chișinău, Republic of Moldova*
[2]*Institute of Applied Physics, Moldova State University, Chișinău, Republic of Moldova*
[*]E-mail: tatiana.gutul@iien.utm.md

Nanocomposite materials based on ferrites have recently become effective heterogeneous catalysts and are widely used in the purification of water systems from organic pollutants [1]. Zinc ferrite occupies a special place as a prospective semiconductor photocatalytic material due to the photoresponse in the visible light spectrum, the band gap is 1,9 eV [2]. Zinc ferrite-based film structures are insufficiently represented, although they have a technological perspective. Thus, the creation of photocatalytic systems based on zinc ferrite is an actual task. In the presented work we obtained $ZnFe_2O_4$/glass film structures using the RF-magnetron sputtering method. The target was made by pressing of zinc ferrite nanoparticles synthesized by us using the solvothermal method. The morphology of $ZnFe_2O_4$ nanoparticles and thin films was characterized by Scanning Electron Microscopy (SEM-Philips XL30 SFEG and TESCAN VEGA 5124). Optical characteristics of the obtained $ZnFe_2O_4$/glass films were measured on the Spectrophotometer UV-VIS T-80.

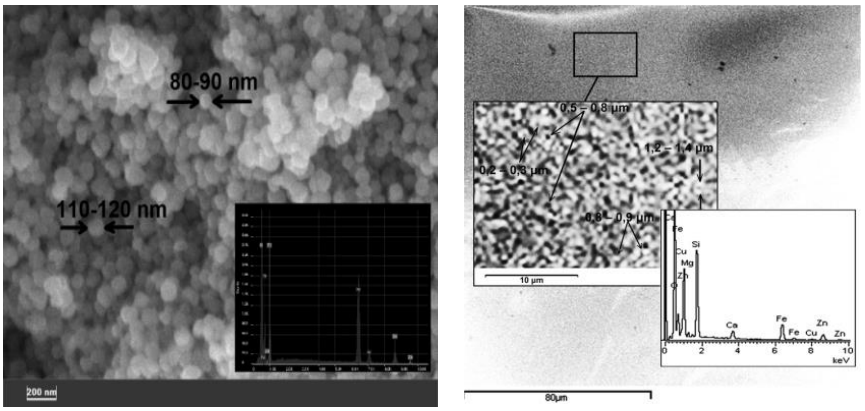

(a) (b)

Figure 1. SEM of $ZnFe_2O_4$ NPs (a) and SEM EDX of $ZnFe_2O_4$/glass thin film (b).

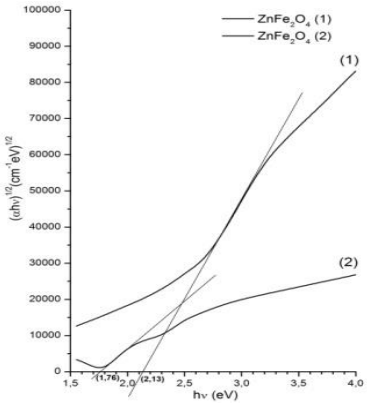

Figure 2. *Tauc's plot* analysis of UV-Vis *absorption spectra* of $(\alpha h\nu)^{1/2}$ $(cm^{-1}eV)^{1/2}$ versus photon energy hν(eV) of $ZnFe_2O_4$/glass structures.

The morphology and sizes of $ZnFe_2O_4$ nanoparticles are shown in Fig.1(a). Nanoparticles have a spherical form with dimensions from 5 to 10 nm. Because of nanoparticles high surface energy, they undergo rapid interparticle interaction and enlarge into spheres with a diameter from 80 to 120 nm. Film structures of $ZnFe_2O_4$ are flexible chain formations consisting of spherical nanoparticles with dimensions from 150 to 250 nm. In Fig.2 the data of spectrophotometric studies for $ZnFe_2O_4$/glass samples with a band gap of 1,76 eV and 2,13 eV are presented.

[1] S. K. Sharma. Spinel Nanoferrites. *Springer* 2022, 315.
[2] C. Zhang, X. Han, F. Wang, L. Wang, J. Liang. *Frontiers in Chemistry* 2021 **9** Art.736369.

FORMATION OF $ZnFe_2O_4$/ZnO:Al THIN FILM HETEROSTRUCTURE WITH THE PEROXIDASE MIMETIC PROPERTIES BY RF-MAGNETRON SPUTTERING METHOD

T.D. Gutsul[1,*], M.C. Lupu[1], E.I. Monaico[2], N.V. Costriucova[3], D.O. Podgornii[3]
[1]*Technical University of Moldova, "D.Ghitu" Institute of Electronic Engineering and Nanotechnologies, Chișinău, Republic of Moldova;*
[2]*Technical University of Moldova, Chisinau, Moldova;*
[3]*Institute of Applied Physics, Moldova State University, Chișinău, Republic of Moldova*
[*]E-mail: tatiana.gutul@iien.utm.md

In recent years analytical methods based on the catalytic activity of nanoparticles with the properties of the peroxidase mimetic, such as palladium nanoparticles, porous cobalt oxide nanostructures and others, have been successfully used to detect pollutants in the environment [1]. In our work we propose $ZnFe_2O_4$/ZnO:Al film heterostructures that were obtained by magnetron sputtering in an argon atmosphere as a mimetic of the peroxidase enzyme for the detection of hydrogen peroxide in model experiments. The morphology and chemical composition of $ZnFe_2O_4$/ZnO:Al thin films were studied using a Zeiss Sigma scanning electron microscope and Tescan Vega TS 5130MM equipped with an Oxford Instruments INCA energy dispersive X-ray system operating at a voltage of 20 kV. The study of the chemical composition obtained using X-ray spectroscopy (EDX) shows in the case of thin layer of ZnO:Al, along with the main elements Zn, O, Al, elements similar to glass (Ca, Si, Mg, O) as well as Zn, Fe, O, for $ZnFe_2O_4$/ZnO:Al film nanostructures. In Fig.1 (a) and (b) are presented SEM EDX of ZnO:Al thin film and $ZnFe_2O_4$/ZnO:Al heterostructure respectively.

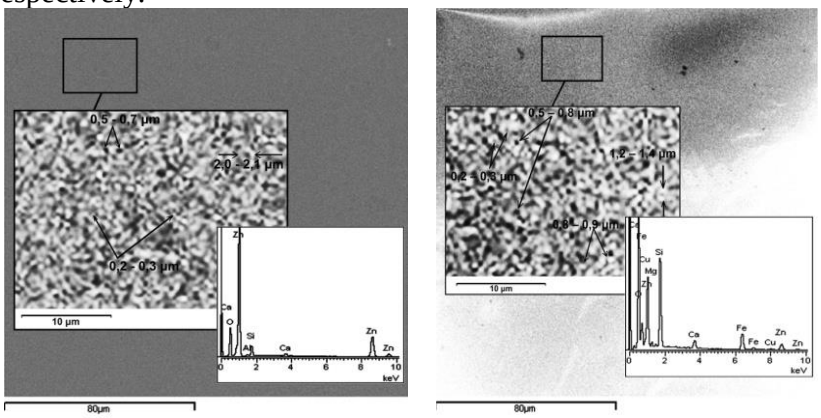

(a) (b)

Figure 1. SEM EDX of ZnO:Al/glass thin film (a) and $ZnFe_2O_4$/ZnO:Al heterostructure (b).

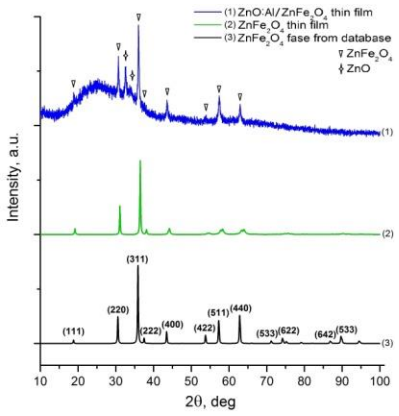

Figure 2. XRD of $ZnFe_2O_4$/glass thin film (2) and $ZnFe_2O_4$/ZnO:Al/glass heterostructure (1).

The comparison of the X-ray diffraction (Desktop X-ray diffractometer Miniflex 600 Rigaku) of the obtained thin films in Fig.2 (2) with a diffraction pattern from the JCPDS database No. 22-1012 presented in Fig.2 (3) shows the presence of peaks corresponding to (111), (220), (311), (222), (400), (422), (511), (440) phases of cubic spinel (Franklinite). In Fig.2 (1) specific peaks related to ZnO in the $ZnFe_2O_4$/ZnO:Al/glass heterostructure are presented. The ZnO sample shows the specific peaks at 2θ = 31.7° (100), 34.4° (002) and 56.5° (110) corresponding to the hexagonal structure of wurtzite type (ICDD No.01-078-2585). The peroxidase activity of the $ZnFe_2O_4$/ZnO:Al/glass films structure was studied using 3,3', 5,5'-tetramethylbenzidine (TMB) as a peroxidase substrate in the presence of H_2O_2 according to the procedure described in [2].

[1] Patent No: AU2020100704. Date of Filing: 2020.05.05. A method of synthesis of ultrathin palladium nanosheet with peroxidase mimetic activity for the colorimetric detection of H_2O_2.
[2] L. Gao, M. Liang, X. Yan. *Nature Protocols* 2018 **13** 1506−1520.

OPTIMAL COMPUTATIONAL PROCESSING OF DIGITAL PHASE MASKS FOR DIGITAL HOLOGRAPHY

V. Cazac*, E. Achimova, V. Abashkin, A. Meshalkin
Institute of Applied Physics, Moldova State University, Chișinău, Republic of Moldova
*E-mail: veronikakazak21@gmail.com

Today, advanced optical components contribute to emerging computer technologies which have an important role and a huge potential of practical applications in various branches of science and industry including digital holography (DH), optical metrology, biology, medicine, material science and many others. Specifically, digital wavefront manipulation can be used for increasing the depth of field, resolution, and compensation of aberrations, noises and image distortion introduced by the optical components of the setup (microscope objective, lenses, etc.) in digital holographic (DH) optical systems [1]. The main purpose of this paper is to prove that by digital wavefront manipulation using a diffraction grating an improved phase reconstruction can be obtained in DH setups. Optimal phase mask parameters were investigated.

For the simplicity of the calculations and reduction of the computational operation time the off-axis DH is considered with a sinusoidal phase modulation at the object plane. The variational algorithm for phase and amplitude reconstruction is based on the algorithm proposed in the paper [2]. In this experiment, the process of digital holographic recording of the wavefront originating from the object with subsequent computer reconstruction of the object's image was modelled. The variability of DG features (period, optical phase, number of rotating angles) allows one to adjust the phase modulation for obtaining more accurate results. Furthermore, the flexibility of the numerical reconstruction approach allows one to selectively use the diffraction orders carrying out useful information.

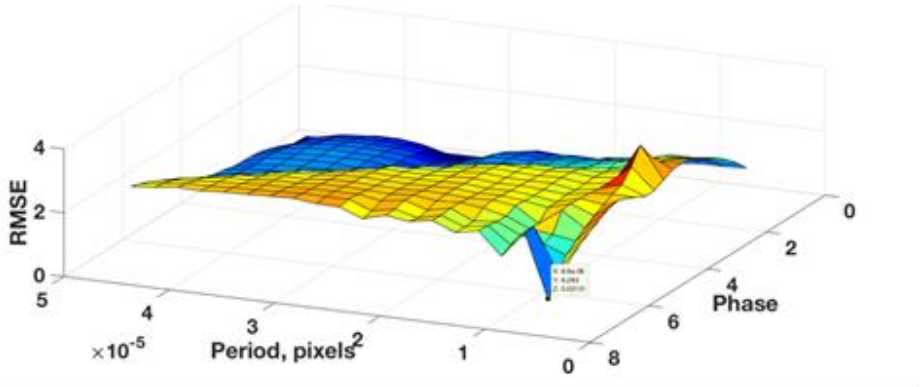

Figure 1. RMSE dependence on phase mask phase and period. The diffraction grating angle is equal to 90°.

Computational simulations results prove that phase imaging enhancement can be obtained by adopting a sinusoidal phase modulation by a diffraction grating for the off-axis DH setup. The following optimal phase mask parameters were identified: the period $\Lambda = 44$ μm, the value of phase modulation was $\varphi = 0.1\pi$ and two positions rotation steps of the phase mask at 0, 90, 180 degrees. The illustration of the root mean square error (RMSE) dependence on grating phase and period is shown in Fig. 1. Due to the optimized diffraction grating parameters (period, phase and number of rotating steps) more information about the high spatial frequencies of the object spectrum is recorded in the CCD sensor from the diffracted orders. Computational experiments show that with sinusoidal phase modulation RMSE values are decreased about 20%.

[1] M. Paturzo, F. Merola, P. Ferraro. *Optics Letters* **volume 35** (2010) pp. 1010-1012.
[2] V. Katkovnik, I.A. Shevkunov, N.V Petrov, K. Egiazarian. *Optics Letters* **volume 40** (2015) pp. 2417-2420.

TECHNOLOGICAL ASPECT ON MORPHOLOGICAL AND ELECTRICAL PROPERTIES OF ZnO AND ZnMgO FILMS

V. Morari[1,*], V. Ciobanu[2], E. V. Rusu[1], V. V. Ursaki[2]
[1]*Institute of Electronic Engineering and Nanotechnologies „D. Ghitu", Technical University of Moldova, Chisinau, Republic of Moldova;*
[2]*National Center for Materials Study and Testing, Technical University of Moldova, Chisinau, Republic of Moldova*
[*]E-mail: vadim.morari@iien.utm.md

ZnO (zinc oxide) films are very important in a range of technological and industrial applications due to their unique physical, optical, and electronic properties. Recent studies have been carried out based on ZnO films obtained by RF magnetron sputtering and pulsed laser deposition method [1,2] for gas sensing application. The effect of deposition time on morphological and electrical properties has a crucial aspect in ZnO and ZnMgO thin films research. Crystal size and morphology can impact the electrical conductivity and optical transparency of the films [1]. It was shown that as the deposition time increases, the film thickness and crystal size of ZnO increases, the optical band gap was decreased from 3.31 to 3.29 eV, and prepared films have a quick response and fast recovery time in the range of 128 s and 163 s. Controlling the deposition time is essential for tailoring the properties of ZnO films to meet specific application requirements, whether for optoelectronic devices, sensors, or other devices (e.g., gas sensors, solar cells). Similar effects occur in ZnMgO films, where Mg incorporation can modify properties.

This paper reports on technological aspects and their impact on the morphological and electrical properties of ZnO and $Zn_{0.8}Mg_{0.2}O$ films obtained on silicon (Si) substrate using spray pyrolysis method with various deposition time, ranging from 1 min to 10 min. Our studies were carried out using atomic force microscopy (AFM) to determine the morphological parameters of the films, and electrical measurements with a Keithley multimeter (2400 Standard Series SMU) to determine the resistance of the thin films. The thickness of the obtained films was determined by scanning electron microscope (SEM) by measuring the samples in cross-section. Zinc acetate and magnesium acetate with a molar concentration of 0.25 M were used as precursors, with methyl alcohol, distilled water and acetic acid in the ratio of 6.5:2.5:1 as solvent. The substrate temperature was 480 °C and the carrier gas flow (O_2) was at a solution injection rate of 1.5 cc/min. It was found that the thickness of both ZnO and ZnMgO films increased constantly with increasing the deposition time from 50 nm (1 min) to 380 nm (10 min), while their resistance changed in a specific manner. It decreased with increasing the deposition time up to 5 min and then increased considerably, an effect that occurs for both types of oxide films (ZnO and ZnMgO). One thing to note is that the concentration of Mg in the films considerably increases the resistance of the material, so that the ZnO films resistance was of 170 kΩ at 10 minutes of deposition, while the resistance of $Zn_{0.8}Mg_{0.2}O$ films was of 420 kΩ for the same deposition time. The roughness of films varied with changing the deposition time, and the crystallites size was found to be improved with increasing the deposition time.

ACKNOWLEDGEMENTS: This work was supported by the institutional subprogram project #02.02.01 no. 4/FI „Nanostructures and advanced materials for applications in spintronics, thermoelectricity and optoelectronics".

[1] S. Bhatia, N. Verma, M. Aggarwal. Effect of deposition time on sputtered ZnO thin films and their gas sensing application, *J Mater Sci: Mater Electron*, **Vol. 29**, (2018), pp. 18136–18143
[2] W. B. K. Putri, N. Yudasari, R. P. Putra, M. A. Anugrah, B. Kang. *AIP Conf. Proc.* **2652 (1)**, (2022), 020005

SONICATION-ASSISTED LIQUID-PHASE EXFOLIATION OF MoS_2 AND WSe_2 LAYERS

V.V. Goremichin*, N. Siminel, L.L. Kulyuk
Institute of Applied Physics, Moldova State University, Chisinau, Moldova
*E-mail: vladimir.goremichin@ifa.usm.md

Sonication-assisted liquid-phase exfoliation is a widely used, cost-effective technique for producing two-dimensional (2D) layered materials such as graphene and transition metal dichalcogenides (TMDs) [1]. This method is particularly advantageous for preparing printable TMD inks for use in scalable technologies like inkjet printing. In this study, MoS_2 and WSe_2 nanosheets were prepared via the direct exfoliation of bulk powders in a Bovine Serum Albumin (BSA)-containing solution, which facilitated strong hydrophobic interactions between the benzene rings of BSA and the TMD layers, enabling efficient exfoliation [2].

Both commercially sourced bulk powders and high-quality homemade single crystals were used, with the latter yielding superior nanosheets. A solution of 500 mg bulk MoS_2 or WSe_2 was dispersed in 100 mL of 1-3 mg/mL BSA solution and sonicated for 48 hours in a cooled ultrasonic bath. The supernatant, collected after centrifugation, was subjected to a 50 mM H_2O_2 solution to remove residual BSA. This exfoliation method aligns well with subsequent techniques for creating engineered holes in nanosheets, which are critical for tuning the intrinsic properties of the material, particularly for bio-sensing applications.

A key focus of the study was the development of MoS_2 nanorings, where chemical dissolution in a pH 4.0, 50 mM H_2O_2 solution created holey MoS_2 nanosheets (h-MoS2). These holey structures significantly enhance the number of edge sites, leading to improved sensitivity and selectivity in biosensors, particularly field-effect transistors (FETs) used for bio-detection [3]. The approach demonstrated here offers a scalable and efficient pathway for fabricating advanced 2D materials for high-performance bio-sensing applications.

[1] M. Telkhozhayeva, E. Teblum, R. Konar, O. Girshevitz. *Higher Ultrasonic Frequency Liquid Phase Exfoliation Leads to Larger and Monolayer to Few-Layer Flakes of 2D Layered Materials Langmuir* (2021)
[2] G. Guan, et al. *Chemistry of Materials* **30(15)** (2018), 5108-5115
[3] H. Park, S. Baek, A. Sen, B. Jung, J. Shim, Y. C. Park, L. P. Lee, Y. Jun Kim, S. Kim. *ACS Nano* 1**6** (2022), 1826−1835

XPS: A POWERFUL TOOL FOR QUALITATIVE AND QUANTITATIVE CHEMICAL ANALYSIS OF HEA MATERIALS

S. Cichon*, P. Hruska, J. Lancok
Institute of Physics, the Czech Academy of Sciences, Prague, Czechia
*E-mail: cichon@fzu.cz

XPS (X-ray Photoelectron Spectroscopy) has become a widely available, fast and efficient analytical method for probing chemistry of all kinds of matter [1-3]. It is primarily a surface sensitive method designated for conductive solid state materials. With the most common instrumental arrangement (Al anode), the probing depth is ≥ 2 nm. However, its technical design has evolved enabling analysis of nonconductive materials in various forms such as organics or liquids: bones, tomato peel, tomato pulp, rubber, blood, etc.. Examples of particular designs are NAP-XPS (Near Ambient Pressure X-ray Photoelectron Spectroscopy) or EnviroESCA that also provide an in operando operation.

The qualitative chemical analysis is based on the so called "chemical shifts" of binding energy of electrons in atom orbitals as a results of chemical bonds. The quantitative chemical analysis uses peak or peak component areas for calculation of concentration of constituent elements.

XPS does not have to be restricted to the first 2 nm of the surface of the sample; compositional profiles are accessible via depth profiling similar to the one employed in SIMS (Secondary Ion Mass Spectroscopy). In the same sense, probing depth can be increased employing HAXPES (Hard X-ray Photoelectron Spectroscopy).

Hence, it is not surprising that also HEA based materials have been widely investigated by XPS [4, 5]. Taking a HEA film deposited by a PVD (Physical Vapor Deposition) technique as an example, we can obtain following information: surface concentration of each constituent metal (element specific segregation), quantitative contribution of each element to the formation of the native oxide overlayer, character of the oxide (oxidation state of each metal), element resolved depth profile of the native oxide, concentration profile of each constituent metal within the film, impurities found within the film (above 0.1 % atomic). The above presented "z" information can be complemented with a mapping, an "x-y" information about the sample composition (the resolution is usually around 100 nm). With a HEAC material, for instance, we can elucidate carbon incorporation into the film: element specific carbide formation, segregation, formation of oxycarbides, etc. With all the above mentioned, it is likely more than clear that XPS is a powerful tool that should not stay out of attention of a HEA scientist.

It should be noted that XPS instruments are usually equipped with other facilities that enable further, also in-situ, sample modifications such as high temperature annealing in vacuum or various gases or deposition of other materials.

[1] The XPS Library, xpslibrary.com
[2] The International XPS Database, xpsdatabase.net
[3] X-ray Photoelectron Spectroscopy (XPS) Reference Pages, www.xpsfitting.com
[4] H. Luo, Z. Li, A. M. Mingers, D. Raabe, Corrosion behavior of an equiatomic CoCrFeMnNi high-entropy alloy compared with 304 stainless steel in sulfuric acid solution, *Corrosion Science* **134** (2018) 131-139.
[5] P. Hruska, F. Lukac, S. Cichon, M. Vondracek, J. Cizek, L. Fekete, J. Lancok, J. Vesely, P. Minarik, M. Cieslar, O. Melikhova, T. Kmjec, M. O. Liedke, M. Butterling, A. Wagner, Oxidation of amorphous HfNbTaTiZr high entropy alloy thin films prepared by DC magnetron sputtering, *Journal of Alloys and Compounds* **869** (2021) 157978.

ACCELERATING THIN FILM PHOTOVOLTAIC TECHNOLOGY DEVELOPMENT THROUGH HOLISTIC CHARACTERIZATION AND ARTIFICIAL INTELLIGENCE-DRIVEN DATA ANALYSIS

J. Garí-Galíndez[1], R. Fonoll-Rubio[1], J. Andrade-Arvizu[1], P. Vidal-Fuentes[1], A. Perez-Rodriguez[1,2], V. Izquierdo-Roca[1], M. Guc[1,*]

[1]*Catalonia Institute for Energy Research – IREC, Barcelona, Spain;*

[2]*Departament d'Enginyeria Electrònica i Biomèdica, IN²UB, Universitat de Barcelona, Barcelona, Spain*

[*]E-mail: mguc@irec.cat

Thin film photovoltaic (TFPV) materials and devices are characterized by their high complexity, featuring multi-scale structures ranging from nm to μm, multi-layer configurations, and multi-element compositions, along with intricate fabrication processes. Addressing this complexity requires a comprehensive evaluation of the compositional, structural, morphological, optical, and electrical properties of TFPV devices. Such comprehensive assessments are crucial for developing models that guide their advancement and optimization. The inherent complexity of these devices demands a holistic research approach, involving three main challenges: 1) systematic characterization using diverse techniques, 2) automating data acquisition to produce a statistically significant volume of data (big data), and 3) creation of automated, rapid, and multidimensional data processing strategies.

This work presents a strategy to address these challenges through the development of a modular and highly customizable platform and methods, which enable fast, holistic, and non-destructive characterization of complex materials and devices. The platform addresses the challenges as follows:

1) Systematic characterization – the platform integrates specialized sensors to assess composition, morphology, crystal structure, thickness, and optoelectronic parameters using various techniques (e.g., XRF, Raman, PL, UV-Vis-NIR reflectance, visual imaging, and I-V measurements).

2) Automated data acquisition – the development of specialized software and protocols ensures systematic and automated data acquisition, along with an efficient data storage architecture to facilitate seamless analysis.

3) Automated and fast multidimensional data processing – the platform employs flexible methodologies and algorithms to automate data conditioning and processing. This includes statistical and AI-assisted data analysis, such as machine learning algorithms, to expedite big data analysis and identify correlations that propel the advance of TFPV technology.

A practical example of this approach is demonstrated through the accelerated research of $Cu_2ZnSnSe_4$-based TFPV (CZTSe) devices. Eleven samples (each measured 5×5 cm^2 size) are systematically studied as an initial step towards the up-scaling production of CZTSe-based PV devices. These devices feature a Glass/Mo/$MoSe_2$/CZTSe/CdS/i-ZnO/ITO structure, with slight uncontrolled variations in the fabrication process. Each sample is segmented into 3×3 mm^2 individual solar cells, resulting in 196 cells per sample, which facilitates the compilation of a comprehensive data library. This enables the collection of detailed cell-by-cell information for statistically relevant analysis. Systematic characterization combining spectroscopic and optoelectronic techniques, as previously described, is performed on each cell. The analysis of the obtained data allows for correlating the physicochemical properties of TFPV materials with variations in device performance. This insight is crucial for understanding the impact of different material and layer properties, their interrelations, and current technological limitations. Such information is vital for advancing CZTSe technology toward high efficiencies and future industrialization. Furthermore, the proposed platform paves the way for developing a process monitoring tool for controlling TFPV devices production, which can be easily adapted to other optoelectronic technologies.

THE LINK BETWEEN FLUCTUATIONS IN THE i-ZnO LAYER AND THE PERFORMANCE HOMOGENEITY OF KESTERITE BASED THIN FILM SOLAR CELLS

V. Rotaru[1,2], M. Miró Llorente[1], R. Fonoll[1], J. Andrade-Arvizu[1], D. Payno[1], M. Guc[1], A. Pérez-Rodríguez[1,3], V. Izquierdo-Roca[1], P. Vidal-Fuentes[1]
[1]*Catalonia Institute for Energy Research – IREC, Sant Adrià de Besòs, Spain.*
[2]*Facultat de Física, Universitat de Barcelona, Barcelona, Spain.*
[3]*Departament d'Enginyería Electrònica i Biomèdica, IN2UB, Universitat de Barcelona, Barcelona, Spain.*
[*]E-mail: vrotaru@irec.cat

Recent achievements in the record efficiency of kesterite based thin film solar cells allowed to reconsider this promising technology for the possible implementation in various applications. One of the crucial points for the industrialization of kesterite based photovoltaic (PV) technology is achieving homogeneity of the deposited layers. On top of improving pixel efficiency at cell level, it involves ensuring large area uniformity and reproducibility using scalable and industrially compatible fabrication processes. This is essential for the successful scale-up and feasibility of the kesterite technology, enabling its commercialization, thus contributing to the EU's transition towards renewable electrification.

One critical aspect to consider when scaling up any thin film PV technology is the presence of shunt paths, which become crucial when dealing with larger areas, as they determine the overall device performance. In the case of kesterite technology, the intrinsic zinc oxide (i-ZnO) nanometric layer deposited at the buffer/TCO interface plays a vital role by providing isolation between the front and back contacts of the devices.

Taking this into account, this study focuses on evaluating the importance of the i-ZnO protection layer in substrate architectures (SLG/Mo/$MoSe_2$/CZTSe/CdS/i-ZnO/ITO) during the scale-up of the kesterite technology. Specifically, this work explores the effect of i-ZnO thickness on the performance of the $Cu_2ZnSnSe_4$ (CZTSe)-based devices by employing an in-depth combinatorial analysis methodology based on such spectroscopic techniques as photoluminescence (PL) and Raman scattering, using a set of discrete samples with thickness variation from 0 to 100 nm.

The results of the device performance in the discrete samples show that varying the i-ZnO thickness improves the devices homogeneity. Thus, the coefficient of variation of the FF is reduced from 16.9 % (25 nm of i-ZnO) to 3.8 % (100 nm) without sacrificing the maximum value, while the Voc of these samples is improved by 15 mV. Together, these two factors define the PCE distribution of the sample towards a positive reduction in dispersion.

In addition, the results of PL and Raman spectroscopies show a presence of fluctuations in the i-ZnO layer features in all samples. For instance, there is shown a variation of the crystalline quality, grain size and surface defects concentration in the i-ZnO layer. Finally, we found that these observed variations of the i-ZnO features clearly correlate with the optoelectronic parameters of the solar cells and constitutes an additional factor that influences the device performance. Moreover, the dispersion of the crystalline quality and grain size of i-ZnO in the device, correlate with the dispersion of the samples' optoelectronic performance. These results show that in order to improve the homogeneity of the kesterite devices it is important to control the i-ZnO layer as it proves to be a key factor for scaling up the CZTSe technology.

STUDY ON THE DEPOSITION AND PROPERTIES OF HAFNIUM-BASED HIGH ENTROPY ALLOYS

R. Udrea[1,2], S.A. Irimiciuc[2], P. Garoi[2], V. Craciun[2]
[1]*Faculty of Physics, University of Bucharest, Bucharest, Romania;*
[2]*Second National Institute for Laser Physics and Radiation Plasma, Magurele, Romania;*
*E-mail: radu.udrea@yahoo.com

High Entropy Alloys consist of four or more elements with concentrations between 5-35%. These alloys were found to exhibit high-strength, high fracture toughness at low temperatures and good corrosion resistance. Our study focused on the Hf-based HfNbTaTiZr alloy which belongs to a group of refractory materials with a high melting point and thermal stability with enhanced ductility and strength.

Thin films of HfNbTaTiZr were prepared through Pulsed Laser Deposition (PLD) at different deposition parameters and in different gas atmospheres.

The films produced through PLD were then analysed through grazing incidence X-ray diffraction (GIXRD), X-ray reflectivity (XRR), atomic force microscopy (AFM). Their electrical properties were studied, obtaining I-V curves and determining the resistivity through 4-point probe measurements. Finally, the mechanical properties of the samples were studied through nanoindentation.

A comparison between the deposition parameters is presented, as well as the differences observed between HEA thin films prepared via PLD, compared to other deposition techniques, such as DC magnetron sputtering or ionized jet deposition. The potential application of such films in domains such as the biomedical sciences are discussed.

ACKNOWLEDGEMENTS: This work was supported by NATO SPS G6153 Project.

DEVELOPMENT AND TUNING OF CHEMICAL COMPOSITION, CRYSTAL STRUCTURE AND ELECTRONIC PROPERTIES OF $ZnSnN_2$ THIN FILMS

Gh. Ghileţchii[1,*], Ig. Narolschi[1], T. Unold[2], S. Schorr[2], M. Rusu[1,2], S. Vatavu[1]
[1]*Physics of Semiconductors and Devices Lab, Faculty of Physics and Engineering, Moldova State University, Chisinau, Republic of Moldova*
[2]*Department Structure and Dynamics of Energy Materials, Helmholtz-Zentrum Berlin für Materialien und Energie, Berlin, Germany*
[*]E-mail: ghiletchii.gheorghe@usm.md

$ZnSnN_2$ semiconductor thin films are of high perspective for electromagnetic radiation detection and conversion due to its high absorption coefficient of 10^4-10^5 cm^{-1} and consisting of earth-abundant elements. However, an easy scalable technology development is still a challenge for this material. This work focuses therefore on a detailed analysis of the chemical composition, morphology, crystal structure and electronic properties of as-prepared and postdeposition annealed (PDA) $ZnSnN_2$ thin films as a function of synthesis conditions.

$ZnSnN_2$ thin films were prepared onto glass substrates by DC reactive magnetron sputtering in N_2 plasma containing ambient by using Zn-Sn sputtering targets with different [Zn]/[Sn] ratios varying between 0.15-0.85. The substrate temperature range was 50-350°C. An in-situ PDA process was performed immediately after the preparation procedure at 350°C either in vacuum or Ar . X-ray Fluorescence and Energy Dispersive X-ray (EDX) methods have been used for compositional analysis. Non-contact atomic force microscopy and scanning electron microscopy were used for morphological analysis. Grazing incidence (0.5°) X-ray diffraction and X-ray reflectivity (XRR) measurements have been used for structural characterization of as-prepared and PDA thin films. Electronic properties vs. technological variations were investigated by Kelvin Probe (KP) and Photoelectron Yield Spectroscopy (PYS).

The tune of the technology showed a high influence of the target composition on the film's stoichiometry. 1:1:2 stoichiometry films were prepared at a substrate temperature of 200°C by use of Zn0.50Sn0.50 target.

The structural analysis of the $ZnSnN_2$ films (15-44 nm thick, as determined by XRR) has proven the formation of single phase, Wurtzite-type structure ($P6_3mc$) (a=b=3.370-3.414 Å; c=5.467-5.600 Å; $\alpha=\beta=90°$; $\gamma=120°$). The determined lattice constants are influenced by the substrate temperature. Microstrain, crystallites' size and electronic properties are highly substrate temperature dependent as well as annealing ambient dependent. A minimum lattice strain is obtained for samples with close to 1:1:2 stoichiometry grown in the 100-200°C temperature range.

Surface electronic properties are influenced by substrate temperature and the applied PDA. For the as-prepared films, the ionization energy revealed by PYS reaches a maximum value of 5.7 eV for samples prepared at a substrate temperature of 150°C with [Zn]/([Zn]+[Sn])=0.6. The ionization energy of PDA films was found to change between 5.45 eV and 5.60 eV with the substrate temperature increase from 150°C to 350°C. The work function determined by KP of the vacuum annealed films increases from 4.6 eV to 4.9 eV, while decreasing from 5.0 eV to 4.7 eV for Ar-annealed layers for substrate temperature variation between 150°C and 350°C. Within the PYS characterization depth, a change from *p* to *n*-type conductivity of the films was found . The transition from *p* to *n*-type is influenced by the [Zn]/([Zn]+[Sn]) ratio and substrate temperature. The 1:1:2 stoichiometric films prepared at $T_{substrate}$ = 200°C are of *p*-type conductivity, while the films prepared at $T_{substrate}$ >300°C and subsequently PDA processed at 350°C in Ar are of *n*-type.

In summary, high crystallinity $ZnSnN_2$ nanometric thin films were prepared on glass substrates by use of an easy upscaling method such as the DC reactive sputtering. PDA films exhibit physical properties suitable for applications in photovoltaic and photodetection devices.

ACKNOWLEDGEMENTS: MEC subprogram 011207

TIME-RESOLVED EMISSION FROM CdSe/CdS/CdZnS QUANTUM DOT FILMS

I.V. Belousov*, V.I. Pavlenko
Moldova State University, Institute of Applied Physics, Chișinău, Republic of Moldova
*E-mail: ivbeloussov@gmail.com

The dynamic and spectral characteristics of close-packed quantum dots excited by a long laser pulse in a thin film were investigated. The same highly luminescent CdSe/CdS/CdZnS quantum dots (QDs) were used as in [1] where their time-resolved photoluminescence in a colloidal solution was studied earlier. Their core size amounts to 5.4 nm and the shell thickness is of 2.6 nm. Their core size dispersion amounts to 8%. The close-packed QD films with a refractive index of 1.8 were produced on glass substrates by drop casting from a toluene solution. The morphology of the films was monitored using an optical microscope. Optically transparent sections of the film with a smooth surface without internal defects were selected. Measurements were carried out on the best of them with a thickness of ~50 μm. The films were studied by optical absorption spectroscopy and luminescence spectroscopy. We found out that the first peak of light absorption corresponds to the size of our QDs [1], and the peak of light emission occurs at a wavelength corresponding to the energy of 1.99 eV. This is the energy of exciton formation. Photoluminescence (PL) was excited by laser pulses with a duration of ~30 ps and a repetition rate of 0.5 Hz by the second harmonic (539 nm) of a $YAlO_3:Nd^{3+}$ laser with a passive mode synchronization. The pulses were directed to the film surface at an acute angle, were focused on the surface and created an excitation spot of ~ 100 μm. PL was collected from the excitation region on the upper surface of the film. All measurements were carried out at room temperature.

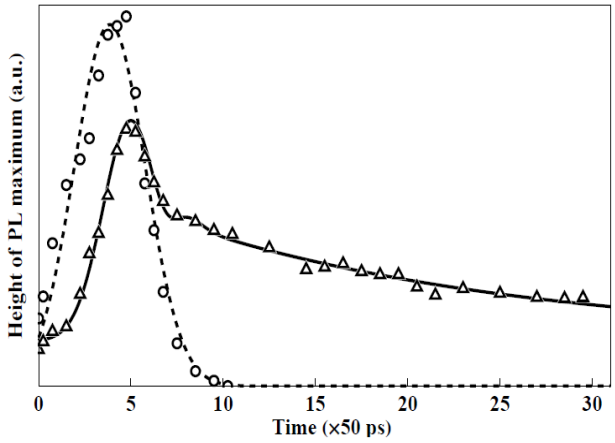

Figure 1. Temporal dependences of the height of maxima of the fitting functions for $\varepsilon = \varepsilon_1$ (circles) and for $\varepsilon = \varepsilon_2$ (triangles). The exciting laser pulse is centered at 117 ps.

The photoluminescence maxima of single excitons (ε_1) and the maxima of amplified spontaneous radiation (ASE) associated with a stimulated decay of biexcitons (ε_2) were obtained. From the spectrogram of the time-resolved photoluminescence the information was obtained about the dynamics of these two types of radiation. The rise and decay of each of them are presented in Fig. 1. It was shown that the radiation peak maximum of single excitons appears by 60 ps later than the maximum of amplified spontaneous radiation, then it slowly becomes narrower and diminishes. The amplified spontaneous radiation lasts for 200 ps. As follows from Fig. 1, the laser pulse excites the ASE, which reaches a maximum value at 190 ps. At the same time, the emission of single excitons appears, which reaches a maximum at 250 ps. The ASE lasts for a very short time period of 200 ps. After reaching the maximum value the ASE peak blurs, its width increases rapidly, and its height decreases to zero. The emission peak of single photons slowly decreases to zero during 2 ns and becomes narrower.

We also obtained a spectrogram of time-resolved PL at a laser excitation intensity of P=1 mJ/cm^2. Its analysis shows that in this case, only spontaneous emission of single excitons is observed, and there is no signal of ASE. In other words, in the figure similar to Fig. 1 only bold solid lines remain, and the dashed lines do not appear.

[1] V. Pavlenko, I. Dobynde, I. Beloussov, D. Ozol. Physica E: Low-dimensional Systems and Nanostructures **115** (2019) 113695.

TIME-INTEGRATED PHOTOLUMINESCENCE FROM CdSe/CdS/CdZnS QUANTUM DOT FILMS

V.I. Pavlenko*, I.V. Belousov
Moldova State University, Institute of Applied Physics, Chișinău, Republic of Moldova
*E-mail: vladimir.pavlenco@ifa.usm.md

The spectral characteristics of close-packed quantum dots excited by a laser pulse in a thin film were investigated. The highly luminescent CdSe/CdS/CdZnS quantum dots (QDs) were used as in [1]. Their core size amounts to 5.4 nm and the shell thickness is of 2.6 nm. Their core size dispersion amounts to 8%. The close-packed QD films were produced on glass substrates by drop casting from a toluene solution. The morphology of the films was monitored using an optical microscope. We found out that the first peak of light absorption corresponds to the size of our QDs, and the peak of light emission occurs at a wavelength corresponding to the energy of 1.99 eV. This is the energy of exciton formation. Photoluminescence (PL) was excited by laser pulses with a duration of ~30 ps and a repetition rate of 0.5 Hz by the second harmonic (539 nm) of a $YAlO_3:Nd^{3+}$ laser with a passive mode synchronization. The time-integrated PL was collected from the excitation region on the upper surface of the film, dispersed in a polychromator and recorded with a multi-channel spectrum analyzer (CCD linear detector) synchronized with the excitation pulse. The results of the measurements performed for different values P, where P1=1 mJ/cm2, P2=3 mJ/cm2, P3=5 mJ/cm2, and P4=6 mJ/cm2 of the laser excitation intensity P are shown in Figure. It can be seen that the dependence of the PL intensity on the intensity P of the excitation pulse has a distinct soft threshold: at P>P3=5mJ/cm2 a maximum appears in the red wavelength region of the photo-luminescence spectrum. With further growth of P, its height increases rapidly, and its width decreases. This feature allows us to assume that below the specified threshold we observe a spontaneous emission of single excitons, and above the threshold - amplified spontaneous emission (ASE) associated with the inversion of populations of biexciton and exciton states. We have shown that the PL of thin QD films CdSe/CdS/CdZnS exhibits a number of features: the ASE band is considerably narrower that the spontaneous emission spectrum and the ASE signal exhibits a distinct soft threshold with the intensity of the pulse of exciting laser radiation.

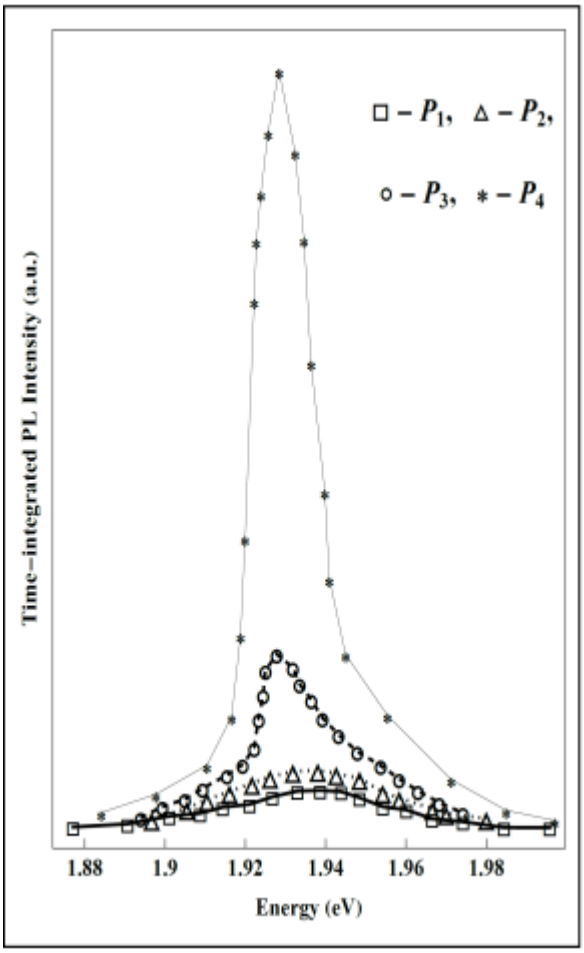

[1] V. Pavlenko, I. Dobynde, I. Beloussov, D. Ozol. Physica E: Low-dimensional Systems and Nanostructures **115** (2019) 113695.

IN-SITU FUNCTIONALITY OF SILVER OXIDE COATINGS TUNED BY PHASE CONTROL DURING PULSED LASER DEPOSITION

O. Gherasim[1,*], R. Udrea[1], V. Grumezescu[1], P. Prepelita[1], B. S. Vasile[2], A. M. Holban[3], S. Chertopalov[4], J. Lancok[4], V. Craciun[1,5], S. A. Irimiciuc[1,4,*]

[1]*National Institute for Laser, Plasma and Radiation Physics, Magurele, Romania;*

[2]*Research Center for Advanced Materials, Products and Processes, National University of Science and Technology Politehnica Bucharest, Bucharest, Romania;*

[3]*Faculty of Biology, University of Bucharest, Bucharest, Romania;*

[4]*Institute of Physics of the Czech Academy of Sciences, Prague, Czech Republic;*

[5]*Extreme Light Infrastructure – Nuclear Physics, Horia Hulubei National Institute of Physics and Nuclear Engineering, Magurele, Romania.*

[*]E-mail: oana.gherasim@inflpr.ro

The pulsed laser deposition (PLD) technique represents an attractive strategy to fabricate high-quality thin coatings for which the nanosize-governed functionality can be tuned during the PLD process by properly adjusting the deposition parameters. The multi-parametric control available within this technique and the well-known flexibility (pulse duration, wavelength, laser fluence, deposition angle, etc.) promotes the PLD method for developing bioactive nano-coatings able to modulate different opportunistic phenomena, such as the microbial contamination and colonization.

Silver (Ag)-based coatings provide a potent alternative for limiting or eliminating the microbial susceptibility of common surfaces, mostly due to Ag^+-driven impairment of microbial metabolism and cellular ultrastructure. Moreover, the intracellular damage of nano-silver-based materials can be boosted due to morphology- and structure-related characteristics.

In this study, different deposition pressures have been considered during PLD experiments performed with an ArF* (193 nm, 25 ns) laser beam to obtain Ag-based nanostructured films. The compositional (XRD, XPS) and morphological (SEM, TEM) data demonstrated the *in-situ* tailoring of as-resulted silver oxide (Ag_xO) thin films. Increasing the O_2 deposition pressure influenced the oxidation (ranging from predominantly metallic to pure oxide mixture) and morphology (nanoparticulate to cauliflower structure) of Ag_xO films. Moreover, the Ag_xO films deposited at higher O_2 pressures resulted in more effective inhibition of bacterial attachment and biofilm formation, with the most prominent antibacterial efficiency being reported against Gram-positive pathogens.

ACKNOWLEDGEMENT: This research is supported by the NATO Science for Peace and Security program through SPS G6153 Project.

POLYMER/CHALCOGENIDE SEMICONDUCTOR STRUCTURE FOR X-RAY IMAGING

A. Chirita[1,*], A. Hustuc[2], N. Nasedchina[1], S. Vatavu[1]
[1]*Physics of Semiconductors and Devices Lab, Faculty of Physics and Engineering, Moldova State University, Chisinau, Republic of Moldova;*
[2]*Alarad SRL, Chisinau, Republic of Moldova*
[*]E-mail: arcadie.chirita@usm.md

The carriers for X-ray imaging (Fig.1a) were prepared as multilayered structure: the flexible polyethylene terephthalate film substrate (1) was covered with a semitransparent chrome electrode (2), the sensitive layer (3) based on $(As_2S_3)_{0,985}Sn_{0,015}$ with a thickness of 3.5 μm (3), and the 0.7 μm thick polyepoxypropylcarbazole thermoplastic layer (4).

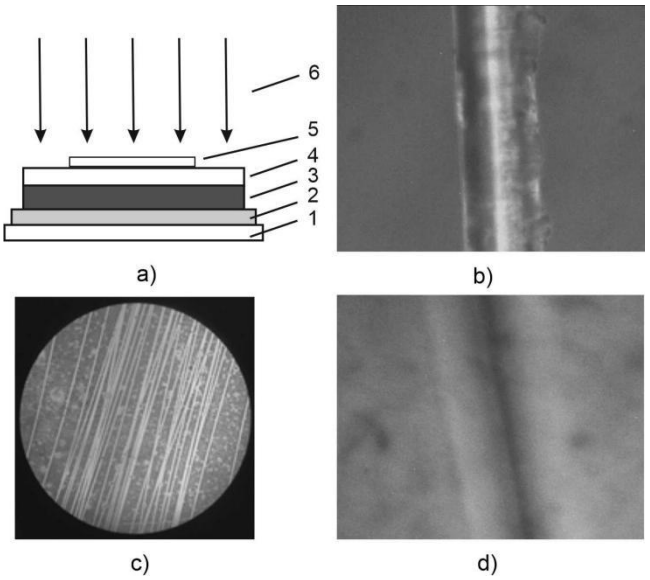

Figure 1. a) Recording process, b) Tungsten wire (magnification 80^x),
c) X-ray image of tungsten wires (magnification 10^x), d) Magnified (80^x) fragment of the wire X-ray image

A tungsten wire with a diameter of 30 μm (Fig.1b) was randomly placed on the surface of the thermoplastic layer (5, Fig.1a). The structure was placed in an X-ray chamber and irradiated with a continuous X-ray spectrum of W-tube (50 kV, 50 mA) the absorbed dose being 1.12 Gy. As the irradiation process is completed, the carrier is removed from the chamber and heated up to a viscous state of the thermoplastic layer (T = 78°C) in the dark and charged for 2.5-3.2 s by use of a high-voltage (7.8 kV) corona discharge. The surface of the thermoplastic layer is charged with positive air ions. The conductivity of the semiconductor layer in the irradiated areas is higher due to a change in specific resistance as a result of X-ray irradiation influence [1-3]. The relief-phase image is formed under the action of the Coulomb interaction of positive charges on the surface of the thermoplastic layer and negative charges in the semiconductor layer. The interaction of charges causes surface deformations of the thermoplastic layer in the irradiated areas and there is no deformation in non-irradiated areas. Fig.1c shows a magnified microscopic image of tungsten wires recorded in X-rays.

ACKNOWLEDGMENTS: This research was funded by MEC subprogram 011207 (DETCONV)

[1] A. Chirita, A. Hustuc, N. Nasedchina, S. Vatavu. *Chalcogenide Letters* **20** (2023) 803-809
[2] A. Chirita., V. Prilepov. *Chalcogenide Letters* **19** (2022) 439-545
[3] A. Chirita, D. Spoiala, S. Vatavu *Chalcogenide Letters* **19** (2022) 683-690

PHOTODETECTION DEVICES BASED ON INDIUM PHOSPHIDE HETEROJUNCTION

P.M. Chetruș, L. Gorceac*, P.I. Chetruș, P. Gaugaș, S. Vatavu
Physics of Semiconductors and Devices Lab, Faculty of Physics and Engineering,
Moldova State University, Chisinau, Republic of Moldova
*E-mail: leonid.gorceac@usm.md

Indium phosphide (InP) and its combinations with other semiconductor compounds: CdS, ZnO, ITO, TiO_2, are preferred for making devices based on the photovoltaic effect.

The results of the research on photovoltaic devices such as photovoltaic cells/modules (PVC/PVM), photodetectors (PD) on InP hetero- and homojunctions are presented in this work.

The junctions were made by using the HVPE (Hydride Vapor Phase Epitaxy) method, (n, pInP), CSS technology (nCdS), magnetron sputtering and spray pyrolysis (nZnO), electron beam evaporation (SiO_2). Electrical parameters such as charge carrier concentration n, p (cm^{-3}) and mobility μ ($cm^2 \times V^{-1}s^{-1}$)) of the component layers of the junctions were as follows: nInP:Te - $(0.9\text{-}2)\times10^{16}$, 1270-1900; pInP:Zn - $(0.5\text{-}5)\times10^{17}$, 32-97; nCdS - 10^{18}-10^{19}, 60-100; ZnO - 1.7×10^{19}, 9.9.

The studies of the load characteristics of PVC on InP hetero- and homojunctions with SiO_2 anti-reflection layer under standard conditions AM1.0 (100 $mW\times cm^{-2}$) had demonstrated that the efficiency of PVC with n^+-p^0-p^+ InP homojunction, at the moment has a value of 7.31%, of those with the simple heterojunction (HJ) nCdS-pInP - 5.5%, and of those of the n^+CdS-p^0-p^+InP type with repeatedly ingrown p^0 intermediate epitaxial layer, S_{ef} = 3 cm^2 is 12%. The efficiency of the presented PVCs differs, primarily, due to the values of the series resistances (R_s) which are respectively 7.47, 14.52 and 3.08 $\Omega\times cm^2$. For nZnO-pInP type PVC the efficiency under the same conditions is currently only 3%.

The photovoltaic module assembled out of 25 mixed-switched nCdS-pInP type photovoltaic cells, with the photoactive surface of 35 cm^2 and SiO_2 anti-reflective layer with the optimal thickness of 80 nm under AM1 conditions generates a power of 1.5 W.

In the functioning of the PD-device for the detection of optical signals, an important role belongs to the external quantum efficiency (EQE) and the absolute photosensitivity (I_{sc}/E).

As a result of the respective research, it was established that the maximum value of EQE of 75-80% in the interval wavelengths range λ=600-900 nm is characteristic for HJ type n^+CdS-p^0-p^+InP (p^0=$(3\text{-}5)\times10^{16}$ cm^{-3}) with SiO_2 antireflective layer, decreasing up to 70% for n^+-p^0-p^+InP type homojunction and 45% for nCdS-pInP type HJ. The application of the SiO_2 anti-reflective layer allows the EQE for all types of photodetectors to be increased by approximately 15%.

It was found that the maximum I_{sc}/E of (500-510) $mA\times mW^{-1}$ is characteristic for the concentration of the intermediate epitaxial layer $p^0=6.5\times10^{16}$ cm^{-3}, and its increase up to the value of 4.7×10^{17} cm^{-3} leads to the decrease of I_{sc}/E up to 430 $mA\times mW^{-1}$.

Thus, the values of PVC efficiency and EQE and I_{sc}/E for PVC and PD based on nCdS-p^0-p^+InP HJ allow their using for the realization of photovoltaic cells and photodetectors for the VIS range of wavelengths.

ACKNOWLEDGEMENTS: MEC subprogram 011207 (DETCONV)

TECHNOLOGY TUNING AND ELECTRONIC PROPERTIES OF GALLIUM SULPHIDE THIN FILMS FOR PHOTODETECTORS

D. Spoială[1*], E. Vatavu[1], L. Dmitroglo[1], Gh. Ghileţchii[1], M. Rusu[1,2], S. Vatavu[1]
[1]*Physics of Semiconductors and Devices Lab, Faculty of Physics and Engineering, Moldova State University, Chisinau, Republic of Moldova*
[2]*Department Structure and Dynamics of Energy Materials, Helmholtz-Zentrum Berlin für Materialien und Energie, Berlin, Germany*
[*]E-mail: dorin.spoiala@usm.md

Gallium Sulphide (Ga_2S_3) has tunable optoelectronic properties, making it a promising material for electromagnetic radiation detection devices. The tunning process of the technological parameters is critical whenever certain physical parameters are targeted. We apply for the deposition of Ga_2S_3 thin films the Closed Spaced Sublimation (CSS) method which allows for high temperature preparation as well as close to stoichiometry sublimation conditions. CSS deposition system uses α'-Ga_2S_3 as source material. *p*-type Si (100) wafers and quartz plates were used as substrates. The substrate temperature range varied between 450-700°C and the source temperature was 800°C. Non-contact atomic force microscopy and scanning electron microscopy was used for films' morphology analysis. The films' morphology is influenced by the substrate temperature (rms up to 510 nm). Structural characterization was performed by grazing (0.5-5.0°) incidence X-ray diffraction and X-ray reflectivity along with Rietveld analysis. A detailed analysis revealed the presence of γ and α phases (γ-Ga_2S_3 cubic a = b = c = 5.215 Å, α-Ga_2S_3 hex. ($P6_1$) a = b = 6.385 Å; c = 18.040 Å) of Ga_2S_3 for diffraction patterns taken at different substrate temperatures. It has been established that crystallites size and γ phase fraction content in film decreases along with the substrate temperature increase, while α phase increases from 65 to 100%. The films deposited on quartz glass substrates contained a phase fraction of GaS ranging between 5 and 48%.

Electronic properties of gallium sulphide were investigated by Kelvin Probe and Photoelectron Yield Spectroscopy. The type of the substrate and its temperature was found to influence the physical properties of the films. Surface photovoltage measurements showed that the layers are of *n*-type conductivity regardless of the applied substrate temperature. The ionization energy varies between 5.7-5.8 eV for films prepared on Si substrates and it is not influenced by the temperature of the substrate, while the work function reaches a maximum value of 4.7 eV for a substrate temperature of 650°C. For the latter substrate temperature, the valence band maximum relative to Fermi level E_{VBM} - E_F = 1.27 eV is calculated. The use of quartz glass substrates resulted in wider ionization energy variations between 4.8-6.1 eV.

This research presents a detailed investigation of the structure, elemental and phase compositions, morphology and electronic properties of gallium sulphide thin films as a function of substrate type and temperature.

ACKNOWLEDGEMENTS: *MEC subprogram 011207 (DETCONV)*

PRINTED FLEXIBLE ELECTRODES BASED ON 2-DIMENSIONAL MATERIALS FOR SENSING AND ENERGY STORAGE APPLICATIONS

A. Uzunoglu[1,*]

[1]*Istanbul Technical University, Faculty of Chemistry-Metallurgy, Materials and Metallurgical Engineering, Istanbul, Turkiye*

[*]E-mail: auzunoglu@itu.edu.tr

Flexible electrodes have been widely implemented in various fields, including energy generation and storage, (bio)sensing, intelligent electronics, and healthcare [1,2]. Inkjet printing is one of the most exploited methods to fabricate flexible electrodes, owing to its fast and cost-effective nature. In addition, direct printing of the functional inks on the desired substrate with high geometric precision renders this technique more appealing [3]. Developing suitable inks with high stability and printability plays a vital role in fabricating flexible electrodes using the inkjet printing process. While two-dimensional materials show great potential in inkjet printing, their hydrophilic nature poses a significant challenge to formulate inks with high stability and concentrations [4]. In addition, the weak physical bonds between the layers result in restacking of 2D materials, leading to the loss of high physical surface area and 2D structure. To circumvent the restacking issue and prepare highly concentrated stable inks, we designed 2D materials with high-defect concentrations. The change in the defect state of the 2D layers resulted in a change in the surface energy of the layers, making them more hydrophilic. Therefore, defect engineering approaches were implemented to develop novel ink formulations, including hole formation on the 2D layers, heteroatom-doping, and reducing the flake size to obtain higher dispersibility. The printability of the inks was assessed using viscosity, surface charge, and average particle size measurements. The printed electrodes were then implemented in electrochemical sensing and energy storage applications.

[1] Sarıkaya, S., et al., *Carbon* **214** (2023), 118362.

[2] Sajedi-Moghaddam, A., E. Rahmanian, N. Naseri. *ACS applied materials & interfaces* **12(31)** (2020), 34487-34504.

[3] Hussain, A., N. Abbas, A. Ali. *Chemosensors* **10(30)** (2022), 103.

[4] Dilsen, M., H.H. Ipekci, A. Uzunoglu. *Journal of Materials Research* (2023), 1-13.

WHITE-LIGHT-SENSITIVE TiO_2/CuO/Ag PHOTOELECTRODES: SYNTHESIS AND PHOTOELECTROCHEMICAL PROPERTIES

R. Levinas[1,*], V. Pakštas[1], A. Jagminienė[1], I. Stankevičienė[1], R. Viter[2], L. Tamašauskaitė-Tamašiūnaitė[1], E. Norkus[1]
[1]*Center for Physical Sciences and Technology (FTMC), Vilnius, Lithuania;*
[2]*Institute of Atomic Physics and Spectroscopy, University of Latvia, Riga, Latvia*
[*]E-mail: ramunas.levinas@ftmc.lt

Efficient utilization of sunlight is a key objective in the renewable energy field. Photoelectrochemistry (PEC) and photocatalysis are fields that are focused on materials with capability to generate electrical current when illuminated with light of a certain wavelength. These materials are used in certain photo-/electrocatalytic processes, such as water splitting to produce H_2 and O_2 or pollutant degradation in wastewater. In particular, transition metal oxides (e.g., WO_3, TiO_2) are a subject of active research due to their favorable semiconductor properties, electrochemical stability, as well as relative abundance. Here TiO_2 films were synthesized by plasma electrolytic oxidation (PEO) at 50 mA cm^{-2} in an alkaline electrolyte. This synthesis formed a film with pore openings of Ø ≤ 1 μm (Fig. 1a). Cu was electrodeposited into these pores, forming a TiO_2/Cu composite (Fig. 1b). Chemical deposition of Ag was carried out on exposed Cu sites, resulting in an Ag-decorated TiO_2/Cu electrode (Fig. 1c). The films were annealed at 300 °C to form Cu_2O and AgO phases for better PEC performance. The PEC properties were characterized in 0.1 M $KHCO_3$ to evaluate the viability of these photoelectrodes for CO_2 photoreduction. Two LEDs were used for photoexcitation: 365 nm, and white light (4100K). All films showed a response to UV light. However, it is most noteworthy that the TiO_2/Cu and TiO_2/CuAg (and their respective annealed) films showed significantly improved visible light activity in contrast to plain TiO_2 (Fig. 1d-f).

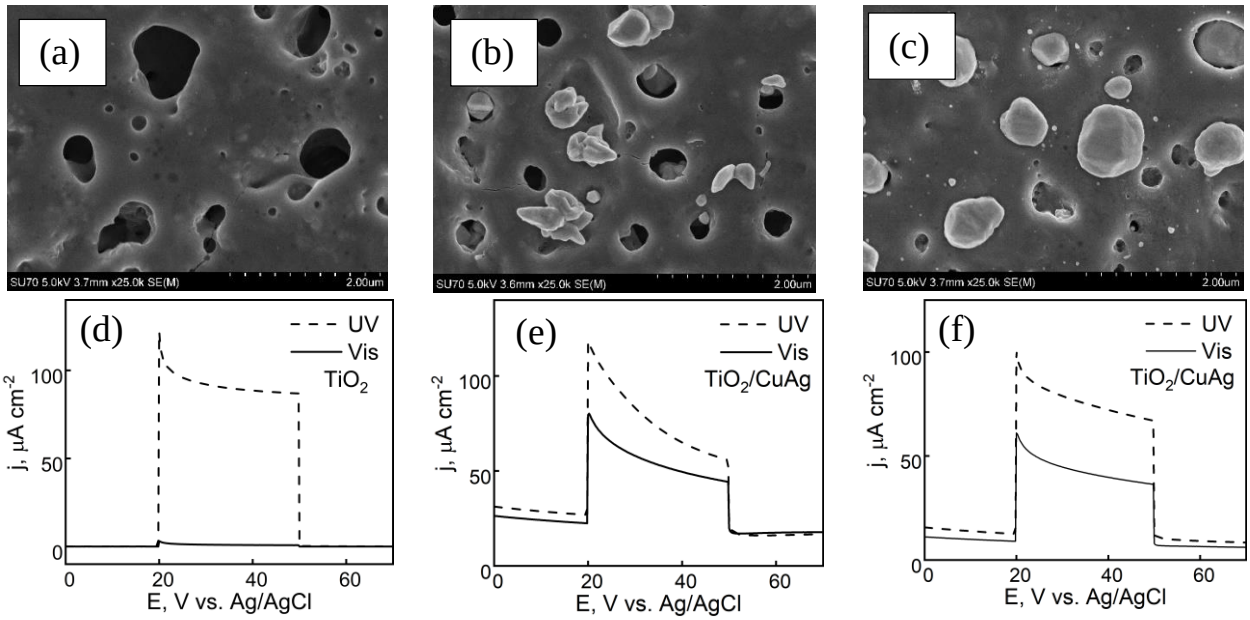

Figure 1. SEM images of TiO_2 (a), TiO_2/Cu (b), TiO_2/CuAg (c); photocurrent pulses at 0.5 V (vs. Ag/AgCl) under UV and white light of TiO_2 (d), TiO_2/Cu (e), and TiO_2/CuAg (f) films.

ACKNOWLEDGEMENTS: This research has received funding from the Research Council of Lithuania (LMTLT), agreement No. S-PD-22-5 (TICAL).

ELECTRODEPOSITED TUNGSTEN-CONTAINING HIGH-ENTROPY ALLOYS AS VERSATILE CATALYSTS OF WELL-CONTROLLED PROPERTIES

Tomasz K. Ratajczyk[1,*], Mikolaj Donten[1]
[1]*University of Warsaw, Faculty of Chemistry, Warsaw, Poland*
[*]E-mail: tk.ratajczyk@uw.edu.pl

Electrodeposition of tungsten-containing alloys has been considered an excellent strategy for obtaining catalytic or protective materials since the previous century. The prominent advantages of this technique include its relative easiness, very low costs and no excessive waste production. For the simplest systems obtainable with this method being already well-studied, namely the binary alloys of tungsten and an iron-group metal, there are visible trends towards more complex materials, ie. consisting of three or more metals. In the far-reaching cases, the deposition of high-entropy tungsten alloys is achievable as well.

The tungsten-containing materials can constitute very efficient catalysts for various processes, eg. for hydrogen or oxygen evolution (water splitting). The electrodeposited tungsten alloys themselves make very good HER catalysts [1, 2]. On the other hand, materials composed of tungsten and iron-group metal oxides make efficient light-driven catalysts for OER [3]. The latter can be also produced from the electrodeposited tungsten alloys, which is being studied in our group.

The approach to the electrodeposition of tungsten alloys has to include strategies of control of the alloy composition, especially for the multinary materials. Monitoring the metal ion levels in the plating bath facilitates obtaining a quinternary high-entropy alloy such as WFeCoNiCu of a desired qualitative composition [4]. The presentation will cover this strategy and its implications, including clarification of relations between the particular metal deposition rates in the unified plating system. It will also focus on physicochemical properties of the mentioned high-entropy alloy such as microstructure or HER performance. The results will be juxtaposed with OER performance of oxide-based catalysts obtained via the very same tungsten codeposition process.

[1] Laszczyńska, A. Mater. Chem. Phys., **314** (2024) 128876. doi:10.1016/j.matchemphys.2023.128876
[2] Vernickaite, E.; Tsyntsaru, N.; Sobczak, K.; Cesiulis, H. Electrochim. Acta **318** (2019) 597–606. doi:10.1016/j.electacta.2019.06.087
[3] Solarska, R.; Bieńkowski, K.; Królikowska, A.; Dolata, M.; Augustynski, J. Funct. Mater. Lett. **7** (2014) 1440006. doi:10.1142/S1793604714400062
[4] Ratajczyk, T.; Donten, M. Materials **17** (2024) 1513 doi:10.3390/ma17071513

THRUST MEASUREMENTS IN A ROTATING DETONATION ENGINE

A. Tcacenco[1], I. Cahanovcshi[1], I. Porumbel[2,*], T. Cuciuc[2,3], A. Bogoi[1,2], M. Gall[1,2], A. V. Cojocea[1,2], D. Asoltanei[2], G. I. Vrabie[2], C. Anton[2]
[1]*National University for Science and Technology "Politehnica", Bucharest, Romania;*
[2]*Romanian National Research & Development Institute for Gas Turbines - COMOTI, Bucharest, Romania;*
[3]*Institute of Applied Physics, Moldova State University, Chișinău, Republic of Moldova*
[*]E-mail: ionut.porumbel@comoti.ro

Rotating Detonation Engines are an innovative approach aiming to harness the enhanced energy release and cycle efficiency of detonation-based combustion [1]. Earlier studies have highlighted the immense potential of thermodynamic cycles centered around pressure gain heat addition in boosting cycle efficiency and energy release rates showing an increase in the thermodynamic cycle efficiency of up to 15 % [2]. Additional benefits encompass design simplicity and reduced weight of the combustion system, and the absence of moving parts.

The paper will focus on thrust measurements at the exhaust of a Hydrogen fueled RDC carried out in the Detonation and Rocket Engines Test Rig of the TESS facility, at COMOTI. The measurements have been carried out using an LCM Systems STA-3-100 load cell, and the pressure, temperature and mass flow rates have been measured using ALICATMQ Series flow meters. The oxidizer used was air. The design is based on the model developed at the University of Southampton [3], optimized by our team. The preliminary data is presented below, as a function of the equivalence ratio.

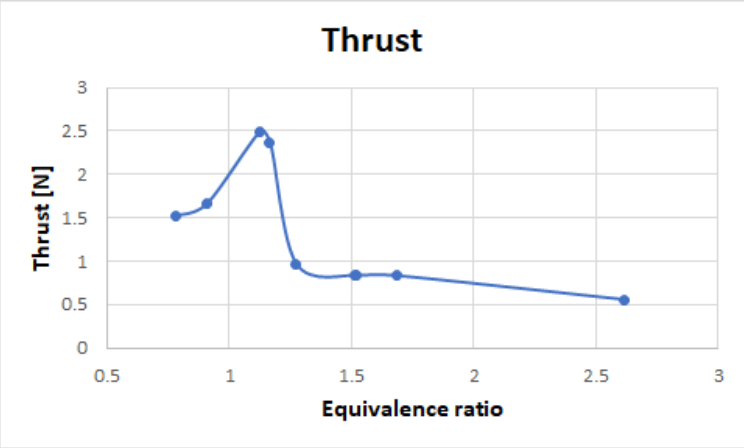

Figure 1. Combustion generated thrust in the RDC

On the average, the jet generated thrust is of about 2.51N, corresponding to an unigntied jet velocity of 55.69 m/s, at the same level as the combustion generated thrust. Even though rotating detonation waves are obtained in the ring shaped channel of the RDC, these supersonic waves propagate in the azimuthal direction in the flow channel, while the axial flow, in the direction of the thrust, remains, lacking a Laval nozzle, in the low subsonic regime, and the combustion generated thrust is low.

The combustion generated thrust reaches a maximum level around 2.5 N, peaking for an Equivalence Ratio (ER) of 1.2. A possible reason for the maximum thrust being achieved for slightly rich combustible mixtures is the imperfect mixing of the fuel and air ahead of the rotating detonation wave. For equivalence ratios above 1.3, the RDC operates in the deflagration regime, and the combustion generated thrust is even lower, below 1N.

[1] K. Kailasanath, *AIAA Journal*, **38** (9), (2000), 1698-1708.
[2] C.F. Cuciumita, T. Cuciuc, I. Porumbel, *ASME Turbo Expo*, Seoul, South Korea, 13-17 June (2016), GT2016 – 57310.
[3] H. Law, T. Baxter, C. Ryan, R. Deiterding, *AIAA Propulsion and Energy 2021 Forum*, August 9-11, (2021).

INVESTIGATION OF THE APPLICATION PROCESS OF Fe-WC COMROSIONAL GALVANIC COATINGS

D. M. Kroitoru[1], S. H. Ivashku[1,*], S. T. Sklifos[2], Z. I. Bobanova[1], S. M. Iatsko[1]
[1]*Institute of Applied Physics, Moldova State University, Chișinău, Republic of Moldova;*
[2]*SRL, AGROFERMOTECH,* Chisinau, Moldova;
[*]E-mail: sergiu.ivascu@ifa.usm.md

It is established that composite electroplating coatings (CEC) based on iron-containing microabrasive powders (e.g., Al_2O_3, SiC, B_4C) as a dispersed phase (DP) are known. At IAP Moldova State University, research is ongoing into the use of tungsten carbide (WC) in CECs, to determine certain properties, in particular wear resistance, without the need for machining of the coatings. A comparison was conducted between Fe-WC composite coatings and those of Fe-Al_2O_3, as well as those obtained through electrosparking.

The electrolyte-suspension (ES) comprised a $FeCl_2$-$4H_2O$ solution with a concentration of 500-600 g/l and microabrasive powders of WC and Al_2O_3, with particle sizes ranging from M1 to M10, at concentrations of 15, 30 and 45 g/l el. The coating was conducted in a vertical two-channel laboratory cell of elevator type, in which one channel was designated for the cathode and anode holders, while the other channel was equipped with a rotating shaft and pumping element. The CEC application was conducted using a DC source. The pH value of the electrolyte suspension (ES) was maintained within the range of 0.7 to 0.8. The wear resistance of the CEC was determined using a reciprocating machine that was adapted to a computer.

Tungsten carbide is incorporated into electrodes (WC8 and T15K6), which are employed in electrospark alloying (ESA) to modify working surfaces. The comparison of test results demonstrated that samples with a Fe-WC CEC exhibited significantly less wear than samples modified with VK8 and T15K6 electrodes. Conversely, the counterbodies of the latter exhibited two and three times more wear than the counterbodies of the former, respectively. Concurrently, the coefficient of friction of Fe-WC coatings in conjunction with Steel 45 is 0.24, whereas coatings obtained by ESA have a coefficient of friction of 0.55.

The results of the conducted studies demonstrate that:

- The nature of the particles of the dispersed phase WC included in the composition affects the size of microroughnesses, with Ra values for coatings containing WC and Al_2O_3 exhibiting significant differences. The roughness index Ra for Fe-WC CEC is an order of magnitude higher than for Fe-Al_2O_3 CEC, which is a noteworthy phenomenon;
- The concentration of tungsten carbide in the CEC coatings affects the microhardness. As the concentration of tungsten carbide increases, the microhardness also increases. In fact, the microhardness increases by 2GPa when the concentration is increased to 42.6% compared to "pure" iron.

The following conclusions may be drawn:

1. The technological process of iron composition deposition provides the opportunity to deposit thin films on Fe-WC parts and to operate them without mechanical treatment.

2. Comparative tests of Fe-WC composite electroplated coatings and coatings obtained by the ESA method demonstrated comparable wear, and in general, friction pairs with Fe-WC coatings exhibited greater efficacy.

ACKNOWLEDGMENTS: This work was supported by the NARD, Moldova within the project "Manufacturing of new Micro- and Nanostructuring Materials by Physic Chemical Methods and the Elaboration on Their Base" (No. 20.8009.5007) and partially from the H2020-MSCA-RISE project Smartelectrodes (No. 778357).

PECULIARITIES OF ELECTRODEPOSITION OF COBALT-TUNGSTEN ALLOYS FROM GLUCONATE ELECTROLYTES

J.I. Bobanova[1], S.P. Yushchenko[1], S.H. Ivashku[1,*], D.M. Croitoru[1], P.G. Globa[2]
[1]*Institute of Applied Physics, Moldova State University, Chișinău, Republic of Moldova;*
[2] *"Nicolae Testemitanu" State University of Medicine and Pharmacy, Chișinău, Republic of Moldova*
[*]E-mail: sergiu.ivascu@ifa.usm.md

Tungsten alloys obtained by induced co-deposition with the iron triad group metals from complex electrolytes have been shown to exhibit enhanced physical and chemical characteristics, thereby rendering them suitable for utilisation as materials in the field of astronautics, particularly in the context of obtaining modulated compositions. In terms of their functional properties, these alloys may offer an alternative to Cr(VI)-based chromium coatings, which are currently used in industry.

Operating experience has demonstrated that alloys obtained from complex electrolytes exhibit low cathodic current efficiency (CE), deposition rate, and are distinguished by a certain degree of instability in their alloy and electrolyte composition, which collectively diminish their performance and operability. The use of a low concentration gluconate electrolyte containing 0.05 M sodium tungstate resulted in the formation of high-quality coatings with a current density of 100 A/m², exhibiting a current efficiency of only 80%.

It was observed that increasing the concentration of each electrolyte component did not result in an improvement in the current efficiency or deposition rate. The current efficiency of the alloy was determined gravimetrically following electrolysis. The theoretical calculation was conducted in accordance with Faraday's law, taking into account the electrochemical coefficient of the alloy, which was found to be equal to 0.31 mg/C. The formation of the coating's roughness and its ability to level, designated as P, was evaluated on samples with a gentle sinusoidal profile, based on the results of profilographic measurements.

In order to enhance the efficiency and functionality of the process and facilitate its implementation in industrial settings, we propose the utilisation of gluconate electrolytes with a high concentration of components and organic ligands at varying molar ratios. The influence of cathodic current density at varying molar ratios on the current efficiency, tungsten content in the alloy, and microdistribution of the coating on the surface was investigated across a wide range of concentrations.

It was discovered that cobalt-tungsten alloy deposits with maximum current efficiency values of 95 -98% are formed in the electrolyte at cobalt and tungsten concentrations of 0.25M and at molar ratios S_{lig}/S_{comp} in the range (5:1). This provides precipitates with high current efficiency and stable composition during long-term use. This behaviour may be attributed to the influence of varying component/ligand ratios on ionic equilibrium and the composition of adsorbed intermediates formed on the surface.

The calculation of the levelling ability of complex electrolytes devoid of any special additives revealed that P = 0, thereby indicating that complex electrolytes are devoid of any levelling ability. Irrespective of the modes and composition of complex electrolytes, levelling is observed solely in coatings with a thickness of 80 – 100 microns. The concentration of metal and ligand salts up to 0.25M has been demonstrated to enhance the micro-distribution of the coating on the surface (P = 0.15).

ACKNOWLEDGMENTS: This work was supported by the NARD, Moldova within the project "Manufacturing of new Micro- and Nanostructuring Materials by Physic Chemical Methods and the Elaboration on Their Base" (No. 20.8009.5007) and partially from the H2020-MSCA-RISE project Smartelectrodes (No. 778357).

IMPROVING THE PERFORMANCE OF EVAPORATION-CONDENSATION SYSTEMS IN AN ELECTRIC FIELD

O.V. Motorin*, M.K. Bologa, I.V. Podlesny
Institute of Applied Physics, Moldova State University, Chișinău, Republic of Moldova
*E-mail: motorin@yahoo.com

Pulsating heat pipe (PHP) is a type of evaporative-condensing system and can be used for cooling various devices, thermal energy storage, low-temperature heat recovery and in renewable energy sources [1]. The efficiency of PHP operation increases if you organize unidirectional circulation of the vapor-liquid mixture, which is usually achieved by including passive control devices in the circuit. The study of the active method of organizing circulation using an EHD pump built into the circuit and its effect on the hydrodynamics of the movement of the vapor-liquid mixture at various orientations in space was considered in [2, 3]. A cone-ring type pump with a maximum static pressure of 1880 Pa at 16 kV was used. In a single-turn PHP, when the EHD pump is turned on and the voltage on it increases, an increase in the period of flow pulsations is observed with a simultaneous decrease in the size of the bubbles. Starting from 10-12 kV, the slug mode of motion of the vapor-liquid mixture turns into a bubble mode, while at the same time the reciprocating motion of the mixture turns into a purely circulation motion. The dependences of the mixture circulation speed on the current strength and supplied thermal power, the local heat transfer coefficient of the internal surface of the heater on the voltage on the EHD pump were obtained for various spatial arrangements of PHP elements (heater at the bottom, heater at the top, all elements are located horizontally).

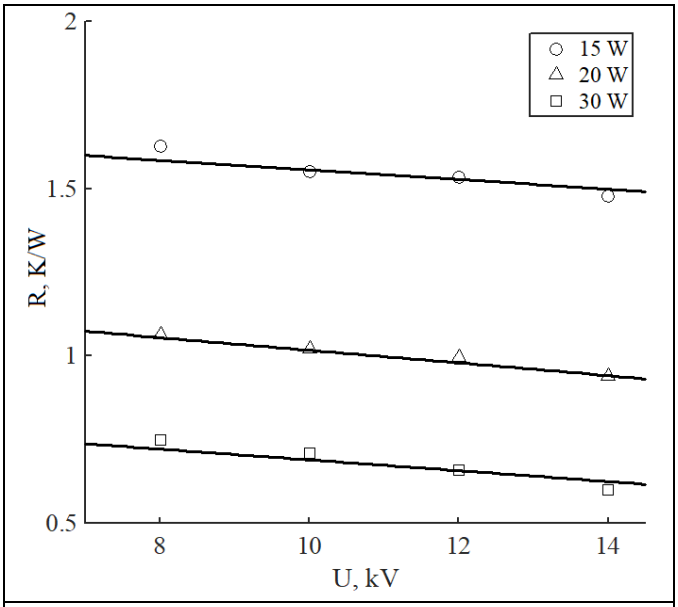

Figure 1. Dependence of thermal resistance on the voltage on the EHD pump.
PHP with 5 turns, heat carrier is n-hexane .

The study of the influence of EHD pumping on thermal resistance, temperatures in the evaporation and condensation zone at various supplied thermal powers was carried out on a three- and five-turn PHP. Fig. 1 shows the dependence of thermal resistance on voltage on the EHD pump. A decrease in thermal resistance with an increase in supplied thermal power is a consequence of an increase in the circulation rate of the vapor-liquid mixture. A generalization of the obtained results has been carried out, which can serve for the design and creation of EHD cooling devices.

The following conclusions can be drawn:

Unidirectional circulation of the vapor-liquid mixture in the PHP improves its heat transfer characteristics; EHD pumping promotes earlier and more reliable start of PHP; the maximum decrease in the evaporator temperature is about 4 °C, thus it becomes possible to regulate the temperature of the evaporation zone using EHD pumping within certain limits.

ACKNOWLEDGEMENTS: The research was carried out thanks to funding from the Ministry of Education and Research of the Republic of Moldova, subprogram 011203.

[1] X. Han, X. Wang, H. Zheng, X. Xu, G. Chen, *Renewable and Sustainable Energy Reviews*, **59** (2016) 692-709
[2] M. K. Bologa, F. P. Grosu, I. V. Kozhevnikov, A. A. Polikarpov, and O. V. Motorin, *Surface Engineering and Applied Electrochemistry*, **50** (2014) 238–245.
[3] M.K. Bologa, F.P. Grosu, I.V. Kozhevnikov, O.V. Motorin, A.A Polikarpov. *IOP Conf. Series: Journal of Physics: Conference Series* **891** (2017) 012012

RECOVERY OF CASEINS AT THE ELECTROACTIVATION OF WHEY

I.V. Paladii[1,*], E.G. Vrabie[1], M.K. Bologa[1], V.G Vrabie[2], T.G. Stepurina[1],
A.A. Policarpov[1], C.Gh. Sprincean[1],
[1]*Institute of Applied Physics, Moldova State University, Chișinău, Republic of Moldova;*
[2]*Moldova State University, Chișinău, Republic of Moldova*
[*]E-mail: irina.paladii@ifa.usm.md

The recovery of whey proteins in protein mineral concentrates (PMCs) depends on the regimes of electroactivation of whey, in particular, the density of the electric current and the specific energy consumption applied per unit volume [1]. The extraction of caseins in PMC is due to the presence of colloidal calcium phosphate, which forms aggregates with caseinate in the form of calcium phosphate-caseinate. Part of the calcium phosphate can be found in the form of a pure solution, and most of it - in the form of a colloidal solution. At the increase of active acidity upon electroactivation, calcium phosphate passes from the colloidal state to the ion-dispersed one, and during ionic flotation it separates in the form of calcium phosphate, or hydro- or dihydrocalcium phosphate, which is "captured" in the PMC at a mechanical level induced by ionic flotation. The same mechanism occurs in the formation of calcium phosphate-caseinate at the interaction of calcium ions with the carboxyl and serine phosphate groups of casein. In this case, calcium reacts with two groups -COOH and -OH- located at small distances, forming intermolecular bridges of calcium: -R-Ca-R-. At the formation of structural bridges (between two phosphoserine radicals) can also participate hydrofosfates -R-Ca-HPO4-Ca-R- or dihydrophosphates -R-Ca-HPO4-Ca-HPO4-Ca-R-. Whey processing involves separation from casein powder, but this procedure still does not allow the complete separation of caseins from the initial whey (IW).

Electrophoretic investigation (SDS-PAGE 15%) of the protein fractions of different types of whey with different protein content (supplied by the "JLC" Joint Stock Company, Chisinau, RM): (1) - whey obtained after the manufacture of granulated cheese "Grăuncior" ; (2) - whey obtained after the manufacture of cow's cheese, with a fat content of 5%; (3) - whey obtained after the manufacture of the cheese product, with a fat content of 18% identifies the presence of CSN. The content of caseins (CSN) is about 18% for IW (1), 12% - IW (2) and 10% for IW (3). The electroactivation of different types of whey in different electrolyzers allows the fractionation of whey proteins and their recovery in PMC with predetermined protein content depending on the processing regimes and the constructive and technical parameters of the electrolyzers [1].

CSNs are extracted in higher amounts in the EDP-2 electrolyser with a parallelepiped casing when processing whey (1) and varies from 16 -21% at current density j=10mA/cm^2 increasing slightly to 26% at j=20mA/cm^2; for whey (2) CSN are extracted unevenly at both electric current densities and vary 10-21%, and for whey (3) CSN are intensively extracted at j=10mA/cm^2, constituting 22-27% and are extracted in insignificant amounts at at j=20mA/cm^2 – 7-9%. At the processing of different types of whey in the EDC-3 electrolyzer with a semi-cylindrical casing, CSN is insignificantly extracted during processing, for whey (1) at j=10 -20 mA/cm^2 and constitutes 3-5% in the first 10 min of treatment. Their extraction is not registred during further processing. For whey (2) CSN extraction constitutes 2-10% at j=10mA/cm^2 and 2-8% at j=20mA/cm^2. The uneven and reduced extraction in the semi-cylindrical casing electrolyser confirms the involvement of CSNs in the formation of high molecular weight proteins (of about 150-240 kDa) that could not be identified by 15% SDS-PAGE electrophoretic analysis. In IW, 2-3 fractions of CSN –α-CSN, β CSN and κ-CSN with the respective molecular mass of 37, 33 and 46 kDa were identified, which contribute to the separation of PMCs from different types of whey in different electrolyzers. The recovery of protein fractions occurs simultaneously with the isomerization of lactose into lactulose.

ACKNOWLEDGMENTS: The participation was financed within the framework of the subproject: 011203 ”Research and development of the advantages of electroconvection, electroactivation and magnetic fluidization at enhancing of heat transfer and processing”

[1] E. G. Vrabie, M. K. Bologa, I. V. Paladii, T. G. Stepurina, et al. *Surface Engineering and Applied Electrochemistry*, **55**, (2019), 197-209.

SUPPRESSION OF CORROSION OF STEELS IN WATER BY MIXTURES OF FURACILIN WITH ORGANIC SUBSTANCES

V.V. Parshutin[1], A.M. Paramonov[1], A.V. Koval'[1,*], V.V. Gorinchoy[2], V.I. Lozan[2]
[1]*Institute of Applied Physics, Moldova State University, Chișinău, Republic of Moldova;*
[2]*Institute of Chemistry, Moldova State University, Chișinău, Republic of Moldova*
[*]E-mail: sasha.covali@mail.ru

It is known, that natural or process water containing activating chloride and sulfate ions is a rather aggressive medium in which corrosion of steel flows at a high rate. The presence of activating chlorine ions in the water leads to the formation of pittings on the walls of the pipes, which in some cases can be through, which leads to an emergency. Moreover, ionized iron, moving into water, accumulates there, degrading its quality. Corrosion control in closed systems of steel pipelines (for example, heat supply systems in which water is a carrier) is a difficult task, because the inhibitor must maintain a given level of corrosion suppression for a long time. The main requirements for the inhibitor are maximum possible corrosion suppression, ability to maintain its properties for a long time, low cost, small concentrations of components, environmental friendliness.

The aim of researches was development of ecologically safe and inexpensive corrosion inhibitors, which will be able to provide effective corrosion suppression in steel pipeline systems containing water. Furacilin (nitrofural) $C_6H_6N_4O_4$ in an amount of 0.05-0.2 was selected as the base. His choice is due to the fact, that it is widely used as an antiseptic and is completely safe. However, the maximum values at a concentration of 0.2 g/l and a test time of 240 hours, inhibition coefficient do not exceed 5.2. This concentration is the limit and is due to its solubility in water. At the same time, in most cases, there is an increase its effect on the corrosion process with an increase in test time.

In the search for a component, that allows to enhance the effect of furacilin, the choice fell on urea - $CO(NH_2)_2$. Studies have shown, that at a concentration of 5 g/l, urea not only does not protect steel in water, but even leads to increased corrosion, especially with increased test time. However, with an increase in its concentration to 10-25 g/l, the corrosion of steel decreases to 3.8 times at 20 g/l and 240 hours of testing. Moreover, the inhibition coefficient increases as the test time increases. It makes no sense to use urea at concentrations above 25 g/l, since its effect on corrosion of steel in water is reduced. The use of a mixture of urea and furacilin as an inhibitor has a positive effect on corrosion suppression. Its introduction into the solution in an amount of 5-25 g/l (optimal concentration - 20 g/l) allowed to reduce corrosion losses by 20 times at 240 hours. Another inhibitor is furacilin and heteronuclear salicylate complex $[FeSr_2(SalH)_2(Sal)_2(NO_3)(DMA)_4]$. The addition of only 0.05-0.75 g/l of the complex reduces the corrosion rate by 11.1 times already at 24 hours of testing. A coating film comprising hardly soluble complexes formed by the interaction of ionized iron with inhibitor decomposition products and enhancing the protective properties of the film provides corrosion protection.

An inhibitor based on a mixture of an aminoguanizon of pyruvic acid (0.05-1.5 g/l) and furacilin showed good results. At their concentrations of 1.5 g/l and 0.2 g/l, respectively, as the test time increases, the corrosion rate begins to decrease significantly and at 240 hours the corrosion process slows down by 16.67 times.

The use of a mixture of these substances positively affects the suppression of the corrosion process. On the one hand, the degree of suppression of the corrosion process increases, and on the other hand, the inhibition coefficient in all cases increases significantly with the increase in test time due to the synergistic effect of the interaction of the mixture components. This is probably due to the formation of denser protective layers on the corrosive surface of the steel.

PROTECTION OF STEELS FROM CORROSION BY EXTRACTS OF A PLANT ORIGIN.

V.V. Parshutin, A.M. Paramonov, A.V. Koval'*, T.D. Kubritskaya
Institute of Applied Physics, Moldova State University, Chișinău, Republic of Moldova
*E-mail: sasha.covali@mail.ru

In recent years, increasing attention has been paid to the selection of non-toxic or low-toxic inhibitors to suppress the corrosion process in water and aqueous media. Often the use of inhibitors is the most advantageous method of protecting metals in liquid media, including those used for electrochemical formation.

Today, the most promising is the development of environmentally friendly and cheap inhibitors or inhibitory compositions based on vegetable products with high efficiency. The availability of plant raw materials and the ease of processing made it possible to hope for the prospect of this area of research.

Initially, owing to the availability, interest was attracted by walnut. Inhibitor of corrosion of steels in water on the basis of water extract of the dried-up leaves of walnut, obtained by extraction of dry leaves in water in a mass ratio of (2-4):10 at a temperature of 70-100°C for 1-3 hours, with subsequent filtration, entered on corrosion medium in number of 10-30 ml per water liter slows down corrosion rate by 5.6 times.

The use of aqueous extracts of dried shrimp grass of amaranth *Amaranthus retroflexus* L. (10-30 ml/l) or birch leaves (10-150 ml/l) allowed to reduce corrosion losses by 7-8.4 times. An important factor is that these inhibitors suppress corrosion quite evenly over a wide range of 24-168 hours. This is an undeniable advantage when it comes to closed extended steel pipeline systems (e.g. heat supply), because it facilitates control and maintenance of corrosion medium parameters within the necessary range.

The developed chestnut-based inhibitor, at a concentration of 50-150 ml/l, provides a reduction in the corrosion rate by up to 6.4 times. True, the peak of its effectiveness is in a small range of 72-120 hours and then corrosion increases sharply.

Studies have shown, that the addition of additional ingredients makes it possible to significantly improve the characteristics of the inhibitor. The use of a mixture of tannin (1-10 g/l) and extracts from dry walnut leaves at a weight ratio of solid substance: liquid 2÷4:10 a inhibition coefficient reaches a value of 12.35.

Mixture of succinic acid dihydrazide (0.1-0.75 g/l) with aqueous extract of dried walnut leaves (10-30 ml/l) allows to reduce corrosion losses of steels in natural and process waters used as heat carrier in closed systems of steel pipelines more than 25 times. The use of mixtures of potassium permanganate (0.5-1.5 g/l) and aqueous walnut leaf extracts (10-30 ml/l) or aqueous extract of greater celandine *Chelidonium majus* (10-40 ml/l), or amaranth *Amaranthus retroflexus* L. (10-30 ml/l) leads to decrease in corrosion losses to 10.8-35 times.

Utilization of the mixture not only makes it possible to significantly reduce corrosion losses as a result of the synergistic effect of the interaction of the inhibitor components. It is important that the steel is uniformly protected against corrosion at different test times and that the inhibition coefficient is not allowed to decrease with increasing test duration. Up to 168 or more hours of testing, a steady reduction in corrosion rate was observed, as opposed to single component inhibitors, in which an increase in corrosion rate was observed after 168 hours.

HIGH-FREQUENCY ELECTROSPARK ALLOYING - AS A WAY TO INCREASE THE PHYSICAL AND CHEMICAL PROPERTIES OF METAL SURFACES.

A.V. Koval'
Institute of Applied Physics, Moldova State University, Chișinău, Republic of Moldova
*E-mail: sasha.covali@mail.ru

Parts of modern engines, machines and mechanisms should ensure their long-term and uninterrupted operation. This is achieved not only by making parts from materials with high physical and chemical properties, but also by various methods of modifying working surfaces.

Electrospark alloying (ESA) method not only restores working surfaces, but also modifies them. ESA allows: to increase hardness, increase wear resistance and corrosion resistance. At the same time, the aspiration to increase the thickness of the resulting layer by increasing the energy in the pulse reduces the corrosion properties of the coating. In addition, the aspiration to obtain thick layers working with high energies leads to overheating of the substrate and reduces other positive aspects of the ESA. It has been found, that the frequency, duty cycle and shape of the pulses have a significant effect on the formation of the coating. Energy accumulation is observed when pulse frequency increases - pulse frequency (or their grouping) and pause between them sets heat accumulation. Too much energy leads not only to greater mass transfer, but also to porosity and cracks. Therefore, energy should be reduced as the pulse frequency increases. During of researches it is noted, that when using a vibration system to accurately calculate the energy going to the ESA, it is necessary that the frequency of pulses coincide with the frequency of vibration of the electrode.

Since the 80s, a manual high-frequency vibrator has been patented, allowing operation at a frequency of up to 2000 Hz. Operation at high frequencies significantly improves the quality characteristics of the obtained coatings due to the effect of heat accumulation in the treatment zone. The use of significantly smaller working capacities than conventional ESA (8-50 μF instead of 200-1000 μF) makes the heat storage process smoother, which dramatically reduces porosity and cracking. This results in a significant increase in corrosion resistance.

The studies revealed features of electrochemical and corrosive behavior of alloyed steel surfaces in acidic, neutral and alkaline media. Various coatings were applied: titanium, nickel, titanium-nickel. The treatment was carried out on installation for high frequency alloying.

Treatment of steel with VK8 (tungsten carbide and cobalt) and titanium with nickel reduces corrosion currents by 2-4.5 times, but alloys of VK-8 and TNM-20 are the most preferred from the point of view of reducing corrosion losses. This result is achieved due not only to putting of corrosion-resistant materials, but also to production of corrosion-resistant iron compounds due to change of energy parameters of spark gap.

Coatings applied by hard-alloy electrodes at high-frequency ESA have not only increased hardness, low roughness, but also high corrosion resistance, especially in water and salt solution.

HETERONUCLEAR SALICYLATE COMPLEX - AS A CORROSION INHIBITOR OF STEEL ST. 3 IN WATER

V.V. Parshutin[1], A.V. Koval'[1,*], V.V. Gorinchoy[2], V.I. Lozan[2]
[1]*Institute of Applied Physics, Moldova State University, Chișinău, Republic of Moldova;*
[2]*Institute of Chemistry, Moldova State University, Chișinău, Republic of Moldova*
[*]E-mail: sasha.covali@mail.ru

Salicylic acid is widely used in medical practice, in analytical and pharmaceutical chemistry, in the synthesis of dyes and various salicylates. It is a dibasic acid. In acidic and neutral solutions it is present as ion $C_6H_4OHCOO^-$ = $SalH^-$ and as undissociated acid $C_6H_4OHCOOH$=H_2Sal. It should be noted, that both salicylic acid itself and its coordination compounds with different metals have found practical applications. Salicylic acid products have long been used as corrosion inhibitors in various media. Thus, salicylic anhydride is HOC_6H_4CHO used to protect copper in solutions of alkali and potassium persulfate. But this inhibitor does not protect the steel surface in water. It is known to use *o*-hydroxybenzoic (salicylic) acid as a corrosion inhibitor of iron and carbon steel in sulfuric acid. However, for example, in the case of corrosion of carbon steel in 15% acid, high concentrations of inhibitor (not less than 50 g/l) are required to achieve a degree of protection above - 66.5%.

Studies were conducted on the effect on the corrosion of St.3 steel in water of the heteronuclear salicylate complex $\{[FeSr_2(SalH)_2(Sal)_2(NO_3)(DMA)_4]\}_n$, where DMA is dimethylacetamide C_4H_9NO, SalH - $C_6H_4OHCOO^-$, Sal - $C_6H_4OCOO^{2-}$. The corrosive medium was Chisinau tap water, in terms of chemical composition of medium or moderate rigidity. Its chemical composition corresponded, mg/l: Ca^{2+} - 42,5, Mg^{2+} - 19,5, HCO_3^- - 97,6, SO_4^{2-} - 203,7, Cl^- - 56,7, with a total salt content of 0.451 g/l. The pH varied between 7.2 and 7.6 and the total stiffness was 5.22 mmol/l.

The most significant effect of inhibitor concentration is observed at 8-72 hours of testing. The independence of the corrosion rate from the holding time is established using the inhibitor after 48 hours, while in water without the inhibitor after 120 hours. It should be noted, that the most uniform reduction in the corrosion rate depending on testing time is observed at an inhibitor concentration of 0.1 g/l. The greatest effect is achieved by using an inhibitor containing 0.5-0.75 g/l of heteronuclear salicylate complex. In this range, at 24 and 72 hours of testing, the corrosion loss is reduced by 12 and 11 times, respectively.

In addition, studies have shown:

1. By IR spectroscopy, X-ray phase analysis and chemical composition analysis, it has been shown, that when steel is corroded in water in the presence of an inhibitor, an oxide-hydroxide coating film is formed on the corrosive surface, which includes hardly soluble complexes formed as a result of the interaction of ionized iron with the decomposition products of the inhibitor and enhancing the protective properties of the film.

2. From these IR spectroscopy of corroded samples it can be stated, that during corrosion on the steel surface the formed layers consist of amorphous oxyhydroxides Fe^{3+}: α-FeO(OH) and/or γ-FeO(OH) and $Fe(OH)_3$. The Mössbauer data, as well as the shape of the Mössbauer spectra of corrosion products are typical for high-spin iron (III) compounds (S = 5/2). Increase of δ_{Fe^+} parameters values with a decrease in sample temperature from 300 K to 80 K is due to the Doppler effect of the second degree.

INVESTIGATION OF CORROSION PROPERTIES OF Ni-Re ALLOYS AND THEIR COMPONENTS

V.V. Parshutin, A.M. Paramonov, A.V. Koval'*
Institute of Applied Physics, Moldova State University, Chișinău, Republic of Moldova
*E-mail: sasha.covali@mail.ru

In the chemical and electrochemical industries, there is an increasing need for cast materials having corrosion resistance in a number of aggressive mediums combined with high strength. Double, triple and with a large number of components, Ni-Re system alloys have high heat, vibration and form stability, combined with processability. Nickel alloying with rhenium leads to sharp hardening of solid solution both in deformed and annealed states and makes it possible to manufacture semi-finished products from these alloys in the form of bars, wire, plates, tape, foil.

Studies of anode and corrosion behavior of both deformed and annealed Ni-Re alloys and their components in various electrolytes and aggressive media were carried out.

Studies have shown, that the corrosion rate of nickel and rhenium is very small in sulfuric, phosphoric and hydrochloric acids (nickel in sulfuric and phosphoric is generally zero), in very significant in nitric acid. Nickel and rhenium corrode slightly in water, NaCl and NaOH solutions.

Alloying significantly affects the corrosion and electrochemical behavior of alloys. In phosphoric acid, Ni-Re alloys, both deformed and annealed, are pasted and not corroded (like nickel) regardless of their rhenium content. In sulfuric acid, nickel alloying with rhenium reduces corrosion resistance compared to both alloy components, and as the rhenium content of the alloy increases, the corrosion rate of the alloy increases. In hydrochloric acid, alloys corrode more slowly than pure nickel, especially it is noticeable as the concentration of the alloying component increases.

In nitric acid, corrosion of alloys is high but significantly less than pure metals. At a rhenium content of 20%, the corrosion rate increases dramatically than at a content of 5 and 10%.

In water, the corrosion rate of all metals is the lowest. At the same time, it is interesting to note, that the more rhenium in the alloy, the less it corrodes in all media. It should be noted, that in all cases the corrosion rate of deformed metals is higher than that of annealed metals.

It has been proven, that the first peak on the potentiodynamic curves of Ni-Re alloys in sulfuric acid is due to the dissolution of nickel from the alloy, and the current therein is less the higher the rhenium content of the alloy. Passivation takes place by forming a film containing NiO oxide partially oxidizing to Ni_3O_4 and a small amount of $Ni(OH)_2$. In the area of transpassive dissolution, there is a re-birth of the film, a transition of nickel into a solution in the form of Ni^{2+} and dissolution of rhenium to form perrenate and simultaneous release of oxygen.

Deformed metal samples corrode significantly more than annealed in all media.

CORROSION PROPERTIES OF NI-RE ALLOYS DOPED WITH ZIRCONIUM, HAFNIUM, TUNGSTEN AND PALLADIUM

V.V. Parshutin, A.M. Paramonov, A.V. Koval'*
Institute of Applied Physics, Moldova State University, Chișinău, Republic of Moldova
*E-mail: sasha.covali@mail.ru

In the chemical and electrochemical industry, there is a need for cast materials with a complex of properties: high corrosion resistance in aggressive media with sufficient strength and form resistance at room and elevated temperatures, ensuring the possibility of making semi-finished products from this material in the form of bars, wire, tape, foil. Rhenium is more efficient than tungsten, molybdenum and other alloying elements, increases the strength of single crystal heat-resistant nickel alloys.

Corrosion and electrochemical behavior, physical and mechanical properties of Ni-Re-based alloys doped with zirconium, palladium, tungsten and hafnium, and the process of high-speed anode dissolution of these alloys were investigated.

Corrosion of all tested metals and alloys is uniform, local destruction (ulcers, pittings) is not detected, there is also no intergranular corrosion. Minimal corrosion of metals is observed in non-oxidizing acids (H_2SO_4, H_3PO_4 and HCl), while in oxidizing acid (HNO_3) and its mixture with hydrochloric acid the corrosion rate increases many times. All the alloys we have studied contain 5 to 20 wt% Re in their composition and fall into the area of solid solutions. It can be assumed in advance that selective dissolution will have a significant effect on the corrosion rate of the alloys, since the second phase is absent and the system is homogeneous. The corrosion rate of alloys may vary due to enrichment as a result of surface corrosion by a more thermodynamic stable element. Such a component is rhenium.

Alloying Ni-Re alloys with zirconium increases their resistance in all acids, which is especially noticeable in concentrated nitric acid and aqua-regia, in which nickel is very non-resistant. The corrosion rate of alloys in neutral and alkali solutions is much lower than observed in acids. Alloying alloys with hafnium, an analogue of zirconium, leads to similar results even if tungsten is present in the alloys. Additional introduction of palladium into the triple alloy Ni-Re-Zr has little effect on the strength characteristics of the alloy, but increases its corrosion resistance in 48% sulfuric acid, concentrated phosphoric and hydrochloric acids, practically without increasing it in concentrated nitric acid and aqua-regia.

X-ray phase analysis has found that the corrosion of Ni-Re alloys in concentrated HCl, HNO_3 and aqua-regia occurs with selective dissolution of nickel, especially in the latter. Amorphous phases appear in the surface layer, as well as hydroxyl chloride $Ni_2Cl(OH)_3$, hydroxide hydrate $3Ni(OH)_2 \cdot 2H_2O$, hydroxide $Ni(OH)_2$ or Ni_2O_3 oxide. In the surface layer, the presence of chlorine 0.25 ± 0.1 and 2.3 ± 0.2 wt% was recorded when etched in hydrochloric acid and aqua-regia, respectively. It has been observed, that annealing deformed alloys results in slowing their dissolution in 48% H_2SO_4 and 20% NaCl.

It has been found, that alloying Ni-Re alloys with zirconium and palladium without changing the dissolution pattern, shifts the active and transpassive dissolution region towards more positive potentials and reduces limit current values.

CAVITATION EXTRACTION OF BIOLOGICALLY ACTIVE SUBSTANCES FROM PLANT RAW MATERIALS FOR PHARMACEUTICALS AND AGRICULTURE

T. D. Kubritskaya, M. K. Bologa, G. K. Balan, T. D. Shemyakova*
Institute of Applied Physics, Moldova State University, Chișinău, Republic of Moldova
*E-mail: shemyakova@yahoo.com

During industrial processing of plant raw materials for the production of fruit and vegetable preserves, tomato paste, and wine, a large amount of solid waste is generated, which contains many useful components. It is recommended to consider such waste as raw materials for processing in order to extract various biologically active substances (BAS) with their subsequent use as food ingredients or pharmacological preparations.

In this work, the effect of ultrasound (US) cavitation action on the process of extraction of biologically active substances (BAS): tomatoside from tomato seeds, capsicoside from pepper seeds, escin from horse chestnut *Aesculus hippocastanum* L. seeds was studied. Tomatoside and capsicoside belong to the group of steroid glycosides (SG). Tomatoside exhibits antiviral action, which exceeds the effectiveness of interferon, the drug "Pacovirin" is proposed based on it. A number of formulations based on SG - moldstim (capsicoside extracted from pepper *Capsicum annuum* L. seeds) and ecostim (tomatoside extracted from tomato *Lycopersicon esculentum* Mill. seeds) - are proposed for use as plant growth bioregulators. Escin (a natural mixture of triterpene saponins) is effectively used in the treatment of chronic venous insufficiency (varicose veins), postoperative edema, exhibits anti-inflammatory and venotonic action, exerts a cytotoxic effect on tumor cells.

The technological scheme for obtaining BAS includes: (1) seed treatment using ultrasonic cavitation and traditional technology, (2) seed extraction with a water-alcohol solution to isolate biologically active substances, (3) concentration of extracts using vacuum, (4) multi-stage purification to isolate the final product, (5) physicochemical study of the obtained product using IR, UV spectroscopy and thin-layer chromatography.

A comparison of the yield of extractive substances from chestnut seeds during ultrasonic treatment and during conventional extraction showed that the yield of biologically active substances during ultrasonic treatment with an optimal treatment time of 60 min and a frequency of 44 kHz is significantly higher (Fig. 1).

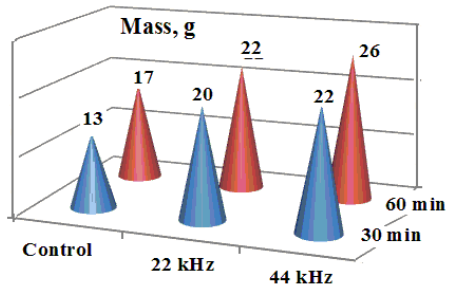

Figure 1. Yield of the sum of extractive substances of chestnut seeds during ultrasonic extraction. Ultrasonic processing frequency 22 kHz and 44 kHz. Extraction duration 30 and 60 min.

The use of ultrasonic cavitation allows extraction to be carried out at a low temperature (30-55°C) without the use of environmentally harmful chemical reagents, provides a significant reduction in the duration of the process, and increases the yield of biologically active substances. According to IR spectroscopy data, the extraction of biologically active substances from tomato, pepper, and chestnut seeds using the ultrasonic cavitation method (at a temperature of 55°C) is not accompanied by a change in the chemical composition of the extracted compound.

ACKNOWLEDGMENTS: Authors acknowledge funding from the Ministry of Education and Research of the Republic of Moldova. Subprogramme CDAETP 011203-IFAUSM.

THE INSTABILITY OF THE CAVITATION FLOW PAST A CYLINDER WITH A TURBULENT BOUNDARY LAYER

T. Cuciuc[1,*], I. Porumbel[2], M. Bologa[1]
[1]*Institute of Applied Physics, Moldova State University, Chișinău, Republic of Moldova;*
[2]*Romanian National Research & Development Institute for Gas Turbines - COMOTI, Bucharest, Romania*
[*]E-mail: tudor.cuciuc@ifa.usm.md

Unstable cavitation flow can be observed in various hydraulic systems and machines or may be triggered in particular by cavitation generators intended for the processing of materials in polyphasic liquid media. Cavitation control in such installations is possible by changing the flow in the boundary layer of the bodies. The paper presents the results of experimental studies on the effect of the turbulent boundary layer on the development of cavitation flow instabilities around a single cylinder. The studies were carried out in a closed circuit hydrodynamic tunnel. Its working chamber has length of 0.8 m and a cross-section of 150 x 70mm^2. The dynamics of the cavitation structures were recorded with a Phantom 42M fast digital camera. The turbulent flow regime in the boundary layer of the cylinder was achieved by injecting hydrogen microbubbles into this layer. In the case of triggering the turbulent regime in the boundary layer by injecting electrolytic hydrogen microbubbles, the effect of cavitation on the flow around the cylinder is explosive and is manifested by the sudden change in the hydrodynamic characteristics, as shown in Figure 1.

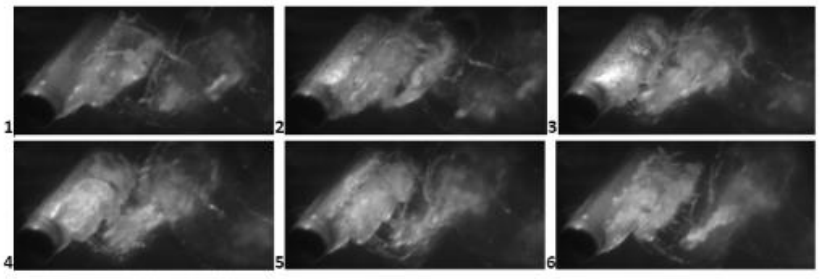

Figure 1. Development of periodic cavitational structures. The time interval between two consecutively captured images is t_i = 228 x 10^{-6}s. d = 14 mm, Re = 1.25x10^5, σ = 1.5, 1 - t_i, 2 - 8 t_i, 3 - 16 t_i, 4 - 18 t_i, 5 - 22 t_i, 6 - 26 t_i.

The periodic development of the singular partial cavity (supercavity) attached either to a part of the surface behind the cylinder (images 1 and 6, lower cavern, in Figure) or to another part of the surface (image 3, upper cavern) was observed. After a short time interval, such caverns also develop on the opposite side of the cylinder (images 2, top and 4, bottom, in Figure). After reaching a certain degree of development, the simultaneously attached partial cavitation zones interact, forming a re-entrant jet directed towards the interfacial layer of the cavity, with a longer length. It was established that the jet, or re-entering jets, transform the flow into a series of new cavitational bubble clouds. The implosion of these new bubbles may generate shock waves in the part of the cavern detached from the surface of the cylinder. Another part of the cavern remains temporarily attached to the surface of the cylinder (image 5, Figure). A cause of the occurrence of this phenomenon may be the development of the Kelvin-Helmholtz instability in the shear layer formed after the implosion of the bubble cloud [1]. It has also been established that this temporary cavity vortex (TVC) plays a special role in the development of transient processes in the cavitational flow. In images 1 and 6 in Figure, the separation and coalescence of the TVC with the downstream main vortex can be observed. The process of detachment of cavitational structures is strictly periodic, although the analysis of these structures highlights their three-dimensional character. It was established that the transition from the periodic regime to the quasi-periodic regime occurs when a critical value of the cavitation number is reached. A possible cause may be coalescence of a TVC with an attached cavitation upstream.

[1] V. Aeschlimann, S. Prothin, S. Barre, H. Djeridi. *European Journal of Mechanics B / Fluids*, **31** (2012), 171–180.

ACTIVATION OF MINERAL RAW MATERIALS IN CONDITION MAGNETOFLUIDIZATION

O.A. Bolotin[1], V.P. Gonciaruc[2,*], M.K. Bologa[2], A.A. Policarpov[2],
S.V. Siutkin[2], Yu.G. Golovko[3]
[1]*Institute of Geology and Seismology, State University of Moldova, Chișinău, Republic of Moldova;*
[2]*Institute of Applied Physics, Moldova State University, Chișinău, Republic of Moldova;*
[3]*Public Institution scientific and Practical Institute of horticulture and Food technologies, Chisinau, Moldova*
[*]E-mail*:* vgonciaruc@mail.ru

Activation is one of the ways to improve the physical and mechanical properties of materials. There are chemical, mechanical and chemical-mechanical activation.

One of the promising methods for activating natural minerals is mechanical activation in a magnetically fluidized bed. Features of devices with a magnetically fluidized bed for crushing solid materials are high-frequency shock loads and frictional forces, which lead not only to crushing of dispersed solid materials, but also to activation of their surface due to deformation of the crystal lattice.

Previously, our work has shown that mechanical activation promotes the formation of defects in the crystal lattice and can be an effective means of improving the properties of quartz sand. Established using X-ray phase analysis, a slight expansion of the main peak of quartz, caused by deformation of the crystal lattice and the accumulation of internal stresses in it, leads to an amorphous surface of quartz and, in turn, contributes to an increase in its reactivity.

The effectiveness of activation of Portland cement in a magnetically fluidized bed in the production of concrete has been shown. Here, mechanical activation occurs as a result of grinding of the material by cylindrical ferromagnetic particles fluidized by a rotating electromagnetic field.

Mechanical activation in a magnetically fluidized bed is an effective method of grinding and a method of increasing the sorption properties of zeolite rocks, which is due to structural changes, an increase in the porosity of the zeolite, an increase in the defectiveness of its surface, the formation of a significant amount of acidic and basic centers such as Si-OH and Al-0H generated under mechanochemical influences, increasing the sorption capacity of not only zeolite minerals, but also impurity minerals.

Thus, it was proven that activated zeolite in a magnetic fluidized bed effectively contributes to the purification of nitrate water. Filtration of model water with an NH^{4+} ion content of 1.73 mg/l through a layer of activated zeolite in a magnetic fluidized bed leads to a decrease in nitrate content to 0.12 mg/l. Activation of a mixture of zeolite and carbon also makes it possible to obtain an effective nitrate absorbent from polluted waters. Modification in a magnetically fluidized bed of zeolite works very well in treating wastewater from heavy metals. Thus, the Fe content decreases from 1.02 mg/L to 0.1 mg/L, and the Pb content from 20.0 mg/L to <0.4 mg/L.

INFLUENCE OF THE STRUCTURE OF THE ANODIC OXIDE SHELL ON THE SPEED OF ANODIC DISSOLUTION IN ELECTROTES FOR ELECTROCHEMICAL MACHINING

E.V. Likrizon*
T.G. Shevchenko Transnistrean State University, Tiraspol, Republic of Moldova
*E-mail: humanth@mail.ru

The influence of anodic oxides shells (AOS) in high-speed anodic dissolution and electrochemical machining has been previously studied in detail in the works electrochemical technologists Ivanovo's State University of Chemistry and Technology under the leadership of E.M. Rumyantsev. At the level of correlations of the nature of their conductivity (shells of semiconductor nature) and indicators of the speed of anodic dissolution distribution over the treated surface, its quantitative characteristics was established the relationship between their nature and indicators of electrochemical machining.

In the following years was developed in relation to description of metal passivity processes quantity theory, which determined the patterns of their formation and dissolution on the basis PDM (point defect model) [1,2]. In [3] based on the research example high-speed anodic dissolution heat-resistant chromium-nickel steels in conditions electrochemical machining (with surface temperature control) was shown the applicability PDM for describe the speed of dissolution in impulse conditions based on PDM-II (barrier oxide shell on the surface to be treated). In this case, there is an equality of speed electrochemical formation AOS and its chemical dissolution. The process changes significantly when switching to direct current (when boiling point is reached), because the shell structure is changing due to the formation of a barrier shell on the confine with solution (PDM-III [2]). In the process of thermokinetic instability (TKI) (thermal explosion) [4], leads to its destruction after which, the speed of dissolution may exceed the Faraday speed (abnormal anodic dissolution).

In the report, using the example of research of high-speed anodic dissolution with surface temperature control of chromium-nickel steel and titanium alloys in nitrate solutions, besides titanium alloys in nitrate and chloride solutions was shown the PDM (depending on the conditions PDM-II or PDM-III) to describe the formation AOS with different structures and their destruction due to TKI [5].

[1] Macdonald, D.D. *Electrochim. Acta.* **56** (2011), 1761.
[2] Macdonald D.D., Engelgardt G.R. *ECS Trans.* **28(24)** (2010), 123.
[3] Dikusar A.I., Silkin, S.A. *Surf Eng Appl Electrochem*, **58 (4)** (2022), 313.
[4] Engelgardt, G.R., Dikusar, A.I. *J. Electroanal. Chem.* **207** (1986) 1
[5] Dikusar A.I., Likrizon E.V. *Surface Engineering and Applied Electrochemistry* **57(1) (**2021), 10 – 18.

HEAT TRANSFER OF ROUGH SURFACES IN AN ELECTRIC FIELD

I.M. Chernica*, M. Ch. Bologa
Institute of Applied Physics, Moldova State University, Chișinău, Republic of Moldova
*E-mail: ion.cernica@ifa.usm.md

The interest in intensifying heat transfer during boiling under the influence of an electric field has increased, mainly in connection with the development of technical devices capable of delivering liquid dielectrics to heat-releasing surfaces in order to ensure specified thermal conditions. However, the electrical method does not always provide the intended temperature conditions.

This work is devoted to an experimental study of the effect of a nonuniform electric field on the process of boiling of a dielectric liquid in a large volume using rough surfaces. Boiling was carried out on single tubes with a diameter of 4 mm and a length of 80 mm, coated with a thin layer of tungsten carbide and stainless steel using the electric spark method and immersed in a relatively large volume of liquid – hexane (with a boiling point of 68.7ºC). The experiments used rectangular and round brass high-voltage electrodes located parallel to the heat-transfer element on top. The coatings had developed roughness: R_a = 3.216, 3.493, 4.316, 5.288 μm (surfaces coated with a layer of tungsten carbide) and R_a = 4.285 μm (surface coated with a layer of stainless steel). The interelectrode distance δ varied within 1.5–8 mm. An electrical circuit with a negative high-voltage potential was used, which was changed stepwise up to 25 kV.

The influence of the field on heat transfer during boiling on rough surfaces appears to a greater extent at low and moderate heat fluxes. For a given q, with increasing field strength, the boiling curves shift to the region of lower thermal pressures, where boiling is less intense and the heat transfer coefficient is higher. The influence of roughness is manifested over the entire range of heat flux densities and field strengths (Fig. 1). For given q and E, with an increase in the arithmetic mean deviation of the profile R_a, a decrease in temperature differences $\Delta T=T_w-T_s$ and a relatively small increase in the heat transfer coefficient are observed.

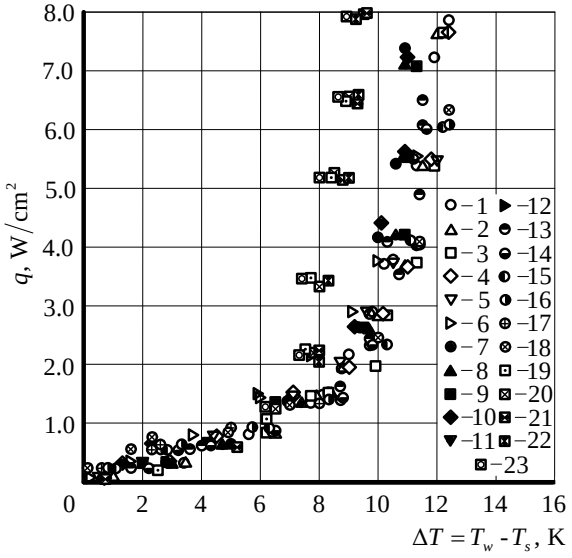

Figure 1. Heat transfer curves during boiling of hexane on modified surfaces of different roughness in an electric field, δ = 3 mm: 1 – E = 0; 2 – 16.67; 3 – 33.33; 4 – 50.00; 5 – 66.67; 6 – 83.33 kV/cm – R_a = 4.316 μm; 7 – E = 0; 8 – 16.67; 9 – 33.33; 10 – 50.00; 11 – 66.67; 12 – 83.33 kV/cm – R_a = 3.493 μm; 13 – E = 0; 14 – 16.67; 15 – 33.33; 16 – 50.00; 17 – 66.67; 18 – 83.33 kV/cm – R_a = 3.216 μm; 19 – E = 0; 20 – 16.67; 21 – 33.33; 22 – 50.00; 23 – 66.67 kV/cm – R_a = 5.288 μm

The possibility of intensifying heat transfer during boiling in an electric field on rough surfaces is shown. The greatest influence on the intensity of heat transfer is exerted by modification of the structure of the heat-releasing surface. At the same time, heat transfer during boiling on rough surfaces in an electric field has a number of significant features.

LAMINAR MOTION OF NON-NEWTONIAN FLUIDS IN CIRCULAR PIPES

I. M. Chernica*
Institute of Applied Physics, Moldova State University, Chișinău, Republic of Moldova
*E-mail: ion.cernica@ifa.usm.md

In nature, technology and medicine there are fluids with complex molecular structures, which do not obey Newton's linear law of deformation, that is, their dynamic viscosity depends not only on the thermodynamic state, but also on the rate of deformation, on the flow history, and on other factors. These abnormally viscous fluids are called non-Newtonian fluids. Since they additionally possess elastic and plastic properties, they flow according to specific laws, which must be known along with the laws for Newtonian fluids.

In non-Newtonian fluids, the best studied flow is a continuous and isothermal laminar flow of some rheological models in a horizontal cylindrical pipe, taking into account their rheological peculiarities and using as methodological apparatus both the Navier–Stokes equations [1] and the classical tools of hydraulics [2]. Regardless of the applied research method, the results coincide. The dynamic study could be simplified, if the continuous laminar flow of the general rheological model was approached, and the obtained results could be extended to simpler rheological models.

Relative to a plane Cartesian coordinate system, the rheological equation for non-Newtonian fluids has the form [1]

$$\tau = \tau_0 + k\left(dv/dy\right)^n, \tag{1}$$

where τ_0 is the tangential limit stress from which the flow starts, called the flow threshold or limit stress, k is the dynamic coefficient of structural viscosity, called consistency, in Pa·s^n, and n is the flow behavior index. In the case of flow through circular pipes, the shear rate dv/dy expressed in cylindrical coordinates is $dv/dy = -dv/dr$. Then the rheological equation (1) becomes

$$\frac{dv}{dr} = -\left(\frac{\tau - \tau_0}{k}\right)^{1/n}. \tag{2}$$

If we also take into account that the tangential shear stress is $\tau = \tau_w\, r/r_0$, we get

$$dv = -\left(\frac{\tau_w\, r/r_0 - \tau_0}{k}\right)^{1/n} dr. \tag{3}$$

By integration with respect to the current radius r, we obtain

$$v(r) = -\int_r^{r_0}\left(\frac{\tau_w\, r/r_0 - \tau_0}{k}\right)^{1/n} dr. \tag{4}$$

Knowing the velocity distribution in the cross-section of the pipeline, the volume flow rate of the fluid transported through the pipeline can be determined as

$$Q_v = \int_0^{r_0} 2\pi r v(r)\, dr = \pi \int_0^{r_0} v(r)\, d(r^2).$$

Assuming that $v(r)$ and $d(r^2)$ are differentiable functions with continuous derivative and using the expression for integration by parts we obtain

$$Q_v = \pi\left[\, r^2\, v(r)\Big|_0^{r_0} - \int_0^{r_0} r^2 dv(r)\,\right]. \tag{5}$$

For $r = 0$ and $r = r_0$, the product $r^2 v(r)$ is zero, so $r^2 v(r) = 0$, and if expression (3) is also taken into account, we get

$$Q_v = \pi \int_0^{r_0} r^2 \left(\frac{\tau_w r / r_0 - \tau_0}{k} \right)^{1/n} dr. \tag{6}$$

Substituting the current radius *r* by the expression $r = r_0 \tau / \tau_w$, for which $dr = (r_0 / \tau_w) d\tau,$ we obtain

$$Q_v = \frac{\pi r_0^3}{\tau_w^3} \int_0^{\tau_w} \tau^2 \left(\frac{\tau - \tau_0}{k} \right)^{1/n} d\tau. \tag{7}$$

Integrating over $\tau,$ initially between 0 and $\tau_w,$ then between τ_0 and τ_w, we obtain for the fluid flow rate passing through the pipe the following relationships

$$Q_v = \frac{\pi n r_0^3}{k^{1/n} \tau_w^3} \left\{ \frac{\tau_0^2}{n+1} \left[(\tau_w - \tau_0)^{\frac{n+1}{n}} - (-\tau_0)^{\frac{n+1}{n}} \right] + \frac{2\tau_0}{2n+1} \left[(\tau_w - \tau_0)^{\frac{2n+1}{n}} - (-\tau_0)^{\frac{2n+1}{n}} \right] + \frac{1}{3n+1} \left[(\tau_w - \tau_0)^{\frac{3n+1}{n}} - (-\tau_0)^{\frac{3n+1}{n}} \right] \right\}, \tag{8}$$

$$Q_v = \frac{\pi n r_0^3}{k^{1/n} \tau_w^3} \left[\frac{1}{3n+1} (\tau_w - \tau_0)^{\frac{3n+1}{n}} + \frac{2\tau_0}{2n+1} (\tau_w - \tau_0)^{\frac{2n+1}{n}} + \frac{\tau_0^2}{n+1} (\tau_w - \tau_0)^{\frac{n+1}{n}} \right], \tag{9}$$

which can be customized. Table 1 presents the calculation relationships of the volume flow of fluid transported in the laminar motion of some specific types of non-Newtonian fluids in circular pipes, for which the tangential shear stress at the wall is given by the relationship $\tau_w = r_0 \Delta p / 2l$.

Table 1

No. crt.	The rheological model	General relationship (8)	General relationship (9)
1.	Newtonian fluid $\tau_0 = 0,\ k = \mu,\ n = 1$	$Q_v = \frac{\pi r_0^4}{8\mu l} \Delta p$	
2.	Pseudoplastic and Bingham fluids $\tau_0 \neq 0,\ k = \mu,\ n = 1$	$Q_v = \frac{\pi r_0^4 \Delta p}{8\mu l} \left[1 - \frac{4}{3} \left(\frac{2l\tau_0}{r_0 \Delta p} \right) \right]$	$Q_v = \frac{\pi r_0^4 \Delta p}{8\mu l} \left[1 - \frac{4}{3} \left(\frac{2l\tau_0}{r_0 \Delta p} \right) + \frac{1}{3} \left(\frac{2l\tau_0}{r_0 \Delta p} \right)^4 \right]$
3.	Pseudo-plastic and dilatants fluids $\tau_0 = 0,\ k \neq \mu,\ n < 1$	$Q_v = \frac{\pi n}{(3n+1)} r_0^{3+1/n} \left(\frac{\Delta p}{2kl} \right)^{1/n}$	

Thus, it was found that in the flow of Newtonian, pseudo-plastic, and dilatant fluids, the fluid's flow rate through the pipe does not depend on the applied boundary conditions. When calculating the flow of pseudo-plastic and Bingham fluids, it is important to take into account the boundary conditions. The pipe of circular section carries a higher flow rate of pseudo-plastic fluid and Bingham fluid when there is a pressure difference, and the tangential shear stress τ becomes equal to the limit stress τ_0.

[1]. D.M. Klimov, A.G. Petrov, D.V.Georgievskii. *Viscoplastic Flows: Dynamic Chaos, Stability, Mixing*. – Moscow, Nauka, 2005. – 394 p.

[2]. G.B. Froishteter, S.Iu. Danilevich, N.V. Radionova. *Flow and heat transfer of non-Newtonian fluids in pipes*. – Kiev, Naukova dumka, 1990. – 215 p.

PRODUCTION AND PROPERTIES OF MAGNETIC MICRO- AND NANOWIRES. SURFACE ENERGY IN NANOWIRES

S. Baranov[1,*]
Moldova State University, Institute of Applied Physics, Chisinau, Moldova
[*]E-mail: serghei.baranov@ifa.usm.md

Technological aspects of the Ulitovsky-Taylor method for the preparation of glass-coated micro and nanowires with different structure of metallic cores are analyzed. The residual stress in micro and nanowires of this type determine the domain structures. The residual stress in cast amorphous micro- and nanowires is studied. Cast glass-coated ferromagnetic amorphous micro and nanowires (CGCFMNWs) are known to exhibit good magnetic properties. CGCFMNWs are composite materials that consist of a metallic core and a glass coating. The glass-coating induces strong residual stress in the core. This residual (mechanical) stress affects the magnetostriction value that is determined by large magnetoelastic anisotropy. The magnetic properties of CGCFMNWs are determined by the composition, which gives the sign and magnitude of their magnetostriction, and metallic core diameter, glass-coating thickness, and their ratio, which are extremely relevant for the level of residual stresses induced during preparation.
The magneto mechanical coupling between residual stresses and magnetostriction is mainly responsible for the distribution of anisotropy axes and domain structure formation. In the preparaion of CGCFMNWs, the residual stresses increase from the axis attaining maximum values on the surface. We have written a simple analytic expression for the switching field dependence on residual stresses, the radius of the metallic core of the microwire, the magnetostriction constant, and temperature; it has been experimentally verified. The macroscopic mechanism of domain wall activation qualitatively explains the main switching field dependence as an exponential form of temperature. Theory of thermoplastic relaxation can be used to show that residual stresses will increase on the surface of a microwire, which corresponds to the previously obtained experimental data. CGCFMNWs exhibit residual magnetization due to the specific distribution of residual stresses. This property of CGCFMNWs can be used for designing long-term magnetic storage elements and other electronic devices. The main technological parameters for the preparation of CGCFMNWs have been described. Particular attention has been paid to parameters determining the casting and cooling rates that are responsible for the microstructure of as-cast CGCFMNWs (amorphous or microcrystalline).

The method of continuous casting of CGCFMNWs has some limitations determined by the properties of the metal and the glass. The diameters of CGCFMNWs obtained by this technique are limited. In addition, there are limitations on quenching rate and metallic alloy composition. The range of working temperatures for casting is specific for a given composition of the metallic alloy and the glass for each metallic alloy-glass pair; it depends on the viscosity of the glass and the metal and other physical properties.

Classical nucleation theory method and within the limits of the statistical concentration density theory receives laws for surface energy of a cylindrical particle. It is shown, that in a linear case it is possible to receive close classical results. For a nonlinear problem results can differ from the standard. Analytical solutions to equations for case the cylindrical surface for the linear and nonlinear Van der Waals theory are analyzed.

STUDY OF AZITHROMYCIN HYDRATE DEGRADATION IN THE UV/H_2O_2 SYSTEM

T. Isac-Guțsul*, E. Tutovan, D.L. Nika
Moldova State University, Chisinau, Republic of Moldova
*E-mail: tatiana.isac.gutul@usm.md

We report on the optimal conditions of a colored compound formed in a strongly acidic medium upon interaction of azithromycin hydrate (AZI) with sulfuric acid 27 N degradation in the UV/H_2O_2 system. This drug is a broad-spectrum antibiotic used to treat respiratory tract infections and sexually transmitted diseases [1]. Azithromycin is spectrophotometrically inactive due to its chemical structure and does not show absorption in the ultraviolet (UV)/visible (VIS) range. As result of AZI interaction with concentrated sulfuric acid, there occurs hydrolytic cleavage at the glycosidic bond, which leads to the formation of the degradant product – erythronolide. This compound is reported to be stable in time and is used for dosing the drug and determining its stability in time [2].

In the research there was used the drug Azax (500 mg tablets, produced by „Nobel", Istanbul, Turkey). The structural formula of azithromycin is shown in Figure 1.

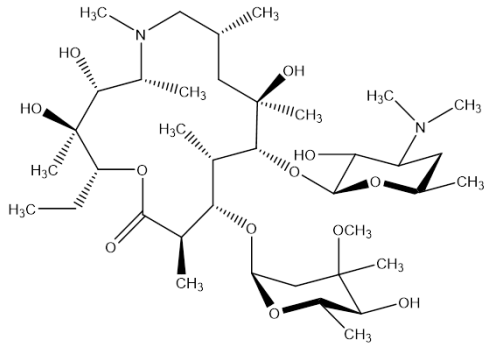

Figure 1. Structural formula of azithromycin

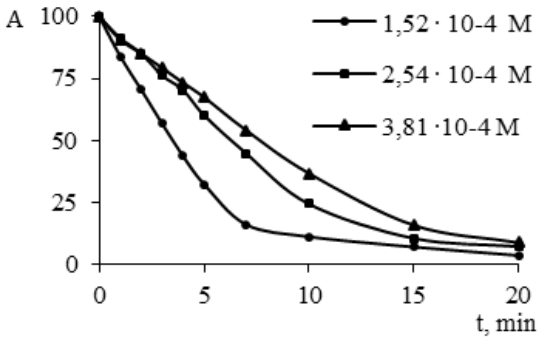

Figure 2. Kinetic curves of AZI hydrate degradationin the AZI-UV system

The degradation of the antibiotic in the AZI/UV system was studied at different concentrations of the drug ranging between (1.52 - 3.81) $\cdot 10^{-4}$ mol/L. To prepare the reactant mixture with a volume of 20 mL was introduced a certain volume of aqueous solution of 1 mg/mL azithromycin hydrate in 0.1 M H_2SO_4 solution, 5 mL of concentrated H_2SO_4 and a certain volume of distilled water was added. At certain time intervals samples were taken from the solution and absorbance values were measured, what allowed the construction of kinetic curves (Figure 2). Based on the obtained data, the degradation degree (DD) of the drug (in %) was calculated, which ranged between 91.2%- 96.4%. The initial rates were determined from the dependences W = f(t), using polynomial approximation with the Microsoft Excel programme. Their values range between (2.27-2.78)$\cdot 10^{-5}$ mol/(L·min). For a more complete drug oxidation, H_2O_2 was added to the system at concentrations of (5.0-2.4) $\cdot 10^{-2}$ mol/L. In the presence of oxidant, the AZI DD increases with increasing H_2O_2 concentration only by 3%, but the oxidation rate increases significantly and ranges between (1.1-2.2)$\cdot 10^{-4}$ mol/(L·min). The rate constant $k_{OH\cdot+AZI} = 6.39 \cdot 10^5$ mol/(L·min) was determined.

Finally we can conclude that the examined AZI colored compound is very unstable under the influence of UV light, and the presence of oxidant stimulates its intense degradation due to the interaction with OH• radicals, which have a very high ability to degrade organic compounds with bulky structures.

ACKNOWLEDGEMENTS: T.I.-G., and D.L.N. acknowledge the financial support from the Ministry of Education and Research of the Republic of Moldova (research program no. 011208).

[1]. I. C. Antonazzo, C. Fornari, D. Rozza at all International Journal of Infectious Diseases, Vol. 124, 2022, pp. 27-342.
[2]. S. NAJMA, A. SAEED, at all *Journal of Pharmaceutical Sciences*, Vol. 19(2), 2006, pp. 99.

PHOTOCATALYSIS vs ADSORPTION on HYBRID PHOTOCATALYST. COMPARISON

T. Datsko*, V. Zelentsov
Moldova State University, Institute of Applied Physics, Chisinau, R. Moldova
*E-mail: datsko.tatiana@yandex.ru

Purification of aqueous solutions from toxic substances is carried out in various ways, among them adsorption and heterogeneous photocatalysis occupy a certain, quite noticeable place. Both of these methods have some common features, namely the adsorption of the target substance on the surface of the catalyst. However, there are significant differences: during the adsorption process, the substance from the solution passes into another (solid) phase without changing its chemical nature, while during photocatalysis the toxic substance adsorbed on the catalyst surface undergoes decomposition ultimately into harmless compounds such as water and carbon dioxide.

Titania (TiO_2) has been perhaps the most promising and most studied semiconductor photocatalyst for removal of toxic substances from water solutions.

Photocatalysis is a complex physicochemical process that occurs in a heterogeneous aqueous system and includes the adsorption of molecules on the surface of a solid, absorption of UV radiation energy and oxidation-reduction reactions according to the scheme:

$$Organic\ waste \Rightarrow TiO_2 / O_2 / h\nu \geq E_g \Rightarrow Intermediates \Rightarrow CO_2 + H_2O$$

Therefore, the adsorption properties of the catalyst play an important role in the photocatalytic decomposition of organic pollutants.

However, the large scale application of this treatment technology is constrained by several factors such as: low adsorption capacity, feeble thermal stability, strong tendency to agglomeration of nano sized TiO_2 particles resulting in reduction or even complete loss of photocatalytic activity; problem of separation of nanosized particle powder in the aqueous media after the photocatalytic process. To overcome these drawbacks is the use the support for TiO_2 nanoparticles. Diatomite is a perfect porous support in preparation of hybrid photocatalyst for its unique physico-chemical properties, as high surface areas, good thermal resistance and mechanical stability, inherent hierarchical porosity, inexpensiveness and easy availability.

Using the example of adsorption and photodecomposition of a model dye methylene blue by a hybrid photocatalyst based on diatomite and nanosized anatase grafted onto it, a comparative analysis of the implementation of dye removal from an aqueous solution was made. The photocatalyst was prepared via heterogeneous hydrolysis of $TiCl_4$ as a precursor of TiO_2 in the presence of diatomite at room temperature and normal pressure. The obtained product was further washed, dried and calcined at 450^{o}C for anatase phase development. The amount of titania in the products varied from 10 to 75%.

All experiments on adsorption and photodegradation were carried out under the following conditions: to 50.0 ml of a solution of MB with a certain initial concentration, 0.1 g of a sample of the sorbent was added with constant stirring for a specified time.

At adsorption in the dark, the percentage of recovery of the dye with its initial content in the solution of 130 mg/l is about 52%. Photocatalysis allows to achieve the purification degree of 84% for the sample of hybrid photocatalyst with 20% of anatase (which is optimal in terms of adsorption and structural characteristics). At the same time, it is always necessary to keep in mind that via photocatalysis a toxic compound decomposes into safe products, while the adsorbed compound can, under certain conditions, be released again into the environment and continue to poison it.

Thus, the purifying of aqueous solution from a highly toxic compound for which other methods such as biodegradation are not applicable due to its toxicity, heterogeneous photocatalysis using the hybrid photocatalyst is the best alternative.

ACKNOWLEDGEMENTS: The work completed within the framework of the project CDAETP 011203

INFLUENCE OF THE MOVEMENT FORM OF PROCESSING ELECTRODES ON THE COATING FORMATION PROCESS DURING ELECTRO-EROSION ALLOYING OF STEELS

V.V. Mikhailov*, S.H. Ivashku, N.N. Kazak, A.I. Yanakevich
Institute of Applied Physics, Moldova State University, Chisinau, Republic of Moldova
*E-mail: valentin.mihailov@gmail.com

The research results on how the form of machining electrode motion affects coating formation, as well as structural and phase transformations in the surface layers of low-carbon steels St.3 and St.35, are presented. Two types of machining electrode motion were analyzed in detail: vibration for compact electrodes made of aluminum and nickel with dimensions 40×5×5 mm, and rotation for wire electrodes made of the same materials with diameters ranging from 1.5 to 2.0 mm in a plane perpendicular to the machined surface. Processing was conducted using electric pulse energies ranging from 3.0 to 6.0 J.

It was experimentally established that the form of motion of the processing electrode relative to the substrate surface, with all other conditions being equal, significantly influences the qualitative parameters of the resulting layers – specifically, their continuity, uniformity, and hardness. These effects associated with vibrating and rotating electrodes are likely due to the following factors: Firstly, with a vibrating anode, its contact with the cathode (substrate) surface is very brief (between 0.6 and 1-2 ms), which is insufficient for significant physicochemical transformations between the anode (Al) and the cathode (Fe). Secondly, the perpendicular movement of the anode relative to the cathode and its subsequent collisions cause some of the liquid phase formed during discharge to remain on the anode and cool down, rather than transferring completely to the cathode surface.

In contrast, with electro-erosion alloying (EEA) using a rotating electrode, the transfer of aluminum and nickel is more continuous and effective. The rotating electrode's tangential movement relative to the cathode surface allows the anode material to be transferred more efficiently. When the electrode-anode approaches within a breakdown distance, a discharge occurs, eroding the anode and forming a liquid phase at its end. This liquid phase, upon contact with the cathode surface, spreads and forms a coating. Additionally, the prolonged contact between the anode and cathode due to the rotation leads to greater heating of the contact zones from the short-circuit current, which results in a more persistent thermal field.

X-ray analysis of coatings obtained via EEA with vibrating and rotating electrodes confirmed the hypothesis that rotating electrodes enhance the interaction between anode and cathode materials. In the surface layers of the cathode subjected to EEA with rotating electrodes, a wide range of intermetallic compounds based on aluminum and nickel were identified, including $FeAl_3$, $FeAl_2$, $FeAl_5$, NiAl, Ni_2Al, as well as solid solutions and oxides.

ACKNOWLEDGEMENTS: The authors are grateful for the support provided by the Ministry of Education and Research of the Republic of Moldova through the subprogram 011204 (2024-2027) titled “Technology for Modifying the Surfaces of Construction and Medical Steels through Complex Actions Including Electrical Impulse Discharges, Plastic Deformation, and Plasmochemical Treatment in Electrolytes.”

ANALYSIS OF COMPOSITION AND STRUCTURE OF SURFACE LAYERS OF SHEET GLASS, THERMOCHEMICALLY TREATED WITH GASEOUS REAGENTS, USING THE METHOD OF SECTION ETCHING BY HF SOLUTION

V. A. Sharagov*, G. I. Curicheru
Alecu Russo Balti State University, Balti, Republic of Moldova;
*E-mail: vsharagov@gmail.com

Industrial glassware is characterized by low mechanical strength and bad thermal stability and as a result losses of production on the stage of manufacturing, transportation and exploitation reach 5 %. The different methods to improve the mechanical properties, thermal stability and chemical resistance of the glassware were developed. Thermochemical treatment with acid gases is the simplest method to improve the surface properties of glass. In laboratory and manufacturing conditions the thermochemical treatment method with gaseous reagents is the most effective for increasing the chemical resistance to water and acids of glass and at the same time increases the mechanical resistance by 20-30 %, microhardness and thermal stability - by 5-10 %.

The aim of the undertaken experiments was to study the composition and structure of the surface layers of sheet glass, thermochemically treated with gaseous reagents, using the method of section etching by HF solution.

The subjects of investigation were sheet glass samples. The chemical composition of glass is the following (weight %): 72.31 SiO_2, 1.46 Al_2O_3, 0.10 Fe_2O_3, 7.69 CaO, 3.83 MgO, 13.82 Na_2O, 0.35 K_2O and 0.31 SO_3. Dealkalization of glass samples has been carried out, using thermochemical treatment with acid gases. Sulfur dioxide, hydrogen chloride, dichlorodifluoromethane, chlorodifluoromethane and mixtures of these gaseous reagents were used for the treatment of glass samples in laboratory and manufacturing conditions. Regimes of treatment of samples in laboratory experiments are the following: temperature – from 300 to 600^{o}C, volume of gaseous reagent to the treatment – 15 L, duration – 15 min. The main regimes of treatment of glass with gaseous media in the manufacturing conditions are: glass temperature – from 600 to 900^{o}C, duration – no more than 20 min.

The analyses of glass surface layers have been carried out with the help of section etching by HF solution. The method consists in section dissolution of glass and analysis of extracts obtained after etching. The thickness of the dissolved layer and rate of dissolution in HF solution of glass surface layers were calculated based on mass losses of the samples before and after etching. The concentration of Na^+, K^+ and Ca^{2+} was measured in extracts after etching by the method of flame photometry. The experiments showed that the rate of dissolution of all the glass samples in HF solution is not stable. The analysis of glass samples, thermochemically treated with gaseous reagents, was carried out at the depth 10 μm.

Gaseous reagents at temperatures above 300 ^{0}C are extracted from the glass of alkali metal cations. The process of dealkalization of gaseous reagents includes a number of the physical and chemical phenomena. The mechanisms of interaction of sheet glass with gaseous reagents and with their mixtures are in generally analogical and can be reduced to dealkalization of the surface layer to the depth of 1.0 μm, at the degree of dealkalization 80%. The close connection between the dealkalization rate of glass by gaseous reagents, physical and chemical properties, composition and structure of its surface layer it is established. The optimal regimes are determined and a technology of thermochemical glass treatment by gaseous reagents is developed.

IMMOBILIZED PHENYLALANINE AMMONIA-LYASE FROM ARABIDOPSIS THALIANA FOR CONTINUOUS-FLOW PRODUCTION OF L-AMINO ACIDS

M. E. Moisă*, M. Pap, C. Paizs, L. C. Bencze, M. I. Toșa
Enzymology and Applied Biocatalysis Research Center, Faculty of Chemistry and Chemical Engineering, Babeș-Bolyai University of Cluj-Napoca, Cluj-Napoca, Romania
*E-mail: madalina.moisa@ubbcluj.ro

Biocatalysis is a valuable tool in chemical synthesis, in both academia and industry. The development of biotransformation-based synthetic processes has significantly progressed in recent years, especially due to advancements in protein engineering, enabling technologies with increased efficacy, productivity and selectivity, diminished costs and environmental impact. Besides high catalytic activity and selectivity, key factors for the successful application of enzymes are stability and recyclability, generally achieved through enzyme immobilization. [1] Additionally, flow technology has proven to be an attractive tool for developing efficient immobilized enzyme-based biocatalytic processes with upgraded productivity as compared to the batch systems. [2]

Phenylalanine ammonia lyases (PALs), catalyzing in nature the non-oxidative deamination of L-phenylalanine to *trans*-cinnamic acid, are well-established biocatalysts for the production of both D- and L-phenylalanine derivatives, useful building blocks in medicinal and synthetic chemistry. [3] PAL from *Arabidopsis thaliana* (*At*PAL) recently proved to be superior to other well-investigated PALs in the biotransformation of several substituted phenylalanine and *trans*-cinnamic acid analogues. [4]

In this work, we explored different immobilization strategies for *At*PAL with the aim of developing robust and active biocatalysts for continuous-flow production of optically pure aromatic amino acids. [5] Adsorption-based binding and three covalent immobilization techniques were investigated: (1) non-specific covalent immobilization employing amino-functionalized supports and a bis-epoxide linker, (2) maleimide-thiol coupling of enzyme's native surficial Cys residues to maleimide-derivatized supports and (3) site-specific maleimide-thiol coupling of engineered enzymes with unique cysteine residues introduced at specific positions on the enzyme surface, to maleimide-functionalized supports. The immobilization supports consisted in commercially available poly(methacrylic) resins functionalized with spacers of different lengths and amino groups. All developed biocatalysts were studied in both ammonia elimination and addition reaction routes. For the two best performing biocatalysts the enzyme load was optimized, their specific activities were determined and their recyclability was investigated. Moreover, the biocatalysts' operational stability and productivity in a packed-bed continuous-flow mini-reactor was explored.

ACKNOWLEDGEMENTS: This work was supported by the project "Advanced (multi)-enzymatic synthesis and purification processes for biobased furan derivatives –ASPIRE" funded by European Union – Nextgeneration EU and Romanian Government, under National Recovery and Resilience Plan for Romania, contract no. 760042/23.05.2023, cod PNRR-III-C9-2022-I8-ASPIRE/PNRR2022, through the Romanian Ministry of Research, Innovation and Digitalization, within Component 9, Investment I8.

[1] A. O'Connell, A. Barry, A. J. Burke, A. E. Hutton, E. L. Bell, A. P. Green, E. O'Reilly. *Chem. Soc. Rev*. **53** (2024) 2828-2850.
[2] M. P. Thompson, I. Peñafiel, S. C. Cosgrove, N. J. Turner. *Org. Process Res. Dev.* **23** (2019) 9-18.
[3] F. Parmeggiani, N. J. Weise, S. T. Ahmed, N. J. Turner. *Chem. Rev.* **118** (2018) 73-118.
[4] S. D. Tork, M. E. Moisă, L. Cserepes, A. Filip, L. C. Nagy, F. D. Irimie, L. C. Bencze. *Sci. Rep*. **12** (2022) 1-12.
[5] J. H. Bartha-Vári, M. I. Toșa, F. D. Irimie, D. Weiser, Z. Boros, B. G. Vértessy, C. Paizs, L. Poppe. *ChemCatChem* **7** (2015) 1122-1128.

IMPROVING PHYSICO-CHEMICAL PROPERTIES OF INDUSTRIAL GLASSWARE BY COMBINING THERMOCHEMICAL TREATMENT WITH GASEOUS REAGENTS AND THERMOMAGNETIC TREATMENT

V.A. Sharagov*, G.I. Curicheru
Alecu Russo Balti State University, Balti, Republic of Moldova;
*E-mail: vsharagov@gmail.com

The aim of the undertaken experiments was to investigate the influence of combining thermochemical treatment with gaseous reagents and thermomagnetic treatment on the physico-chemical properties of industrial glassware.

Objects of investigation were jars, bottles and flasks of colorless glass. Dichlorodifluoromethane, chlorodifluoromethane, hydrogen fluoride and chloride, sulfur dioxide, other gaseous reagents, and constant, alternating and impulse magnetic fields may be used for combining treatment of glassware in manufacturing conditions. Parameters of glassware combining treatment are as follows: temperature – between 500 and 600 ºC, volume fraction of gaseous reagent (gaseous reagent volume vs. container capacity) between 0.05 and 5.0 %, duration – between 1 and 8 s, vector's magnitude of magnetic induction - up to 0.25 T, magnetic field strength – 0.064 MA/m, duration of an impulse - 25 μs, pulses follow at a frequency - between 1 and 10 Hz. There are three possible variants of combined treatment: 1) thermomagnetic treatment of glassware, then thermochemical treatment; 2) thermochemical treatment of glassware, then thermomagnetic treatment; 3) simultaneous treatment of glassware with acid gases and electromagnetic fields. Glassware was treated in different places: final blowing of containers, conveyor for transportation of glassware towards annealing and lehr. The reagents were fed into the glassware mainly in gaseous state and in the form of solutions and solid substances. Thermochemical dealkalization with gaseous reagents and thermomagnetic treatment of glassware was carried out in conditions of stable operation of glass-forming machine. No special measures were taken to prevent damaging the glass surface.

Jars, bottles and flasks were tested for by water resistance, resistance to internal hydrostatic pressure, microhardness, and thermal stability. For jars, the resistance to the compression force was additionally determined in the direction perpendicular to the walls of the body. In our experiments, the maximum mechanical strength and thermal stability of glassware were measured. For this purpose, the glassware was tested to its complete destruction.

As a result of the combining treatment of hollow glassware with magnetic field and dealkalization with gaseous reagents, water resistance of the glass surface increases by tens times, as well as increases the mechanical strength - by 30-50 %, the thermal stability and microhardness - by 10-15 %. The greatest effect in increasing the water resistance, mechanical strength, thermal stability and microhardness of glass containers was obtained as a result of simultaneous treatment of glassware with gaseous reagents and electromagnetic fields.

This research determined the influence of the following factors on the physico-chemical properties of glassware exposed to combining treatment: glass temperature, vector's magnitude of magnetic induction value, duration of treatment, frequency of pulses, and the position of magnetic field lines in relation to the plane of the walls of the glassware. The higher the temperature of glass and the value of the vector's magnitude of magnetic induction, the longer the duration of treatment, the greater the thermomechanical properties of the glassware.

HIGH-Tc CUPRATES – STORY OF TWO ELECTRONIC SUBSYSTEMS

Neven Barišić[1,2,*]
[1]*Institute of Solid State Physics, TU Wien, Wien Austria;*
[2]*Department of Physics, University of Zagreb, Zagreb, Croatia;*
[*]E-mail: nbarisic@phy.hr

The experimentally established universalities in high-T_c cuprates will be presented [1-7]. Based on them we show that the phenomenology of cuprates across the phase diagram is fully captured by the simple charge conservation relation:

$$1 + p = n_{loc} + n_{eff}$$

Here, p is the doping while n_{eff} is the carrier density and n_{loc} is the density of localized charge within a CuO_2 plaquette. The corresponding superfluid density is related to both components:

$$\rho_S = n_{eff} \cdot (O_S\, n_{loc}).$$

where all terms can be experimentally determined directly. The charge n_{loc} is responsible for all the strangeness of these compounds, which includes the pseudogap phenomenon and the superconducting glue. [7-9]

The compound-dependent constant, O_S, is fine-tuned by the local crystal structure. It arises from the *p–d–p* fluctuation by the Cu-localized holes visiting the neighboring planar–oxygen atoms and can be determined from NMR [9].

[1] N. Barišić et al., *New J. Phys.* **21** (2019) 113007 (see also *arXiv*:1507.07885 (2015)).
[2] Y. Li et a., *Sci. Adv.* **5** (2019) eaap7349.
[3] N. Barišić et al., *Proc. Natl. Acad. Sci. U.S.A.* **110** (2013) 12235.
[4] S. I. Mirzaei et al., *Proc. Natl. Acad. Sci. U.S.A.* **110** (2013) 5774.
[5] M. K. Chan et al., *Phys. Rev. Lett.* **113** (2014) 177005.
[6] P. Popčević et al., *npj Quantum Mater.* **3** (2018) 42.
[7] C. M. N. Kumar et al., *Phys. Rev. B* **107** (2023) 144515.
[8] D. Pelc et al., *Sci. Adv.* **5** (2019) eaau4538.
[9] N. Barišić & D. K. Sunko. *J Supercond. Nov. Magn.* **35** (2022) 1781.

COMMENSURABILITY EFFECTS AND LONG-TERM STABILITY OF PINNING LANDSCAPES IN COPPER-OXIDE SUPERCONDUCTORS FABRICATED BY FOCUSED He-ION-BEAM NANOPATTERNING

B. Aichner[1,*], S. Keppert[2], M. Karrer[3], K. Wurster[3], C. Magén[4], C. Schmid[3], R. Hutt[3], J. D. Pedarnig[2], R. Kleiner[3], E. Goldobin[3], D. Koelle[3], W. Lang[1]

[1]*Faculty of Physics, University of Vienna, Wien, Austria;*

[2]*Institute of Applied Physics, Johannes Kepler University of Linz, Linz, Austria;*

[3]*Physikalisches Institut, Center for Quantum Science (CQ) and LISA$^+$, Universität Tübingen, Tübingen, Germany;*

[4]*Instituto de Nanociencia y Materiales de Aragón (INMA), CSIC-Universidad de Zaragoza, Zaragoza, Spain*

[*]E-mail: bernd.aichner@univie.ac.at

The focused beam of a helium ion microscope (HIM) is an excellent tool for creating closely spaced nanocolumns in thin films of copper-oxide superconductors [1]. Within these nanocolumns, the critical temperature T_c is reduced or entirely suppressed due to the disruption of the superconducting charge carrier pairs by scattering on numerous point defects. Most irradiation-induced displacements affect oxygen atoms while not reducing the overall oxygen content in the sample. It is widely accepted that the oxygen atoms are displaced only a few unit cells, which implies that moving back only requires minimal energy.

To optimize the conditions for creating nanostructures suitable as Abrikosov-vortex pinning arrays via focused He^+-beam irradiation (He-FIB), we have investigated the impact of various irradiation parameters on the structural and superconducting properties of $YBa_2Cu_3O_{7-\delta}$ (YBCO) thin films. An important point is the optimal number of 30 keV He^+ ions needed to irradiate a dot of the nanocolumn lattice for maintaining the crystalline framework of YBCO intact while suppressing its superconductivity. Using aberration-corrected scanning transmission electron microscopy, we identified a critical dose of approximately 13,000 ions/dot beyond which the YBCO film becomes amorphous. Conversely, lower doses do not cause any visible damage. Still, they affect the behavior of magnetic flux quanta, influencing the efficiency of the vortex pinning lattices formed by the columnar defects [1]. Moreover, we demonstrate that the He-FIB technique can also be applied to $Bi_2Sr_2CaCu_2O_{8+x}$ thin films to produce efficient pinning landscapes in this highly anisotropic superconductor.

One topic to be investigated is the stability of these defects over long timescales. To address this, we investigated the efficiency of pinning arrays in YBCO films over several years of storage at room temperature. The critical temperature T_c increased during an initial healing period of about three years and then showed a marginal decrease up to a total storage period of almost six years. The long-term storage in dry air did not compromise the vortex-matching signatures. This analysis suggests that room-temperature annealing reduced the defect density surrounding the columnar defect channels while maintaining robust pinning potential at their cores [2]. Our results carry significant implications for potential applications in fluxonics.

ACKNOWLEDGMENTS: The research was funded by a joint project of the Austrian Science Fund (FWF), grant I4865-N, and the German Research Foundation (DFG), grant KO 1303/16-1. It is based upon work from COST Actions CA19140 (FIT4NANO), CA21144 (SuperQuMap), and CA19108 (Hi-SCALE) supported by COST (European Cooperation in Science and Technology). B.A. acknowledges financial support from the Austrian Science Fund, grant I6079.

[1] M. Karrer, B. Aichner, K. Wurster, C. Magén, C. Schmid, R. Hutt, B. Budinská, O.V.Dobrovolskiy, R. Kleiner, W. Lang, E. Goldobin, D. Koelle, Phys. Rev. Applied, **22** (2024) 014043.

[2] S. Keppert, B. Aichner, P. Rohringer, M.-A. Aurel Bodea, B. Müller, M. Karrer, R. Kleiner, E. Goldobin, D. Koelle, J. D. Pedarnig, W. Lang, Int. J. Mol. Sci., **25** (2024) 7877.

VORTEX MATTER IN COPPER-OXIDE SUPERCONDUCTORS WITH PERIODIC DEFECTS

W. Lang[1,*], B. Aichner[1], L. Backmeister[1], M. Karrer[2], K. Wurster[2], R. Kleiner[2], E. Goldobin[2], D. Koelle[2]
[1]*Faculty of Physics, University of Vienna, Wien, Austria;*
[2]*Physikalisches Institut, Center for Quantum Science (CQ) and LISA$^+$, Universität Tübingen, Tübingen, Germany*
[*]E-mail: wolfgang.lang@univie.ac.at

The talk will focus on understanding how strategically placed topological defects affect the arrangement of Abrikosov vortices in a superconductor. This involves creating a precise potential landscape that can pin the vortices in place. It is crucial to ensure that these vortices are magnetically coupled, and hence, their separation should not exceed the London penetration depth at the desired operating temperature. The latter should be significantly lower than the superconductor's critical temperature T_c to minimize the impact of thermodynamic fluctuations. Achieving nanoscale resolution is particularly challenging in copper-oxide superconductors due to their complex atomic structure and susceptibility to environmental influences. Traditional lithographic methods are limited in this context, but these challenges can be overcome using a focused beam from a helium ion microscope (He-FIB). The 30 keV He^+ ion beam is employed to create various arrays of defect columns in thin films of $YBa_2Cu_3O_{7-\delta}$ (YBCO). These nanocolumns suppress T_c due to pair-breaking caused by numerous point defects, making them effective pinning sites for Abrikosov vortices.

The distinctive layout of our pinning landscapes leads to several noteworthy phenomena. The interaction between vortex pinning at artificial regular and intrinsic irregular sites results in the creation of an ordered Bose glass of vortices [1,2]. A periodic pinning pattern with voids allows us to study the competition between pinning and elastic forces that seek to restore the genuine hexagonal vortex arrangement [3]. In ultradense hexagonal pinning landscapes, we observe reentrant zero resistance at an applied magnetic field of 3.8 T, accompanied by a pronounced peak in the pinning force density of the vortex ensemble caused by commensurability effects. When the vortex density aligns with the precisely known density of defect columns, we can determine the pinning force exerted on an individual vortex by an artificial defect. We will also discuss how this pinning force varies with temperature in the context of Ginzburg-Landau theory.

ACKNOWLEDGMENTS: The research was funded by a joint project of the Austrian Science Fund (FWF), grant I4865-N, and the German Research Foundation (DFG), grant KO 1303/16-1. It is based upon work from COST Actions CA19140 (FIT4NANO), CA21144 (SuperQuMap), and CA19108 (Hi-SCALE) supported by COST (European Cooperation in Science and Technology).

[1] L. Backmeister, B. Aichner, M. Karrer, K. Wurster, R. Kleiner, E. Goldobin, D. Koelle, W. Lang, Nanomaterials **12** (2022) 3491
[2] B. Aichner, L. Backmeister, M. Karrer, K. Wurster, R. Kleiner, E. Goldobin, D. Koelle, W. Lang, Condens. Matter **8** (2023) 32.
[3] B. Aichner, B. Müller, M. Karrer, V. Misko, F. Limberger, K. L. Mletschnig, M. Dosmailov, J. D. Pedarnig, F. Nori, R. Kleiner, D. Koelle, W. Lang, ACS Appl. Nanomater., **2** (2019) 5108.

ENHANCEMENT OF FLUX PINNING BY CREEP, - NONMONOTONIC RELAXATION OF CAMPBELL PENETRATION DEPTH

V. Geshkenbein*
Institute for Theoretical Physics, ETH Zurich, Zurich, Switzerland
*E-mail: dimagesh@phys.ethz.ch

In the traditional view of magnetic flux creep in type-II superconductors, all relevant observables relax monotonically, as the vortex density gradient decays with time. Here, we propose a revised model where vortices, initially freed from shallow pinning sites by thermal fluctuations, are re-trapped by deeper sites with larger average curvature [1]. This process dominates in the initial stages of relaxation and can be observed by measuring the Campbell response, which probes the linear response of the vortices inside the pinning wells. Direct experimental measurements confirm the predicted non-monotonic behavior, validating this new, general picture of the vortex creep mechanism [2].

[1] F. Gaggioli, G. Blatter, V. B. Geshkenbein, Phys. Rev. Research **4**, 013143 (2022)
[2] S. Ghimire et al arXiv:2403.14891

SUPERCONDUCTING ARTIFICIAL NEURAL NETWORKS

A. Sidorenko*
Technical University of Moldova, D.Ghitu Institute of Electronic Engineering and Nanotechnologies, Chișinău, Republic of Moldova
*E-mail: sidorenko.anatoli@gmail.com

The need of radical reduction of energy consumption is becoming a decisive parameter limiting the development of new supercomputers. Recently it was started a very rapidly development of novel research direction: design of non-von Neumann computers with a brain-like architecture or artificial neural networks - superconducting ANNs. That requires the development of base elements of neural network - a nonlinear switching neurons and linear elements synapses, changing connection strength or "weight" of neurons in ANN [1].

The results of the design and research of artificial superconducting ANNs, based on superconducting spin valves and superconducting synapses constructed from layered superconductor-ferromagnetic hybrid nanostructures are presented.

Layered Nb/Co heterostructures demonstrate a change of the superconducting order parameter in thin niobium films due to switch from parallel to antiparallel magnetic ordering of adjacent ferromagnetic layers. Such heterostructures can be used as a base elements of superconducting ANN [2,3]. Computer designed on superconducting ANN using these two basic elements - artificial neurons and artificial synapses, makes it possible to reduce for several orders of magnitude the power consumption compared to the existing computers built on semiconducting elements.

ACKNOWLEDGMENTS: The research was supported by the project of the Moldova State Program «Functional nanostructures and nanomaterials for industry and agriculture» no. 20.80009.5007.11.

[1] I.I Soloviev, N.V. Klenov, S.V Bakurskiy, M.Y. Kupriyanov, A.L Gudkov., A.S. Sidorenko, *Beilstein J. Nanotechnol.* **8** (2017), 2689–2710
[2] I.I. Soloviev, A.E. Schegolev, N.V. Klenov, S.V. Bakurskiy, M.Yu Kupriyanov, M.V. Tereshonok, A.V. Shadrin, V.S. Stolyarov, A.A. Golubov, *Journal of Applied Physics* **124** (2018), 152113
[3] A. Schegolev, N. Klenov, S. Bakurskiy, I. Soloviev, M. Kupriyanov, M. Tereshonok, A. Sidorenko, *Beilstein J. Nanotechnol.* **13** (2022), 444–454

CROSSOVER FROM ISOLATED YSR STATES TO GAPLESS SUPERCONDUCTIVITY IN 2H-NBSE$_{2-x}$S$_x$ AT THE ATOMIC SCALE

J.A. Moreno[1,*], V. Barrena[1], M. Roig[2], E. Herrera[1], A. Fente[1], A. Montoya[3], S. Mañas-Valero[3], A. Smeets[1], B. Wu[1], M.N. Gastiasoro[4], J. Aragón Sánchez[5], Y. Fasano[5], E. Coronado[3], J.J. Baldoví[3], B.M. Andersen[2], I. Guillamón[1], H. Suderow[1]

[1]*Laboratorio de Bajas Temperaturas y Altos Campos Magnéticos, Departamento de Física de la Materia Condensada, Instituto Nicolás Cabrera and Condensed Matter Physics Center (IFIMAC), Universidad Autónoma de Madrid, Madrid, Spain;*

[2]*Niels Bohr Institute, University of Copenhagen, Copenhagen, Denmark;*

[3]*Instituto de Ciencia Molecular (ICMol), Universidad de Valencia, Paterna, Spain;*

[4]*Donostia International Physics Center, Donostia-San Sebastian, Spain;*

[5]*Centro Atómico de Bariloche and Instituto Balseiro, CNEA, CONICET and Universidad Nacional de Cuyo, San Carlos de Bariloche, Argentina.*

[*]E-mail: josea.moreno@uam.es

Anderson's theorem states that the superconducting gap of s-wave superconductors remains fully open even in presence of a large amount of non-magnetic impurities. A single isolated magnetic impurity leads to in-gap states, called Yu-Shiba-Rusinov (YSR) states. These states produce local density of states oscillations and have been extensively studied in pure 2H-$NbSe_2$ with a small number of magnetic impurities[1,2]. Here we study 2H-$NbSe_{2-x}S_x$ with highly diluted Fe impurities (0.02 at.%) and find that gapless superconductivity sets in over large areas[3]. The characteristic electron-hole asymmetry of the density of states of isolated YSR states is lost in the gapless regime. YSR oscillations exhibit wavevectors which differ from the ones found in pure 2H-$NbSe_2$, unveiling features in the electronic band structure such as the van Hove anomaly along the Γ-M direction. We show through density functional calculations that substitutional Se-S disorder leads to a band structure with enhanced quasi two-dimensional character. However, at the same time, the charge density wave of pure 2H-$NbSe_2$ is destroyed by in-plane disorder, leading to in-plane isotropic vortex cores in the gapless regime. Our experiments show that electronic correlations and disorder produce gapless superconductivity even with minute amounts of magnetic impurities.

[1] G. Ménard et al., *Nature Phys* **11** (2015), 1013–1016.
[2] S. Park et al., *Nat Commun* **12** (2021), 4668.
[3] S. Skalski, et al., *Phys. Rev.* **136** (1964), A1500.

MAGNETOTRANSPORT PROPERTIES OF BISMUTH WIRES BELOW 25 K

E. Condrea*
Technical University of Moldova, D.Ghitu Institute of Electronic Engineering and Nanotechnologies, Chișinău, Republic of Moldova
*E-mail: elena.condrea@iien.utm.md

In this paper we report on magnetotransport measurements of single crystalline bismuth wires at high magnetic fields and low temperatures. These investigations are motivated in part by the unusual electronic properties of the semimetal bismuth that reflect its unique location in an intermediate position between good metals and semiconductors and present the fundamental and practical interest.

Measurements of the magnetoresistance (MR) and magnetothermopower (Seebeck coefficient) in the range of magnetic field up o 20 T reveal a various behavior of quantum oscillations for the different values of temperatures that persist from 4.2 to 25 K. Observed Shubnikov-de Haas oscillations exhibit anomalies in their amplitude up to 15 T which deviates from the conventional Lifshitz-Kosevich behavior below the magnetic ordering temperature and around 20 K. The latter, which has so far not been observed, suggests a field- and temperature-induced electronic structure transition.

Thermopower (S) of the 1.1 μm wire with high resistance residual ratio (R(300K)/R(4.2K) = 30) exhibits a non-linear temperature dependence with $\partial S/\partial T < 0$ at B = 0 (Figure 1(b)). In standard low-temperature measurements of bulk Bi crystals such behaviour is associated with the phonon drag effect that dominates the total thermopower of being the sum of diffusion (Sd) and phonon drag term (Sg) at liquid helium temperature. The phonon-drag effect ($S \propto 1/T$) has been observed in the set of Bi wires a higher crystalline perfection as compared with submicron nanowires with low resistance residual ratio (Figure 1(a)).

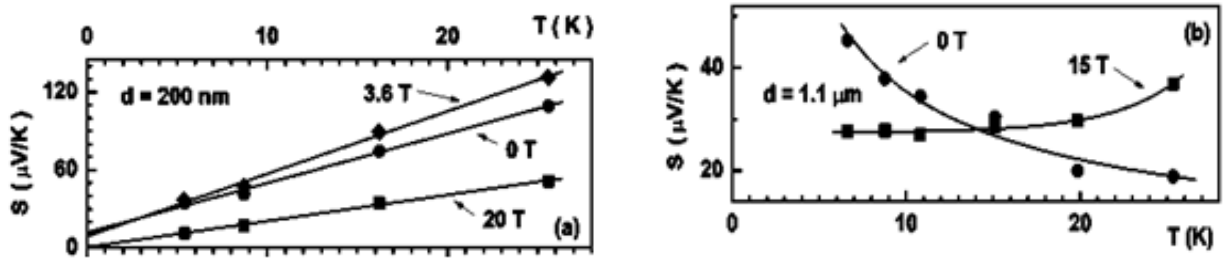

Figure 1. Dependence of the thermopower with temperature at various values of longitudinal magnetic field for the submicron nanowire (200 nm) (a) and 1.1 μm wire (b).

As shown in figure 1(b), the curves of temperature dependence S(T) have different shapes at magnetic field of B = 0 and 15 T. The observed change from $\partial S/\partial T < 0$ to $\partial S/\partial T > 0$ suggests that increasing the magnetic field enhances the relative contribution of the diffusion TEP and decreases the phonon drag contribution.

We provide a thorough analysis of the different samples, highlighting the importance of sample quality for elucidating details in the transport behavior.

ACKNOWLEDGMENTS: The study was supported by the Project "Nanostructures and advanced materials for implementation in spintronics, thermoelectricity and optoelectronics" no. 020201.

HIGH-TEMPERATURE BIPOLARONIC SUPERCONDUCTIVITY IN MULTILAYER PERIODIC STRUCTURES

S. I. Beril, A. S. Starchuk*
T. G. Shevchenko Pridnestrovian State University, Tiraspol, Republic of Moldova
*E-mail: starchukas@gmail.com

The possibility of realizing high-temperature superconductivity (HTSC) in multilayer structures was predicted by Ginzburg [1]. In a theoretical study of HTSC in a three-layer structure of the Ginzburg sandwich type: $SrTiO_3$/FeSe (monolayer)/$SrTiO_3$, it was shown [2] that the experimentally detected HTSC in these structures [3] can be explained on the basis of a bipolaronic mechanism. The estimates of the binding energy (E_{bp}) of the bipolaron and the critical temperature (T_c) in the FeSe layer are in the range $E_{bp} \sim (150 \div 500)\ K$ with a maximum value of $T_c \sim 140\ K$, i.e. bipolarons are stable quasi-particles and can exist in the structure under consideration at a temperature significantly higher than the temperature T_c of their condensation.

The theory makes it possible to simulate the material and geometric parameters of multilayer periodic structures in which critical temperatures T_c can be reached in the range of room values $T_c \sim 300\ K$.

For the considered mechanism of HTSC occurrence, the most promising multilayer structures are multilayer structures, the layers of which, along with FeSe, CuO_2, are such layers as SrO, TiO_2, BaO and a number of others proposed in [2], [4].

[1] V. L. Ginzburg. *UFN* **95** (1968) 91–95.
[2] S. I. Beril, A. S. Starchuk. *American Journal of Physics and Applications* **11** (2023) 8–20
[3] S. Zhang, J. Guan, X, Jia, B. Liu, W. Wang, F. Li, L. Wang, X. Ma, Q. Xue, J. Zhang, E. W. Plummer, X. Zhu, J. Guo. *Phys. Rev. B.* **94** (2016) 081116 (R).
[4] Lee D. H. What Makes the T_c of FeSe/$SrTiO_3$ so High? // arXiv: 1508.02461v1[cond-mat.str-al] 11Aug.2015.

QUANTUM SIZE EFFECTS ON ANDREEV TRANSPORT IN JOSEPHSON JUNCTIONS

B. Ujfalussy[1,*], G. Csire[2], N. Kucska[1]
[1]*HUN-REN Wigner Research Centre for Physics, Budapest, Hungary;*
[2]*Materials Center Leoben Forschung GmbH, Leoben, Austria*
[*]E-mail: ujfalussy.balazs@wigner.hu

In this talk we discuss the experiments in epitaxial Nb(110)/Au(111)/Nb(110) trilayers, where the critical current density, the superconducting coherence length, and the superconducting transition temperature all show an oscillating behavior as a function of the Au-layer thickness. Such behavior cannot be understood based on simple models of the Josephson Effect, therefore we apply the first principles-based microscopic theory of inhomogeneous relativistic superconductivity to understand both the fundamentals and the specifics of the underlying physical mechanism of this behavior. We study the effects of spin-orbit coupling, and the effect of confinement and show that they induce a complex structure of Andreev states in the superconducting state which in turn modifies the quasi-particle spectrum and the Josephson supercurrent. Our study reveals the coexistence of two superconducting phases in the gold layers, the usual intraband s-wave phase and an additional Fulde-Ferrell-Larkin-Ovchinnikov (FFLO) phase stemming from interband pairing (without magnetic field). The results indicate the rich interplay between quantum size and proximity effects which suggests the possibility of modifying superconducting transport properties by exploiting thickness-dependent quantum size effects.

ENGINEERING QUANTUM STATES IN RADICAL MOLECULES ON SUPERCONDUCTING SURFACES

V. Pokorný[1,*], M. Žonda[2], C. Li[3]
[1]*FZU - Institute of Physics, Czech Academy of Sciences, Prague, Czech Republic;*
[2]*Department of Condensed Matter Physics, Faculty of Mathematics and Physics, Charles University, Prague, Czech Republic;*
[3]*Department of Physics, University of Basel, Basel, Switzerland*
[*]E-mail: pokornyv@fzu.cz

Engineering quantum states in metal-free organic molecules is challenging due to their complex nature and inherent limitations. We investigated the properties of molecular assemblies engineered from a radical molecule tetrabromo-tetraazapyrene on a Pb(111) superconducting surface. We used scanning tunneling microscopy and spectroscopy in combination with theoretical calculations based on density functional theory and the numerically exact solution of the superconducting Anderson impurity model to study the behavior of the Yu-Shiba-Rusinov (YSR) states. Tunneling spectra show that YSR states lie close to the Fermi energy in isolated molecules. A quantum phase transition from singlet to doublet ground state can be induced by the change in the scanning tip distance. Additionally, we show that the presence of a second molecule allows us to tune the energy of the YSR state by changing the relative distance and can induce splitting of the YSR state for certain relative orientations. Constructing odd- and even-numbered molecular chains gives evidence of a periodic arrangement of charged and neutral molecules along the chains. Furthermore, the charge state of a tetramer chain can be manipulated by external electric fields induced by the presence of the scanning tip, opening the possibility to store information in these structures. Together, we show that the different molecular assemblies can be utilized as highly tunable building blocks for superconducting molecular quantum technologies.

SUPERFLUIDITY ON NON-TRIVIAL GEOMETRIES IN A MAGNETIC FIELD AND FINITE TEMPERATURES IN THE CONTEXT OF THE BOSE-HUBBARD MODEL

M. Rodríguez Martín*, T.A. Zaleski
Institute of Low Temperature and Structure Research, Polish Academy of Sciences, Wrocław, Poland
*E-mail: m.rodriguez@intibs.pl

Quantum materials exhibit unique properties that make them suitable for the development of new technologies as well as for the improvement of existing devices. Many of these applications exploit the superconducting capabilities of the materials, allowing further development of a wide range of areas, such as metrology or quantum computation. It is well known that there exists a very close relationship between superconductivity and superfluidity, so advancements in the study of superfluid systems can be translated into an improvement of the understanding of superconductivity.

In this work we study the properties of the Bose-Hubbard model, which exhibits a superfluid phase, making use of the quantum rotor approach, which carefully includes the spatial correlations. This allows us to investigate a complicated form of the system: three-dimensional lattice under a uniform synthetic magnetic field with reduced dimensionality, i.e. with finite thickness in the direction perpendicular to the field. This opens up new possibilities, e.g. to analyze the correlations between strongly interacting bosons under the influence of a magnetic field in terms of the distance to the system's edge, visualizing effects of non-trivial topology of the band structure, or discovering parallels between finite and infinite systems in certain conditions. Furthermore, we are able to improve the accuracy on the account of the thermal fluctuations, which allows us to properly describe the state of the system at non-zero temperature. These elements allow for a better understanding of the Bose-Hubbard model, in particular of its superfluid phase, which can in turn be related to superconductivity.

VORTEX DYNAMICS SIMULATIONS IN 3D CURVED SUPERCONDUCTOR MEMBRANES

I. Bogush[1,*], V. M. Fomin[2,3], O. V. Dobrovolskiy[1]
[1]*Cryogenic Quantum Electronics, EMG and LENA, Technische Universität Braunschweig, Braunschweig, Germany;*
[2]*Institute for Emerging Electronic Technologies, Leibniz IFW Dresden, Dresden, Germany;*
[3]*Moldova State University, Chișinău, Republic of Moldova*
[*]E-mail: igori.bogus@tu-braunschweig.de

Superconductor 3D nanoarchitectures are a subject of extensive theoretical and experimental studies due to their potential for tuning superconducting properties by their geometry. In this regard, of special interest are effects emerging because of the extension of planar thin films into the third dimension and the impact of the 3D geometry on phenomena studied extensively for planar systems [1, 2]. In particular, vortex dynamics in superconductor films are strongly influenced by the component of the magnetic field that is normal to the film surface. When a curved thin film is exposed to a homogeneous magnetic field, the normal component of this field exhibits a complex spatial profile. Vortices tend to move along the region where the magnitude of the normal magnetic field is the largest [3]. This enables a vortex steering on curved superconducting surfaces, which can additionally be tuned by adjusting the magnitude and direction of the external magnetic field.

In this talk, I will introduce a formalism we developed based on differential geometry and conformal mappings for numerical simulations of curved surfaces using a finite difference approach. Differential geometry is a powerful tool that describes spaces with curvature or curvilinear coordinates, e.g., in General Relativity. Conformal mapping transforms the initial surface into a domain of plane with the geometry being encoded in a conformal factor and an extrinsic curvature tensor. This formalism allows us to apply the finite difference method to simulations of curved films by incorporating these conformal factors and curvatures into the model equations.

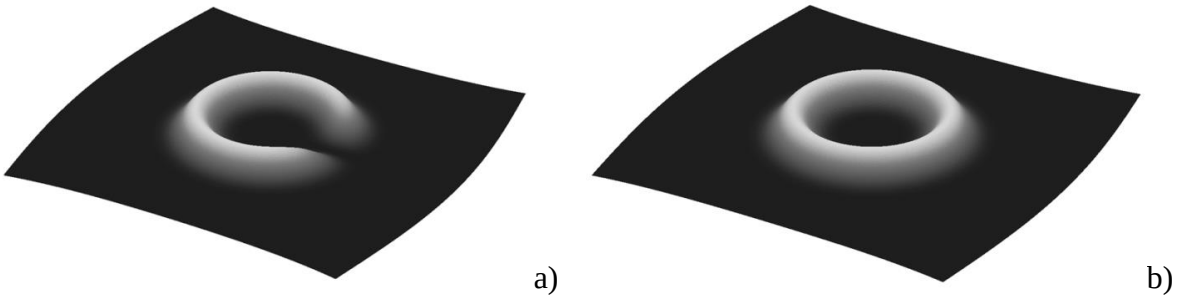

Figure 1. Examples of the considered geometries: (a) C-shaped well, (b) ring-shaped well.

I will discuss several theoretical aspects of the formalism and illustrate its application to the Schrödinger equation for a charged particle in static electric and magnetic fields. Further, the method is applied to the time-dependent Ginzburg-Landau equation for the superconducting order parameter. The considered geometries include a ring-shaped well and a C-shaped well (Fig. 1). It is demonstrated that vortices can be pinned by geometrical effects and that a vortex ratchet effect can be achieved by geometric adjustments alone. Both pinning and vortex ratchet effects can be controlled by varying the external magnetic field.

[1] I. Bogush, V. M. Fomin, Phys. Rev. B **105** (2022) 094511
[2] I. Bogush, O. V. Dobrovolskiy, V. M. Fomin, Phys. Rev. B **109** (2024) 104516
[3] I. Bogush, O. V. Dobrovolskiy, V. M. Fomin, Nanomaterials **14** (2024) 420

FRACTIONAL VORTICES AND FLUX-FLOW INSTABILITIES IN TWO-BAND SUPERCONDUCTORS

A.O. Pokusinskyi[1,2,*], A.L. Kasatkin[2], O.V. Dobrovolskiy[1]
[1]*Cryogenic Quantum Electronics, EMG and LENA, Technische Universität Braunschweig, Braunschweig, Germany;*
[2]*Taras Shevchenko National University of Kyiv, Kyiv, Ukraine;*
[*]E-mail: anton.pokusinskyi@tu-braunschweig.de

Multiband superconductors entail rich physics associated with the coexistence of different order parameters and competing interactions. Therein, the dynamics of vortices is of special interest as novel approaches to fluxon steering can be elaborated via tuning intensity and type of pinning sites, vortex structure, and the intervortex interaction. In particular, it was predicted theoretically [1] and proved experimentally [2] that fractional components of a composite vortex in two-band superconductors can exist separately as vortices with different parameters (e.g. magnetic penetration depth, coherence length) associated with the respective superconducting condensates. Usually, the fractional components of composite vortices tend to combine in the form of a composite vortex with full magnetic flux quantum, which can be explained by an interband attraction between two vortices from the different condensates [3,4]. A moving composite vortex behaves as a single-band Abrikosov vortex with effective parameters of the two-band system, which is why experimental observations of the two-band vortex nature in resistive measurements are challenging. However, the possibility for a moving two-band vortex to dissociate into vortices of two fractional components, due to the disparity of the vortex viscosity and flux of the vortex in the different bands [3], allows for emerging features in the current-voltage (I-V) curve of the superconductor.

In my talk, I will present the results of our theoretical studies of possible mechanisms for the dissociation of composite vortices in two-band superconductors under the action of a strong rf current in the presence of strong pinning sites [5]. The problem is considered on the basis of a nonlinear dynamic equation for a single composite vortex interacting with a single pinning potential trough. For the case of a rather strong pinning, we predict that a resistive branch in the I-V curve will occur due to the depinning of a more mobile vortex fractional component, while a less mobile fractional vortex component remains pinned. By contrast, for the case of a weak pinning, the depinning of composite vortices is followed by a dissociation of a composite vortex into a slow-moving vortex component whose velocity can even drop to zero and a fast-moving fractional component, giving rise to instability jumps in the I-V curves. Fractional instabilities observed recently experimentally for superconductor 2D films and 3D nanoarchitectures will be commented within the framework of the considered model.

[1] E. Babaev. *Phys. Rev. Lett.* **89** (2002) 067001.
[2] Y. Iguchi et al. *Science* **380** (2023) 1244–1247.
[3] S.-Z. Lin, L. N. Bulaevskii. *Phys. Rev. Lett.* **110** (2013) 087003.
[4] M. A. Silaev. *Phys. Rev. B* **83** (2011) 144519.
[5] A. O. Pokusinskyi, A. L. Kasatkin. *Low Temp. Phys.* **50** (2024) 111–116.

ENHANCED MAGNETIC FLUX PINNING AND CRITICAL CURRENT IN SUPERCONDUCTORS WITH NON-PERIODIC PINNING ARRAYS

V. R. Misko[1,2,*], F. Nori[2,3]
[1]*Department of Chemical Engineering, Vrije Universiteit Brussel, Brussels, Belgium;*
[2]*Theoretical Quantum Physics Laboratory, Cluster for Pioneering Research, RIKEN, Wako-shi, Saitama, Japan;*
[3]*Physics Department, University of Michigan, Ann Arbor, Michigan, USA*
[*]E-mail: veaceslav.misco@vub.be

Non-periodic arrays of pinning sites (APS) are generally thought to be inefficient in magnetic flux pinning, since these APS are incommensurate with periodic vortex lattice whose deformations lead to an increase in the elastic energy. However, pinning properties of a superconductor can be even improved by using these APS. We demonstrate enhanced pinning in quasiperiodic (QP) and hyperbolic-tessellation (HT) APS.

Periodic APS are efficient for matching flux, resulting in a narrow peak in the critical current J_c. We found that a five-fold Penrose-tiling APS provided a broad maximum in $J_c(\Phi)$ [1], as verified in experiments with APS of antidots [2] and magnetic dots [3]. We demonstrated theoretically and experimentally [4, 5] that QP APS can enhance J_c in the important range above the matching flux. Thus, QP APS could be useful for applications demanding high J_c over a broad range of fields.

HT APS are characterized by a gradient density of pinning sites. Vortex matter in this device can coexist in three different phases: in a liquid phase, in a viscous liquid phase, and in a solid phase [6]. The penetration of magnetic flux in HT APS is strongly inhomogeneous, in contrast to the conventional Bean model. The magnetization of this device displays a remarkable hysteresis. Due to the enhanced asymmetry of the surface barrier for vortex entry and exit, HT APS could be used as a "capacitor" to store magnetic flux. The enhanced pinning efficiency of graded APS was demonstrated [7] by magnetization and MOI measurements in superconducting *a*-$Mo_{79}Ge_{21}$ thin films with antidots.

Recently, using the focused beam of a helium ion microscope, ultradense kagomé-like patterns have been fabricated in thin films of the cuprate superconductor $YBa_2Cu_3O_{7-\delta}$ [8]. In these kagomé-like patterns, the voids lead to magnetic caging of vortices, resulting in unconventional commensurability effects that manifest themselves as peaks in the critical current and minima in the resistance versus applied magnetic field up to ∼0.4 T. These findings open the way for a controlled manipulation of vortices in cuprate superconductors by artificial sub-100 nm pinning landscapes.

[1] V. Misko, S. Savel'ev, and F. Nori, *Phys. Rev. Lett.* **95** (2005) 177007; *Phys. Rev. B* **74** (2006) 024522.
[2] M. Kemmler *et al.*, *Phys. Rev. Lett.* **97** (2006) 147003.
[3] A. V. Silhanek *et al.*, *Appl. Phys. Lett.* **89** (2006) 152507.
[4] V. R. Misko *et al.*, *Phys. Rev. B* **82** (2010) 184512.
[5] D. Bothner, R. Seidl, V. R. Misko, R. Kleiner, D. Koelle, M. Kemmler, *Supercond. Sci. Technol.* **27** (2014) 065002.
[6] V. R. Misko and Franco Nori, *Phys. Rev. B* **85** (2012) 184506.
[7] M. Motta *et al.*, *Appl. Phys. Lett.* **102** (2013) 212601.
[8] B. Aichner, B. Mueller, M. Karrer, V. R. Misko *et al.*, *ACS Appl. Nano Mater.* **2**, (2019) 5108.

ESTIMATION OF CARRIER DENSITY IN Te-DOPED BISMUTH MICROWIRES

A.A. Nikolaeva[1,*], L.A. Konopko[1], T.E. Huber[2], G. Para[1], I. Gherghishan[1]
[1]*Technical University of Moldova, Ghitu Institute of Electronic Engineering and Nanotechnologies, Chişinău, Republic of Moldova*
[2]*Howard University, Washington, DC 20059, USA.*
[*]E-mail: albina.nikolaeva@iien.utm.md

In this report a new approach to characterizing the carrier density *n* in Te-doped Bi micro-wires is described. Carrier density is a fundamental parameter for determining the electrical transport properties of micro- and nanowires to optimize their performance for different applications, such as thermoelectrics. Measurements of the Hall effect, which is basically a 2D phenomenon, may be inapplicable for microwires and the Shubnicov–de Haas (SdH) oscillations for highly doped microwires. To determine the carrier density *n* of different Te-doped Bi microwires, we used measurements of Seebeck coefficient α(*n*) at 300 K at relative resistance $R_{300}/R_{4.2}(n)$. Glass-insulated Bi-Te microwires were prepared by liquid-phase casting by the Ulitovsky method [1]. The samples had a strictly cylindrical shape, the (1011) orientation along the wire axis, a diameter of >0.2 μm, and a length of a few tens of meters.

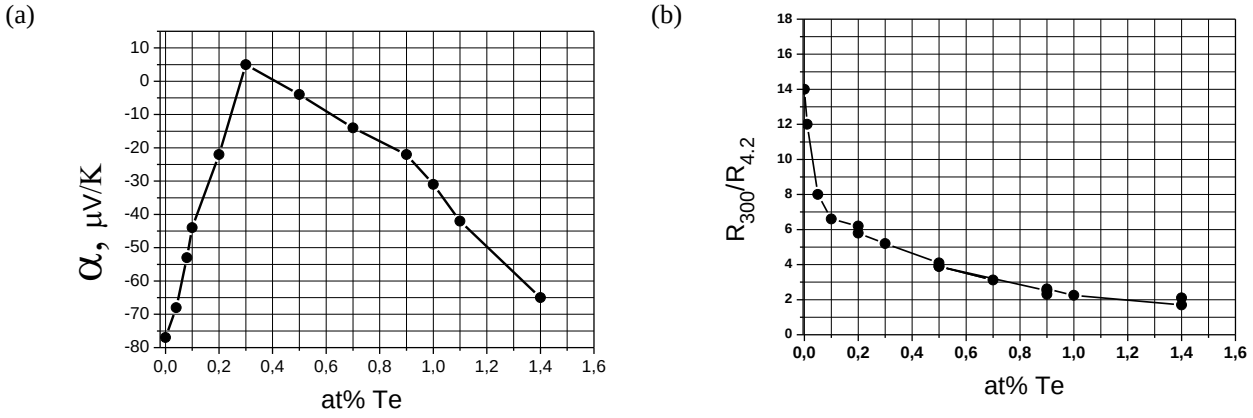

Figure 1. (a) Concentration dependences of coefficient Seebeck α(n) at 300 K and (b) - $R_{300}/R_{4.2}$ (n) of Bi-Te wires.

The From (SdH) oscillations(to 0,4 at %Te) it was estimated Te concentration (in sm^{-3}) at 4.2K. At concentration- 0.3 at %Te there is a sign change thermopover which is a reference point and corresponds Lifshits's to topological transition [2].- to occurrence T- zone of conductivity at alloying. The results offer practical to optimize these parameters during preparation micro-wires for different applications.

ACKNOWLEDGEMENTS: This work was supported by the Ministry of Education and Research of R. Moldova within the program no. 020201 in Moldova. In the U.S., the work was sponsored by the U.S. National Science Foundation STC Center for Integrated Quantum Materials, Grant 1231319, The Boeing Company, and the Keck Foundation.

[1] N.B.Brandt, D.V.Gitsu, A.A.Nikolaeva, Y.G.Ponomarev *Sov. Phys. JETP* **45**(6) (1977) 1226-1232.
[2] L. Varlamov A.A.Egorov V.S.Panatsulaya. *Adv.Phys.* **38**(5) (1989) 469-564.

QUANTUM OSCILLATIONS AT THE TOPOLOGICAL INSULATOR MICROWIRE/TOPOLOGICAL SUPERCONDUCTOR INTERFACE

L.A. Konopko[1,*], A.A. Nikolaeva[1], T.E. Huber[2]
[1]*Technical University of Moldova, Ghitu Institute of Electronic Engineering and Nanotechnologies, Chișinău, Republic of Moldova*
[2]*Howard University, Washington, DC 20059, USA.*
[*]E-mail: leonid.konopko@iien.utm.md

In this work, the magnetoresistance (MR) of topological insulator (TI) single-crystal $Bi_{0.83}Sb_{0.17}$ and polycrystalline Bi_2Te_2Se glass-coated microwires in contact with In_2Bi superconducting (SC) leads was investigated. To study the TI/SC interface, the glass-coated microwire was connected to copper leads on one side using In_2Bi superconducting alloy (T_c=5.6 K) and on the other side using gallium. Gallium has superconductivity at temperatures below 1 K, so it was a normal metal in our measurements. The topologically nontrivial 3D superconductor In_2Bi has proximity-induced superconductivity of topological surface states. The *h/2e* oscillations of magnetoresistance in longitudinal and transverse magnetic fields (up to 1 T) at the TI/SC interface were observed at different temperatures (4.2 K–1.5 K) [1,2] (see Fig. 1). To explain the observed oscillations, we used magnetic flux quantization, which requires a multiply connected geometry where flux can penetrate into normal regions surrounded by a superconductor. The effective width Δr of the closed superconducting area of the TI/SC interface was determined to be 15 nm based on the analysis of FFT spectra and the beats of the MR oscillations for two different directions (longitudinal and transverse) of the magnetic field.

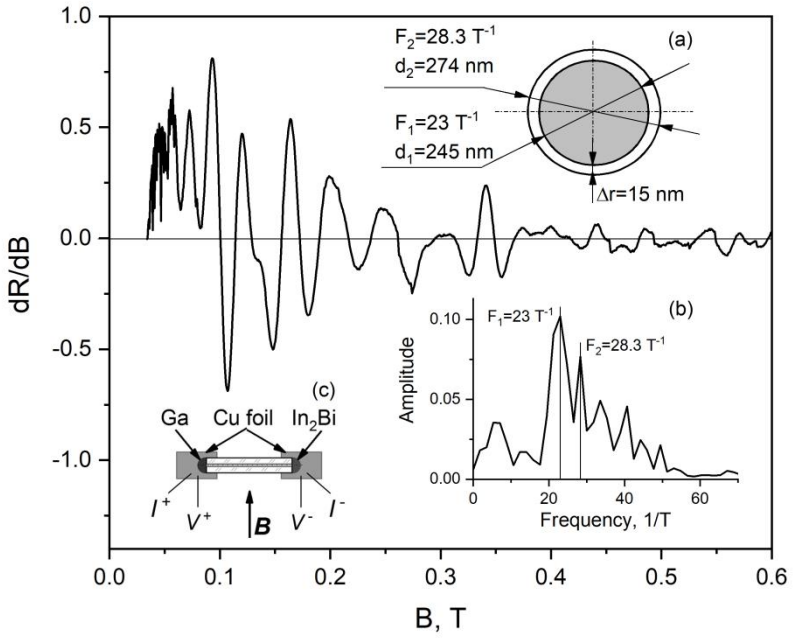

Figure1. Magnetic field dependence of the derivative of transverse MR for the $Bi_{0.83}Sb_{0.17}$ glass-coated microwire, D = 19 μm, d = 1.7 μm measured at 1.5 K (monotonic part is subtracted); Insert (a): The TI-SC contact area, for example, is presented in the form of a circle; Insert (b): FFT of the oscillating part of the derivative of transverse MR; Insert (c): Sketch of microwire mounting.

ACKNOWLEDGEMENTS: This work was supported by the Ministry of Education and Research of R. Moldova within the program no. 020201 in Moldova. In the U.S., the work was sponsored by the U.S. National Science Foundation STC Center for Integrated Quantum Materials, Grant 1231319, The Boeing Company, and the Keck Foundation.

[1] L.A. Konopko, A.A. Nikolaeva, T.E. Huber, K. Rogacki. *Physica B Condens. Matter.* **536** (2018) 259-261.
[2] L. Konopko, A. Nikolaeva, T. Huber. *IFMBE Proceedings* **91** (2023) 293-302.

THERMOELECTRIC POWER STUDY OF 2D DICHALCOGENIDES THROUGH SCANNING THERMOPOWER MICROSCOPY ADAPTED IN A SCANNING TUNNEL MICROSCOPE

J.D. Bermúdez-Perez[1,2,*], E. Herrera-Vasco[2], H. Rojas-Páez[3], O.L. Herrera-Sandoval[4], H. Suderow[2], P. Giraldo-Gallo[3], J. Augusto Galvis[1]
[1]*School of Engineering, Science and Technology, Universidad del Rosario, Bogotá, Colombia;*
[2]*Laboratorio de Bajas Temperaturas, Departamento de Física de la Materia Condensada, Instituto de Ciencia de Materiales Nicolás Cabrera, Condensed Matter Physics Center (IFIMAC), Facultad de Ciencias Universidad Autónoma de Madrid, Madrid, Spain;*
[3]*Department of Physics, Universidad de Los Andes, Bogotá, Colombia;*
[4]*Facultad de Ingeniería y Ciencias Básicas, Universidad Central, Bogotá, Colombia*
[*]E-mail: josed.bermudez@uam.es

Nanotechnology requires the use of specialized experimental techniques to investigate the physical properties of materials at the nanoscale. One such powerful technique is Scanning Tunneling Microscopy (STM), which allows the study of material surfaces at the atomic level. In STM, a sharp metal tip is positioned extremely close to the sample surface, typically of the order of angstroms. At this proximity, electrons can tunnel between the tip and the sample, generating a tunneling current [1]. This current is measured and used to produce images of the surface topography with atomic resolution, as well as to probe the local density of states through tunnel conductance.

STM can be modified to incorporate additional measurement modes, enabling the exploration of physical phenomena beyond those addressed by the conventional technique [2]. In this poster, we present a novel approach involving the development of a high-resolution Scanning Tunneling Microscope adapted as a Thermopower Microscope (STM/SThEM), which operates in a high vacuum environment and at room temperature. This innovative setup allows for the measurement of the Seebeck coefficient (S), a critical parameter in thermoelectric studies, and offers valuable insights into material properties. We demonstrate the application of this technique using our custom-built STM/SThEM microscope to study the effect of chemical doping on the thermoelectric power of the transition metal dichalcogenide WSe_2, a novel material with additional properties such as ferroelectricity and ferromagnetism [3].

[1] G.Binnig and H.Rohrer. Surf.Sci **126**, 236 (1983).
[2] Bermúdez-Perez, J.D., Herrera-Vasco, E., Casas-Salgado, J. et al. Ultramicroscopy **261**, 113963 (2024)
[3] Cardenas-Chirivi, G., Vega-Bustos, K., Rojas-Páez, H. et al. npj 2D Mater Appl **7**, 54 (2023).

SUPERCONDUCTING NANOSTRUCTURES FOR SPINTRONICS

V. Boian, M. Lupu, A. Sidorenko*
Technical University of Moldova, D.Ghitu Institute of Electronic Engineering and Nanotechnologies, Chișinău, Republic of Moldova
*E-mail: sidorenko.anatoli@gmail.com

Increasing energy consumption and the necessity of the energy efficiency and the radically reduction of the power consumption level becomes a crucial parameter constraining the advance of supercomputers. The most promising solution is design and development of the non-von Neumann computers with brain-like architecture, first of all – the Artificial Neural Networks (ANN) based on superconducting elements. Superconducting ANN needs elaboration of two main elements – functional nanostrtuctures: nonlinear switch similar to the neuron, and linear connecting elements similar to synapse [1]. There are presented results of design and investigation of artificial neurons, based on superconducting spin valves, and superconducting synapses, based on layered hybrid nanostructures superconductor-ferromagnet. Are presented results of the theoretical and experimental study of the proximity effect in a stack-like superconductor/ferromagnet (S/F) superlattices with Co-ferromagnetic layers of different thicknesses and coercive fields, and Nb-superconducting layers of constant thickness equal to coherence length of niobium.

The superlattices Nb/Co demonstrate change of the superconducting order parameter in thin niobium films due to switching from the parallel to the antiparallel alignment of neighboring ferromagnetic layers. We argue that such superlattices can be used as suitable base elements for superconducting spintronics for ANN engineering [2]. Design of the ANN using that two base elements, artificial neurons and artificial synapses, allows construction of the computer with several orders of magnitude lower energy consumption in comparison with the traditional computer designed from semiconducting base elements.

ACKNOWLEDGEMENTS: The study was supported by the project of the Moldova State Program «Functional nanostructures and nanomaterials for industry and agriculture» no. 20.80009.5007.11.

[1] A. Sidorenko, H. Hahn, V. Krasnov. Beilstein J. Nanotechnol. 2023, 14, 79–82
[2] A. Sidorenko (Editor). Functional Nanostructures and Metamaterials for Superconducting Spintronics. Springer, 2018

EDGE MAGNETISM IN ARMCHAIR GRAPHENE NANORIBBONS

S. Šćepanović[1,2,3,*], J. Mirković[1,2], T. Klamroth[4], A. Hassanien[3]
[1]*University of Montenegro, Podgorica, Montenegro;*
[2]*PRONA - Montenegrin Science Promotion Foundation, Podgorica, Montenegro;*
[3]*Jozef Stefan Institute, Ljubljana, Slovenia;*
[4]*Institute of Chemistry, University of Potsdam, Potsdam, Germany*
[*]E-mail: stefanscepanovic@gmail.com

Interest in magnetically active graphene nanoribbons stem from the fact that they have great potential for applications in topological spintronic devices. However, due to their high reactivity, the edges are passivated during the synthesis process which leads to quenching of these magnetic states. Using scanning tunneling microscopy and spectroscopy, we find that magnetism can be revived through post annealing process, where unpassivated atoms are located near the termini. Namely, a pair of intense Kondo resonances emerges at each end of zigzag terminus, of as-grown 7 atom-wide-armchair GNR on Au (111), revealing the many-body screening effects of local magnetic moments. Although the Kondo resonance originates from a missing local orbital, it extends to a distance of 2.5 nm along the side of GNR. In contrast, the signal intensity sharply drops towards the bulk of the ribbon indicating no appreciable interactions with extended π state electrons. From the temperature dependence of the half width at half maximum we determine, a Kondo temperature of 68 K. The results are complemented by density functional theory (DFT) calculations which suggest a possible coupling between Kondo states despite screening effects of substrate electrons. These findings highlight a possibility of inducing magnetic ordering in passivated GNR by de-hydrogenation of atoms at the peripheries of zigzag termini.

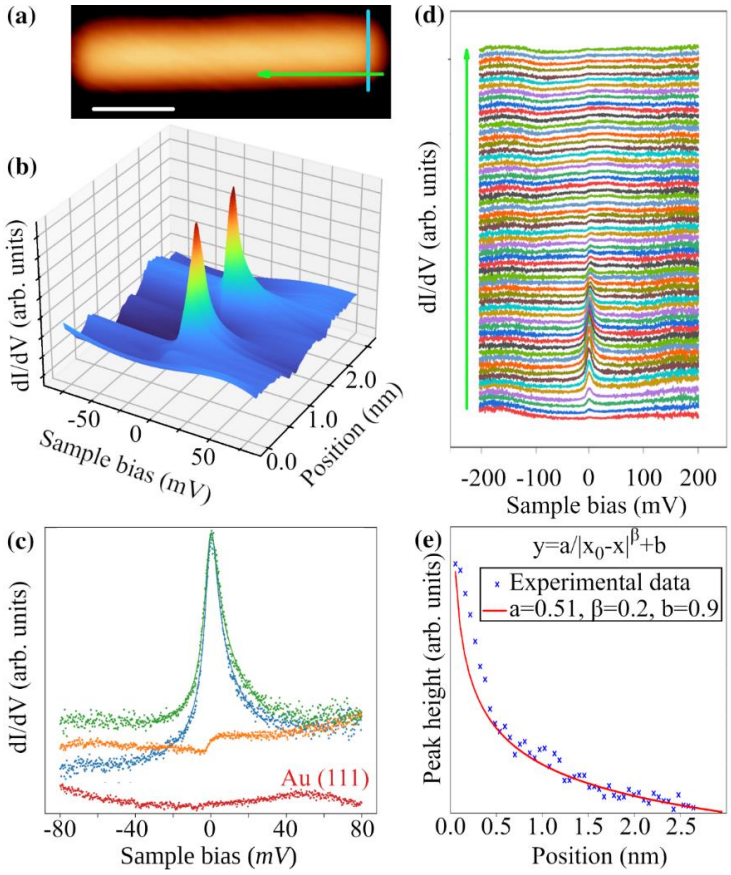

D

E

F

G

N

O

P

R

S

Ș

T

U

10TH INTERNATIONAL CONFERENCE ON MATERIALS SCIENCE AND CONDENSED MATTER PHYSICS

OCTOBER 1-4, 2024

Bun de tipar *20.09.2024.* Formatul *70x100 1/12*
Coli de tipar 18,4
Comanda 115/24. Tiraju 230 ex.

Centrul Editorial-Poligrafic al USM
str. Al. Mateevici, 60, Chișinău, MD-2009
email: cep1usm@mail.ru; usmcep@mail.ru